

School of Molecular and Life Science

**Studies Towards Sulfate Sensing by Voltammetry at Liquid-liquid
Interfaces**

Nasib Kalaci

**This Thesis is presented for the degree of
Doctor of Philosophy of
Curtin University**

May 2023

Declaration

To the best of my knowledge and belief, this thesis contains no material previously published by any other person except where due acknowledgement has been made.

This thesis contains no material which has been accepted for the award of any other degree or diploma in any university or institution for higher education.

Nasib Kalaei

PhD Candidate

30/05/2023

Table of Contents

Declaration.....	i
Table of Contents.....	ii
Tables:.....	vi
Figures.....	vii
Dedication	xii
Acknowledgements	xiii
Glossary	xiv
Roman Symbols:.....	xiv
Greek Symbols:.....	xv
Abbreviations.....	xv
Abstract.....	xvii
1. Introduction	1
1.1. Fundamental of electrochemistry.....	1
1.1.1. Electron transfer at electrodes	1
1.1.2. Faradic and non-Faradic processes.....	2
1.1.3. Polarisable and non-polarisable electrodes.....	2
1.1.4. The electrical double layer.....	3
1.1.5. Mass transport.....	5
1.2. Electrochemistry at the Interface between Two Immiscible Electrolyte Solutions	6
1.2.1. Background.....	6
1.2.2. Basic theoretical relationships at the ITIES.....	7
1.2.3. The interface structure of the ITIES	9
1.2.4. Polarizable and non-polarizable ITIES.....	11
1.2.5. Potential window at the ITIES	13
1.2.6. Forms of charge transfer at the ITIES.....	15
1.3. Macro-ITIES	15
1.3.1. Electrochemical set up of the ITIES.....	15
1.4. Micro-ITIES	16
1.4.1. Miniaturisation of the ITIES	16
1.4.2. Different arrangements of the ITIES and their effect on electrochemical signal	17
1.4.3. Electrochemical set up of the μ -ITIES	20
1.4.4. Electrodes and electrolytes at the ITIES	21
1.4.5. Facilitated ion transfer at the micro-ITIES.....	22
1.4.6. Cyclic Voltammetry at the ITIES.....	26
1.4.7. Differential pulse voltammetry (DPV):	27
1.5. Principles of ion selective electrodes	28
1.5.1. Introduction	28

1.5.2.	Structure of conventional ISEs and Nernstian behaviour	28
1.5.3.	Selectivity of ISEs	31
1.5.4.	Solid state ion selective electrodes	32
1.5.5.	Different solid contact ion selective electrodes.....	33
1.6.	Aims and goals of this work (sulfate sensing):.....	34
2.	Characterisation of facilitated ion transfer at micro-interface arrays supported on laser-ablated glass membranes.....	36
2.1.	Introduction:.....	36
2.2.	Experimental Section.....	37
2.2.1.	Reagents and materials.....	37
2.2.2.	Micro-pore array fabrication and characterization	37
2.2.3.	Electrochemical procedure at the micro-ITIES array:	39
2.3.	Results and discussion	40
2.3.1.	Mechanism of the ion transfer.....	40
2.3.2.	Evaluation of reversibility of the system	42
2.4.	Screening of sulfate ionophores by FIT at glass micropore array	46
2.4.1.	Introduction	46
2.5.	Experimental Section: Facilitated Sulfate Transfer at ITIES.....	47
2.5.1.	Reagents and materials:.....	47
2.5.2.	Electrochemical set up for sulfate sensing:	48
2.5.3.	Results and Discussion:.....	49
2.5.4.	Nernstian behaviour of facilitated sulfate transfer:.....	52
2.6.	Conclusion	54
3.	Evaluation of a Ru-bipod complex as a redox transducer for membrane-based voltammetry of anions	55
3.1.	Introduction:.....	55
3.2.	Experimental section	58
3.2.1.	Reagents.	58
3.2.2.	Instrumentation and measurements.....	59
3.2.3.	Film preparation.....	59
3.2.4.	Synthesis of Ru-bipod complex.....	59
3.3.	Results and Discussion	59
3.3.1.	Cyclic Voltammetry Confined in Thin Films.	61
3.3.2.	Electron transfer kinetic study	67
3.3.3.	Stability evaluation during potential cycling	68
3.3.4.	Nernstian behaviour of the thin film:.....	70
3.3.5.	Selectivity study:	72
3.4.	Conclusion	74
4.	New Ru complexes to develop solid contact ion selective electrodes to sense Sulfate.....	76

4.1.	Introduction.....	76
4.2.	Experimental section	77
4.2.1.	Reagents	77
4.2.2.	Instrumentation and measurements.....	77
4.2.3.	Film preparation.....	78
4.2.4.	Synthesis of Ru(bipod)(dmbb) and Ru(bipob)(bipob).	78
4.3.	Result and discussion.....	78
4.3.1.	Electrochemical properties of the complexes	78
4.3.2.	Stability during scans in the presence of sulfate ions:	81
4.3.3.	Thin film behaviour in the presence of sulfate ions:	83
4.3.4.	Hofmeister series and selectivity of thin film to sense sulfate over other anions:	84
4.3.5.	Potentiometric behaviour of the thin films and calibration curves:	85
4.3.6.	Sensitivity and selectivity of the membrane with Ru(bipod)(dmbb) and Ru(bipod)(bipob):	89
4.3.7.	Electrochemical behaviour of thin film in the presence of sulfate ionophores:	90
4.4.	Conclusion	96
5.	Immobilization of Janus type Ru complex on ITO electrodes and investigation of its electrochemical behaviour	97
5.1.	Introduction.....	97
5.2.	Experimental	98
5.2.1.	Reagent:.....	98
5.2.2.	Modification of ITO electrodes:	98
5.2.3.	Instrumentation and measurement:.....	99
5.3.	Results and discussion	99
5.3.1.	Characterization of Janus-Ru complex modified ITO electrode:	99
5.3.2.	Electrochemical responses of the modified ITO electrode in the presence of different anions: 102	
5.3.3.	Sensitivity of the immobilised ITO electrode with the thin film:.....	104
5.4.	Conclusion:	106
6.	Conclusions	107
6.1.	General Conclusions.....	107
6.2.	Suggestions for future work	109
	References:.....	111
	Appendix A: Synthesizing the Ru-bipod complex and its characterisation (all the information in this section is the group of Pro. Haga, Chuo University, Japan) (related to chapter 3)	123
	A-1: Synthesis of Ru-bipod and its characterisation:	123
	Appendix B: Synthesis of Ru(bipod)(bipob) and Ru(bipod)(dmbb) and their characterisation (all the information in this section is the group of Pro. Haga, Chuo University, Japan) (related to Chapter 4)	126
	B-1: Materials:	126

B-2: Physical Measurements:	126
B-3: Synthesis of (2-nitrophenyl)-(2-octyldodecyl)amine	127
B-4: Synthesis of N-(2-octyl dodecyl)-benzene-1,2-diamine	128
B-5: 1,3-Bis(N- (2-octyl dodecyl)benzimidazol-2-yl)benzene (bipob)	128
B-6: Synthesis of [Ru(bipod)Cl₃]	128
B-7: Synthesis of [Ru(bipod)(bipob)](PF₆)	128
B-8: Result and discussion:	130
B-8-1: Synthesis	130
B-8-2: Electrochemical properties:	131
B-8-3: UV-vis spectral change by chemical oxidation of [Ru(bipod)(bipob)]⁺ by Ce(IV) ion	131
B-8-4: Preliminary result of X-ray single crystal analysis.	132
B-8-5: Phase transitions from DSC measurement	133
Appendix C: Results (related to chapter 3)	136
Appendix D: Attribution Statement	138

Tables:

Table 2.1 Dimensions of the pores characterized by SEM and Image J software (n=4).....	38
Table 2.2 Reversibility factors achieved by two types of the membrane configurations including: peak to peak separation, proportion of peak current of forward to reverse scan, linear relation of peak current with square root of scan rate, no shifting in potential with scan rate (n=3).	46
Table 3.1 : Different electroactive materials which used in SC-ISEs.....	56
Table 3.2 : Different compositions of the membranes (M1-M10) in total mass which is 12.5 mg in 500 μ l THF. (a: mmol/ kg, b : mg, S.I : Sulfate Ionophore).	60
Table 3.3 Kinetic parameters calculated from the data in Fig5 for the kinetics of Ru-bipod in the presence of NPOE or DOS as plasticizers. α : electron transfer coefficient, v_a and v_c : anodic and cathodic critical scan rates, respectively, $k_{app,a}$ and $k_{app,c}$: anodic and cathodic electron transfer rate constants, respectively, and $k_{app,ET}$: total electron transfer rate constant.....	68
Table 3.4 The peak area under first scan which is representative of the charge which is transferred in the first peak with and without ETH500 in the presence 10 mM of KPF_6 and with and without sulfate ionophore in the presence of 10 mM of K_2SO_4 (n = 6).....	70
Table 3.5 selectivity coefficients of NO_3^- ions over PF_6^- and ClO_4^- by FIM and SSM methods.....	73
Table 4.1 Kinetic parameters calculated from the data in Figure 4.13 : Plots of the oxidation and reduction peak potentials of the Ru-bipod complex in membranes a) 65 mmol/ kg Ru(bipod)(dmdbb) and b) 65 mmol/ kg Ru(bipod)(bipob), 66% NPOE and 33% PVC) in the presence of aqueous 10 mM K_2SO_4 versus logarithm of scan rate with(n=3).for the kinetics of Ru(pod)(pob) and Ru(pod)(dmdbb) in the presence of 10 mM KPF_6 . α : electron transfer coefficient, v_a and v_c : anodic and cathodic critical scan rates, respectively, $k_{app,a}$ and $k_{app,c}$: anodic and cathodic apparent electron transfer rate constants, respectively, and k_{app} : total apparent electron transfer rate constant.....	88
Table 4.2 : Kinetic parameters calculated from the data in Figure 4.13 for the kinetics of Ru(pod)(pob) and Ru(pod)(dmdbb) in the presence of 10 mM K_2SO_4 . α : electron transfer coefficient, v_a and v_c : anodic and cathodic critical scan rates, respectively, $k_{app,a}$ and $k_{app,c}$: anodic and cathodic apparent electron transfer rate constants, respectively, and k_{app} : total electron transfer rate constant.	89
Table 4.3 : selectivity coefficients of the thin film with Ru complexes in the presence and absence of T.Thio. bisCF ₃ with sulfate over chloride and nitrate ions by separate solution method.....	95

Figures

Figure 1.1.1 The current/potential curves for polarisable a) and non-polarisable b) electrodes. Dashed lines represent practical behaviour of electrodes while solid lines show ideal behaviour.	3
Figure 1.1.2 Electrical double layer of Helmholtz model (left) of the electrode and electrolyte solution interface and its similarity to a capacitor (right).	4
Figure 1.1.3 : The electrical double layer including the Inner Helmholtz Plane (IHP) and the Outer Helmholtz Plane (OHP).	5
Figure 1.2.1 Schematic of mixed solvent layer which is similar with electrical double layer at ITIES.	11
Figure 1.2.2 Polarizable and non-polarizable set up at the ITIES. At the polarizable interface, A^+ and B^- are very hydrophilic while C^+ and D^- are very hydrophobic. At the non-polarizable interface, (left) A^+ and B^- are common ions in both phases, and (right) A^+ is a common ion in two phases and B^- is very hydrophilic and C^- is very hydrophobic.	13
Figure 1.2.3 Cyclic voltammogram of 10 mM LiCl in aqueous phase and 10 mM BTPPATPBCl in organic phase (1,6-dichlorohexane). Scan rate: 10 mV/s.	14
Figure 1.3.1 Electrochemical cell showing the typical four electrodes set up at ITIES, which includes two counter electrodes (CE) and two reference electrodes(RE), one of each in aqueous and organic phases.	16
Figure 1.4.1 Three different electrode geometries and their diffusion modes. For each electrode geometry, there is a limiting current (I_{lim}) equation which describes their different dependencies. In the equations, n is number of electrons transferred, F is the Faraday constant, C is the concentration, r is the electrode radius and L is the recessed depth.	18
Figure 1.4.2 Diagram representing single micro interface formed at the mouth of a micropore. There are two diffusion modes: radial diffusion of ion in aqueous phase (left) and linear diffusion of ions from organic phase to aqueous phase (right).	18
Figure 1.4.3 Illustration of hexagonal (left) and cubic (right) arrangement of micro disc arrays. d is the distance between two pores and grey part shows the diffusion zone that forms around each micro-ITIES.	19
Figure 1.4.4 Two electrodes set up with micropore array membrane for form a micro-ITIES array.	21
Figure 1.4.5 Illustration of the four types of complexations at the ITIES, which are aqueous complexation followed by transfer (ACT), transfer to the organic phase followed by complexation (TOC), transfer by interfacial complexation (TIC) and transfer by interfacial dissociation (TID).	24
Figure 1.4.6 Applied potential versus time in cyclic voltammetry.	26
Figure 1.4.7 cyclic voltammogram a) for linear diffusion b) for radial diffusion in forward scan and linear diffusion in backward scan.	27
Figure 1.4.8 Potential versus time waveform in differential pulse voltammetry (DPV) (this figure is taken from ⁹⁰ reference).	28
Figure 1.5.1 Schematic of a conventional ion selective electrode with a reference electrode.	29
Figure 1.5.2 Separation solutions method (SSM) to measure K_{IJ}	31
Figure 1.5.3 Fixed Interference Method (FIM) to measure K_{IJ}	32
Figure 2.1 Facilitated potassium ion transfer by DB-18-C-6 in conical shaped micropores in glass membranes functionalised to be hydrophobic on either a) the laser exit side or b) the laser entry side and consequent formation of the ITIES at the a) laser exit side or b) laser entry side.	38
Figure 2.2 SEM images at laser exit side a) hydrophobic side pore and b) hydrophilic side pore, and at laser entry side c) hydrophilic side pore d) hydrophobic side pore	39
Figure 2.3 The electrochemical cell composition (Y mM is concentration of KCl).	39
Figure 2.4 Cyclic voltammograms for the transfer of K^+ across W/DCH interface in the absence (dotted line) and presence (solid line) of DB18-C-6 (10 mM KCl and 1 mM DB18-C6) in pores with interfaces located at laser entry side a) , and pores with interface located at laser exit side b)	41
Figure 2.5 Cyclic voltammograms for the transfer of $TPrA^+$ across W/DCH interface located at the laser entry side (wider pore diameter at the hydrophilic side of the membrane) (solid line) and the interface located at laser exit side (narrower pore diameter at the hydrophilic side of the membrane) (dotted line)(the potential is versus the experimentally used reference electrodes).	42

Figure 2.6 CVs for potassium ion concentrations: 0.5, 1, 2, 4, 7 and 10 mM and in presence of 0.5 mM DB18-C6 in organic phase and 1 mM $MgCl_2$ as background electrolyte in aqueous phase, with laser entry side pore a) and with laser exit side pore b) and plot of mid-point potential of potassium transfer across the interface with Log $[K^+]$ with laser entry side pore c) and with laser exit side pore d) (10 mV/s scan rate). ..43	43
Figure 2.7 a) Peak to peak separation at different concentrations of aqueous phase potassium in the presence of 0.5 mM DB-18-C6 in the organic phase with two the membrane configurations b) ratio of forward and reverse peak currents at different concentrations of aqueous potassium in the presence of 0.5 mM DB-18-C6 in the organic phase with the two membrane configurations.44	44
Figure 2.8 CVs of facilitated potassium transfer by 0.5 mM DB-18-C6 in organic phase and 10 mM KCl in aqueous phase at micro-ITIES array with sweep rate: 5, 10, 15, 20, 25, 30, 35, 40, 50, 60, 70 mV/s at laser entry side a) and laser exit side b) and confirm of reversibility by the linear dependence of peak current with square root of scan rate (c) laser entry side pores (d) laser exit side pores ((the potentials are transposed to Galvani Scale)).45	45
Figure 2.9 Structure of different sulfate ionophores N,N'-bis(2-acetamidophenyl)-5-(tert-butyl)isophthalamide (DCC-286), N,N',N''-(nitrilotris(ethane-2,1-diyl))tris(pyrrole-2-carboxamide) (DCC-287) and N',N''-(3,6-di-tert-butylcarbazole-1,8-diyl)bis(N-phenylthiourea) (PGP-59) (Synthesised by the group of Dr. David Curiel, Murcia University, Spain).48	48
Figure 2.10 Structure of a) Tren-Phenyl and Tren-Antracence b) (2-aminoethylamine)(Tren)bis-CF ₃ (Tren-bis CF ₃) (Synthesised by the group of Prof. Katrina Jolliffe, University of Sydney).48	48
Figure 2.11 Electrochemical set up to sense sulfate ionophore49	49
Figure 2.12 Cyclic voltammograms for the transfer of SO_4^{2-} across W/NPOE interface in absence (dotted line) and presence (solid line) of 0.25 mM a) DCC-286 b) DCC-287 and c) PGP-59 in the presence of 10 mM Li_2SO_4 pores with laser entry side.....50	50
Figure 2.13 Cyclic voltammograms for the transfer of SO_4^{2-} across W/NPOE interface in absence (dotted line) and presence (solid line) of 0.25 mM a) Tren-Antracene b) Tren-Phenyl in the presence of 10 mM Li_2SO_4 pores with laser entry side.....51	51
Figure 2.14 Cyclic voltammograms for the transfer of SO_4^{2-} across W/NPOE interface in absence (dotted line) and presence (solid line) of 0.25 mM Tren-bis CF ₃ in the presence of 10 mM Li_2SO_4 pores with laser entry side, inside is the cyclic voltammograms of transferring TEA (50 μ M) at W/NPOE interface52	52
Figure 2.15 a) CVs for sulfate ion concentrations : 5×10^{-5} , 10^{-4} , 5×10^{-4} , 10^{-3} , 2×10^{-3} , 4×10^{-3} , 7×10^{-3} and 10^{-2} M of SO_4^{2-} and in presence of 0.25 mM Tren-bis CF ₃ in 10 mV/s scan rate b) plot of mid-point potential of potassium transfer across the interface with Logarithm of SO_4^{2-} (n=3).53	53
Figure 2.16 a) DPV back ground subtraction responses related to sulfate interfacial complexation at Water/NPOE interface in the presence of different concentrations of SO_4^{2-} ions (5×10^{-8} , 10^{-7} , 10^{-6} , 10^{-5} , 5×10^{-5} , 10^{-4} , 10^{-3} and 5×10^{-3} M) (which is obtained by subtraction of each voltammogram from the experiment in which SO_4^{2-} concentration is zero), b) Calibration curve of logarithm of different concentrations of sulfate ions versus current (n=3).54	54
Figure 3.1 a) Structure of Ru-bipod complex b) Schematic illustration of the working mechanism of the thin film electrode for anion detection. The film contains the Ru-bipod complex. An applied potential provokes oxidation at the electrode surface (GC) and excess of positive sites ($Ru(III)$) are generated at the GC-film interface. The excess positive charge is balanced by ingress of anions from the aqueous solution into the thin film. Once the reversed potential is applied, anions are expelled from the membrane to maintain electroneutrality.60	60
Figure 3.2 Cyclic voltammetry obtained using membrane M5 (Table S1, containing 65 mmol/kg Ru-bipod complex, 33% PVC and 66% NPOE) in the absence (dashed line) and presence (solid line) of 10 mM KPF ₆ . Scan rate: 10 mV/s.....61	61
Figure 3.3 Hofmeister Series for different anions (10 mM of different anions, PF_6^- (red), ClO_4^- (green), NO_3^- (blue), Cl^- (orange) and SO_4^{2-} (black) using a) M3 b) M4 , c) M6 and d) M5 as the membranes with scan rate 10 mV/s (n=6).....63	63
Figure 3.4 First scan of the membrane M3 (table S1) in the presence of 10mM of different anions, PF_6^- (red), ClO_4^- (green), NO_3^- (blue), Cl^- (orange) and SO_4^{2-} (black).....64	64

Figure 3.5 a) Comparison of half width potential by using different plasticizer of NPOE (solid line) (M5, 65 mmol/Kg Ru-bipod, 33% PVC, 66% NPOE) and DOS (dotted line) M4 (65 mmol/Kg Ru-bipod, 33% PVC, 66% DOS) in presence of 10 mM KPF_6 b) comparison of peak to peak separation by using NPOE (square shapes) and DOS (triangle shapes) as a plasticiser in presence of different concentrations of KPF_6 (n=6)....	65
Figure 3.6 a) Cyclic voltammograms in 10 mM KPF_6 using membrane with two different plasticisers NPOE (M5, 65 mmol/kg Ru-bipod, 33% PVC , 66% NPOE) and b) DOS (M4, 65 mmol/Kg Ru-bipod, 33% PVC , 66% DOS) at different scan rates (10, 15, 20, 25, 30, 40, 50, 60, 70, 90 and 100 mV/ s), and scan rate dependence for cathodic and anodic peaks c) with NPOE and d) DOS (n=3).	66
Figure 3.7 Plots of the oxidation and reduction peak potentials of the Ru-bipod complex in membranes M5 (65 mmol/kg Ru-bipod, 33% PVC , 66% NPOE) (left) and M4 (65 mmol/kg Ru-bipod, 33% PVC , 66% DOS) (right) in the presence of aqueous 10 mM KPF_6 versus logarithm of scan rate with a) NPOE (M5), b) DOS (M4). Linear regression data shown for the higher scan rates where $E_p - E_{0'} > 100$ mV). (n=3)	68
Figure 3.8 Demonstrating electrochemical stability of thin film (using membrane M5) in the presence of a) 10 mM KPF_6 , b) 10 mM KNO_3 , c) K_2SO_4 and d) the thin film (using membrane M11 , with sulfate ionophore) in the presence of 10 mM K_2SO_4 , scan rate 10 mV/s (50 scans).	69
Figure 3.9 Comparison of membrane a) M5 (with ETH500) and b) M10 (without ETH500) in the presence of 0.1 mM of KPF_6 c) M5 and d) M10 in the presence of 10 mM KNO_3 , e) M5 and f) M10 in the presence of 10 mM $KClO_4$, g) M4(with ETH500) and h) M9 (without ETH500) from in the presence of 10 mM KPF_6 with scan rate 10 mV/s.....	71
Figure 3.10 Cyclic voltammograms for increasing concentrations of a) different concentrations of KPF_6 with membrane M5 (65 mmol/kg Ru-bipod, 33% PVC , 66% NPOE). b) relationship between log of concentration and midpoint potential, with a Nernst slope for PF_6^- . Scan rate: 10 mV/s. (n=3).	72
Figure 3.11 Cyclic voltammograms for increasing concentrations of a) different concentrations of KNO_3 with membrane M5 (65 mmol/kg Ru-bipod , 33% PVC , 66% NPOE). b) relationship between log of concentration and midpoint potential, with a Nernst slope for NO_3^- Scan rate: 10 mV/s. (n=3).	73
Figure 3.12 Selectivity study of solid contact with membrane M5 (65 mmol/kg Ru-bipod , 33% PVC and 66% NPOE) in the presence of different concentrations of a) NO_3^- (0.5, 1, 1.2, 1.5, 2, 5, 10, 30, 50, 100 and 200 mM); a) in presence of 0.1 mM ClO_4^- b) in presence of 0.1 mM PF_6^- and c) relation of mid-point potential to logarithm of NO_3^- concentration (n=3): NO_3^- ions in presence of 0.1 mM ClO_4^- (triangles) and NO_3^- ions in presence of 0.1 mM PF_6^- (squares) (n=3).	74
Figure 4.1 : Structure of Ru complexes: Ru(bipod)(dmdbb) and Ru(bipod)(bipob).	78
Figure 4.2 : Cyclic voltammograms of 0.5 M Ru(bipod)(bipob) together with 0.3 M Ru-bipod in CH ₃ CN with 0.1 M TBAPF ₆ as a supporting electrolyte. Working electrode, glassy carbon electrode at 25°C (Data provided by research group of Prof. Haga, Chuo University, Japan).	79
Figure 4.3 : Schematic of sulfate ions transfer in forward (left) and reverse scan (right) which is triggered by oxidation and reduction of the Ru complex, respectively.	79
Figure 4.4 : Cyclic voltammograms of 65 mmol/kg Ru(bipod)(dmdbb) complex, 65 mmol/kg ETH500, NPOE and PU, in the presence (solid line) and absence of PF_6^- (dashed line). scan rate: 10 mV/s.	80
Figure 4.5 : Cyclic voltammetry obtained using membrane containing 65 mmol/kg Ru-bipod complex (blue) and 65 mmol/ kg Ru (bipod)(bipob) (red) and 65 mmol/ kg Ru(bipod)(dmdbb), 33% PVC and 66% NPOE in the presence of 10 mM KPF_6 . Scan rate: 10 mV/s.	81
Figure 4.6 : Stability of the membrane containing a) 65 mmol/ kg Ru(bipod)(dmdbb) complex and b) Ru(bipod)(bipob), 65 mmol/ kg ETH500, 50% NPOE and 50% PU during 50 runs in presence of 10 mM sulfate (first scan (solid line), last line (dotted line)).	82
Figure 4.7 : CVs after twice rinsing of thin film containing 65mmol/kg Ru(bipod)(dmdbb), 130 mmol / kg ETH500, 50% NPOE and 50% PU a) and 50% PVC b).....	83
Figure 4.8 : Cyclic voltammograms in 10 mM K_2SO_4 using thin film containing a) 65 mmol/ kg Ru(bipod)(dmdbb) and b) Ru(bipod)(bipob), 130mmol/kg ETH500, PU=NPOE in different scan rate (10, 20, 30, 40, 50, 70, 90, 100 mV/s).	84

Figure 4.9 : Hofmeister series with thin film containing 65 mmol/ kg Ru(bipod)(dmdbb)(a) Ru(bipod)(bipob), 130 mmol/ kg ETH500, PU=NPOE, in the presence of 10 mM (from right to left) sulfate (dotted line), chloride, nitrate, perchlorate and hexafluorophosphate. Scan rate 10 mV/s. (n=3).....	85
Figure 4.10 : Response of thin film membrane containing 65mmol/kg Ru (bipod) (dmdbb), 130mmol/ kg ETH500, 50% NPOE and 50% PU in presence of different concentration of KPF_6 . (375 μ M, 1.25 mM , 3.75 mM ,10 mM, 17.5 mM , 27.5, 52.5 mM). (n=3).	86
Figure 4.11 : Response of thin film membrane containing 65mmol/ kg of a) Ru (bipod) (dmdbb) and b) Ru(bipod)(bipob), 130mmol/kg ETH500, NPOE=PU in presence of different concentration of SO_4^{2-} (5×10^{-5} , 10^{-4} , 5×10^{-4} , 10^{-3} , 5×10^{-3} , 10^{-2} , 5×10^{-2} , 10^{-1} M) and c) and d) relationship between log of the concentrations of SO_4^{2-} and midpoint potential related to the membrane containing Ru(bipod)(dmdbb) and Ru(bipod)(bipob), respectively. (n=6).....	87
Figure 4.12 : Plots of the oxidation and reduction peak potentials of the Ru-bipod complex in membranes a) 65 mmol/kg Ru(bipod)(dmdbb), NPOE=2PVC and b) 65 mmol/ kg Ru(bipod)(bipob), 66% NPOE and 33% PVC (right) in the presence of aqueous 10 mM KPF_6 versus logarithm of scan rate with(n=3).	88
Figure 4.13 : Plots of the oxidation and reduction peak potentials of the Ru-bipod complex in membranes a) 65 mmol/kg Ru(bipod)(dmdbb) and b) 65 mmol/ kg Ru(bipod)(bipob), 66% NPOE and 33% PVC) in the presence of aqueous 10 mM K_2SO_4 versus logarithm of scan rate with(n=3).	89
Figure 4.14 : Response of thin film membrane containing a) 65mmol/kg Ru (bipod)(dmdbb), and b) 65mmol/ kg Ru(bipod)(bipob), 130mmol/kg ETH500, 50% NPOE and 50% PU in presence of different concentration of K_2SO_4 and the midpoint potential versus logarithm of the different concentrations of sulfate ions with thin film containing c) Ru(bipod)(dmdbb) and d) Ru(bipod)(bipob) (n=3).....	91
Figure 4.15 : a) structure of commercial sulfate ionophore (S.I) b) structure of Tren thiourea bis CF3 (T.Thio. bisCF3).....	92
Figure 4.16 : 10 first scans of thin film containing 65 mmol/kg Ru(bipod)(dmdbb), 130 mmol/ kg ETH500, 130 mmol/kg Sulfate ionophore, 50% NPOE and 50% PU.	92
Figure 4.17 : CVs of the thin film: a) 65 mmol/ kg Ru(bipod)(dmdbb) b) 65 mmol/ kg Ru(bipod)(bipob) , 130mmol/kg ETH500, 50% NPO, 50% PU and excess of S.I in the presence of different concentrations of sulfate and the midpoint potential versus logarithm of the different concentrations of sulfate ions with thin film containing c) Ru(bipod)(dmdbb) and d) Ru(bipod)(bipob).	93
Figure 4.18 : Response of thin film membrane containing a) 65mmol/kg Ru (bipod) (dmdbb) , and b) 65mmol/ kg Ru(bipod)(bipob) 130mmol/ kg ETH500, excess amount of T.Thio. bisCF3 ionophore, 50% NPOE and 50%PU in presence of different concentration of K_2SO_4 (10^{-8} , 5×10^{-8} , 10^{-7} , 5×10^{-7} , 10^{-6} , 5×10^{-6} , 10^{-5} , 5×10^{-5} , 10^{-4} , 5×10^{-4} , 10^{-3} , 5×10^{-3} , 10^{-2} , 5×10^{-2} , 10^{-1} M) and the midpoint potential versus logarithm of the different concentrations of sulfate ions with thin film containing c) Ru(bipod)(dmdbb) and d) Ru(bipod)(bipob) (n=3).	94
Figure 4.19 : CVs related to responses of the membrane contains a) 65 mmol/ kg Ru(bipod)(dmdbb) and b) Ru(bipod)(bipob), 130 mmol/ kg ETH500, excess amount of T.Thio. bisCF3 ionophore and 50% NPOE and 50% PU in the presence of 10 mM SO_4^{2-} , Cl^- and NO_3^- ions.....	95
Figure 4.20 : Response of thin film in the presence of 10 mM of Sulfate ions. (scan rate: 10 mV/s) in the presence of a) Ru(bipod)(dmdbb) and b) Ru(bipod)(bipob). (from right to left: without any ionophore, with S.I and with T.Thio. bisCF3 ionophore.	96
Figure 5.1 : The structure of the Janus Ru complex ²³⁷ employed in this work.....	98
Figure 5.2 : Voltammograms of the ITO electrode which is modified with Janus Ru complex at different scan rates in aqueous solution containing 10 mM KPF_6 b) the linear relationship between peak currents and scan rates (10, 25, 35, 55, 75, 100 mV/ s) in forward and backward scans (n=3; error bars show standard deviation, and are not visible if smaller than the symbol size).....	100
Figure 5.3 : Cyclic voltammogram of modified ITO electrode (solid line) by J-Ru complex and bare ITO electrode (dotted line) in the presence of 10 mM KPF_6 in aqueous solution (Scan rate :55 mV/s).	100
Figure 5.4 : Scheme of anion transfer by thin film which is spin coated on immobilised ITO electrode, R^+ and R^- are tetradodecylammonium and tetrakis(4-chlorophenyl)borate ions , respectively.....	101

Figure 5.5 : Voltammograms of the immobilised ITO electrode with the polymeric thin film containing 65 mmol/ kg ETH00, PVC and NPOE, at different scan rates (10, 25, 35, 55, 75, 100 mV/s) in solution containing 10 mM KPF_6 ; b) the linear relationship between peak current and scan rate in forward and backward scans (n=3; error bars show the standard deviation; where error bars are not visible, the error bars are smaller than the symbol size).....	102
Figure 5.6 : CVs (third scan) related to immobilised ITO electrode which is spin coated by thin film (containing 65 mmol/ kg ETH500, PVC, NPOE) in the presence of different 10 mM aqueous solutions of anions, PF_6^- (orange), ClO_4^- (blue), NO_3^- (green) and SO_4^{2-} (red).	103
Figure 5.7 : 10 first scans of the modified ITO electrode with polymeric thin film containing 65 mmol/kg ETH500, PVC and NPOE, in the solution containing 10 mM KPF_6 (Scan rate:10 mV/s).....	103
Figure 5.8 : Comparison of CV of the modified ITO with polymeric thin film membrane with (solid line) and without (dotted line) added ETH500 in the solution containing 10 mM KPF_6 (Scan rate:10 mV/s).	104
Figure 5.9 : a) Response of the immobilised ITO electrode in the presence of different concentrations of PF_6^- (2.5, 7.5, 15, 30 and 50 mM). b) relationship between log of concentration and midpoint potential, with a Nernst slope for PF_6^- Scan rate: 10 mV/s. (n=3).	104
Figure 5.10 : a) Response of the immobilised ITO electrodes with thin film membrane containing 65 mmol/ kg ETH500, PVC and NPOE in the presence of different concentrations of PF_6^- (2.5, 7.5, 15, 30 and 50 mM). b) relationship between log of concentration and midpoint potential, with a Nernst slope for PF_6^- Scan rate: 10 mV/s. (n=3).....	105
Figure 5.11 : Electrochemical response of the modified ITO with thin film contains 65mmol/kg ETH500, PVC, NPOE and with 130 mmol/ kg S.I (solid line) and without S.I (dotted line). In the solution contains 10 mM K_2SO_4 (Scan rate: 10 mV/s).....	105

Dedication

To my mum, who taught me resilience.

To my dearest Armita, who had to shoulder much more than her age, and was robbed of her mother's time and attention, but did give back love and taught me compassion.

And to all the brave young girls (and boys) of my country, IRAN, who are putting their lives on the line, in their century long fight for freedom.

Woman, Life, Freedom

زن، زندگی، آزادی

Acknowledgements

I would like to extend my sincere thanks to my supervisor, prof. Damien Arrigan who gave me this fantastic opportunity as one of his research group members. I am so grateful to have his invaluable advice, support, encouragement, and patience during my PhD study. Always it has been a pleasure and my honor be under his supervision and take his guidance to make my journey more interesting and easier.

To the supportive and knowledgeable person in sensor group, Dr. Terence Henares for his Scientific and technical support during my research. I shared with him all my tears and happiness during this journey. For all the lunch and coffee times that we had and had electrochemistry discussions about sulfate sensor project.

I would like to thank Prof. Haga and his research group from Chuo University, Japan, who provided for me the very important part of my project which is redox prob complexes, and for their collaborations in this project.

I would like to thank Prof. Kate Jolliffe and her research group from The University of Sydney for collaboration in this project and providing synthesized sulfate ionophores.

I would like to extent my thanks to Curtin university to provide my Scholarship from and funding for laboratory consumables via Australian Research Council (Linkage project) and Water Corporation. Without their support, this research never has been taken place.

To other members in sensor groups, Bren, Ben, Jahir, Shahada, Hum and Nazanin who have been there always in my PhD journey. To Ben and Jahir to spend time and use their knowledge to provide SEM images for dimensions of the micro pores of glass membrane. For the moments I spend with them and had Scientific discussions.

Finally, to my love, Majid, the most reliable, supportive life partner who first inspired me and supported me to put my step in this amazing journey. Always he reminds me of my abilities in research and out of the box thinking and encourages me to go forward. He was the only reason I put my step in this journey.

Glossary

Roman Symbols:

Symbol	Definition	Unit
O	oxidised species	-
R	reduced species	-
e^-	electrons	-
n	number of transferred electrons	-
E_{eq}	equilibrium potential	V
E°	the formal potential	V
R	the universal gas constant	J K ⁻¹ mol ⁻¹
T	temperature	K
F	Faraday Constant	$Cmol^{-1}$
Q	total charge	C
N	number of moles	-
E	potential	V
C	capacitance	F
χ	distance of ionic species	cm
J_i	flux	mol s ⁻¹ cm ⁻²
D	diffusion coefficient	$cm^2 S^{-1}$
C_i	concentration of the ionic species	mol cm ⁻³
Z_i	charge of the ionic species	-
i	ionic species	-
A	electrode area	cm^2
a_i^a	activity of i species	-
R_s	resistance of solution	Ω
I_{lim}	limiting current	A
r	electrode radius	cm
L	recessed depth	cm
d	centre to centre distance	cm
K_a^O	association constant	-
i_c	charging current	A
i_f	faradic current	A
$E_{D,ref}$	liquid junction potential	V
E_M	membrane potential	V
$K_{I,J}$	selectivity coefficient	-
M	slope of the calibration graph	-
ΔE	difference potential of the ISE	V
C_L	concentration of ionophore in organic phase	mol cm ⁻³
C_M	concentration of the ions in aqueous phase	mol cm ⁻³
n	stoichiometry of the ion and ionophore	-
$E_{p,c}$	athodic peak potential	V
$E_{p,a}$	anodic peak potential	V
K_{app}	apparent rate constant of electron transfer	s^{-1}
$K_{app,a}$	anodic electron transfer rate constant	s^{-1}
$K_{app,c}$	cathodic electron transfer rate constant	s^{-1}

Symbol	Definition	Unit
$K_{app,ET}$	total electron transfer rate constant	s^{-1}
E_{mid}	midpoint potential	V

Greek Symbols:

Symbol	Definition	Units
$v(\chi)$	hydrodynamic velocity	$cm\ s^{-1}$
$\Delta_o^w \phi$	Galvani potential	V
ϕ^w	Galvani potential at the aqueous phase	V
ϕ^o	Galvani potential at the organic phase	V
μ_i^a	electrochemical potential	V
$\Delta_o^w \phi_{1/2}$	half wave potential	V
γ_i	Activity coefficient of ion i	-
r	pore radius	cm
δ	diffusion zone thickness	cm
ν	scan rate	V/s
ϕ	Electrical potential	V
μ_i	Chemical potential	$kJ\ mol^{-1}$
μ_i'	Electrochemical potential of species	$kJ\ mol^{-1}$
μ_i^0	Standard chemical potential of the ion	$kJ\ mol^{-1}$
β	equilibrium binding constant	-
$\Delta_o^w \phi_{M^+}^0$	standard potential of ion transfer across the interface	V
α	electron transfer coefficient	-
ν_a	anodic critical scan rate	V/ s
ν_c	cathodic critical scan rate	V/ s
Γ	surface coverage	mol/cm^2
ϵ_r	Dielectric constant	-

Abbreviations

abbreviation	Definition
ACT	aqueous complexation followed by transfer
BTPPATPBCl	bis (triphenylphosphoranylidene) ammonium tetrakis (4-chlorophenyl) borate
CE	counter electrodes
CV	cyclic voltammetry
CWEs	coated wire electrodes
DB-18-C6	dibenzo-18-crown-6
DCC-286	N,N' -bis(2-acetamidophenyl)-5-(<i>tert</i> -butyl)isophthalamide
DCC-287	N,N',N'' -(nitriлотris(ethane-2,1-diyl))tris(pyrrole-2-carboxamide
DCH	dichlorohexane
DOS	bis(2-ethylhexyl) sebacate
DPV	Differential pulse voltammetry
EMF	electromotive force
ET	electron transfer

abbreviation	Definition
Fc	Ferrocene
FIB	focused ion beam
FIB	focused ion beam
FIM	fixed interference method
FIT	facilitated ion transfer
GC	glassy carbon
IFS	inner filling solutions
IHP	inner Helmholtz plane
IPE	Ideal polarised electrodes
iR	ohmic drop
ISEs	ion selective electrodes
ISM	ion selective membrane
IT	ion transfer
ITIES	The interface between two immiscible electrolyte solutions
ITO	indium tin oxide
MD	molecular dynamics
MD	molecular dynamics
MVN	modified Verwey–Niessen
NPOE	nitrophenyloctylether
OHP	outer Helmholtz plan
PEDOT	poly(3,4-ethylenedioxythiophene)
PET	Polyethylene terephthalate
PGP-59	<i>N,N'</i> -(3,6-di-tert-butylcarbazole-1,8-diyl)bis(<i>N</i> -phenylthiourea
POT	poly(3-octylthiophene)
PU	polyurethane
PVC	polyvinylchloride
RE	reference electrodes
RE	reference electrode
RO	reverse osmosis
S.I	sulfate ionophore
SAMs	self-assembled monolayers
SC-ISEs	solid contact ion selective electrodes
SECM	scanning electrochemical microscopy
SHE	standard hydrogen electrode
SSM	separate solution method
T.Thio. bis	Tren thiourea bis
TIC	transfer by interfacial complexation
TID	transfer by interfacial dissociation
TOC	transfer to the organic phase followed by complexation

Abstract

Detection of anions is of considerable importance for their clinical and environmental applications. The focus of this thesis is investigation of electrochemical methods for sensing of sulfate ions. One of the main applications of sulfate sensing is in water recycling plants and using of sulfate as an indicator to assess the performance of reverse osmosis membranes which are used as a powerful barrier to remove contamination from wastewater. The basis of electrochemistry at the interface between two immiscible electrolyte solutions (ITIES) is the occurrence of ion transfer at the polarizable interface, which is formed between two solutions, one aqueous and the other organic, when they are brought into contact. This provides the possibility of anion detection. Amongst various anions, the anions with low hydration energy can be detected more easily because of their low hydrophilicity. However, detection of hydrophilic anions, which have greater hydration energy, is more challenging than for other anions. Among different inorganic anions, sulfate has the highest hydration energy and consequently is one of most challenging anions for detection.

For this purpose, different synthesized ionophores were evaluated to provide facilitated sulfate transfer at the ITIES as the basis for detection. However, before study of sulfate transfer at the ITIES, facilitated potassium transfer by dibenzo-8-crown-6, as a well-known process, was evaluated at two configurations of micro-ITIES arrays located at micropore arrays in glass membranes. These two configurations were the location of the ITIES at either the wider pore opening (laser entry side) or the narrower pore opening (laser exit side) at the conical micropores formed in the glass membranes by laser ablation. The highest sensitivity for potassium was achieved by the membrane with the micro-ITIES located at the laser entry side, and this membrane was chosen for sulfate detection studies at the ITIES. The results suggest for both ions that complexation and decomplexation are occurring at the interface. Based on the cyclic voltammetric profile achieved with different sulfate ionophores, Tren-bis CF_3 was chosen as the better ionophore because the transfer potential for sulfate anions in the presence of this ionophore is more positive than other ionophores. In addition to cyclic voltammetry, differential pulse voltammetry (DPV) was applied to enhance sensitivity of sulfate sensing and improve detection limit.

Facilitated ion transfer at the liquid-liquid interface can be replaced by a more robust method. Synthetic sulfate ionophores can be used in thin organic films on electrodes, referred to as solid contact electrodes, to provide more robust solid contact ion selective electrodes (SC-ISEs). In this method, the thin polymeric layer contains redox probes (as electroactive molecules) and plasticizers and was spin coated onto electrodes. The redox probes that were used in this study to sense sulfate and other anions were synthetic ruthenium complexes. A hydrophobic Ru-bipod complex (where bipod is the tridentate ligand 2,6-bis(1-(2-octyldodecyl)benzimidazol-2-yl)pyridine) was used as a

redox probe, polyvinylchloride (PVC) as the polymer and 2-nitrophenyloctylether was the plasticizer. The thickness of the thin film was estimated by the charge under CV peaks and was found to be 0.9 ± 0.3 μm . Different thin film membrane compositions were prepared and based on CV profiles, the best composition was chosen. The Ru complex in the thin film acts as an ion-to-electron transducer. The CVs show stable and Nernstian behavior in the presence of hexafluorophosphate, perchlorate and nitrate ions. However, the CVs were not stable and reversible in the presence of sulfate and chloride ions. Furthermore, the CVs related to the thin film with a commercial sulfate ionophore showed unstable responses, with different peaks being present. Although the thin film with Ru-bipod showed very stable response in the presence of more hydrophobic anions, because of the high redox potential of the complex in the presence of sulfate, promising electrochemical responses were not achieved.

To address the problems encountered with Ru-bipod-based thin films, two heteroleptic Ru complexes (Ru-(bipod)(dmdbb) includes two tridentate ligand 2,6-bis(1-(2-octyldodecyl)benzimidazol-2-yl)pyridine) (L_1N) and benzene (L_2C), and Ru-(bipod)(bipob) with four tridentate ligand 2,6-bis(1-(2-octyldodecyl)benzimidazol-2-yl)pyridine) (L_1N) with benzene (L_2C)) were evaluated as redox probes in the thin film to sense sulfate. Both complexes have the same core composition as Ru-bipod, but the difference is a cyclometalated bond. The thin films employing these new Ru complexes displayed stable electrochemical response in the presence of sulfate ions. The redox potentials of the new complexes were 0.7 V lower than that of Ru-bipod. This difference makes the thin films totally stable in the presence of sulfate ions. Voltammetric scan rate study suggested thin film behavior in the presence of Ru(bipod)(dmdbb) and Ru(bipod)(bipob). Potentiometric behavior was studied in the presence of sulfate ions and although plotting of mid-point potential versus logarithm of concentration of sulfate showed a linear response, there was deviation from a Nernstian slope (-20 mV/dec). A kinetic analysis study was carried out by application of Laviron's model, and it showed this deviation from Nernstian behavior can be related to the hydrophilic nature of sulfate ions. The semi-logarithmic range of sulfate response in the presence of both Ru complexes was between 10^{-4} M and 0.1 M. The detection limit for Ru(bipod)(bipob) and Ru(bipod)(dmdbb)-based thin film electrodes were 31 and 38 μM . To improve the selectivity and sensitivity of the thin films, commercial and synthetic sulfate ionophores were applied in the thin films. The mid-point potential versus logarithm of concentration of sulfate was not linear in the presence of the commercial sulfate ionophore. However, the plot in the presence of Tren thiourea bis CF3 (synthetic sulfate ionophore) was linear with logarithm of concentration in the range 5×10^{-6} to 0.1 M. The detection limit achieved with the membranes containing either Ru(bipod)(dmdbb) or Ru(bipod)(bipob) was 2.86 μM and 2.60 μM , respectively. A selectivity study was carried out with thin films without and with Tren thiourea bis CF3 ionophore.

Based on the selectivity coefficients, which were obtained by the separate solution method, better selectivity for sulfate over chloride was achieved in the presence of the ionophore, while in the absence of the ionophore the redox potentials of the Ru-bipod in the presence of sulfate and chloride are very close to each other. The selectivity coefficients for sulfate over nitrate were worse in the presence of the sulfate ionophore compared to the thin film without the ionophore.

One of the main issues for polymeric thin films on electrode surfaces formed by spin coating is using high concentrations of the redox probes for effective ion transfer process. This is a serious issue when an ionophore is used in thin film. By immobilization of the redox probe on the electrode surface, this issue can be addressed. A Janus Ru complex with hydrophilic phosphonate groups which can be chemisorbed on indium tin oxide (ITO) electrodes was evaluated in this study. By a voltammetric scan rate study, thin film behavior was shown, and the surface coverage of Ru complex was measured at 4.5×10^{-11} mol/cm². However, based on the CVs, the peak half-width potential was much higher than the theoretical value. Polymeric thin films were spin coated on the modified ITO electrodes. CVs obtained from the thin film coated modified electrodes in the presence of different anions suggest that the thin film is not selective with different anions. Potentiometric responses of the modified electrodes with and without thin films showed that although there is an improvement in potentiometric slope with thin film compared to the modified electrodes without thin films, still there is significant deviation from the Nernstian slope even in the presence of the more hydrophobic hexafluorophosphate anions.

The results presented within this thesis provide a basis for anion sensing by simple, portable, and rapid electrochemical methods based on voltammetry. Sulfate sensing was achieved by ion transfer at thin films on electrodes containing new Ru complexes as ion to electron transducers.

1. Introduction

1.1. Fundamental of electrochemistry

This chapter serves as a background to the thesis topic. Hence, it introduces key concepts that are directly relevant. The basic principles of electrochemistry at solid electrodes are introduced as these also enhance the comprehension of electrochemistry at liquid-liquid interfaces. The mechanism of electrochemical response at liquid-liquid interfaces is controlled by the transfer of charged species from one solution to another, which can be determined by Gibbs free energy. The mechanism can be classified into three types: ion transfer, facilitated ion transfer, and electron transfer, which enable label-free detection of ionized molecules. From an analytical standpoint, the thesis explores the benefits and significance of utilizing charged species transfer at liquid-liquid micro-interfaces and at solid contact electrodes. Accordingly, this chapter provides an in-depth overview of the pertinent research conducted at the interface between two immiscible electrolyte solutions (ITIES). Subsequently, the significance and scope of this study are discussed.

Chemical reactions in which there is charge transfer across interfaces between chemical phases like electrodes and electrolyte are defined as electrochemical processes.¹ This definition of electrochemistry is the basis of electroanalytical sensors. In this section, aspects of electrochemistry will be introduced which are important in discussion about charge transfer at the Interface between Two Immiscible Electrolyte Solutions (ITIES).

1.1.1. Electron transfer at electrodes

Electrochemistry happens when there is electron transfer between electronic conductors (or electrodes), like carbon, metallic electrodes or semi-conductors, and an ionic conductor (electrolyte) when they are in contact. In electrochemical systems, the transfer of electrons occurs when potential is imposed on electrodes and then current passes as a result of this charge transfer. Charge transfer in electrolyte solution is carried out by movement of ionic species. However, this transfer at the surface of electrodes involves oxidation and reduction phenomena. Oxidation process results from the loss of electrons from a chemical species on an electrode surface, while reduction is due to gain of electrons by the chemical species at the electrode surface. These processes are shown in equations 1.1.1 and 1.1.2 in which O and R are oxidised and reduced species, respectively.



The redox reaction on an electrode surface can be in equilibrium when thermodynamic and kinetic parameters are favourable. The reaction is governed by Faraday law and can be demonstrated by the

Nernst equation, which is the relationship of the concentrations of oxidised [O] and reduced [R] species with the equilibrium potential (E_{eq}) at the electrode surface ($x=0$) and at t time, as shown in equation 1.1.3:

$$E_{eq} = E^{\circ} + \frac{RT}{nF} \ln \frac{[O](0,t)}{[R](0,t)} \quad \text{Equation 1.1.3}$$

Where E° (V) is the formal potential of the redox couple, R is the universal gas constant ($8.314 \text{ JK}^{-1}\text{mol}^{-1}$), T (K) is the temperature, n is number of transferred electrons via the redox reaction, and F is the magnitude of the electric charge when one mole electrons is transferred at the electrode surface and also is known as the Faraday Constant ($96,485.4 \text{ C mol}^{-1}$).²

1.1.2. Faradic and non-Faradic processes

As mentioned above, the oxidation and reduction reactions of electroactive species at electrodes can be governed by Faraday's law and hence are known as Faradic processes. These reactions obey equation 1.1.4.

$$Q = nFN \quad \text{Equation 1.1.4}$$

Where Q (C) is the total charge due to the redox reaction at the electrodes, n is the number of electrons in each redox reaction which is transferred at the electrodes, F is the Faraday constant and N is the number of moles of electroactive species which undergo reaction. In addition to Faradic current which is a portion of the measured current, another type of current called non-faradic current is present which does not result from chemical reactions at the electrode-solution interface. Meanwhile non-Faradic currents can be due to adsorption or desorption processes which can cause accumulation of charge at the electrode-electrolyte interface. Non-Faradic current results from charging current (or background current) at electrodes and is caused by electrical double layer (which will be discussed later) in which the structure of the metal-solution interface can be affected by potential or solution composition.²⁻⁴

1.1.3. Polarizable and non-polarizable electrodes

Ideal polarised electrodes (IPE) are the electrodes at which there is no electron transfer even by imposing potential from outside sources. In reality, no electrodes can be total IPEs over an unlimited range of potential. The relation between current and potential for these kinds of electrodes is illustrated in **Figure 1.1.1 a**. On the other hand, ideally non-polarised electrodes present no difference in potential when current is passing at the electrodes. (**Figure 1.1.1 b**).

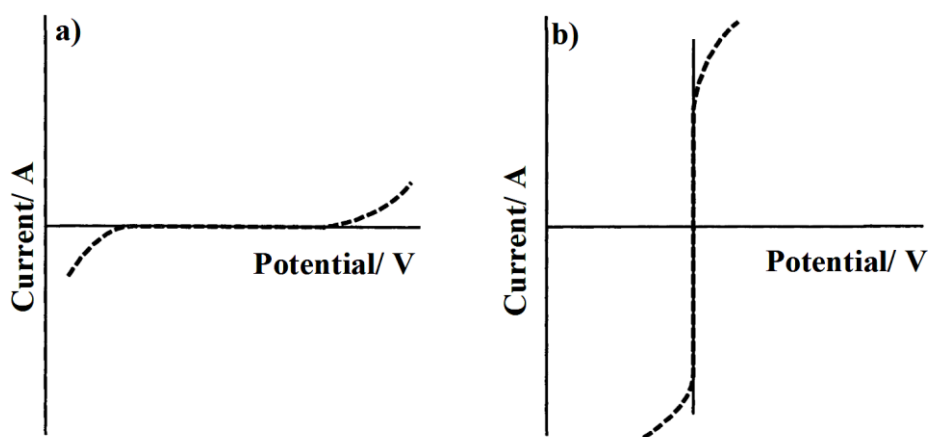


Figure 1.1.1 The current/potential curves for polarisable a) and non-polarisable b) electrodes. Dashed lines represent practical behaviour of electrodes while solid lines show ideal behaviour.

1.1.4. The electrical double layer

Since Faradic and non-faradic current simultaneously have contribution on measured current at electrodes, it is needed to distinguish non-Faradic current from Faradic current as much as possible. As mentioned earlier, charging current can be explained by the electrical double layer which was introduced by Helmholtz.⁵ The charging currents result from non-faradic processes at electrode-electrolyte interface. Electrical double layer is composed of electrical charge on electrode surface formed when potential is imposed on the electrode and the ions in solution which are in vicinity to the electrode surface and causes the charging current (non-faradic current). The interface of the electrode and solution mimics a capacitor (**Figure 1.1.2**).⁵ A capacitor is an electrical circuit component that is composed of two metal plates and once potential is imposed on these planes positive and negative charges assemble on them which can be defined as in equation 1.1.5:

$$C = \frac{Q}{E} \quad \text{Equation 1.1.5}$$

Where Q (C) is the stored charged on the capacitor, E (V) is the imposed potential and C (F) is the capacitance.

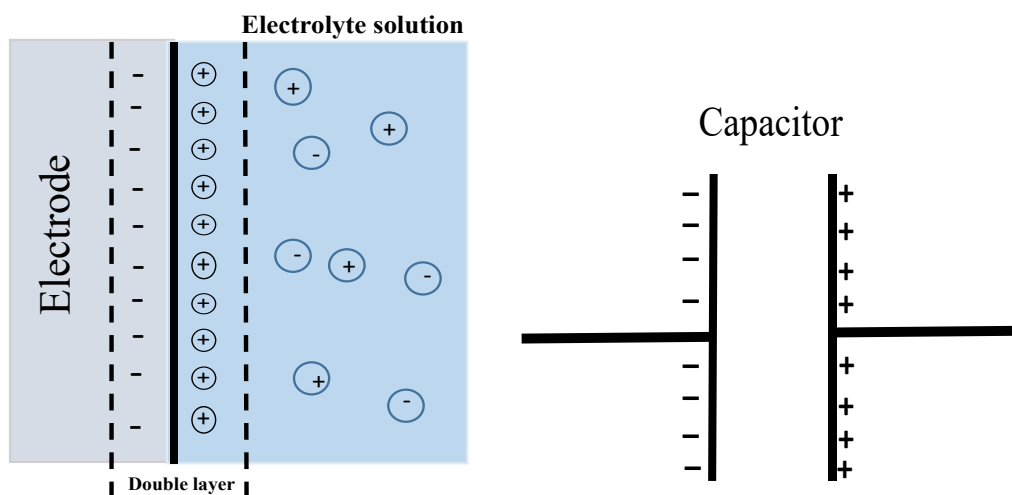


Figure 1.1.2 Electrical double layer of Helmholtz model (left) of the electrode and electrolyte solution interface and its similarity to a capacitor (right).

In addition to the Helmholtz theory about the electrical double layer, over the years this concept was modified by different explanations like the Gouy and Chapman theory.¹ Their theory explains that ionic charge in solvents cannot be confined on an electrode surface and the thickness of the double layer is dependent on the concentration of ions in solution and the imposed potential. The thickness of the double layer in solution with very low concentrations of ions is high, to compensate the charge on the electrode surface, so it needs to be extended in a diffuse layer, and the applied potential has an impact on the diffuse layer of ionic species at the surface of electrodes. Higher potentials can result in greater electrostatic forces at an electrode surface and then lower thickness in the diffuse layer. Since the ionic charges in solutions are not point-charges, so these theories seem to not be very realistic because the ionic species are not moving on the surface of the electrodes arbitrarily; because they have finite size and practically, they cannot approach on the surface of electrodes at lower than their diameter size. Thus, more modification of the Gouy Chapman model is needed which can define the approaches that occur at the vicinity of the electrode surface. Stern and Grahame modified these theories by defining two Helmholtz planes. The first plane (the inner Helmholtz plane or IHP) is composed of solvent and specifically adsorbed ions which are partially solvated (**Figure 1.1.3**) located at x_1 distance of electrode surface; the second plane (the outer Helmholtz plan or OHP) consists of solvated ions. The ions are surrounded by solvent molecules and are not closer than x_2 distance of the electrode surface.⁵

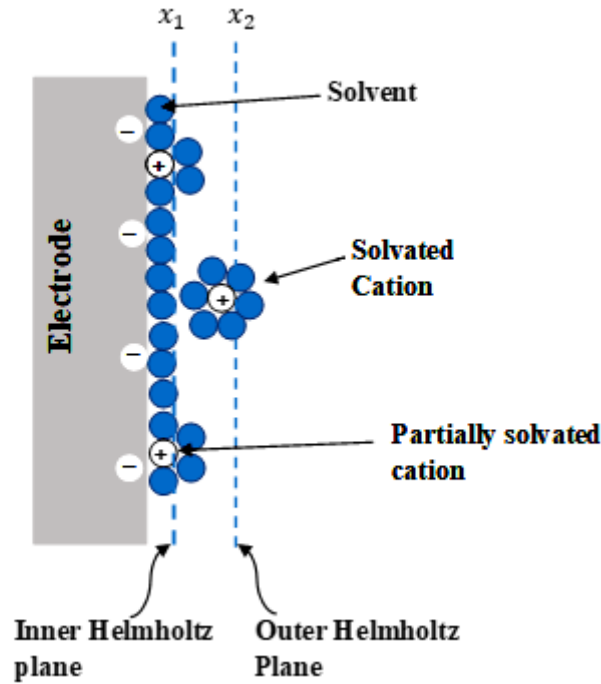


Figure 1.1.3 : The electrical double layer including the Inner Helmholtz Plane (IHP) and the Outer Helmholtz Plane (OHP).

1.1.5. Mass transport

When electroactive species are moving towards or away from the surface of electrodes, there is mass transport. Three approaches result in mass transport at the surface of electrodes: 1) diffusion, in which there is transport of ions based on concentration gradients, 2) migration, in which the movements occur because of an electric field, 3) convection, which results from mechanical forces such as differences in temperature or stirring. All three types of mass transport of species i as the flux J_i (mol $\text{cm}^{-2}\text{s}^{-1}$) are defined in the Nernst-Planck equation:

$$J_i(x) = -D_i \frac{\partial C_i(x)}{\partial x} - \frac{z_i F}{RT} D_i C_i \frac{\partial \phi(x)}{\partial x} + C_i v(x) \quad \text{Equation 1.1.6}$$

Where x (cm) is the distance of ionic species to the electrode surface, and D , C , z are the diffusion coefficient (cm^2s^{-1}), the concentration (mol cm^{-3}) and the charge of the ionic species, respectively. $\frac{\partial C_i(x)}{\partial x}$ and $\frac{\partial \phi(x)}{\partial x}$ represent the concentration and potential gradients along the x axis, respectively; then, $v(x)$ is the hydrodynamic velocity (cm s^{-1}). Three parts of the equation (from left to right) are showing diffusion, migration, and convection, respectively. The favourable part of this equation is the diffusion part. To make the diffusion part of this equation the major contributor, simply a large concentration of background electrolyte can be added to the experimental solution and the experiment can be carried out in stationary conditions and at stable temperature to minimise the migration and convection parts, respectively. Thus, an electrochemical reaction occurs at the surface of an electrode, a concentration gradient of (usually) analyte (i) can produce diffusional flux of ionic species (i). This

phenomenon is shown by Fick's first law (Equation 1.1.7) in which there is a direct relation between the fluxes with gradient of concentration at position x of the electrode surface and time t :

$$J_i(x, t) = -D_i \frac{\partial C_i(x, t)}{\partial x} \quad \text{Equation 1.1.7}$$

For aqueous environments, usually the diffusion coefficients of different ionic species are in the range from 10^{-6} to 10^{-5} (cm^2s^{-1}) and the value is dependent on the viscosity of the solvent, the temperature, and the molecular size of the species which diffuses through the solution. Also, the negative sign of the equation in Fick's first law shows the opposite tendency of species with the concentration gradient. Fick's second law, which is derived from the first law, shows the diffusional flux relation at time t (Equation 1.1.8):

$$\frac{\partial C_i(x, t)}{\partial t} = D_i \frac{\partial^2 C_i(x, t)}{\partial x^2} \quad \text{Equation 1.1.8}$$

On the other hand, current I , which has direct relation with the flux, can be defined as equation 1.1.9 below:

$$I = -nFA \frac{\partial C_i(x, t)}{\partial x} \quad \text{Equation 1.1.9}$$

$$I = nFAD_i \frac{\partial C_i(x, t)}{\partial x} \quad \text{Equation 1.1.10}$$

Where n is number of electrons transferred per molecule, A is electrode area (cm^2) and F is Faraday constant. If migration and convection parts of the Nernst-Planck equation are suppressed by the methods which were mentioned earlier, equation 1.1.10 can be obtained from combination of equations 1.1.7 and 1.1.9:

This equation 1.1.10 is one of the most important equations in electrochemistry because it shows the relationship between the evolution of the concentration profile in the vicinity of the electrode and the current flow from the electrochemical instrument.¹

1.2. Electrochemistry at the Interface between Two Immiscible Electrolyte Solutions

1.2.1. Background

The interface between two immiscible electrolyte solutions (ITIES) is formed when two electrolyte solutions with nearly zero mutual miscibility are in contact with each other. One of the solutions is aqueous phase with hydrophilic ions (e.g. LiCl) as an electrolyte and the other is a polar organic solvent with moderate to high dielectric constant to dissociate (or partially dissociate) the hydrophobic electrolyte (e.g. bis(triphenylphosphoranylidene)ammonium tetrakis(4-chlorophenyl)borate, BTPPATPBCl).⁶⁻⁸ By imposing a potential across the ITIES one ion is

transferring from one phase to the other phase across the ITIES, electrochemically this interface is considered as a polarisable interface. Although the key strength of the ITIES in electroanalytical chemistry is the ability to sense non-redox active species at electrode surfaces,⁷ redox reactions can happen at the interface as well, but it is not as common as ion transfer at the interface.⁹ In addition to sensing of non-redoxactive species, several advantages contribute to the great interest of the ITIES. First, the ITIES can mimic half of a biological cell membrane in which phospholipids have two sides, one hydrophobic and one hydrophilic.^{6, 10, 11} This characteristic of the ITIES can be applied to sense different biomolecules.^{7, 12} Also, the ITIES can be used in electroanalysis, ion extraction and electrocatalysis or phase transfer catalysis.⁶ In addition, although the ITIES was originally conducted as macro (e.g. millimetre or centimetre) structures,^{13, 14} but it can be easily compatible with miniaturised ones¹⁵⁻²⁰ (e.g. micro and nano scales) to provide more sensitive and portable electrochemical sensing methods, which will be discussed later in the miniaturisation of the ITIES section.

For the first time, the concept of the ITIES was introduced by Nernst's and Riesenfeld's experiment in which the coloured species were transferred across a water-phenol interface.²¹ After that for decades this method was used to distribute salts across interfaces between two immiscible phases.⁵ ²¹ In continue, to apply ITIES in transfer reactions, for the first time Gavach utilized a galvanic potential at the ITIES to make the interface polarised. Consequently, the difference in potential at the interface can be a driving force of ion transfer reactions.²² For macro-ITIES, always high iR (i is current and R is resistance) drop is problematic for study of different aspects of charge transfer at interfaces. Thus for the first time, Samec and his group used a four electrodes cell to compensate resistance at interfaces to study kinetic charge transfer at the ITIES.²³ By these modifications in the ITIES over the time which were mentioned earlier and more than them, several applications of ITIES have been opened until now. For example, using dynamic electrochemistry methods like voltammetry and amperometry to sense different ions,²⁴⁻²⁶ including a wide range of inorganic ions²⁷⁻³⁰ and biological species like different proteins.^{31, 32}

1.2.2. Basic theoretical relationships at the ITIES

Generally, as mentioned above, at the ITIES, there are different types of charge-transfer processes including electron transfer, ion transfer or coupled electron-ion transfer. This PhD thesis is focused on ion transfer, therefore all theoretical relationships in this section are focusing on ion transfer processes. When two liquid phases with their background electrolytes are in contact with each other, an interface called the ITIES is formed. Then charged species of the electrically conducting liquids partition between the two phases because of a difference of the Galvani potentials ($\Delta_G^w \phi$) of the two

sides of the interface, ϕ^w and ϕ^o which are the Galvani potential at the aqueous phase and the Galvani potential at the organic phase, respectively.^{6,33} The equilibrium Galvani potential difference is shown in equation 1.2.1:

$$\Delta_o^w \phi = \phi^w - \phi^o \quad \text{Equation 1.2.1}$$

If the electrochemical potentials of the ion i in the two phases are equal and at same constant temperature and pressure, the condition of ion transfer equilibrium is in place, as shown in 1.2.2 equation:

$$\bar{\mu}_i^w = \bar{\mu}_i^o \quad \text{Equation 1.2.2}$$

The electrochemical potential ($\bar{\mu}_i^a$), the potential needed to transfer a species, i , from vacuum phase to a liquid phase, is demonstrated in equation 1.2.3:

$$\bar{\mu}_i^a = \mu_i^a + z_i F \phi^a \quad \text{Equation 1.2.3}$$

Where μ_i^a and $z_i F \phi^a$ are chemical and electrical contributions, respectively. In this equation, if the electrical part is considered as zero ($z=0$) in solution, so the electrochemical potential (μ_i^a) can be illustrated just with the chemical potential which is shown in equation 1.2.4:

$$\mu_i^a = \mu_i^{0,a} + RT \ln a_i^a \quad \text{Equation 1.2.4}$$

In the equation 1.2.4, a_i^a is the activity of i species and can be defined in 1.2.5 equation:

$$a_i^a = \gamma_i^a C_i^a \quad \text{Equation 1.2.5}$$

Where, γ_i and C_i are the activity coefficient and concentration of ion i , respectively.

Then equation 1.2.3 can be rewritten as equation 1.2.6:

$$\bar{\mu}_i^a = \mu_i^{0,a} + RT \ln a_i^a + z_i F \phi^a \quad \text{Equation 1.2.6}$$

In thermodynamic equilibrium (equation 1.2.2), the electrochemical potential of species i in the two phases are equal, which is shown in equation 1.2.7:

$$\mu_i^{w,0} + RT \ln a_i^w + z_i F \phi^w = \mu_i^{o,0} + RT \ln a_i^o + z_i F \phi^o \quad \text{Equation 1.2.7}$$

From rearrangement of equation 1.2.7, the Galvani potential difference will be achieved (equation 1.2.8):

$$\Delta_o^w \phi = \phi^w - \phi^o = \frac{\mu_i^{o,0} - \mu_i^{w,0}}{z_i F} + \frac{RT}{z_i F} \ln \left(\frac{a_i^o}{a_i^w} \right) \quad \text{Equation 1.2.8}$$

In addition, the standard molar Gibbs energy of ion transfer from water to organic phase ($\Delta G_{Transfer,i}^{0,W \rightarrow O}$) can be defined by the difference of standard Gibbs energy of solvation of the ion in water and in

organic phases. As a result, there is a relation between $\Delta G_{Transfer,i}^{0,W \rightarrow O}$ and the standard Galvani potential ($\Delta_o^w \phi_i^0$) of species i given by equation 1.2.9:

$$\Delta_o^w \phi_i^0 = \frac{\Delta G_{Transfer,i}^{0,W \rightarrow O}}{z_i F} = \frac{\mu_i^{o,0} - \mu_i^{w,0}}{z_i F} \quad \text{Equation 1.2.9}$$

Finally, Nernst equation at the ITIES for transfer of ion species i at the water/organic interface can be achieved by combination of equation 1.2.8 and 1.2.9:

$$\Delta_o^w \phi = \phi^w - \phi^o = \Delta_o^w \phi_i^0 + \frac{RT}{z_i F} \ln \left(\frac{a_i^o}{a_i^w} \right) \quad \text{Equation 1.2.10}$$

The Nernst equation at the ITIES tells us that, when an external energy source is applied, the standard ion transfer potential term $\Delta_o^w \phi_i^0$ remains constant while the ratio of $\frac{a_i^o}{a_i^w}$ changes in response to the external energy source. Changing of ion activities in both phases results from movement of ions across the interface to make equilibrium circumstance at the interface. These movements across the interface can be translated to an electrochemical current at the interface. According to all of these occurrences due to applied potential via an external energy source, the achieved current can be a function of the potential.

On the other hand, the Nernst equation at the ITIES (equation 1.2.10) with concentration of ionic species instead of their activity is obtained by using equation 1.2.5 in the Nernst equation (1.2.10) and rewrite it as:

$$\Delta_o^w \phi = \Delta_o^w \phi_i^0 + \frac{RT}{z_i F} \ln \left(\frac{\gamma_i^o C_i^o}{\gamma_i^w C_i^w} \right) \quad \text{Equation 1.2.11}$$

By introducing the formal Galvani potential ($\Delta_o^w \phi_i^{0'}$):

$$\Delta_o^w \phi_i^{0'} = \Delta_o^w \phi_i^0 + \frac{RT}{z_i F} \ln \left(\frac{\gamma_i^o}{\gamma_i^w} \right) \quad \text{Equation 1.2.12}$$

and by rearrangement of equation 1.2.11, and combination with equation 1.2.12, finally the following form of the Nernst equation at the ITIES based on the concentration of ion species in both water and organic phases is achieved:

$$\Delta_o^w \phi = \Delta_o^w \phi_i^{0'} + \frac{RT}{z_i F} \ln \left(\frac{C_i^o}{C_i^w} \right) \quad \text{Equation 1.2.13}$$

1.2.3. The interface structure of the ITIES

From surface tension measurements at the ITIES, the so-called modified Verwey–Niessen (MVN) model introduced the structure of the interface, which was two back-to-back diffuse layers, with one of the layers containing excess positive charges and the other one excess negative charge. These two

layers are separated by oriented separate solvent molecules³⁴⁻³⁷. However, the MVN model is mainly limited to water/nitrobenzene interface and limited organic background electrolytes, which are typically tetraalkylammonium tetraphenylborate salts. These conditions cause the experimental potential window for these systems to be very narrow. Thus the validity of the MVN model cannot be investigated with different organic solvents and organic salts.³⁸ After Verwey–Niessen, Gavach et. al. proposed the hypothesis of the two compact non-ionic inner layers which are surrounded by ions in diffuse layers which can make two diffuse double layers, one in each phase, separated from each other.³⁴ In continuation of the MVN theory modification, Girault and Schiffrin suggested that the inner layer is a mixed solvent layer (**Figure 1.2.1**), and the composition of this layer is changing, constantly.³⁹

Electrolyte composition and concentration in the aqueous phase has an impact on the surface tension of the non-polarised ITIES.³⁸ The ions which are present in the interface have impact on both physical properties and stability of the ITIES. According to computer simulations and experimental results, the capacitance of the ITIES depends on overlap of aqueous and organic ionic layers at the interface.³⁸ In addition, Schmickler's research shows the solubility of the two solvents can have an impact on the mixed solvent layer.⁴⁰ Nonlinear optical spectroscopy results suggested that the aqueous and organic molecules have special orientation. This orientation can cause different dielectric constant of the mixed solvents at the interface.³⁸ Therefore, in addition to electrolytes in two phases at the ITIES, the solvents can have an impact on the potential profile of the interface. Ion transfer at the ITIES based on potential-current dependency are explained by two mechanisms. Some authors suggest that ion transfer through the ITIES is due to electrochemical reaction while others suggest that ion transfer at the ITIES is a mass transport phenomenon.³⁸ The presence of other ions at the ITIES can be problematic to study ion transfer mechanism at the ITIES. However, ion transfer can be studied at the nano-ITIES without background electrolytes. Some experiments at the nano-ITIES showed that the alkali metal ions 'shuttle' from aqueous to organic phase. On the other hand, the results from same method showed that very hydrophilic ion transfer cannot happen at the ITIES while transfer of aqueous clusters into the organic phase can be occur. Moreover, very recent simulations did not show the shuttle mechanism of ion transfer at the ITIES while the results showed water fingers into the organic phase. However, until now both mechanisms have been proved by different experiments and different ions.³⁸

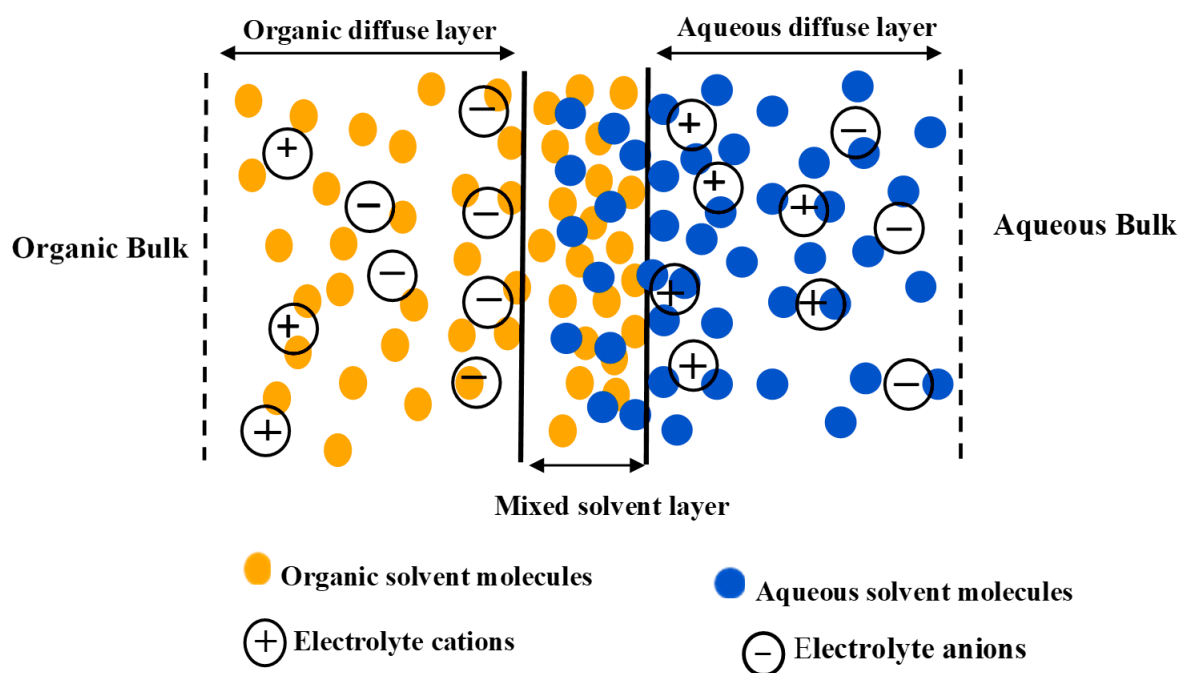


Figure 1.2.1 Schematic of mixed solvent layer which is similar with electrical double layer at ITIES.

In recent years, modern experimental approaches such as X-ray reflectivity and neutron reflection methods have been applied to probe the structure of the ITIES. For example, the interfacial thickness and characteristics of water/alkane interfaces was measured by synchrotron X-ray reflectivity, based on the electron density at the interface^{41,42}. The experimental data are in concordance to theoretical simulation results carried out by a molecular dynamics (MD) method in which estimation of ion distribution was carried out.⁴³ An interfacial thickness between water/alkane, which was examined by x-ray reflectivity, was 3.5-6 Å,⁴¹ while the interfacial thickness between water/dichloroethane was 10 Å via neutron reflection and scanning electrochemical microscopy (SECM) methods.⁴⁴ To comprehend all these achievements about the interfacial structure of the ITIES, ion-ion and ion-solvent correlations should be considered at nanoscales, because they have an impact on the thickness and structure of the interface.

1.2.4. Polarizable and non-polarizable ITIES

In the same way as described for solid electrodes and liquid electrolytes (as mentioned earlier), polarizability and non-polarizability can be defined at the ITIES depending on if there is a relation between the potential difference between the two phases ($\Delta_o^w \phi$) and the concentrations of ions.⁶ Polarization at the ITIES is an ionic approach in which, by imposing an external Galvani potential difference, two back-to-back Gouy-Chapman diffuse layers are present, one with excess positive charge and the other one has excess negative charges.⁴⁵ The polarisable interface acts as a working

electrode where the processes of interest are occurring. Based on the electrolytes in the two phases, polarizability of the interface can be determined.

The Ideal polarizable interface is an interface in which the electrolytes in both phases have infinite Gibbs transfer energies. However, practically all ions have finite Gibbs transfer energies to different phases. In this regard, to make the interface to be polarised, the choice of electrolytes for each phase is important - very hydrophilic electrolytes (A^+ , B^-) for water phase (e.g. LiCl, HCl, $MgCl_2$ and $MgSO_4$) and very lipophilic electrolytes (C^+ , D^-) for the organic phase (e.g. tetrabutylammonium, tetraphenylarsonium, or bis(triphenylphosphoranylidene)ammonium cations with tetraphenylborate, tetrakis(4-chlorophenyl)borate or tetrakis[3, 5-bis(trifluoromethyl)phenyl]borate anions) (**Figure 1.2.2**). However, choosing background electrolytes in aqueous phase and organic phase depends on the interest range of potential window for the experiment, which will be discussed later.

The non-polarised ITIES can be defined in two categories. One is where the electrolyte (A^+ , B^-) in the aqueous phase and the organic phase is common (by assuming the charge for all anions and cations is unit). In this case, the Nernst equation at the ITIES (equation 1.2.10) can be written separately for anion and cation:

$$\Delta_o^w \phi = \Delta_o^w \phi_{A^+}^0 + \frac{RT}{z_i F} \ln \left(\frac{a_{A^+}^o}{a_{A^+}^w} \right) \quad \text{Equation 1.2.14}$$

$$\Delta_o^w \phi = \Delta_o^w \phi_{B^-}^0 + \frac{RT}{z_i F} \ln \left(\frac{a_{B^-}^o}{a_{B^-}^w} \right) \quad \text{Equation 1.2.15}$$

Since solubilities of the ions are different in the two solvents, the potential distribution across the interface can be affected by activity coefficients instead of concentrations of ions. Then, the Nernst equation can be rewritten as equation 1.2.16:

$$\Delta_o^w \phi = \frac{\Delta_o^w \phi_{A^+}^0 + \Delta_o^w \phi_{B^-}^0}{2} + \frac{RT}{2F} \ln \left(\frac{\gamma_{A^+}^o \gamma_{B^-}^o}{\gamma_{A^+}^w \gamma_{B^-}^w} \right) \quad \text{Equation 1.2.16}$$

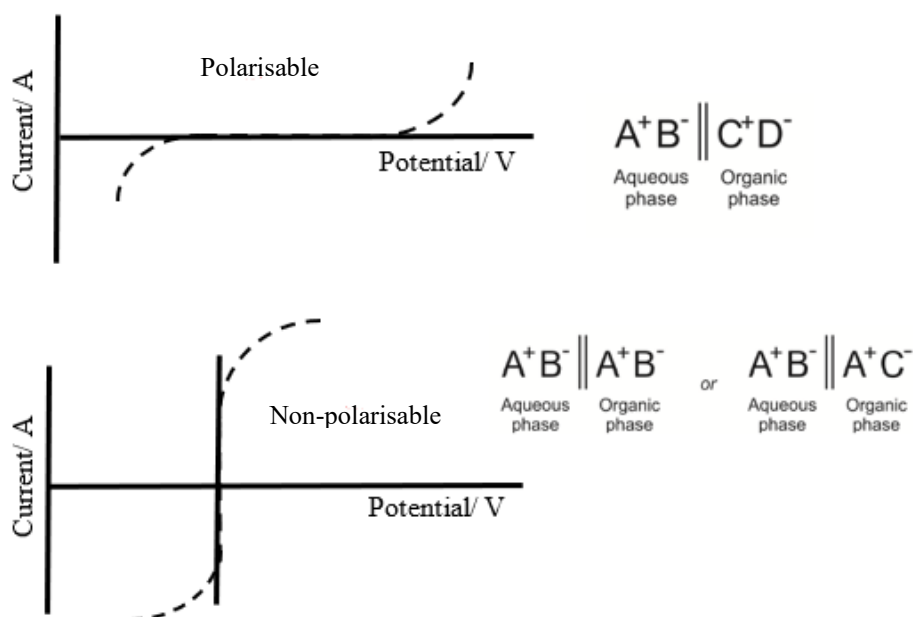


Figure 1.2.2 Polarisable and non-polarisable set up at the ITIES. At the polarisable interface, A^+ and B^- are very hydrophilic while C^+ and D^- are very hydrophobic. At the non-polarisable interface, (left) A^+ and B^- are common ions in both phases, and (right) A^+ is a common ion in two phases and B^- is very hydrophilic and C^- is very hydrophobic.

The second form of the non-polarised ITIES is when there is just one common ion (for example A^+), and other counter ions (like B^- and C^-) are sufficiently hydrophilic and hydrophobic to remain in the aqueous and organic phases, respectively. Consequently, the potential distribution of the common ion can be written as equation 1.2.17:

$$\Delta_o^w \phi = \Delta_o^w \phi_{A^+}^0 + \frac{RT}{F} \ln \left(\frac{a_{A^+}^o}{a_{A^+}^w} \right) \quad \text{Equation 1.2.17}$$

1.2.5. Potential window at the ITIES

Generally, the potential window at the ITIES is the range of potential in which there is not transferring any ions across the interface; obviously the ion transfer current in this range should be zero or nearly zero. As mentioned above, if this potential window is wider, there are more possibilities to detect a wider range of ions at the ITIES by voltammetric methods. To make this window wider, it is required to have a more hydrophilic pair of ions in the aqueous phase and a more lipophilic pair of ions in the organic phase. In cyclic voltammetry, typically, the imposed external potential is starting from low positive potential in forward scan and then comes back to starting potential in backward scan, and positive currents are present in forward scans (positive potential) while negative ones are generally present with backward scans (negative potentials). At the polarised ITIES, by imposing a positive

potential for forward scans, cations are transferring from aqueous phase to organic phase or anions from organic phase to aqueous phase, while for backward scan all these transfers are reversed. On the other hand, by imposing less positive potential (or negative potential) in which the current is negative, there is transfer of cations from organic phase to aqueous phase and anions from aqueous phase to organic phase.⁴⁶ All these trends are shown in **Figure 1.2.3** Between these two positive and negative potential limits, there is a region within which transfers of analytes occur and this is considered as a desired potential window.

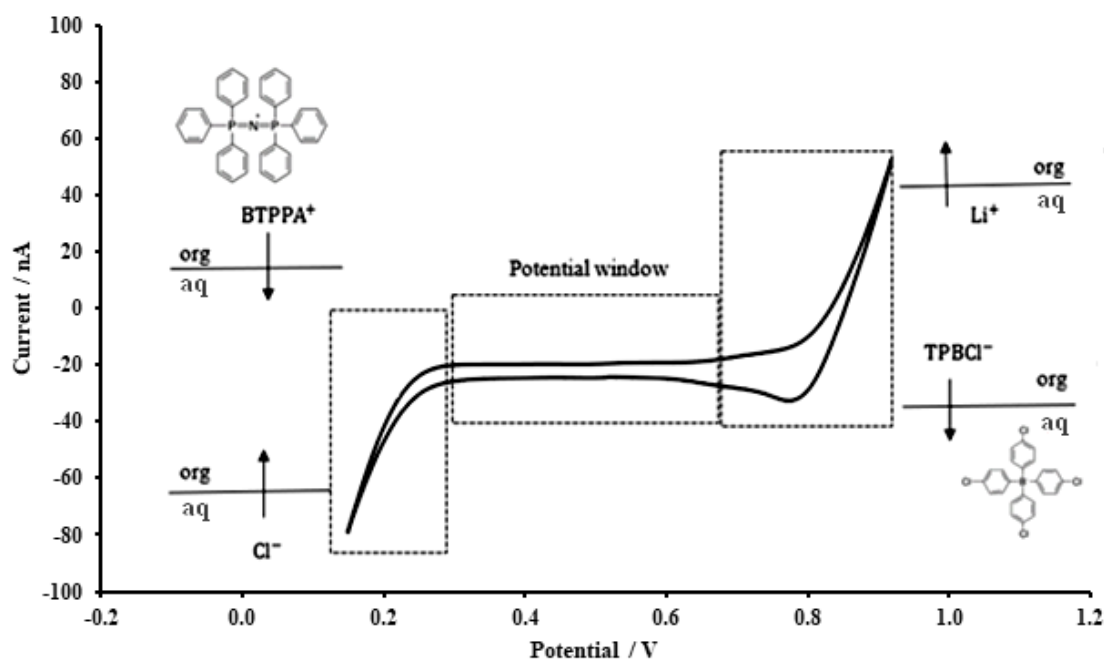


Figure 1.2.3 Cyclic voltammogram of 10 mM LiCl in aqueous phase and 10 mM BTPPATPBCl in organic phase (1,6-dichlorohexane). Scan rate: 10 mV/s.

In the example CV (**Figure 1.2.3**), the range of applied potential is between 0.05 to 1.0 V; as shown in the figure, it can be divided to three parts. The first part is at more positive potential (between 0.8-1.0 V) in which, in the forward scan, Li⁺ and TPBCl⁻ are transferring from aqueous to organic and organic to aqueous phase, respectively. For the reverse scan, these transfers are reversed. In the second region (which is in the range 0.8-0.2 V), there is no transferring of background electrolyte ions between the two phases, and this is called the potential window region or polarisation region. This part is the ideal section to detect analyte signals. Finally in the third region (between 0.2-0.05 V), in the forward scan, there is transfer of Cl⁻ and BTPPA⁺ from aqueous phase to organic and organic to aqueous phase, respectively, in the backward scan, these are reversed.

1.2.6. Forms of charge transfer at the ITIES

There are three types of charge transfer at the ITIES. First one is simple ion transfer (IT) which is transfer of ions by imposing an external potential. The potential should overcome the Gibbs transfer energy of the ions between two phases. The transfer potential of ions which are in the potential window region can be related to different concentrations of the ions by Nernst equation.⁶ Another charge transfer at the ITIES is facilitated ion transfer (FIT)¹⁴ in which by using an ionophore or ligand in the other phases (can be organic or aqueous phase), and complexation of the ions with the ionophore, the Gibbs transfer energy of the complexed form of ions are lower than the Gibbs transfer of non-complexed ions and it is within the potential window range. This type of charge transfer will be discussed later.

Third type of charge transfer at the ITIES is electron transfer (ET) which occurs between redox active species in each phase, as illustrated in equation 1.2.19:



The Nernst equation related to this kind of charge transfer at the ITIES can be defined as equation 1.2.20:

$$\Delta_o^w \phi = \Delta_o^w \phi_{ET}^0 + \frac{RT}{F} \ln \left(\frac{a_{R_1}^w a_{O_2}^o}{a_{O_1}^w a_{R_2}^o} \right) \quad \text{Equation 1.2.20}$$

Electron transfer at the ITIES is complex, because of the need to choose the redox species which are compatible with the potential window in addition to all of redox products should not transfer across the ITIES, because the current related to their transfer has a masking effect with the current related to electron transfer.⁴⁷

1.3. Macro-ITIES

1.3.1. Electrochemical set up of the ITIES

Samec was the first to introduce the four-electrode electrochemical cell for the ITIES²³, which includes two reference and two counter electrodes, as shown in **Figure 1.3.1**.

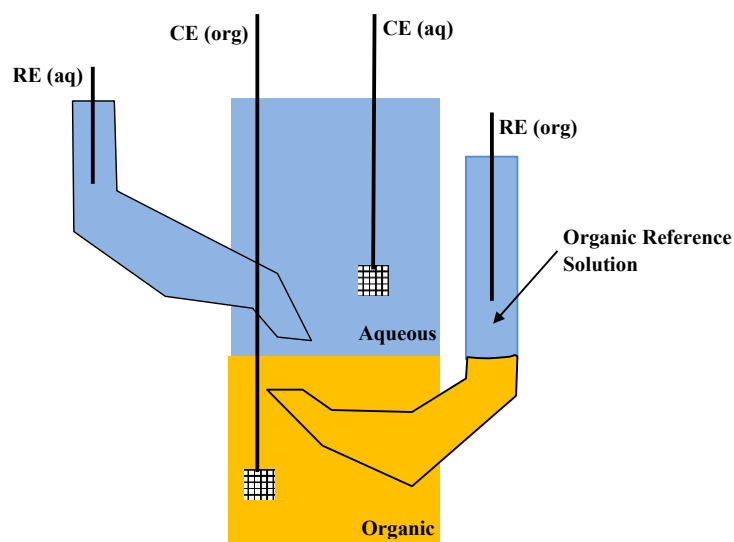


Figure 1.3.1 Electrochemical cell showing the typical four electrodes set up at ITIES, which includes two counter electrodes (CE) and two reference electrodes (RE), one of each in aqueous and organic phases.

Usually, the counter electrodes are platinum mesh and one of them is inserted in the organic phase, and reference electrodes are silver/silver chloride. Usually this set up is applied for macro-ITIES in which the size of the interface between the organic and aqueous phases is between millimetre squared and centimetre squared, and a four electrode cell is used because of the high resistance in this scale. In this thesis, a two electrode set up is used because the size of the interface is around micrometre squared and ohmic drop is much lower than at macro-scale ITIES (**Figure 1.3.1**).

1.4. Micro-ITIES

1.4.1. Miniaturisation of the ITIES

Since, as mentioned before, the ITIES is considered as a working electrode. The improvement of solid electrodes to ultra-micro or nanoelectrodes, therefore, miniaturisation of the interface between two immiscible electrolyte solutions can give several advantages. These advantages are due to lower current values with miniaturised ITIES, and then resulting in lower iR or ohmic drop at these interfaces. Resistance at the ITIES mostly is related to the organic phase.⁵ Based on Ohm's law, when there is a potential between the working electrode and reference electrode, a voltage drop is present which is shown by the equation 1.4.1.

$$i = \frac{V}{R} \quad \text{Equation 1.4.1}$$

Where, i is the current which flows between two points and is proportioned to potential difference V of these two points and the resistance R . Resistance in the ITIES cell is related to the resistance of solution (R_s) and it is considered that the resistance in aqueous solutions is negligible compared to that of the organic phase with low permittivity values. Thus, by miniaturisation of the ITIES, R_s will

be reduced and then the voltage drop (iR_s) is also reduced, so just two electrode cell set up can be applied for the miniaturised ITIES⁵. This capability of ITIES electrochemical set up (just two electrodes) also can provide a wide range of advantages such as more portability, lower cost and higher possibility to combine with other techniques.^{48, 49}

The first report of miniaturised ITIES was by Taylor and Girault, who reported the ITIES at micrometre size (25 μm) supported by a glass pipette. The cell set up is u-tube shape where organic phase solution is between the working aqueous solution and the reference aqueous solution.¹⁵ Micro-ITIES was obtained by micropipette with borosilicate glass or quartz to provide hydrophilic properties inside of the micropipette to keep aqueous phase⁵⁰ and by silanization of the glass pipette tips, hydrophobic properties were obtained.⁵¹ Eventually the research ventured into nanometre size. Nano-ITIES by glass pipette were provided.⁵² Despite addressing the ohmic drop issue by micro- and nanoscale ITIES, still low current values were there. This issue directed the ITIES to micro- and nano-ITIES arrays. There are several fabrication techniques to provide miniaturised ITIES which have been developed in the last decades, such as using electron-beam lithography combined with chemical etching techniques on silicon materials to achieve microscale and on silicon nitride to achieve nanoporous membranes.^{53, 54} Another common technique used to obtain single nano- or micro-ITIES interface was CO_2 -laser pipette pullers to develop nano- or micro-sized glass pipettes.^{55, 56} Also laser micromachining was applied to make single micrometre size holes on different polymeric substrates like polyester,⁵⁷ polyimide⁵⁸ and polyvinylchloride films.⁵⁹ Although single holes or micropipettes can overcome iR_s drop, they have been faced with an important issue, which is low current, and which can be problematic with some applications. To address this issue, microarray format has been developed. UV excimer laser was applied to ablate 66 micro-hole arrays on Polyethylene terephthalate PET substrate.⁶⁰ In continues, glass membrane with microscale holes was achieved by laser ablation method.⁶¹ Arrays of 100 micropores were achieved in 130 μm thick borosilicate glass and the glass was functionalised with trichloro(1H,1H,2H,2H-perfluorooctyl) silane on one side to provide a hydrophobic side to make it suitable for the organic phase of the ITIES. Depending on laser exit side and entry side, the pore diameters have different dimensions and conical pores are formed.⁶¹

Finally, miniaturisation of the ITIES has been reached to arrays of nano-ITIES. Arrays of nanopores have been fabricated on Si_3N_4 by focused ion beam (FIB) milling to obtain radii between 30-80 nm which were used to support formation of nano-ITIES arrays.^{62, 63}

1.4.2. Different arrangements of the ITIES and their effect on electrochemical signal

Different geometries and arrangements of solid-liquid electrochemistry have significant impacts on the electrochemical signal. For example, the diffusion-controlled current resulting from different

electrodes such as recessed disc, inlaid disc, and hemispherical electrode shapes^{64,65} follow different formulations, which are shown in **Figure 1.4.1**.

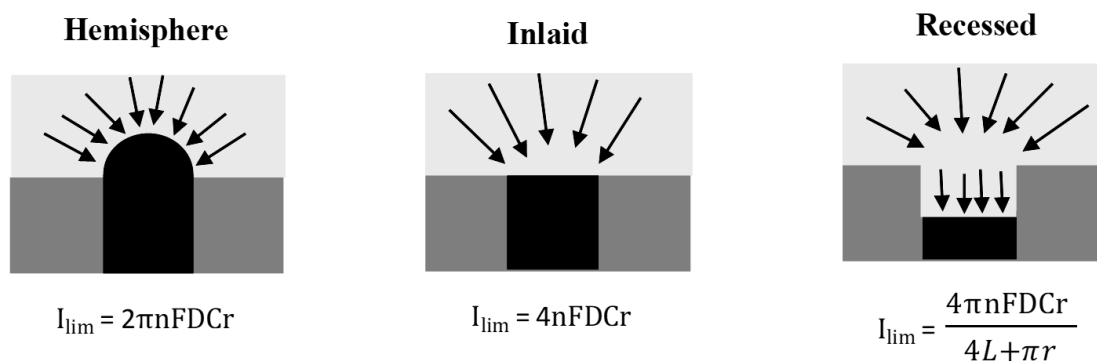


Figure 1.4.1 Three different electrode geometries and their diffusion modes. For each electrode geometry, there is a limiting current (I_{lim}) equation which describes their different dependencies. In the equations, n is number of electrons transferred, F is the Faraday constant, C is the concentration, r is the electrode radius and L is the recessed depth.

In the same way, the geometric features of soft interfaces, like the liquid-liquid interface (the ITIES), which is considered as the working electrode, has an impact on the generated electrochemical signal as well. The formulations in **Figure 1.4.1** can be used for the ITIES just by replacing n by the charge number of ions (z) which are transferred at the interface. As shown in **Figure 1.4.2** for the case of a single microscale ITIES formed at the mouth of a micropore, when ions are moving from the aqueous phase to the organic phase, there is radial diffusion, while when they are moving from the organic to the aqueous phase, there diffusion is linear diffusion.

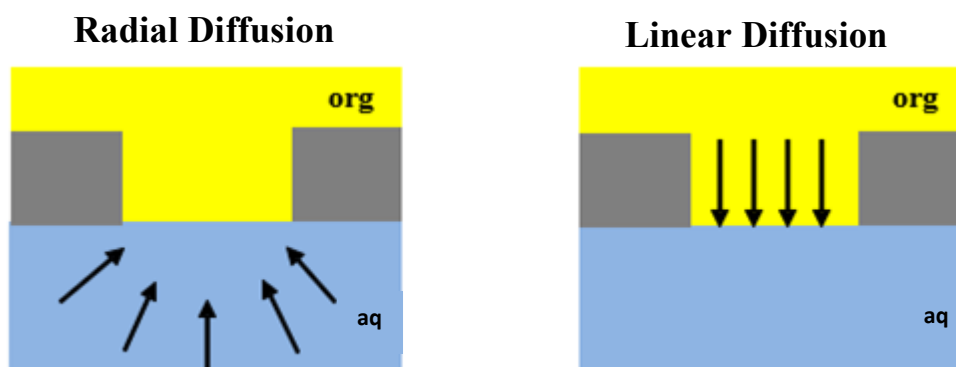


Figure 1.4.2 Diagram representing single micro interface formed at the mouth of a micropore. There are two diffusion modes: radial diffusion of ion in aqueous phase (left) and linear diffusion of ions from organic phase to aqueous phase (right).

When the imposed potential in an array of micro-ITIES formed at an array of micropores is similar, the electrochemical signal is depending on the dimensions of each pore in the array and the density of the pores. For example, if the pores in the array are very close to each other, diffusion to each pore can have a competition effect on another adjacent pore, and this effect can result in a decrease in the electrochemical signal at each individual micro-ITIES. The distance between pores in such arrays was studied with different arrangement of arrays such as a cubic, hexagonal, and random arrangement, based on both theoretical and experimental aspects.^{66, 67} In addition to the density of pores, pore to pore centre distance, pore dimensions including radius and depth, experimental time scale and diffusion coefficient of each analyte are key factors in the electrochemical signal.⁶⁸ In **Figure 1.4.3**, it is shown cubic and hexagonal arrangements for micro disc arrays.

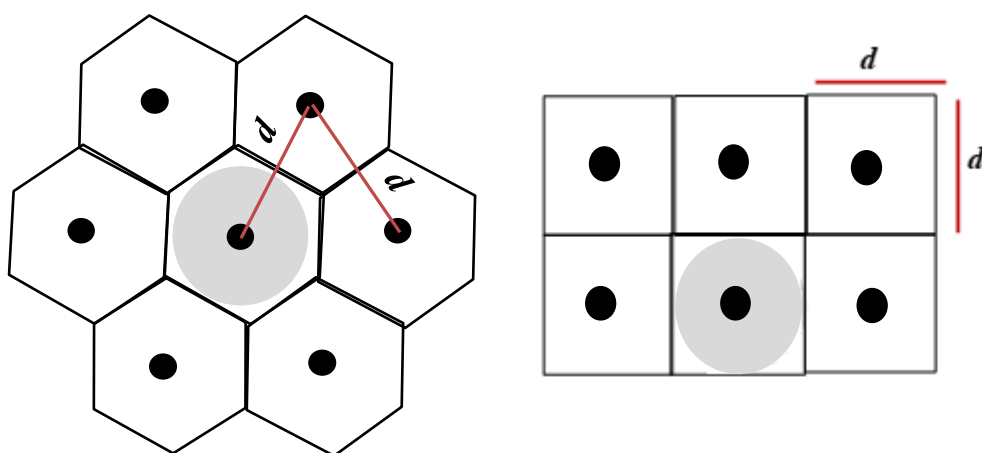


Figure 1.4.3 Illustration of hexagonal (left) and cubic (right) arrangement of micro disc arrays. d is the distance between two pores and grey part shows the diffusion zone that forms around each micro-ITIES.

To achieve the best arrangement in which each pore can act independently from other pores so as to obtain the optimum electrochemical signal, it is important to have enough distance between the pores. To study the optimal centre to centre distance between pores on a micro disc array, there are two assumptions, that a steady state response is achieved, and this response is independent of sweep rates. Based on these conditions, to obtain the optimum signal, the centre to centre distance (d) should be more than 12 times the pore radius (r).⁶⁹ Another research modified this proportion and suggested that the d value should be higher or equal to 20 times the pore radius,⁷⁰ as shown in equation 1.4.2:

$$d \geq 20r \quad \text{Equation 1.4.2}$$

Further modification occurred to estimate the diffusion zone thickness δ which is shown in Equation 1.4.3⁷¹:

$$\delta > \sqrt{2D_i \frac{\Delta(\Delta_{\beta}^a \phi)}{v}} \quad \text{Equation 1.4.3}$$

D is the diffusion coefficient of species i , v is the scan rate and $\Delta(\Delta_{\beta}^a \phi)$ represents the potential range from where the faradaic current is started to the steady state current or peak current. This equation suggests that, against the previous studies, the diffusion zone is independent of the radius of pores, but it is related to the time, which comes from the scan rate. This equation is driven from the assumption that the diffusion is one dimensional.⁶⁷

If the diffusion zone is more than half of the pore-to-pore centre distance (or $\delta < 0.5d$ the micro array will experience nonlinear diffusion. In this case, the whole electrochemical signal is determined by multiplying the number of pores in arrays by the current for one single pore. If $\delta > 0.5d$, diffusion zones are overlapping due to neighbouring effect of pores on each other and then ions diffuse linearly in this condition.^{67, 68} When all of these equations and conditions are true, the radius of each pore is not less than 1 μm ; in pores with less than 1 μm of radius, these assumptions are not suitable.⁶⁷

Strutwolf and co-workers reported electrochemical results of simple ion transfer at water/gelled 1,6-dichlorohexane (DCH) interfaces in different arrangements of microporous silicon membranes with pores of different radii (between 10-25 μm), pore depth of 100 μm and different pore to pore centre separations (99 and 986 μm). They compared the experimental results with computational results obtained by COMSOL simulation program. For some arrangements the centre-to-centre distance was not more than 12 times the pore radius, and there was diffusion zone overlapping. With some arrays which were not compatible with equation 1.4.3, there was a peak shaped CV which is showing diffusion overlapping as well.⁶⁸

In another study, Alvarez de Eulate and co-workers showed some experimental and theoretical results of simple ion transfer at water/DCH interface which are formed at the micropore arrays composed of 100 pores in a glass membrane. The conical shape pores are formed by laser ablation so that pore radii were different on the laser entry side and laser exit side (with radii on the entry side around 26.5 μm and on the exit side around 11 μm) and each pore has 130 μm depth. There is good agreement between experimental results and the results from computer simulation.⁶¹

In this thesis, facilitated ion transfer will be investigated at the ITIES located at micropore arrays formed in glass membranes like those used in the recent report,⁶¹ but in this case the radii of each pore at laser entry side and exit side are around 40 and 20 μm , respectively.

1.4.3. Electrochemical set up of the μ -ITIES

In μ -ITIES, two reference electrodes (Ag/AgCl) are used. After sealing the micro-pore array membrane onto a glass cylinder, the organic phase is introduced into the glass cylinder. Then the

cylinder with organic phase is inserted in the aqueous phase in a beaker. After that, it is needed to add the organic reference solution on top of the organic solution in the cylinder.⁵⁴ As a result, a micro-interface array was formed between organic phase in the cylinder and aqueous phase in the beaker (illustrated in **Figure 1.4.4**).

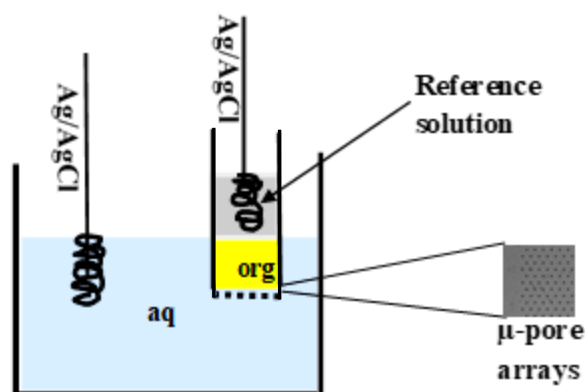


Figure 1.4.4 Two electrodes set up with micropore array membrane for form a micro-ITIES array.

If all of the interfaces are considered in this set up (**Figure 1.4.4**), there are two liquid-liquid interfaces including the interface between the reference solution and the organic solution inside the cylinder, and the interface between the organic solution and water in the beaker. To provide pure electrochemical signal, which is just due to ion transfer between organic and aqueous phase in the beaker, it is required to make just this interface to be polarisable and to make the other one to be non-polarisable. In this regard, it is required to add proper electrolyte in the organic reference solution on top of the organic solution in the cylinder, to make common ions between the two phases. The electrolyte contains a common cation (e.g. bis(triphenyl) phosphoranylideneammonium, BTPPA⁺), so the interface between the organic reference solution and organic solution is a non-polarised interface.

1.4.4. Electrodes and electrolytes at the ITIES

Generally, in solid-liquid electrochemical set up, working electrodes are defined as electrodes at which the redox reaction of interest occurs. Redox reaction also occurs at the counter electrode. For the liquid-liquid interface or the ITIES set up, the interface is considered as the working electrode because the charge transfer of interest happens at this interface. An ideal reference electrode (RE) in a solid-liquid electrochemical set up needs to provide a very stable and reproducible reference potential. One of the most common RE is silver-silver chloride or Ag/AgCl/Cl⁻ and the standard half-cell reaction in this electrode is shown in equation 1.4.4:



The standard potential E^0 of Ag/AgCl/Cl⁻ is +0.222 Volts versus the standard hydrogen electrode (SHE).⁷² Based on the Nernst equation (equation 1.4.5) related to the Ag/AgCl electrode, its potential is proportional to the activity of chloride ions.

$$E_{\text{Ag/AgCl}} = E_{\text{Ag/AgCl}}^0 - \frac{RT}{F} \ln a_{\text{Cl}^-} \quad \text{Equation 1.4.5}$$

In solid-liquid system, the source of chloride is KCl or NaCl solution while for liquid-liquid interface system, it is needed to add background electrolyte like chloride salts to make the interface between Ag/AgCl and water non-polarisable. In addition, for Ag/AgCl electrode on the organic side of the ITIES in the organic reference solution, it is needed to have BTPPACl as a background electrolyte with 10 mM lithium chloride to make the interface between Ag/AgCl and the organic reference solution to be non-polarised as well.

In the micro-ITIES array electrochemical cell, as mentioned before, the interface between organic solution in cylinder and the water phase in the beaker (**Figure 1.4.4**) is considered as the working electrode, and this interface should be a polarisable interface. On the other hand, the non-polarised interface between reference organic solution and organic solution in cylinder is considered as a reference interface.⁸ Because of the presence of the common ion (BTPPA⁺) between these two solutions in the cylinder, so the equilibrium and interfacial potential difference based on equation 1.2.13 will be achieved. On the other hand, the external applied potential is different with the Galvani ion transfer standard potential ($\Delta_o^w \phi_i^0$). Then, the imposed potential difference is the difference in potential between the two reference electrodes, which shows the difference potential of the interface. To have reproducibility in measurement of potential difference at the ITIES, tetraalkylammonium cations can be used as reference ions. The potential axis of the analyte can be adjusted by transposing the experimental half-wave potential of tetraalkylammonium cations to the Galvani scale by knowledge of their formal transfer potential of these cations on the Galvani scale from the literatures.

1.4.5. Facilitated ion transfer at the micro-ITIES

As mentioned earlier, there are three types of charge transfer at the ITIES, namely simple ion transfer (IT), electron transfer (ET) and facilitated ion transfer (FIT). The main focus of this study is facilitated ion transfer (FIT) in which a ligand or ionophore can selectively complex with the ion of interest. Generally, use of hydrophobic ionophores in the organic phase in ion selective electrodes (ISEs) has been highly developed. New synthesised ionophores considerably have been used in ISEs by potentiometric approaches.⁷³ On the other hand, these ionophores can be applied at the ITIES by

amperometric sensing methods. The main difference between the two approaches is the first one is at equilibrium while the second one is a non-equilibrium method, because in amperometric methods, the current is changing.⁷⁴

Koryta¹⁴ pioneered FIT at the ITIES and in this study, the facilitated transfer of alkali metal ions by valinomycin and a crown polyether at the macro ITIES was investigated with different electrochemical methods, including cyclic voltammetry, chronopotentiometry and polarography. The study can be a platform for tremendous applications of the ITIES including environmental and biological sciences. In FIT at the ITIES, the complexation can overcome the Gibbs transfer energy of the ion of interest and then the electrochemical signal related to transfer of the ion of interest can be visualised within the available potential window. Furthermore, in terms of designing ion sensors, the main advantage of using ionophores at the ITIES is improvement of selectivity for the target ions over other ions. As mentioned before, there are four mechanisms of facilitated ion transfer at the ITIES: aqueous complexation followed by transfer (ACT), transfer to the organic phase followed by complexation (TOC), transfer by interfacial complexation (TIC) and transfer by interfacial dissociation (TID)⁷⁴ (**Figure 1.4.5**).

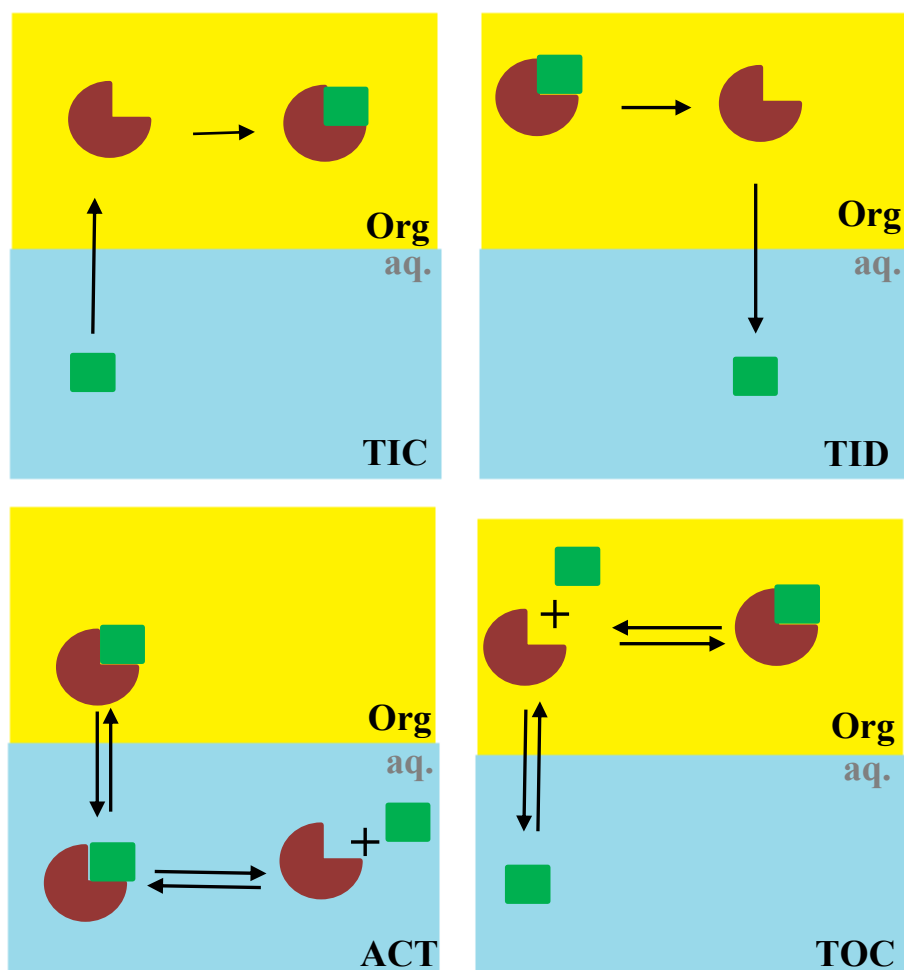


Figure 1.4.5 Illustration of the four types of complexations at the ITIES, which are aqueous complexation followed by transfer (ACT), transfer to the organic phase followed by complexation (TOC), transfer by interfacial complexation (TIC) and transfer by interfacial dissociation (TID).

Since usually different ionophores have very low solubility in water, most of FIT transfers are following TIC, TOC and TID mechanisms. Due to varieties of ion to ligand stoichiometry, Girault et al.⁷⁵ defined thermodynamic equations for facilitated ion transfer based on 1:m ion to ligand stoichiometry. On the other hand, Matsuda et al.⁷⁶ proposed the relevance of FIT reactions based on half wave potential via two limiting conditions, which are excess of the ligand in the organic phase compared to ion in aqueous phase and excess of ion in aqueous phase relative to ligand concentration in organic phase. Other assumptions to simplify the FIT mechanism are always that both complexation and de-complexation are faster than diffusion of ions and ionophores, which results in both association and dissociation between ions and ionophores are in equilibrium. By assumption that the ion to ionophore proportion is 1:1, the equilibrium between ion and ionophore and the association constant (K_a^O) can be defined (equation 1.4.6):



Where a_{ML}^O , a_M^W and a_L^O are activity of complex, ion in aqueous phase(w), ionophore and complex in organic phase (O), respectively. Also, the Galvani potential difference ($\Delta_O^W \phi$) is shown in equation 1.4.7:

$$\Delta_O^W \phi = \Delta_O^W \phi_{ML}^0 + \frac{RT}{zF} \ln \left(\frac{a_{ML}^O}{a_M^W} \right) \quad \text{Equation 1.4.7}$$

In which $\Delta_O^W \phi_{ML}^0$ is the standard transfer potential of the complex, and since the ionophore does not have any charge, z is the charge of the ion or complex, which are the same. By considering that the concentration of ions in the aqueous phase is in excess compared to the ligand in the organic phase, and replacing concentration instead of activity, the association constant (K_a^0) has the following relation to the half wave potential ($\Delta_O^W \phi_{1/2}$) (equation 1.4.8):

$$\Delta_O^W \phi_{1/2} = \Delta_O^W \phi_M^0 - \frac{RT}{zF} \ln (C_M^W K_a^0) \quad \text{Equation 1.4.8}$$

Where $\Delta_O^W \phi_M^0$ is the formal transfer of the cation from aqueous phase to organic phase.

Several reports have been carried out to study of FIT for cations especially for alkali metals with crown ethers as ionophores.^{77, 78} Furthermore, other types of ionophores are applied to investigate alkali metals, such as calixarene structures.^{79, 80} Fundamental results achieved from recent studies for alkali metals with FIT methods can be exploited for a wide range of analytes even organic molecules like neurotransmitters, amino acids and oligopeptides in their protonated forms by using crown ethers.⁸¹⁻⁸³ In these systems, these analytes can form hydrogen bonding with oxygen in the structures of crown ethers.

Although numerous investigations have been conducted for FIT of inorganic cations and the organic compounds which were mentioned above, still just a few reports were dedicated to inorganic anions. Challenges of anion detection by FIT at the ITIES are due to larger ion size compared to cations, their sensitivity to pH, and their interaction with solvents.⁸⁴ In addition to these issues to sense anions by FIT at the ITIES, fewer synthesised ionophores are available compared to ionophores for cations. The main focus of this thesis is anion sensing by using selective commercial and synthesised ionophores to detect sulfate.

In addition, at the liquid/liquid interface, to obtain more robustness, FIT can be studied at ion selective membranes on top of solid electrodes. For example, Bond et al. studied both anion and cation sensing by dynamic electrochemical methods (cyclic voltammetry) via 1 μ m thick PVC-based membranes containing commercial ionophores, an electroactive species, a plasticizer (like NPOE) and organic background electrolyte.^{85, 86} This study was an introduction to solid contact ion selective electrodes (SC-ISEs) which will be discussed more in the next section.

1.4.6. Cyclic Voltammetry at the ITIES

One of the most useful techniques in electrochemistry is cyclic voltammetry (CV). Kinetic and thermodynamic information can be achieved by CV. Also, some data related to analytes including diffusion, adsorption and the number of electrons which are transferred in electron transfer reactions can be obtained by CV.⁸⁷ In this method, by sweeping the potential from an initial potential E_1 to a different potential E_2 (**Figure 1.4.6**),⁸⁸ the current will be recorded. E_1 and E_2 in electrochemistry at the ITIES will be related to the background electrolytes in both organic and aqueous phases because these electrolytes can restrict the working potential window in CV.

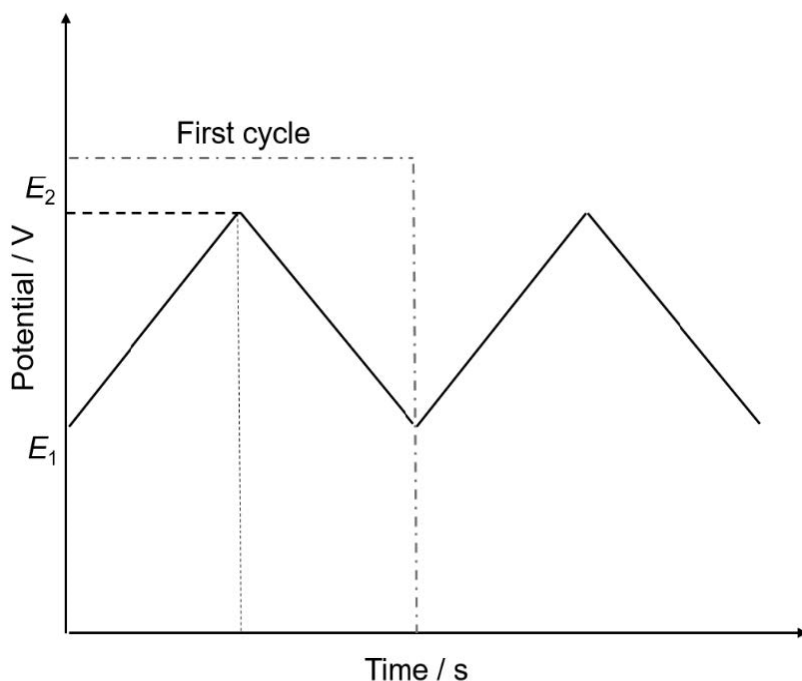


Figure 1.4.6 Applied potential versus time in cyclic voltammetry.

The values which are important in CV are the peak current (I_p) and the peak potential (E_p) (**Figure 1.4.7**).⁸⁹ Two types of diffusion behaviour are shown in **Figure 1.4.7** a), shows the situation where diffusion on both sides of the ITIES is linear, while in **Figure 1.4.7** b), the forward scan in the CV shows radial diffusion and the backward scan shows linear diffusion of ion transfer.

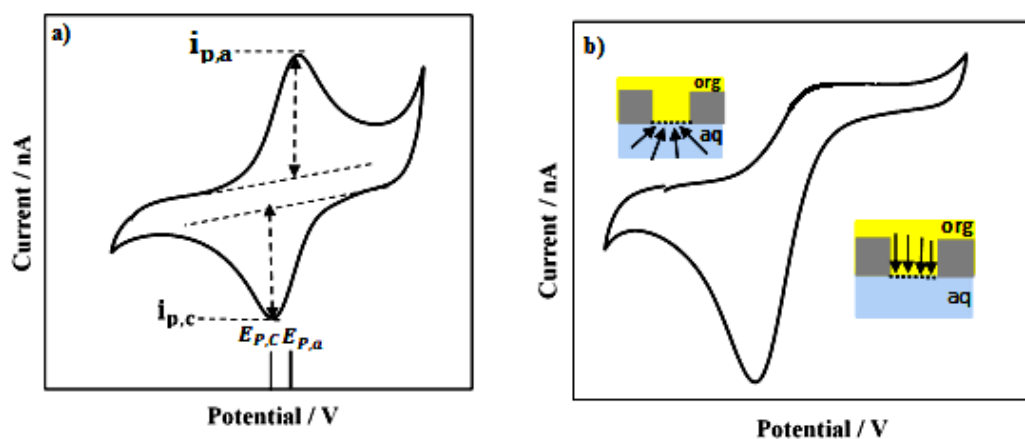


Figure 1.4.7 cyclic voltammogram a) for linear diffusion b) for radial diffusion in forward scan and linear diffusion in backward scan.

For the case with linear diffusion, the peak current can be defined by the Randles-Sevcik equation:

$$I_p = (2.69 \times 10^5) z_i^{3/2} A D_i^{1/2} C_i v^{1/2} \quad \text{Equation 1.4.9}$$

Where, I_p is the peak current, z_i is the charge of the ion, D_i is diffusion coefficient of the ion, C_i is the concentration of the ion, A is the interface area and v is scan rate. In linear diffusion at a flat interface, the peak current is proportional with the square root of the scan rate ($v^{1/2}$).³ In this system, the method to evaluate reversibility is plotting the peak current (I_p) with square root of scan rate ($v^{1/2}$) and both forward and backward I_p are proportional with $v^{1/2}$. In addition, for reversible system, the peak-to-peak separation between peak potential of forward (the transfer potential of the ion from aqueous phase to organic phase) and peak potential of backward (the transfer potential of the ion from organic to aqueous phase) is around 59 mV/ z_i at 25 °C.

1.4.7. Differential pulse voltammetry (DPV):

Differential pulse voltammetry (DPV) is an electroanalytical method in which the sensitivity is increased by reducing the ratio of charging current (i_c) to faradic current (i_f). This can be possible because i_f decreases by $\frac{1}{t^{1/2}}$ whereas i_c decreases faster.² A pulse potential waveform (**Figure 1.4.8**⁹⁰) is applied in DPV and the current is sampled at two points: first, current is sampled before the pulse application (i_1), and, second, at the end of the pulse application (i_2). The difference between two sampled currents resulting in peak-shaped which is final out put of DPV method.

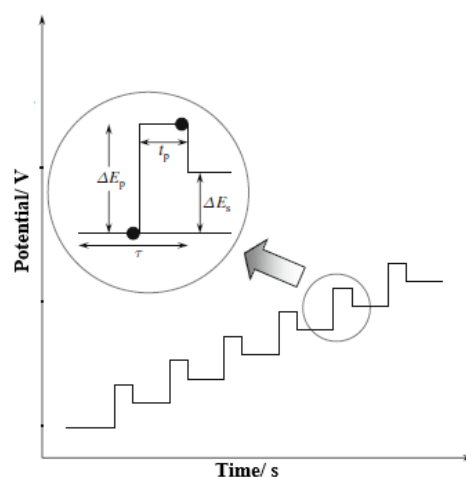


Figure 1.4.8 Potential versus time waveform in differential pulse voltammetry (DPV) (this figure is taken from ⁹⁰ reference).

1.5. Principles of ion selective electrodes

1.5.1. Introduction

Generally, ion selective electrodes (ISEs) are applied to sense activities of different ions. These devices can be used in wide range of applications such as medical and environmental science. In comparison to different analytical methods, these tools are very low cost, portable with low energy consumption.⁹¹ The electroanalytical method which is mostly used in these devices is potentiometry, in which the potential difference is measured between ISEs and reference electrodes (**Figure 1.5.1**) and can be expressed by the Nernst equation 1.5.1:

$$E = E^{\circ} + \frac{RT}{zF} \ln C_i \quad \text{Equation 1.5.1}$$

Where E° is the formal potential and it is constant, C_i is concentration of i species in solution, and z is charge of this ion.

1.5.2. Structure of conventional ISEs and Nernstian behaviour

Conventional ISEs contain an ion selective polymeric membrane which is placed between a sample solution and an inner filling solution (**Figure 1.5.1**). The ion selective membrane includes a polymer (e.g. PVC), a plasticizer or membrane solvent such as 2-nitrophenyloctylether (o – NPOE) or bis(2-ethylhexyl) sebacate (DOS), lipophilic ionic sites or ion exchangers which have one lipophilic ion that does not partition into the water solution and an inorganic ion which is an exchangeable ion, ionophores with which the ions of interest have more affinity to make complex with over other ions, and, finally, a lipophilic background electrolyte to increase the ion conductivity of the membrane.

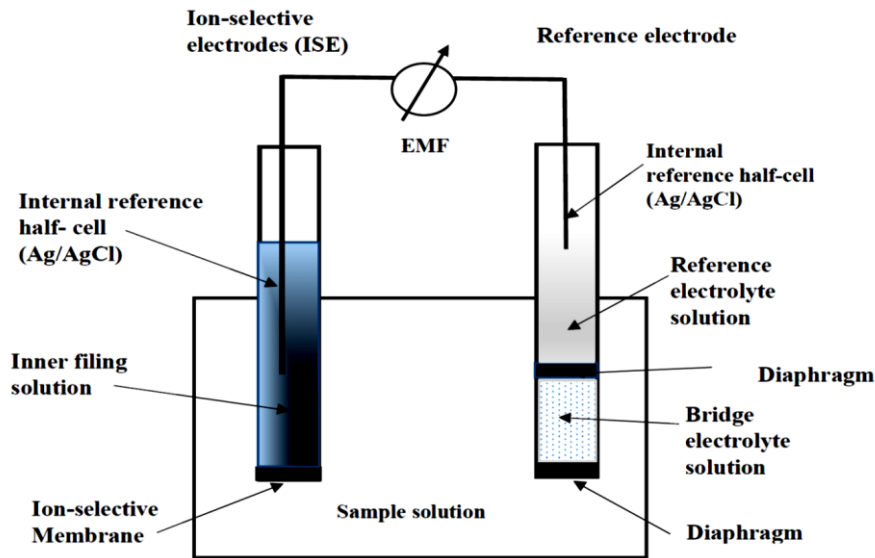


Figure 1.5.1 Schematic of a conventional ion selective electrode with a reference electrode.

In typical potentiometric set up (**Figure 1.5.1**), the electromotive force (EMF) is the sum of the potential differences between the two electrodes at zero current. For EMF, just two potential differences are related to sample concentration: 1) the liquid-junction potential ($E_{D,ref}$) and 2) the membrane potential (E_M) can be written as equation 1.5.2. Other contributions which are not dependent on the sample are constant (E_{const}).

$$EMF = E_{const} + E_{D,ref} + E_M \quad \text{Equation 1.5.2}$$

The liquid junction potential ($E_{D,ref}$) is because of differences in ion mobilities at the phase boundary between the sample solution and the bridge electrolyte and can be negligible by using a high concentration bridge electrolyte. The membrane potential (E_M) consist of three parts, which are the potential difference at the sample solution - membrane interface, the potential difference between the internal filling solution and the membrane, and the diffusion potential inside the ion selective membrane. Among these three potentials, the potential difference between the inner filling solution and the membrane is not related to the sample concentration and can be constant, and the diffusion potential is negligible. So E_M can be written as in equation 1.5.3:

$$E_M = E_{M,const} + E' \quad \text{Equation 1.5.3}$$

Where $E_{M,const}$ is sum of the diffusion potential and the potential difference between inner filling solution and the membrane, and E' is the potential difference at the sample solution - membrane interface which can be derived from thermodynamic theory. The electrochemical potential of species

i (μ_i') in the aqueous phase can be divided into two parts: electrical potential ($\phi(aq)$) and chemical potential of the ion ($\mu_i(aq)$), as shown in equation 1.5.4:

$$\mu_i'(aq) = \mu_i(aq) + z_i F \phi(aq) \quad \text{Equation 1.5.4}$$

Where, z_i is the charge of the ion, F is the Faraday constant. In this equation, chemical potential of the ion (i) (μ_i) can be defined as (equation 1.5.5):

$$\mu_i(aq) = \mu_i^0(aq) + RT \ln a_i(aq) \quad \text{Equation 1.5.5}$$

in which R is the gas constant, T is absolute temperature, a_i is the activity of ion and μ_i^0 is the standard chemical potential of the ion. By combination of equation 1.5.4 and 1.5.5, electrochemical potential of ion i in aqueous phase can be rewritten in equation 1.5.6:

$$\mu_i'(aq) = \mu_i^0(aq) + RT \ln a_i(aq) + z_i F \phi(aq) \quad \text{Equation 1.5.6}$$

Also, the electrochemical potential of ion in the ion selective membrane can be written in the same way by equation 1.5.7:

$$\mu_i'(org) = \mu_i^0(org) + RT \ln a_i(org) + z_i F \phi(org) \quad \text{Equation 1.5.7}$$

Since at equilibrium time, electrochemical potential of the ion in both phases are the same, the electrical potential difference between two phases at the interface can be written in equation 1.5.8:

$$E' = \phi(org) - \phi(aq) = -\frac{\mu_i^0(org) - \mu_i^0(aq)}{z_i F} + \frac{RT}{z_i F} \ln \frac{a_i(aq)}{a_i(org)} \quad \text{Equation 1.5.8}$$

By combining all sample independent potentials in equation 1.5.3 and 1.5.8 into the constant parameter E^0 and the activity of the interested ion in membrane is constant, the Nernst equation can be achieved which is dependent on activity of ion species in the aqueous phase:

$$E_M = E^0 + 2.303 \frac{RT}{z_i F} \log a_i(aq) \quad \text{Equation 1.5.9}$$

By replacing ion activity by concentration, these potential differences have correlation with different concentrations of ions, as shown in equation 1.5.10:

$$E_M = E^{0'} + 2.303 \frac{RT}{z_i F} \log C_i \quad \text{Equation 1.5.10}$$

In which $E^{0'}$ is the formal potential, which is constant. By plotting of E_M versus $\log C_i$, a calibration curve of the ISE is achieved. So, by the Nernstian behaviour of ISEs, sensing of ions can be obtained.

1.5.3. Selectivity of ISEs

Selectivity in ISEs means the ability of ISEs to discriminate between the primary ions and other ions in solution or interfering ions. Thus, selectivity can be considered a factor by which the performance of ISEs can be evaluated. Selectivity of ISEs is defined as selectivity coefficient ($K_{I,J}$) and usually can be presented as $\log(K_{I,J})$. For example, when $K_{I,J}$ is 1, it means that the response and the sensitivity of ISEs to the primary ion (I) is same as to the interfering ion (J). A lower value of $K_{I,J}$ represents a better selectivity of the primary ion (I) over the interfering ion (J). Selectivity can be determined by different methods.⁹²⁻⁹⁴ The most common methods to measure selectivity coefficients are the separate solution method (SSM) and the fixed interference method (FIM). In SSM, the electrode is calibrated in both interfering ion solution and primary ion solution separately. The potential difference between these two solutions ($\Delta E = E_J - E_I$) is used to determine the selectivity coefficient of the primary ion (I) over the interfering ion (J) (**Figure 1.5.2**). The selectivity coefficient can be calculated by the equation 1.5.11.

$$\text{Log}(K_{IJ}) = \frac{\Delta E}{M} \quad \text{Equation 1.5.11}$$

In this equation ΔE is the difference potential of the ISE in solutions of primary ion (I) and interfering ion (J) at the same concentrations or activities and M is the slope of the calibration graph of different concentrations of primary ions versus potentials (**Figure 1.5.2**).

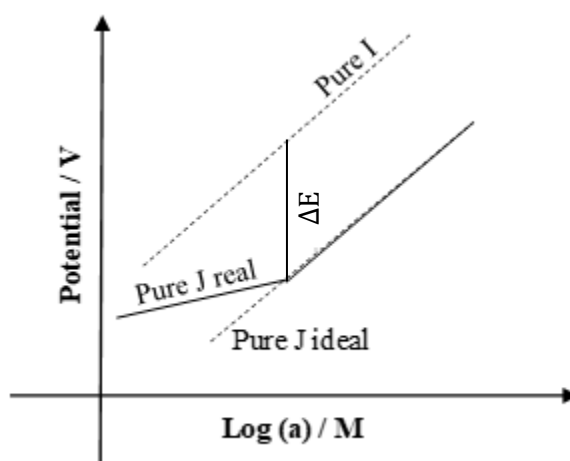


Figure 1.5.2 Separation solutions method (SSM) to measure K_{IJ}

The selectivity coefficient can be determined also by the fixed interference method (FIM). In this method, the electrode is calibrated in the pure primary ion solutions and then placed in solutions with fixed concentrations of interference ions and with different concentrations of primary ions. At higher activity of interfering ions, the calibration curve related to primary ions is changed (**Figure 1.5.3**).

However, in higher activity of the primary ion, the calibration curve is linear. In other words, in FIM, the detection limit of the primary ion is lower in the case without interfering ions. The selectivity coefficient by this method is defined by the Nikolsky-Eisenman equation⁹⁵ :

$$E = E^0 + \frac{RT}{z_1 F} \ln(a_I + \sum (K_{IJ} a_J)) \quad \text{Equation 1.5.12}$$

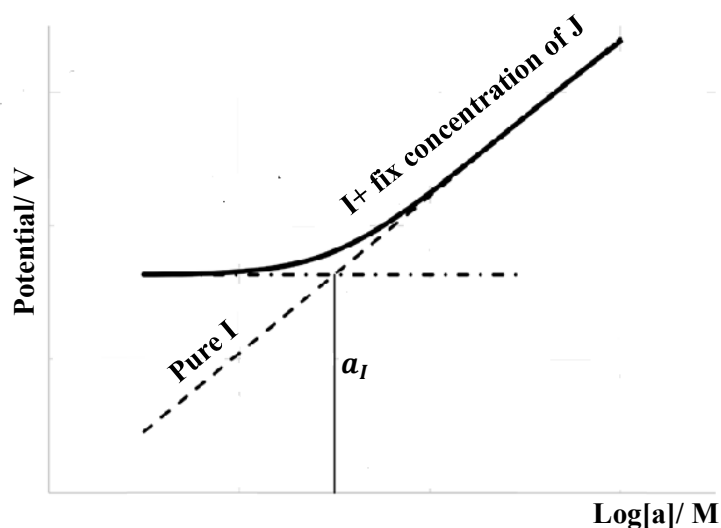


Figure 1.5.3 Fixed Interference Method (FIM) to measure K_{IJ}

The selectivity coefficient by FIM is obtained by equation 1.5.13:

$$K_{IJ} = \frac{a_I}{a_J} \quad \text{Equation 1.5.13}$$

In this equation, a_I is the intercept achieved by the two extrapolated lines in **Figure 1.5.3** and a_J is fixed interfering ion activity in solution. As it is shown in **Figure 1.5.3** the linear range of the solution with primary ion (I) in the presence of interfering ion (J) is less than the solution just with primary ion (I). For equations 1.5.11 and 1.5.13 to be valid the following three conditions must be reached: 1) Nernstian behaviour of both primary and interfering ion, 2) both ions should have same charge, 3) there are no fluxes.^{96, 97}

1.5.4. Solid state ion selective electrodes

In the same way as miniaturisation of the ITIES which can address challenges related to the macro-ITIES for sensing of ions, miniaturisation of conventional ISEs can provide several advantages in view of implantable devices, easy maintenance, measurements in very small volume of sample, and mass production.⁹⁸ On the other hand, one big challenge of conventional ISEs is the inner filling solutions (IFS) due to their sensitivity to temperature and pressure. The volume of inner filling solutions cannot be lower than the millilitre level.⁹⁹ However, microelectrodes based on micropipettes

have been developed for a long time,¹⁰⁰ but their fabrication is a very delicate process and also they are fragile. The first step towards solid state ISEs (i.e. ISEs without inner filling solutions) was coated wire electrodes (CWEs)⁹⁸ with very simple design (**Figure 1.5.2 b**). In this design, ion selective membrane (ISM) was deposited on electrodes such as Au, Pt or glassy carbon.¹⁰¹ A big disadvantage of CWEs compared to conventional ISEs is a lack of reproducibility in potential from sensor to sensor, and they need frequent calibrations. The next step towards solid state ISEs was use of hydrogels as an ion-to-electron transduction layer (**Figure 1.5.2 c**) instead of IFS. However, the issue related to hydrogel-based electrodes is absorption of water or small neutral molecules like CO₂ to the ISM.⁹¹ Moreover, these ISEs need long equilibrium time, and can be problematic in some applications like single used sensors and short turnaround time sensors. These issues related to CWEs and hydrogel-based electrodes drive efforts to design new ISEs with short equilibrium times, very low potential drifts and calibration free electrodes.^{91, 99, 102} In this regard, many compounds with ion-to-electron transduction properties were used between ion-sensing membranes and electrodes. The layer containing these components is called the solid contact and the role of the solid contact in ISEs is providing well-defined interfacial potentials between electrodes and ISMs (**Figure 1.5.2 d**).

1.5.5. Different solid contact ion selective electrodes

To design solid contact ion selective electrodes (SC-ISEs), a wide range of solid contact materials can be used as an intermediate ion-to-electron transducing layer, including self-assembled monolayers (SAMs),¹⁰³ carbon-based materials like three dimensioned macro-porous carbon, carbon nanotube, fullerene and graphene,¹⁰⁴ organic compounds¹⁰⁵ and conducting polymers.¹⁰⁶ Although conducting polymers such as poly(3-octylthiophene) (POT), polyaniline and poly(3,4-ethylendioxythiophene) (PEDOT) have been widely used as intermediate compounds in solid contact ISEs, their use is limited due to low redox capacity and significant difference between anodic and cathodic peaks.^{106, 107} Similar to hydrogel-based ISEs, a water layer containing ions or neutral molecules (e.g. CO₂) forms between the solid contact and the ISM. These issues can be addressed by inserting electroactive materials directly into the ISM and instead of two layers (ISM layer and transduction layer), there is just one layer that can act as a SC-ISE layer. These compounds are molecular redox probes which can be easily dissolved in the ISM or can be covalently attached to ISM matrixes.¹⁰⁸⁻¹¹¹ One of the most common redox probe complexes is ferrocene and its derivatives but the major disadvantage of these compounds is an irreversible electrochemical behaviour in the presence of chloride ions, due to formation of a complex with chloride ions.¹¹¹ Another category of redox probes is cobalt complexes, which were introduced by Buhlmann.^{112, 113} To overcome instability of anion detection by POT, a lipophilic osmium complex was applied as a molecular redox probe.¹¹⁴ However, anion sensing by these compounds are strongly depends on the concentration of these complexes in the ISM. In a very recent study, functionalised helicene compounds were applied

in a solid contact layer¹¹⁵ and showed very stable and reversible responses. However, in the presence of ionophore, the compound leaked from the ISM. In continue, by excess amount of ionophore and use of polyurethane as a polymer instead of PVC in the ISM, the leakage issue was addressed.¹¹⁶ In this thesis, lipophilic ruthenium complexes were investigated for anion sensing.

1.6. Aims and goals of this work (sulfate sensing):

The general aim of this work is to investigate the use of electrochemical methods to selectively detect sulfate at the interface between two immiscible electrolyte solutions. In this research, different approaches were applied to sense sulfate, including ion transfer at liquid-liquid interfaces and at solid contact electrodes. Newly synthesised sulfate ionophores were evaluated in this thesis to assess their suitability for sulfate sensing.

In chapter 2, facilitated ion transfer at μ ITIES arrays was studied in order to compare electrochemical responses at micropore arrays which were located at either laser entry side or laser exit side of laser ablated glass membranes. Facilitated potassium transfer by dibenzo-18-crown-6 (DB-18-C6) was used as an established model to characterise the FIT process at these laser-ablated pore-based ITIES. Then the micropore arrays located at the laser entry side of membranes, which showed best sensitivity, were chosen in order to study sulfate sensing. Newly synthesised sulfate ionophores were examined for sensing of sulfate.

In chapter 3, in order to develop a more robust sensing system of different anions, solid contact electrodes containing a new lipophilic Ru complex as a redox probe was used to evaluate the detection of sulfate and other anions. The aim of the work was to evaluate this new Ru complex as an ion-to-electron transducer in solid contact electrodes and to assess suitability for ion sensing. Different compositions of membrane were assessed to optimise electrochemical responses. Two plasticizers were studied, and their responses were compared, and for the first time, kinetic studies were carried out to provide information about the ion-to-electron transduction systems at solid contact electrodes.

In chapter 4, in order to provide stable sulfate ion selective electrodes, two new Ru complexes were examined. Nernstian behaviour was evaluated, and the nearly Nernstian slope was achieved. In order to provide more selective electrodes, two different newly synthesised sulfate ionophores were assessed, and their electrochemical responses were compared to responses obtained with a commercial sulfate ionophore.

In chapter 5, in order to provide more robust ion to electron transduction system, the immobilisation of a new Ru complex on indium tin oxide (ITO) electrodes was studied. The chemical immobilization

occurred on the ITO electrodes' surface. This method was used to investigate anion sensing on ITO electrodes, including with thin polymeric layers spin coated on the surface.

In Chapter 6, general conclusions of this thesis and suggestion for future investigations are discussed.

2. Characterisation of facilitated ion transfer at micro-interface arrays supported on laser-ablated glass membranes.

2.1. Introduction:

Ion transfer electrochemistry at the interface between two immiscible electrolyte solutions (ITIES) has attracted much attention for fundamental and applied studies of chemical and biological systems.¹¹⁷⁻¹¹⁹ Facilitated ion transfer (FIT) at the ITIES deals with the movement of ions from aqueous to organic phase through the binding affinity of the ion (in the aqueous phase) with the ionophore present in the organic phase upon perturbation by an applied potential. This FIT concept was pioneered by Koryta,¹⁴ allowing thermodynamic and kinetic parameters to be obtained which are critical to the mechanistic understanding for the development of ion-selective sensors.

The FIT process could be investigated with either macro- or micro-scale liquid-liquid interfaces. The ground-breaking work of Koryta in 1979¹⁴ on the transfer of potassium ion from water to nitrobenzene assisted by dibenzo-18-crown-6 (DB-18-C-6) was conducted on macro interface by conical glass capillary with a four electrodes cell setup (with two auxiliary electrodes and two reference electrodes). Kudo et al. have also demonstrated the FIT process of Li^+ , Na^+ and K^+ by different crown ether ionophores¹²⁰ while Beni et al. studied the selective dopamine detection by DB-18-C-6,¹²¹ both of which were performed across a polarized macroscopic liquid-liquid interface. Although macro-ITIES mostly has been employed for kinetic and thermodynamic studies of ion transfer, it suffers from mechanical instability, high iR drop and capacitive current, and complicated four-electrode electrochemical cell. Miniaturization has been able to address the above mentioned challenges of the macro-ITIES system by enhancing the rate of mass transport and reducing the impact of cell resistance.¹²² It also comes with a simpler two-electrode system while further benefitting for the significant reduction of reagent consumption. The first miniaturised version of ITIES was in a glass micropipette (25 μm diameter) introduced by Taylor and Girault.¹⁵ Since then, different arrangements of miniaturised supported ITIES with various materials and fabrication procedures have been applied to study the FIT process, such as micropipette prepared from borosilicate glass capillary with silanized outer wall to provide a hydrophobic side,¹²³ FIT investigation at quartz nano-pipettes,¹²⁴ facilitated ammonium transfer by bexakis (2,3,6-tri-O-acetyl)- α -cyclodextrin at micro-hole ITIES on polymer substrate¹²⁵ and simple and facilitated ion transfer across dual micropipette.¹²⁶ Later on, to increase the efficient surface area of the interfaces and consequently to enhance the mass transport rates, an array of micro- or nano-ITIES which are based on polymer, silicon and glass porous membranes have been developed.¹²⁷ First micro-hole arrays including 66 holes was fabricated on polyethylene terephthalate film (PET) substrates by UV

laser ablation.¹²⁸ Surprisingly, to our knowledge, there are few studies of FIT at ITIES with the micro- or nano-pore arrays.

Our group has previously reported the simple ion transfer on a borosilicate glass microporous membrane with 100 micropores with 10 x 10 square array format.⁶¹ The conical shaped pores were produced by laser ablation to provide an array holder for electrochemical sensing at liquid-liquid interface. According to the electrochemical responses and the simulation analysis of the membranes, higher sensitivity was achieved by locating the ITIES at the laser entry side, which is wider, while lower variability in the voltammetry was achieved by the interface located at the laser exit side, with narrower dimensions.⁶¹ Here, electrochemical responses at the micro-ITIES arrays located at either laser entry and laser exit side were investigated and compared. An established K⁺ ion - DB-18-C-6 ionophore FIT system was applied to evaluate the thermodynamic and kinetic differences in these two configurations. This study was conducted to achieve the best configuration of glass membrane to evaluate new ionophores for FIT of sulfate ions for development of sulfate sensors.

2.2. Experimental Section

2.2.1. Reagents and materials

All chemicals were provided from Sigma Aldrich, without further purification. MgCl₂ (10 mM) is used as aqueous phase background electrolyte and was prepared in ultrapure water (with a resistivity of 18.2 MΩ cm) Milli-Q from a USF Purelab plus UV, Millipore Pty. Ltd. Australia. The organic phase background electrolyte, bis (triphenylphosphoranylidene) ammonium tetrakis (4-chlorophenyl) borate (BTPPATPBCl), was obtained by metathesis of equimolar amounts of potassium tetrakis(4-chlorophenyl)borate (KTPBCl) and bis (triphenylphosphoranylidene) ammonium chloride (BTPPACl). In these experiments, 1,6-dichlorohexane (DCH) and 2-nitrophenyl octyl ether (NPOE) were used as organic solvents. In the first section which is facilitated potassium transfer, DCH was used to dissolve BTPPATPBCl and DB-18-C-6 ionophore, and in the second section which is facilitated sulfate transfer, NPOE was used as an organic solvent to dissolve BTPPATPBCl and sulfate ionophores.

2.2.2. Micro-pore array fabrication and characterization

The array of miniaturized liquid-liquid interfaces was formed across 100 pores in 10×10 square array arrangement (Fig. S.1). The pores were drilled by laser ablation method at the Optofab Node (ANFF-OptoFab, Macquarie University, New South Wales), as previously reported.⁶¹ As demonstrated in previous work⁶¹, one side of the microporous glass membrane was adhered by blue tape and the other side was functionalised by trichloro(1*H*,1*H*, 2*H*,2*H*-perfluorooctyl)silane under vacuum for 1 hour. Since the contact angle of water drops on the hydrophobic side is less than the contact angle on

hydrophilic side, easily the hydrophobic side can be distinguished from hydrophilic side of the membrane.

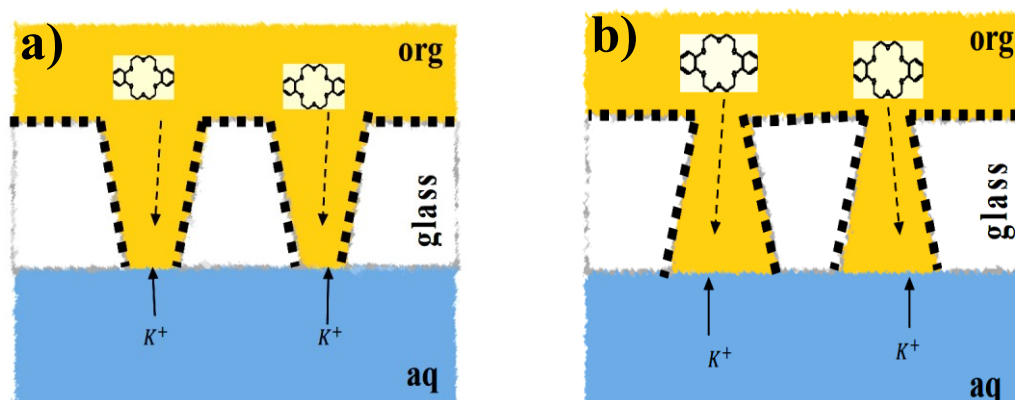


Figure 2.1 Facilitated potassium ion transfer by DB-18-C-6 in conical shaped micropores in glass membranes functionalised to be hydrophobic on either a) the hydrophobic treatment is on the laser entry side or b) the hydrophobic treatment is on the laser exit side. The laser entry side and consequent formation of the ITIES at a) the ITIES is formed at the laser exit side (the narrower end of the pore) b) the ITIES is formed on the laser entry side (the wider end of the pore).

The geometries of the array (including the number of the pores, pore size of both sides and pore to pore centre distances) were characterised by Scanning Electron Microscopy (SEM) (using a Tescan Mira3 FESEM) (**Figure 2.2**). The data from SEM images were processed by Image J software (**Table 2.1**). The shape of the pores in both membranes is conical, as determined by the dimensions of the pores on the laser entry side (wider radii) and laser exit side (narrower radii) side (**Figure 2.1**).

Table 2.1 Dimensions of the pores characterized by SEM and Image J software (n=4).

Distance (μm)	Laser exit side	Laser entry side
Linear centre to centre distance	297.85 (± 0.78)	313.85 (± 2.7)
Diagonal centre to centre distance	421.85 (± 0.25)	445.33 (± 2.1)
Hydrophilic side pore diameter	21.02 (± 0.68)	41.43 (± 0.82)
Hydrophobic side pore diameter	42.12 (± 1.7)	23.42 (± 0.57)

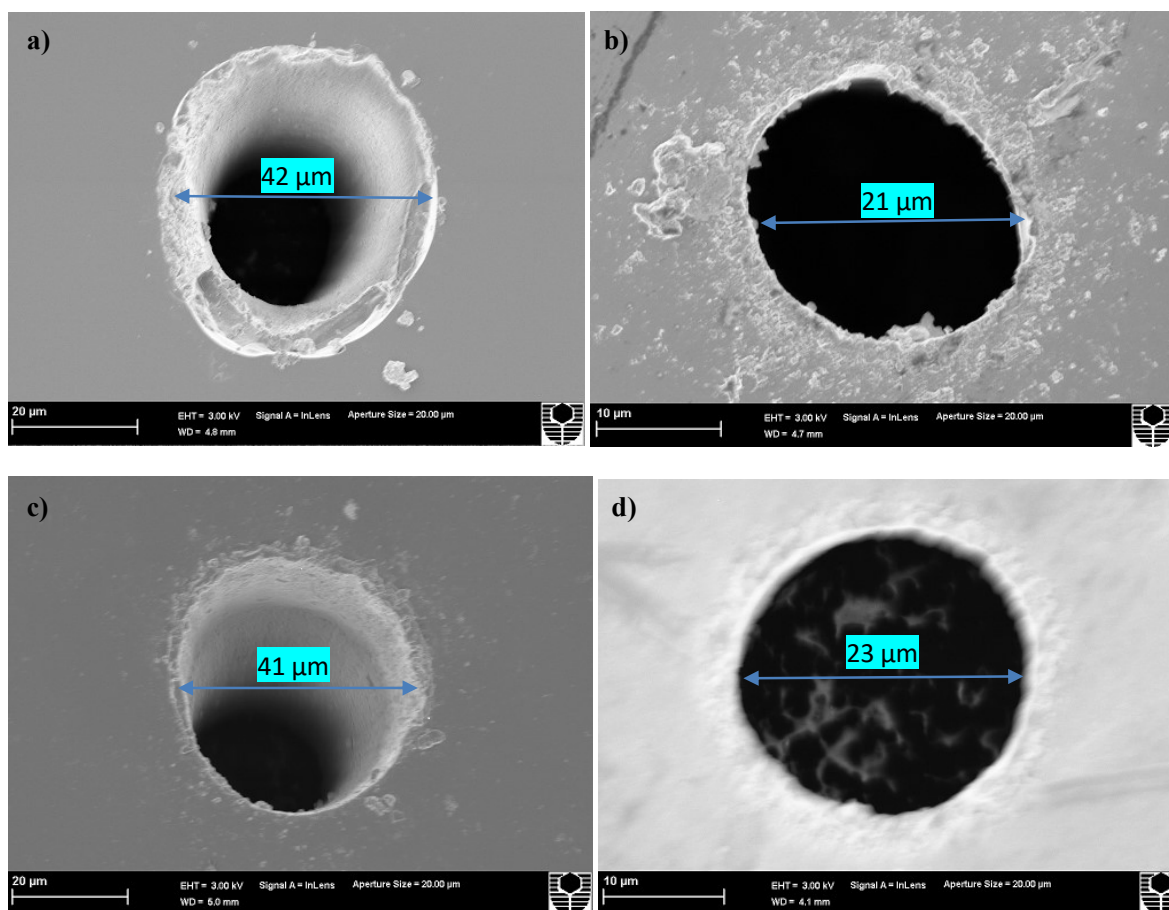


Figure 2.2 SEM images at laser exit side a) hydrophobic side pore and b) hydrophilic side pore, and at laser entry side c) hydrophilic side pore d) hydrophobic side pore

2.2.3. Electrochemical procedure at the micro-ITIES array:

The microporous glass chips were glued onto glass cylinders with silicone rubber while the hydrophobic side is facing the cylinder. 150 μL of the organic solution was inserted in the cylinder and after immersing in aqueous solution, 250 μL of aqueous reference solution was added to top of the organic solution. The electrochemical setups consisting of two Ag/AgCl electrodes and liquid electrolytes were implemented (**Figure 2.3**).



Figure 2.3 The electrochemical cell composition (Y mM is concentration of KCl).

Tetrapropylammonium chloride (TPrACl) was used as an internal standard to provide half wave potential on the Galvani potential scale at the end of each experiment, and based on the tetraphenylarsonium tetraphenylborate (TATB) assumption, the formal transfer potential of TPrA⁺ from water to DCH is -0.08V.⁶¹ Metrohm Autolab PGSTAT101 electrochemical analyser together with NOVA 1.9 software were used for all CV experiments. Moreover, measurement of uncompensated resistance (U_R) was carried out using a CHI900B potentiostat (CH Instruments Inc., USA) at the open circuit potential, and the values of U_R , which were around 230 and 300 kOhm for the interface at laser exit side and laser entry side, respectively, were compensated by NOVA 1.9 software. The potentials are transposed to Galvani Scale by using TPrA⁺ as an internal standard to provide the Galvani potential scale for these experiments.

2.3. Results and discussion

2.3.1. Mechanism of the ion transfer

In FIT, mass transport is more complicated than in simple IT, although it was simplified by two limiting conditions: 1) much higher concentration of ionophore in organic phase than ions in aqueous phase ($C_L \gg C_M$), 2) greater concentration of the ions in aqueous phase than the concentration of ionophore in organic phase ($C_L \ll C_M$).⁷⁶ Based on these limiting conditions, it is always assumed that both complexation and de-complexation are faster than the diffusion of species.¹¹⁹ All of experiments were carried out in the limiting condition in which the concentration of K⁺ in the aqueous phase is sufficiently greater than the concentration of DB-18-C-6 in the organic phase ($c_L \ll c_M$).

The well-known potassium FIT process across water/DCH was used to characterise the behaviour of the glass micropore array ITIES. The cyclic voltammograms (CV) (**Figure 2.4**) were recorded for experiments with aqueous solutions containing potassium (10 mM KCl) in contact with organic phases either with or without DB18-C6 for membranes with pores in two configurations (**Figure 2.1**).

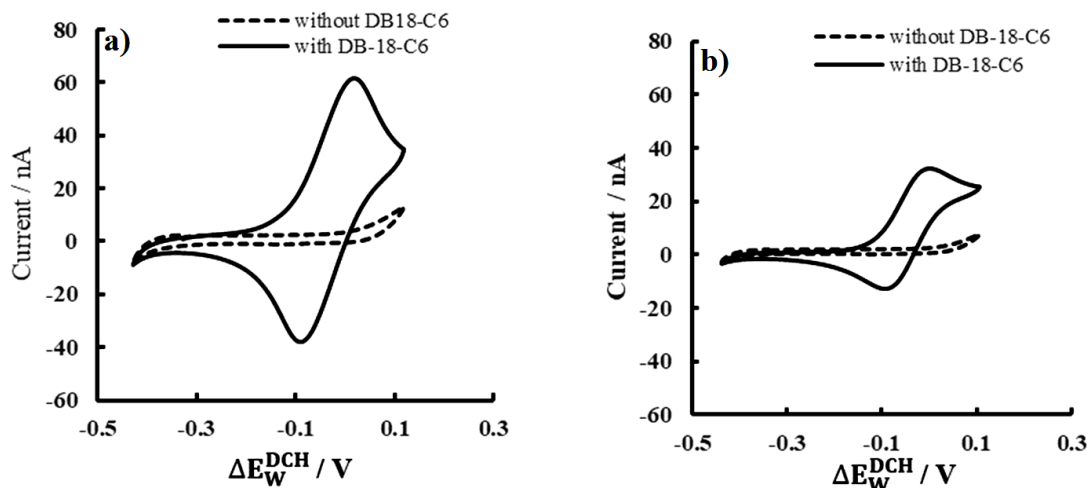


Figure 2.4 Cyclic voltammograms for the transfer of K^+ across W/DCH interface in the absence (dotted line) and presence (solid line) of DB18-C-6 (10 mM KCl and 1 mM DB18-C6) in pores with interfaces located at laser entry side **a)**, and pores with interface located at laser exit side **b)**

In both membranes configurations, without DB18-C-6, there is an increase in current at the positive end of the potential window which is related to transferring K^+ , while in the presence of the ionophore, both positive and negative peak currents in forward and reverse scans, respectively, occurred at more negative potential: these peaks correspond to facilitated transfer of K^+ by DB-18-C-6. The cyclic voltammogram profile (**Figure 2.4**) presents a diffusion-controlled regime of K^+ ions transfer across the interface from water to organic phase and vice versa which is linear. This is attributable to the limiting condition ($c_L \ll c_M$), and the results indicate the transfer of K^+ is controlled by ionophore diffusion in the organic phase which filled the pores in both types of membrane configuration. These results confirm complexation and de-complexation of K^+ with DB18-C6 is occurring at the interface in both pore configurations (with wider or narrower pore diameter on hydrophilic (aqueous) side of the membrane). Also these results are in agreement with previous work with silicon membrane-based ITIES.^{17, 129} However, there is a significant difference in amount of ion transfer between the two phases in these two types of pores. In pores with the interface located at the laser entry side (wider pore diameter at the hydrophilic side of the membrane), the peak current, which is related to diffusion of DB18-C-6 (forward scan) and diffusion of its complex with potassium (backward scan), is significantly higher (**Figure 2.4 a)** than the peak current in pores with the interface located on the laser exit side (narrower pore diameter at the hydrophilic side of the membrane) (**Figure 2.4 b)**.

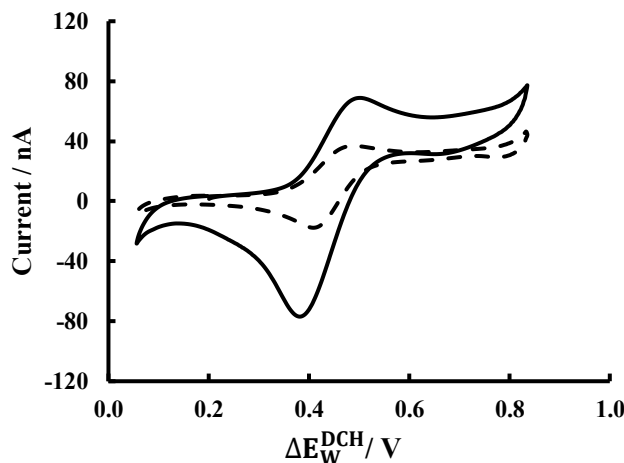


Figure 2.5 Cyclic voltammograms for the transfer of $TPrA^+$ across W/DCH interface located at the laser entry side (wider pore diameter at the hydrophilic side of the membrane) (solid line) and the interface located at laser exit side (narrower pore diameter at the hydrophilic side of the membrane) (dotted line) (the potential is versus the experimentally used reference electrodes).

In another study, $TPrA^+$ transfer of from aqueous phase to organic phase across interfaces located at laser entry side and exit side was investigated (**Figure 2.5**). $TPrA^+$ was used as a standard to provide the half-wave potential on the Galvani potential. As shown in **Figure 2.5**, the current due to $TPrA^+$ at interfaces located at laser entry side pores is significantly higher than current value at interfaces located at laser exit side.

2.3.2. Evaluation of reversibility of the system

In the limiting condition ($C_L \ll C_M$) in which the ionophore controlled all the processes across the interface, and with the reversible transfer of ions across the interfaces, the half-wave potential of ion transfer is defined as by equation 2.1 which is derived from the Nernst equation for a reversible ion transfer across the ITIES.¹³⁰

$$\Delta_o^w \phi_{1/2} = \Delta_o^w \phi_{M^+}^0 + \frac{0.059}{n} \log \frac{D_L}{D_{ML^+}} - \frac{0.059}{n} \log (\beta C_{M^+}) \quad \text{Equation 2.1}$$

Where $\Delta_o^w \phi_{1/2}$ is half-wave transfer potential of the ion, $\Delta_o^w \phi_{M^+}^0$ is the standard potential of ion transfer across the interface, n is the stoichiometry of the ion and ionophore, D_L and D_{ML^+} are diffusion coefficient of ionophore and complex in organic phase, respectively, which are assumed to be nearly the same, β is the equilibrium binding constant between ion and ionophore, and C_{M^+} is the concentration of ion in the aqueous phase. CVs of assisted transfer of different concentrations of K^+ are shown in **Figure 2.6**. With increasing ion concentrations, the transfer potential of K^+ is shifting to more negative values (as expected in eq. 2.1). This experiment was carried out in two types of

pores of glass membrane (Figure 2.6). Based on the equation 2.1, midpoint potential (E_{mid}) is plotted with concentration of K^+ (Figure 2.6).

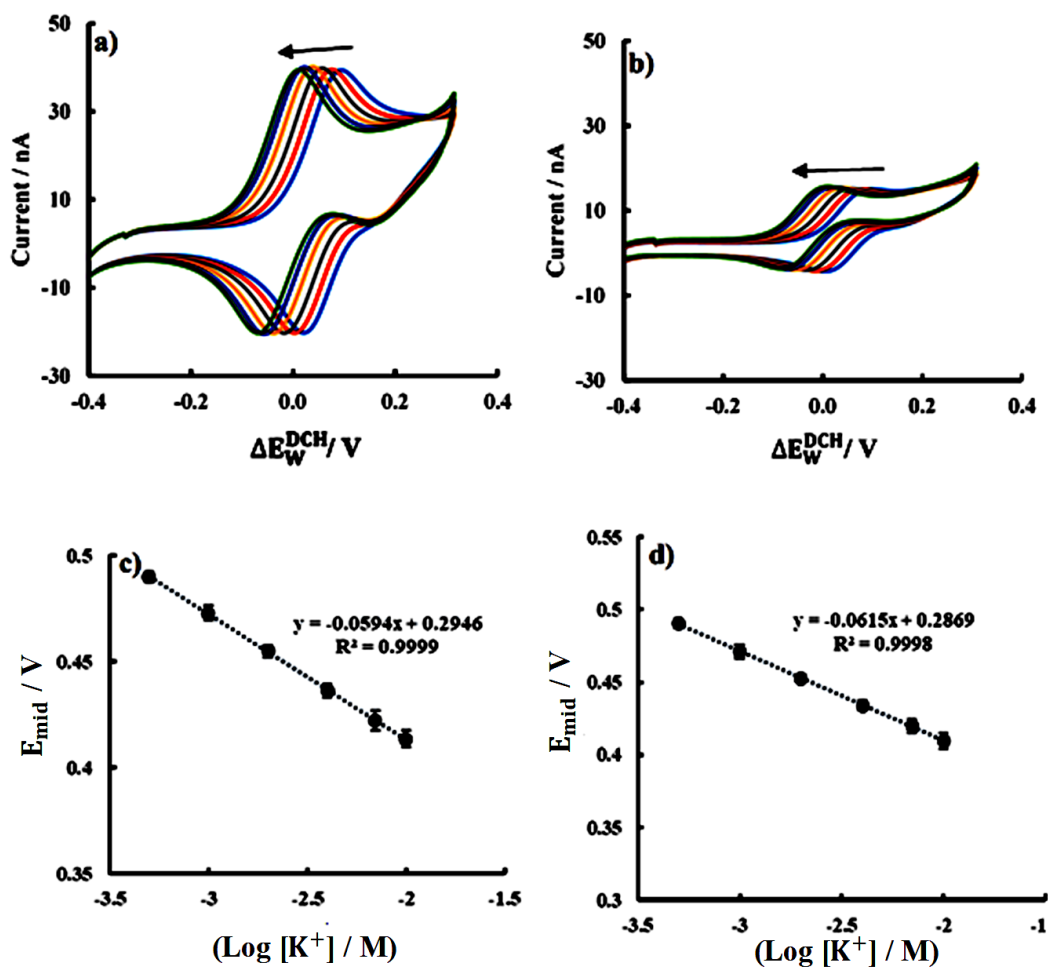


Figure 2.6. CVs for potassium ion concentrations: 0.5, 1, 2, 4, 7 and 10 mM and in the presence of 0.5 mM DB-18-C6 in the organic phase and 1 mM $MgCl_2$ as background electrolyte in the aqueous phase, with laser entry side pore **a)** and with laser exit side pore **b)** and plot of mid-point potential of potassium transfer across the interface with $\text{Log} [K^+]$ with laser entry side pore **c)** and with laser exit side pore **d)** (10 mV/s scan rate).

Regarding the average slope values for both membrane configurations (0.06 V/dec) which is close to the Nernst value ($\frac{0.059}{n}$ V/dec) where $n=1$, indicating stoichiometry of the ionophore and potassium is 1:1, which agrees with other reports.¹³¹⁻¹³⁶ Regarding the results for the binding constant (β) for K^+ with DB-18-C6, which can be calculated from the intercept value of the Nernst equation, and considering the value of $\Delta_{\text{DCH}}^{\text{W}} \phi_{K^+}^0 = 0.584$ V reported by Katano et al.¹³⁷ and using the equation 2.1, $\log \beta = 5.1$ was achieved for the binding constant between K^+ and DB-18-C6. There is no report to investigate facilitated transferring of K^+ by DB-18-C6 across water and DCH. However, the results obtained was compared with the calculated binding constant in other reports. For example, binding constants between K^+ and DB-18-C6 in 1,2-dichloroethane,¹³⁸ nitrobenzene,¹³¹ acetonitrile¹³³ were 9.9, 6.9, 4.7 respectively. Stability constant of different crown ethers with alkali metals depends on

ion solvation energy in different solvents. Comparison of the complex stability of DB18-C6 with alkali metals between water and different organic solvents shows that in the low polar solvents, there is an enhancement in binding constant.¹³⁸ Based on the value of the intercept, which is equal in both type of membrane configurations, it is expected the binding constant value between potassium and DB-18-C6 is independent of the size of pores.

After IR compensation of the voltammograms, the peak-to-peak separation values ($E_p^F - E_p^R$) for the ion transfer process at the two membrane configurations were different, as plotted with different concentrations of potassium (**Figure 2.7 a**). In the experiments with the interfaces located at membranes with higher diameter pores, the peak-to-peak separation was lower and closer to the Nernst value (60 mV) compared to the interfaces located at membranes with lower radii.

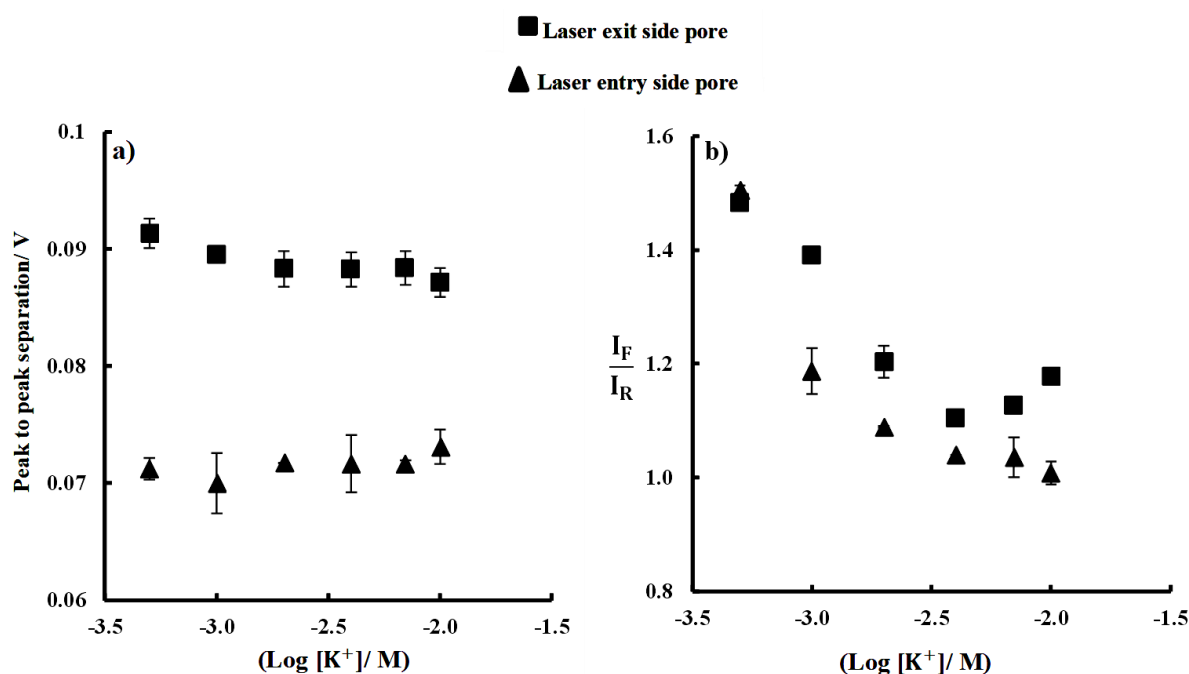


Figure 2.7 a) Peak to peak separation at different concentrations of aqueous phase potassium in the presence of 0.5 mM DB-18-C6 in the organic phase with two the membrane configurations b) ratio of forward and reverse peak currents at different concentrations of aqueous potassium in the presence of 0.5 mM DB-18-C6 in the organic phase with the two membrane configurations.

Another important parameter for reversibility of the system is the ratio of peak current in forward scan with peak current in reverse scan (I_p^F/I_p^R), which for reversible ion transferring is 1. This parameter was assessed for the two configurations of pores. For both pore types, especially with higher concentrations of potassium, the ratio is close to one (**Figure 2.7 b**) because with higher concentration of potassium the ionophore can control ion transfer process and the Nernst equation (equation 2.1)

can be achieved in this condition. In another study, with both membrane configurations, the results (**Figure 2.8**) show that the peak currents relate linearly with square root of scan rate, which is expected from the Randles-Sevcik equation for a linear diffusion regime.¹¹⁹ The diffusion coefficient of DB18-C6 in the organic phase based on this equation was determined to be 4.5×10^{-6} cm/s, which has good agreement with different reports.^{129, 138} Reversibility of the system was assessed in both membrane configurations, which are demonstrated in **Table 2.2**.

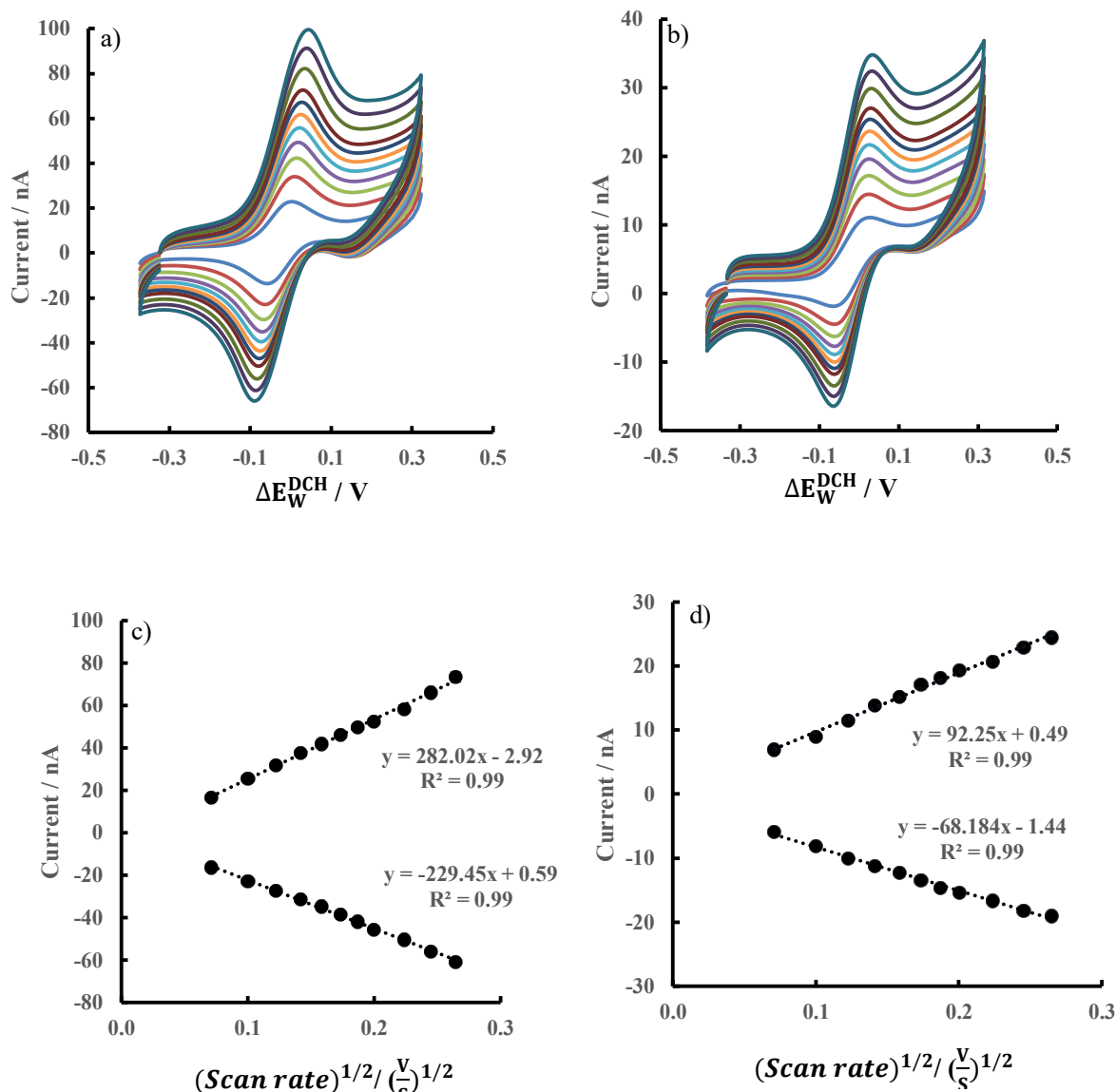


Figure 2.8. CVs of facilitated potassium transfer by 0.5 mM DB-18-C6 in organic phase and 10 mM KCl in aqueous phase at micro-ITIES array with sweep rate: 5, 10, 15, 20, 25, 30, 35, 40, 50, 60, 70 mV/s at laser entry side a) and laser exit side b) and confirmation of reversibility by the linear dependence of peak current with square root of scan rate (c) laser entry side pores (d) laser exit side pores (the potentials are transposed to Galvani Scale).

Table 2.2 Reversibility factors achieved by two types of the membrane configurations including: peak to peak separation, proportion of peak current of forward to reverse scan, linear relation of peak current with square root of scan rate, no shifting in potential with scan rate (n=3).

Membrane configuration	$E_p^F - E_p^R$ (V)	$\frac{I_p^F}{I_p^R}$	$I_p \propto \sqrt{v}$	E_p Shifting with v
Interface located at laser exit side pores	0.088(±0.002)	1.14(±0.01)	Linear	No
Interface located at laser entry side pores	0.072(±0.001)	1.25(±0.02)	Linear	No

Moreover, there was no shifting in peak potential with different scan rates in both forward and backward CV scans. According to the electrochemical results demonstrated in **Table 2.2**, facilitated potassium transfer across the micro-ITIES in both membrane configurations of pores, with wider and narrower in hydrophilic side, seems to be reversible. However, the membranes with interfaces located at the wider diameter pores on hydrophilic side show a higher amount of ion transfer which make this membrane more sensitive compared to narrower one.

2.4. Screening of sulfate ionophores by FIT at glass micropore array

2.4.1. Introduction

The sensing of anions is very challenging because of their large and different size, pH dependence, and their high hydration energies.¹³⁹⁻¹⁴² Among the Hofmeister series anions, (organic anions > ClO_4^- > SCN^- > $\text{I}^- \approx \text{salicylate}$ > NO_3^- > Br^- > Cl^- > HCO_3^- > $\text{HPO}_4^{2-} \approx \text{F}^- \approx \text{SO}_4^{2-}$), sulfate has highest hydration energy (1059 kJ mol^{-1} compared to 314 and 229 kJ mol^{-1} for NO_3^- and ClO_4^- , respectively).¹⁴³ So, quantification of sulfate anions in aqueous environment is very challenging compared to other anions.¹⁴⁴ Despite this, sulfate can be used as a surrogate in wastewater recycling plants so that there is a need to make a system to sense sulfate to allow evaluation of the performance and integrity of reverse osmosis (RO) membranes used in wastewater recycling, so determination of sulfate in water after RO and its comparison with the level of sulfate in water before RO can be an important factor for integrity of RO performance in wastewater recycling plants.¹⁴⁵ In addition, in biosynthesis and detoxification of endogenous and exogenous compounds in human cells, sulfate plays very important roles. Furthermore, sulfate is one of the end stage products in metabolic processes of sulphur-containing amino acids in biological cells.^{146, 147} According to these reasons, there are environmental, clinical, and pharmaceutical applications to sense sulfate ions. One of the most common methods to sense sulfate is ion chromatography coupled with conductometric detection

(IC-CD). However, for routine measurement this method is very expensive and complex¹⁴⁸. There are both optical and electrochemical method to sense sulfate. Optical methods include colorimetry and spectroscopy. In both methods, there is a lack of sensitivity and selectivity.^{149, 150} On the other hand, electrochemical methods are simple and reproducible with low equipment cost and online detection capability. In this study, electrochemical methods including cyclic voltammetry and differential pulse voltammetry were applied to sense sulfate. In addition, to selectively sense sulfate a new synthesised ionophore was used to detect sulfate.

2.5. Experimental Section: Facilitated Sulfate Transfer at ITIES

2.5.1. Reagents and materials:

In this study, synthesised sulfate ionophores were used in the organic phase to investigate interfacial complexation at water/NPOE interface by using of the glass micropore arrays with the interface located at the laser entry side. NPOE was used as the organic solvent instead of DCH, because the dielectric constant of this solvent is much higher than DCH and the more polar sulfate ionophores can be dissolved more easily and in higher concentration. Different synthesised sulfate ionophores were used, including *N,N'*-bis(2-acetamidophenyl)-5-(*tert*-butyl)isophthalamide (DCC-286), *N,N',N''*-(nitrilotris(ethane-2,1-diyl))tris(pyrrole-2-carboxamide) (DCC-287) and *N',N''*-(3,6-di-*tert*-butylcarbazole-1,8-diyl)bis(*N*-phenylthiourea) (PGP-59) (**Figure 2.9**) (from Murcia University in Spain) and Tris(2-aminoethylamine) (Tren) Tri-Squaramide with phenyl (Tren phenyl), anthracene (Tren anthracene) and 2-aminoethylamine (Tren)bis- CF_3 (Tren-bis CF_3) (from University of Sydney, Australia) (**Figure 2.10** a and b, respectively) were used for investigation of sulfate transfer at the interface. The potentials are transposed to Galvani Scale by using of TPrA⁺ and tetraethylammonium (TEA⁺) to provide the Galvani potential scale for these experiments with the Spain ionophores and Sydney ionophores, respectively.

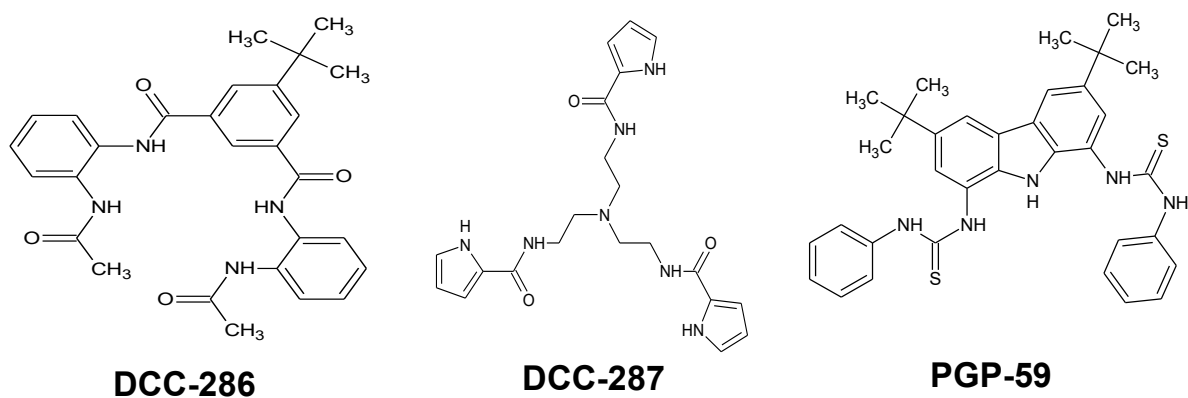


Figure 2.9 Structure of different sulfate ionophores *N,N'*-bis(2-acetamidophenyl)-5-(tert-butyl)isophthalamide (DCC-286), *N,N',N''*-(nitriлотris(ethane-2,1-diyl))tris(pyrrrole-2-carboxamide) (DCC-287) and *N',N''*-(3,6-di-tert-butylcarbazole-1,8-diyl)bis(*N*-phenylthiourea) (PGP-59) (Synthesised by the group of Dr. David Curiel, Murcia University, Spain).

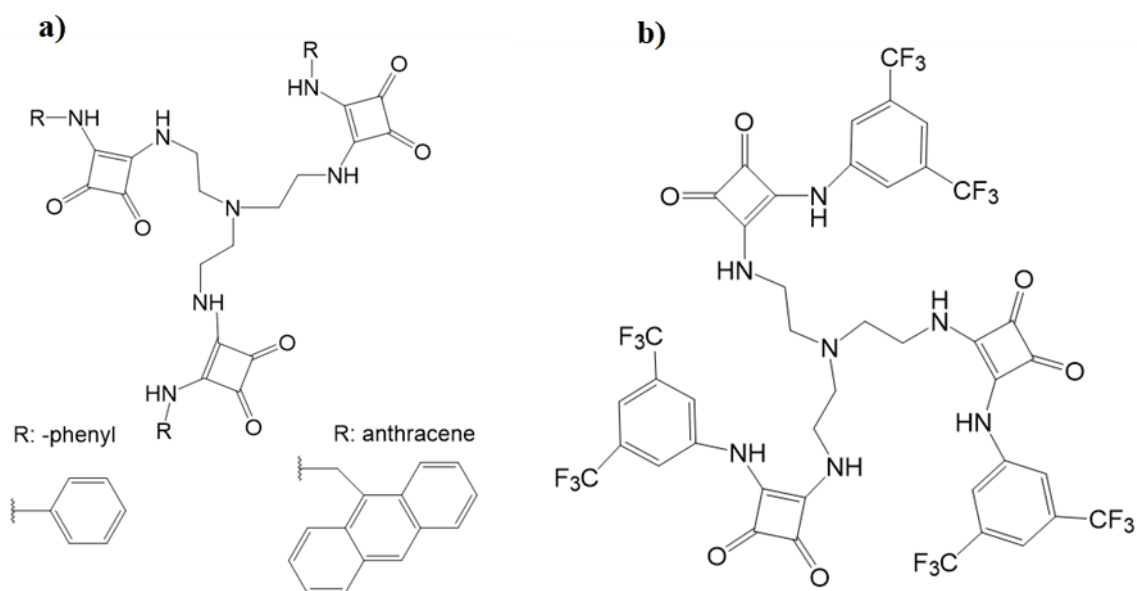


Figure 2.10 Structure of a) Tren-Phenyl and Tren-Antracence b) (2-aminoethylamine)(Tren)bis- CF_3 (Tren-bis CF_3) (Synthesised by the group of Prof. Katrina Jolliffe, University of Sydney).

2.5.2. Electrochemical set up for sulfate sensing:

The electrochemical set up for sensing of sulfate is same as the set up for K^+ , just there is not a background electrolyte in aqueous solution because the presence of any background electrolyte interferes with sulfate. In addition, instead of Ag/AgCl in the aqueous phase, Ag electrode is used because the Ag/AgCl electrode can impact on sulfate response because of Cl^- ions. The electrochemical cell composition to sense sulfate ions is shown in **Figure 2.11**. In addition, in this experiment NPOE was used as the solvent, because the dielectric constant of NPOE is higher than DCH and sulfate ionophore solubility is higher than in DCH. NPOE is a safer solvent compared to DCH and it is better alternative for development of a sulfate sensor.

Ag	AgCl	1 mM BTPPACl (10 Mm LiCl)	10 mM BTPPATPBCl 0.25 mM Sulfate Ionophre(NPOE)	Aqueous phase, Y mM Li ₂ SO ₄	Ag
----	------	------------------------------------	---	--	----

Figure 2.11 Electrochemical set up to sense sulfate ionophore

The electrochemical set up was applied to sense SO_4^{2-} by CV and DPV methods. In CV, the scan direction is from more positive potentials to more negative potentials with scan rate 10 mV/s. In DPV method same as CV, the scan direction is from more positive potentials to more negative potentials (0.550 to 0.05 V), conditioning potential is 0.550 V and equilibration time and modulation time are 60 s and 0.05 s, respectively.

2.5.3. Results and Discussion:

CVs were recorded for experiments with aqueous solutions containing sulfate (10 mM Li_2SO_4) in contact with organic phases either with or without the ionophores for at interfaces located at laser entry side pores. CVs in the presence and absence of DCC-286, DCC-287 and PGP-59 in the organic phase are shown in **Figure 2.12** a, b and c. As it is shown interfacial complexation of sulfate was achieved in the presence of these ionophores, and it is shown in the higher current values than the CVs in the absence of these ionophores. However, the sulfate transferring potential is very close to the transfer potential of organic cations (BTPPA^+) from organic phase to aqueous phase. So, there is no ability to distinguish between the current related to sulfate transfer and the organic cation transfer.

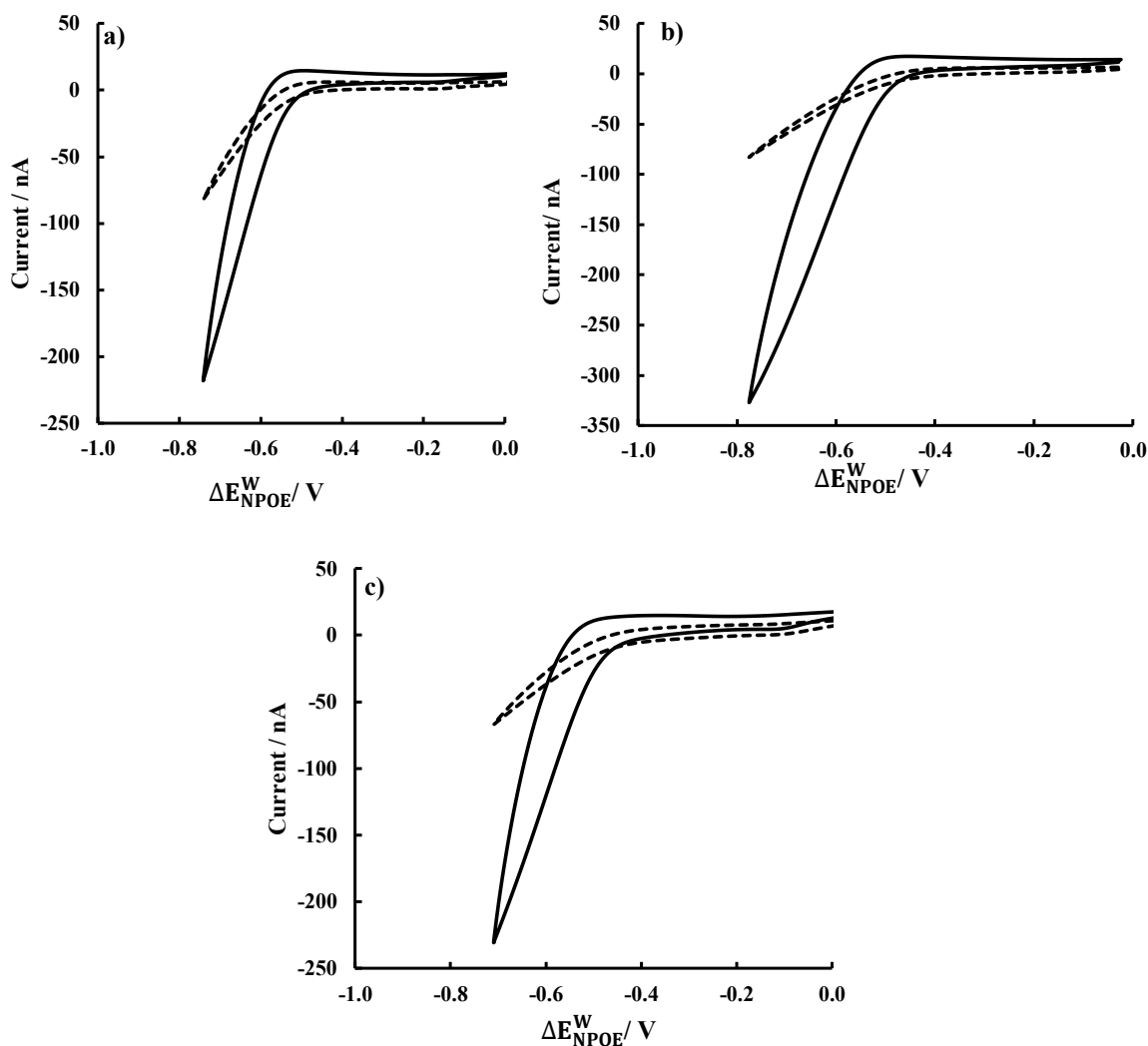


Figure 2.12 Cyclic voltammograms for the transfer of SO_4^{2-} across W/NPOE interface in absence (dotted line) and presence (solid line) of 0.25 mM a) DCC-286 b) DCC-287 and c) PGP-59 in the presence of 10 mM Li_2SO_4 pores with laser entry side.

In the same study, Tren phenyl, anthracene (Tren anthracene) and Tren-bis CF_3 (from University of Sydney, Australia) (**Figure 2.10** a, b and c, respectively) were used to investigate sulfate transfer at the interface. CVs related to response of interfacial sulfate complexation at the interface in the presence and absence of Tren phenyl and Tren anthracene were shown in **Figure 2.13** Cyclic voltammograms for the transfer of SO_4^{2-} across W/NPOE interface in absence (dotted line) and presence (solid line) of 0.25 mM a) Tren-Anthracene b) Tren-Phenyl in the presence of 10 mM Li_2SO_4 pores with laser entry side and b, respectively. There is strong complexation effect of sulfate with Tren phenyl in more positive potential compared to organic cation (BTPPA⁺) transfer (**Figure 2.13** b) while there is not strong complexation between sulfate and Tren anthracene (**Figure 2.13** b).

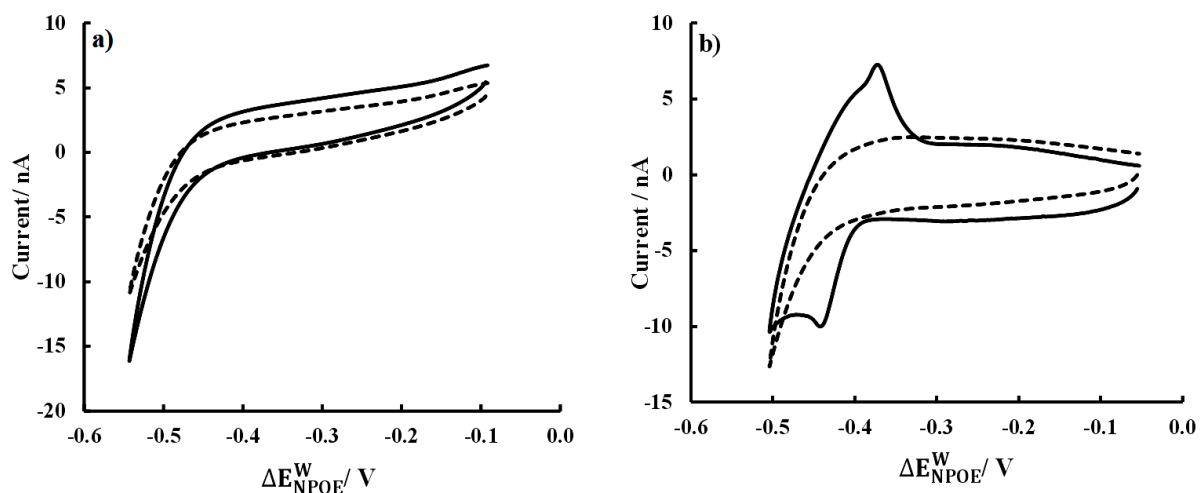


Figure 2.13 Cyclic voltammograms for the transfer of SO_4^{2-} across W/NPOE interface in absence (dotted line) and presence (solid line) of 0.25 mM a) Tren-Antracene b) Tren-Phenyl in the presence of 10 mM Li_2SO_4 pores with laser entry side

Another synthesised sulfate ionophore called Tren-bis CF_3 (From University of Sydney, Australia) was used (**Figure 2.10 b**) to investigate sulfate transfer at ITIES. CVs related to the organic phase with and without the ionophore (**Figure 2.14**) showed that there is interfacial sulfate complexation in more positive potential than $BTPPA^+$ transfer potential, and the potential in the presence of Tren-bis CF_3 is more positive than Tren phenyl. Thus, Tren-bis CF_3 was chosen as best ionophore for facilitated sulfate transfer among the different synthesised sulfate ionophores. The CV profile (**Figure 2.15**) presents diffusion shape regime of SO_4^{2-} ions across the membrane from water to organic phase and vice versa which is attributable to the limiting condition ($c_L \ll c_M$) which is mentioned earlier with complexation of K^+ with DB-18-C6. Thus transferring of SO_4^{2-} is controlled by the ionophore diffusion in organic phase which filled the pores, and these results which confirm complexation and de-complexation of assisted SO_4^{2-} with Tren-bis CF_3 is occurring at the interface in the pores (**Figure 2.14**). Based on the tetraphenylarsonium tetraphenylborate (TATB) assumption, formal transfer potential of $TPrA^+$ and TEA^+ from water to NPOE are -0.116 and -0.003 V, respectively.^{151, 152}

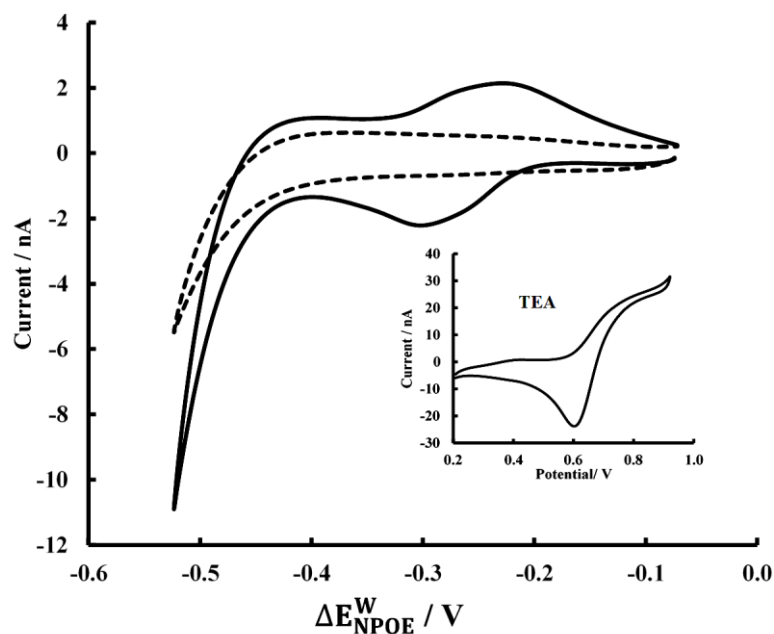


Figure 2.14 Cyclic voltammograms for the transfer of SO_4^{2-} across W/NPOE interface in absence (dotted line) and presence (solid line) of 0.25 mM Tren-bis CF_3 in the presence of 10 mM Li_2SO_4 pores with laser entry side, inside is the cyclic voltammograms of transferring TEA (50 μM) at W/NPOE interface

2.5.4. Nernstian behaviour of facilitated sulfate transfer:

Nernstian behaviour of CVs of facilitated ion transfer of different concentrations of SO_4^{2-} ions are shown in **Figure 2.15 a**. These show that with increasing of the ion concentrations, the transfer potential of SO_4^{2-} is shifting to more positive values (as expected in eq. 2.1). This experiment was carried out the glass membrane configuration with the ITIES located at the laser entry side. Based on the equation I, midpoint potential (E_{mid}) is plotted with concentration of SO_4^{2-} (**Figure 2.15 b**). Since SO_4^{2-} has two negative charge and based on the Nernst equation, the Nernstian slope for 1:1 complexation of SO_4^{2-} with Tren-bis CF_3 is around 0.030 V and the real Nernstian slope in **Figure 2.16 b** is $0.024(\pm 0.003)$ V.

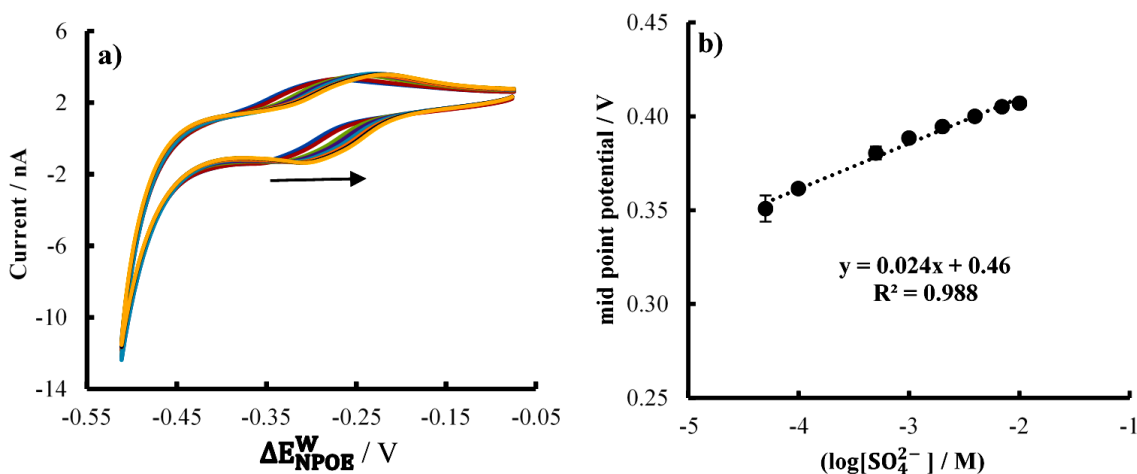


Figure 2.15 a) CVs for sulfate ion concentrations : 5×10^{-5} , 10^{-4} , 5×10^{-4} , 10^{-3} , 2×10^{-3} , 4×10^{-3} , 7×10^{-3} and 10^{-2} M of SO_4^{2-} and in presence of 0.25 mM Tren-bis CF_3 in 10 mV/s scan rate b) plot of mid-point potential of potassium transfer across the interface with Logarithm of SO_4^{2-} ($n=3$).

Differential pulse voltammetry (DPV) was utilized to reduce the detection limit of SO_4^{2-} at the micro-ITIES arrays, in an effort to achieve even greater improvement in sensitivity of SO_4^{2-} . As mentioned earlier, DPV is a widely recognized technique that can attain a lower detection limit (**Figure 2.16 a**). The sensitivity was further enhanced through the utilization of background subtraction. At the onset of the run, a blank experiment (zero concentration of SO_4^{2-}) was recorded for the purpose of performing background subtraction. Subsequently recorded differential pulse voltammetric responses to SO_4^{2-} were each subjected to subtraction by the previously recorded blank response (**Figure 2.16 a**). The low detection limit was estimated from the calibration curve by linear extrapolation of current versus logarithm of SO_4^{2-} concentrations (**Figure 2.16 b**) and is 18 μM . Thus, by DPV method more sensitivity is achieved to sense SO_4^{2-} ion compared to cyclic voltammetry.

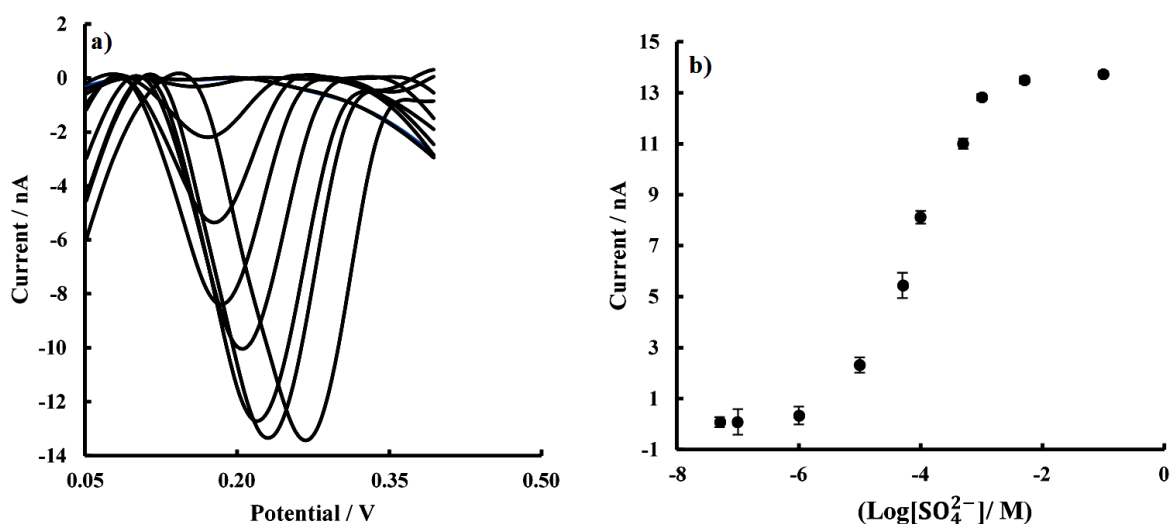


Figure 2.16 a) DPV back ground subtraction responses related to sulfate interfacial complexation at Water/NPOE interface in the presence of different concentrations of SO_4^{2-} ions (5×10^{-8} , 10^{-7} , 10^{-6} , 10^{-5} , 5×10^{-5} , 10^{-4} , 10^{-3} and 5×10^{-3} M) (which is obtained by subtraction from each voltammogram the experiment in which SO_4^{2-} concentration is zero), b) Calibration curve of logarithm of different concentrations of sulfate ions versus current ($n=3$).

2.6. Conclusion

Facilitated potassium transfer by DB18-C6 was investigated across micro-ITIES formed at micro-pore arrays with two types of pores for interfaces located at the laser entry side and the laser exit side. Investigation of thermodynamic parameters shows there is no significant difference between these two types of pores while kinetically there is considerable difference between two pores, because the amount of mass transfer across the interfaces in the pores at the laser entry side (wider at hydrophilic side) was significantly higher than mass transfer in pores in laser exit side (narrower at hydrophilic side) and consequently higher sensitivity for these types of pores. In second part of this chapter, different synthesised sulfate ionophores were evaluated for facilitated sulfate transfer at water/NPOE interfaces formed at laser entry side of glass membranes. There is interfacial complexation of SO_4^{2-} with two of the ionophores (including Tren-phenyl and Tren-bis CF_3). Nernstian behaviour was examined with different concentrations of SO_4^{2-} ions in the presence of Tren-bis CF_3 ionophore. DPV was used to determine the limit of detection of sulfate in pure water, which is 18 μ M. Facilitated ion transfer at liquid/liquid interface can be used to develop ion sensors, but it suffers from instability and to provide more robustness of the sulfate sensor, can be obtained by using the synthesised sulfate ionophores in organogel or using them in a solid contact sensor format.

3. Evaluation of a Ru-bipod complex as a redox transducer for membrane-based voltammetry of anions

3.1. Introduction:

Detection methods based on ion transfer between aqueous samples and polymeric membranes have developed rapidly due to their clinical and environmental applications.¹⁵³⁻¹⁵⁵ In some cases, zero current potentiometry has been replaced by dynamic electrochemical methods to improve limits of detection, selectivity and recalibration frequency.^{156, 157} Additionally, conventional configurations of ion selective electrodes (ISEs) with fragile internal solutions have been replaced by more promising solid contact ion selective electrodes (SC-ISEs)¹⁵⁸ in which the sensing thin polymeric layer is directly in contact with a conductive electrode and with an ion-to-electron transducer material. This approach was introduced by Shi and Anson^{159, 160} to evaluate electron transfer chemistry of redox molecules (e.g. ferrocene) dissolved in a thin layer of organic solvent interposed between a graphite surface and an aqueous phase. Subsequently, Bond and co-workers used the redox behavior of 7, 7, 8, 8-tetracyanoquinodimethane to control ion transfer into such a thin film^{161, 162}. To maintain electro-neutrality in the film, redox reactions are accompanied by ion transfer. Using voltametric approaches, the oxidation and reduction potentials of the redox compound within the thin film depend on the concentration of transferring ion in the contacting the aqueous phase and can be used as an analytical signal. A wide range of electroactive materials were used as SC-ISEs which part of them mentioned in table 3.1.

A key component in these thin films is the redox material. Some of the most widely-used such materials are conducting polymers like poly (3,4-ethylenedioxythiophene) (PEDOT) and poly(3-octylthiophene) (POT) which are commonly applied in SC-ISEs.¹⁶³⁻¹⁶⁶ However, their low redox capacity, significant difference between anodic and cathodic currents, lack of device-to-device reproducibility, and electrochemical instabilities specifically in anion sensing have driven the search for alternatives as ion-to-electron transducers¹⁶⁷ A range of electroactive materials has been used in SC-ISEs, such as ferrocene derivatives, cobalt and osmium complexes, and cationic [6]-helicenes.^{112,}

115, 168-170 Generally, these materials are directly dissolved in the membranes or covalently attached to the sensing layers.^{171, 172} Ferrocene (Fc) has been applied to sense heparin or carbonate but it did not behave reversibly and was unstable in the thin film, specifically in the presence of chloride¹⁶⁸ Another approach to improve the stability of Fc is its immobilization as a monolayer on glassy carbon electrodes¹⁵⁵ but this limits the choice of redox materials to those suitable for surface modification.¹⁷³ Molecular redox materials can be immobilized by covalent attachment¹⁷⁴ or by $\pi - \pi$ interactions which can exhibit limitations like slow electron transfer kinetics or instability on the electrode surface, respectively. As an alternative redox probes, more promising osmium complexes were applied and produced more stable and reversible responses compared to Fc.¹⁶⁹ However, the electrochemical response related to this complex was strongly dependent on the concentration of background electrolytes and their proportion to the complex concentrations, and can be responsive to both cations and anions, and to develop sensors to provide sensitivity just to anions which is the purpose of this study can be problematic.

Table 3.1 : Different electroactive materials which used in SC-ISEs

Redox materials	Analyte [Reference]
CWEs (1971)	$Ni^{2+}, Cu^{2+}, Mg^{2+}, Ba^{2+}, Sr^{2+}, Pb^{2+}$ and Zn^{2+} ¹⁷⁵
PPY (1992)	$BF_4^-, Cl^-, NO_3^-, ClO_4^-$ and SCN^- ¹⁷⁶
POT (1994)	Ca^{2+}, Li^+ and Cl^- ¹⁷⁷
PANI (1995)	Li^+ and Ca^{2+} ¹⁷⁸
PEDOT (1999)	K^+ ¹⁷⁹
SAMs (2000)	K^+ ¹⁸⁰
C_{60} and CNT_s (2008)	K^+ ^{181, 182}
3DMC (2007)	K^+ ¹⁸³
GR and $AuNP_s$ (2011)	K^+ ^{184, 185}

Redox materials	Analyte [Reference]
<i>PtNP_s</i> , <i>AuNC_s</i> and CB (2012)	K^+ ¹⁸⁶⁻¹⁸⁸
Co^{2+}/Co^{3+} and <i>IL_s</i> (2013)	K^+ ^{112, 189}
<i>IC_s</i> (2013)	Li^+, K^+ and Na^+ ¹⁹⁰
CIMC and NP-Au (2014)	K^+ ^{104, 191}
TCNQ (2015)	K^+ and Na^+ ¹⁰⁵
TTF(2015)	NO_3^- ¹⁹²
<i>MoS₂</i> nanoflowers(2016)	K^+ ¹⁹³
μ PC(2017)	K^+ ¹⁹⁴
Os(II)/Os(III) (2017)	Na^+ and ClO_4^- ¹⁶⁹
LIG(2018)	NH_4^+ and NO_3^- ¹⁹⁵
<i>MOF_s</i> (2018)	K^+ and NO_3^- ¹⁹⁶
Cationic[6] Helicenes (2018)	Na^+ and CO_3^{2-} ^{115, 170}
<i>RuO₂</i> nanoparticles MXenes (2019)	K^+ and Ca^{2+} ^{197, 198}

Although several studies reported reliable and stable SC-ISEs, knowledge about the ion-to-electron transduction mechanism is incomplete, and there is an on-going need to investigate new redox materials to broaden the range of redox transduction materials and to find and better understand these sensing methods. In this regard, Ruthenium (Ru) transition complexes can be promising alternative to study ion transfer at liquid-liquid interface, because studies suggested that the redox potentials and solubility of Ru complexes in organic phase can be changed by their design around coordination sphere.¹⁹⁹ This property of Ru complex brings flexibility as a redox material in ion to electron transduction system. Very recently, a hetroleptic Ru complex was used at three-phase junction system²⁰⁰ The complex exhibited sensitivity to different anions at this system and its redox potential is

tunable by changing aqueous phase pH. However, three phase junction system with organic liquid phase (nitrobenzene) is unsuitable for development of sensors.²⁰⁰

In different reports, different plasticizers were used to investigate their effect on sensitivity and selectivity of the ISEs²⁰¹⁻²⁰³ because one of the key components of polymeric layer in ISEs is plasticizers and their proportion, lipophilicity, minimum exudation from polymeric layer, low vapor pressure are important to choose proper plasticizer for polymeric membrane in ISEs²⁰⁴. Additionally, dielectric constant of plasticizers should be enough, because some studies suggested that the polymeric-based substrates with plasticizer with higher dielectric constant, show more ionic conductivity.²⁰⁵⁻²⁰⁷ Since in different membrane compositions 60 to 70 percentage of the weight of the membranes are plasticizers,²⁰⁸ dielectric constant of the plasticizers are key factor in liquid membrane²⁰⁴ and can determine dielectric constant of polymeric membranes.²⁰⁹

In this work, we have investigated a hydrophobic homoleptic bis-tridentate Ru-bipod complex $[\text{Ru}(\text{bipod})_2]^{2+}$ (where bipod is 2,6-bis(1-(2-octyldodecyl)benzimidazol-2-yl)pyridine)) as a redox-active ion-to-electron transducer in thin polymeric films. The aim of this study was to investigate a new material suitable for use in ion-to-electron transduction and to assess its suitability for anion detection in a SC-ISE sensing system. Cyclic voltammetry was used to characterize the anion responses with thin film compositions incorporating the Ru-bipod complex. Furthermore, for first time, effect of plasticizers on ion-to-electron transduction system were evaluated by usage of two plasticizers with high dielectric constant (NPOE; ϵ_r : 23.6) and low dielectric constant (DOS; ϵ_r : 3.9).

3.2. Experimental section

3.2.1. Reagents.

Potassium chloride, potassium hexafluorophosphate, potassium nitrate, potassium perchlorate, potassium sulfate, tetrakis(4-chlorophenyl)borate tetradodecylammonium salt (ETH500), bis(2-ethylexyl)sebacate (DOS), 2-nitrophenyloctylether(NPOE), anhydrous tetrahydrofuran (THF), high molecular weight poly(vinyl chloride) (PVC) and the sulfate ionophore (S.I.) were purchased from Sigma Aldrich in analytical grade. Aqueous solutions were prepared in deionized water (resistivity 18.2 M Ω cm; USF Purelab with UV). 2-Octyl-1-dodecanol (Sigma Aldrich) and Ruthenium (III) trichloride hydrate (Heraeus GmbH) were used without further purification. 1-Bromo-2-octyldodecane was prepared from 2-octyl-1-dodecanol according to literature method²¹⁰.

3.2.2. Instrumentation and measurements

A three-electrode electrochemical cell was used for all measurements, comprising a thin film-coated glassy carbon (GC) disc working electrode (3 mm diameter) (CH Instruments), a Ag/AgCl/3 M NaCl reference electrode (model MF-2056, BASi), and a platinum disc as counter electrode, and placed in a Faraday cage. Electrochemical experiments were conducted with an Autolab PGSTAT302N electrochemical workstation (Metrohm, The Netherlands) with NOVA software. A CH1900b potentiostat (CH Instruments Inc., USA) was used to measure uncompensated resistance. The organic thin films were spin-coated onto GC electrodes using an inverted overhead stirrer (model IKA RW20).

3.2.3. Film preparation

Same as other reports of preparation of thin film^{115, 170} different thin film membrane compositions were prepared (Table 3.2). For each formulation, all components (total mass 12.5 mg) were dissolved in 0.5 mL THF. Then 20 μ L of this cocktail easily was spin coated on a GC electrode by reversed stirrer at 1500 rpm for one minute. The electrode was then immediately used for measurements. The thickness of the spin-coated films was calculated by estimating the volume of the cocktail remaining on the surface after spinning, from the charge under the voltammetric peaks, and considering the density of PVC-NPOE membranes;²¹¹ the estimated thickness is 0.9 ± 0.3 μ m (n = 15).

3.2.4. Synthesis of Ru-bipod complex.

The Ru-bipod complex (**Figure 3.1**) was synthesized as described in the Appendix A (**Figure A-1**) and characterized by ESI-MS, ¹H NMR and cyclic voltammetry (**Figures A-2, A-3, A-4**, respectively).

3.3. Results and Discussion

The synthesis and characterization of the new Ru-bipod (**Figure 3.1 a**) as a molecular redox transducer for thin voltammetric sensing membranes are reported here. The membrane contains the complex which acts as an ion-to-electron transducer. By imposing an oxidizing potential, oxidation of Ru-bipod is accompanied by anion transfer into the membrane to compensate the positive charge resulting from oxidation of the complex. When that oxidized complex is subsequently reduced, anions are expelled from the membrane back into the aqueous phase, as summarized in **Figure 3.1 b**.

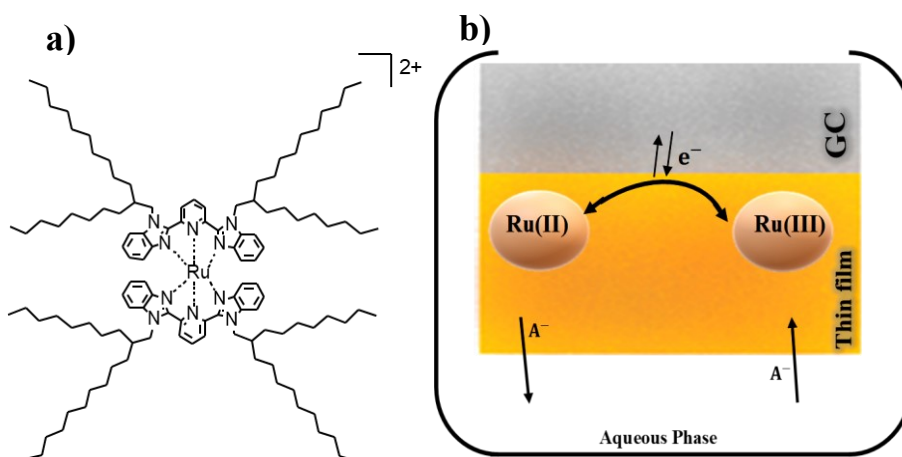


Figure 3.1 a) Structure of Ru-bipod complex b) Schematic illustration of the working mechanism of the thin film electrode for anion detection. The film contains the Ru-bipod complex. An applied potential provokes oxidation at the electrode surface (GC) and excess of positive sites (*Ru(III)*) are generated at the GC-film interface. The excess positive charge is balanced by ingress of anions from the aqueous solution into the thin film. Once the reversed potential is applied, anions are expelled from the membrane to maintain electroneutrality.

Table 3.2 : Different compositions of the membranes (M1-M10) in total mass which is 12.5 mg in 500 μ l THF. (a: mmol/ kg, b : mg, S.I : Sulfate Ionophore).

Membrane	ETH500 ^a	Ru complex ^a	PVC ^b	DOS ^b	NPOE ^b	S. I ^a
M1	130	22	3.3	6.6	-	-
M2	130	33	3.2	6.4	-	-
M3	130	65	2.9	58	-	-
M4	-	65	3.6	7.2	-	-
M5	-	65	3.6	-	7.2	-
M6	130	65	3.2	-	6.6	-
M7	130	22	3.3	-	6.6	-
M8	130	33	3.2	-	6.4	-
M9	65	65	3.2	6.5	-	-
M10	65	65	3.2	-	6.5	-
M11	-	65	3.2	-	6.5	130

3.3.1. Cyclic Voltammetry Confined in Thin Films.

The electrochemical behavior of redox molecules in organic solution is very similar to that in polymeric sensing films.¹⁶⁹ As reported previously about SC-ISEs, the membrane response can be tuned to be responsive to either cations or anions. In this study, the membrane compositions were adjusted to be responsive to anions.¹⁶⁹ In all, two membrane configurations for anion transfer were investigated, with and without sulfate ionophore. The Ru-bipod complex was easily dissolved in the hydrophobic membrane. The thin film containing the Ru-bipod complex is responsive to anions, regardless of the presence or absence of ETH500 as a lipophilic background electrolyte. Once a sufficiently positive potential is imposed, the Ru-bipod complex is oxidized, and anions are extracted from the aqueous phase into the membrane to compensate this unbalanced positive charge. This phenomenon is reversed when the complex is reduced, resulting in anion expulsion from the membrane to the aqueous phase.

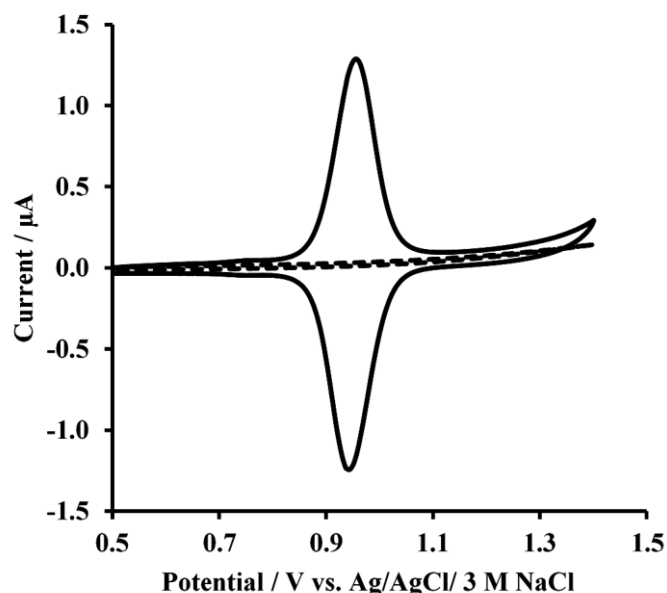


Figure 3.2 Cyclic voltammetry obtained using membrane M5 (Table S1, containing 65 mmol/kg Ru-bipod complex, 33% PVC and 66% NPOE) in the absence (dashed line) and presence (solid line) of 10 mM KPF_6 . Scan rate: 10 mV/s.

Figure 3.2 (solid line) shows a typical CV of the Ru-bipod complex within a polymeric thin film. It shows oxidation and reduction processes with features as expected for a thin film, including reversibility, narrow peak width at half-height (90 mV) as shown in **Figure 3.2** (solid line),²¹² low peak-to-peak separation (close to 0 mV), and no redox reaction in the absence of anions in the aqueous phase (Figure 3.2, dashed line). Although the behaviour strongly depends on the characteristics of the electroactive species, it is also affected by the composition of the polymeric membranes. Different PVC-based membrane compositions were evaluated (Table 3.1). Consecutive CVs for each membrane

formulation were recorded in the presence of aqueous 10 mM KPF_6 (Figure C-1 in Appendix C). The best CV response was achieved with 65 mmol/kg of the Ru-bipod complex (**Figure 3.2**). It seems that in contrast to earlier reports in which lipophilic background electrolyte (i.e. ETH500) can promote fulfilment of electro-neutrality in anion sensing,^{169, 170} here no evidence was found for lower resistance and better sensitivity in the presence of ETH500 (Figure C-1 in Appendix C). In addition, the responses toward different anions (Hofmeister series) indicate better selectivity in the absence of ETH500 (**Figure 3.3**), i.e. the responses in the presence of different anions are better separated along the potential axis. In addition, except for sulfate, there is a linear relation between the CV mid-point potential of the membrane response with the hydration energies of the anions studied (Figure C-2 in Appendix C.). However, that sulfate does not fit this linear response can be attributed to its two negative charges, while the other anions have a single negative charge. Thus, the observed voltammetric response is a combination of the oxidation of the Ru-bipod complex and the transfer of counter-anion into the membrane film. More hydrophilic anions result then in a higher overall potential for this combined process.

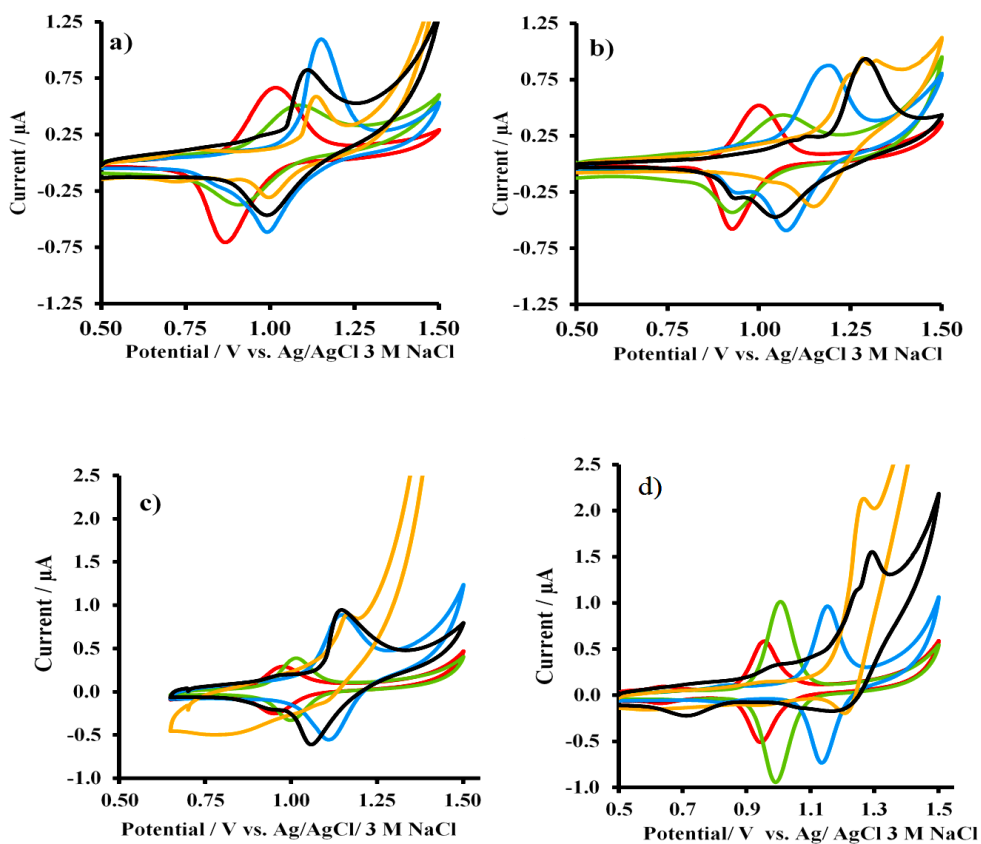


Figure 3.3 Hofmeister Series for different anions (10 mM of different anions, PF_6^- (red), ClO_4^- (green), NO_3^- (blue), Cl^- (orange) and SO_4^{2-} (black) using a) **M3** b) **M4** , c) **M6** and d) **M5** as the membranes with scan rate 10 mV/s (n=6).

Based on the first scan of each membrane containing ETH500, a current was observed in the forward scan due to oxidation of ETH500 (**Figure 3.4**). This large oxidation current has a negative impact on selectivity (as observed in the Hofmeister series responses for different compositions of the membrane (**Figure 3.3**)). Thus, the observed redox potential of the Ru-bipod complex in the presence of different anions is affected by oxidation of ETH500, resulting in the midpoint potentials recorded in the presence of different anions being closer to each other.

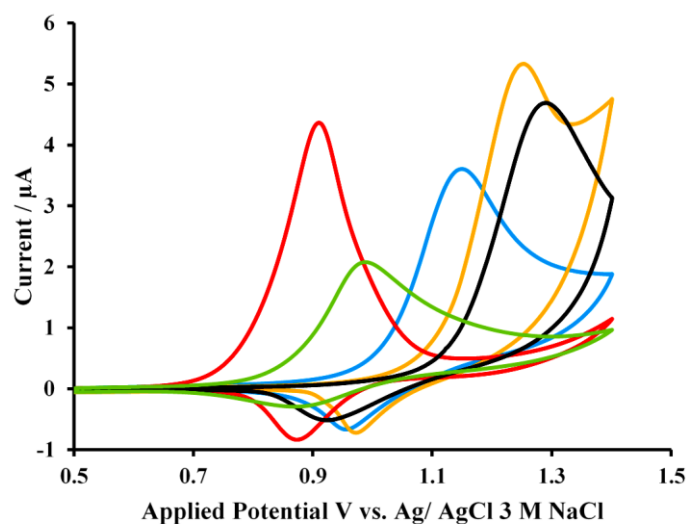


Figure 3.4 First scan of the membrane **M3** (table S1) in the presence of 10mM of different anions, PF_6^- (red), ClO_4^- (green), NO_3^- (blue), Cl^- (orange) and SO_4^{2-} (black).

Since the percentage of the plasticizers in the polymeric membrane is more than 60 percentage of the whole weight of the membrane, dielectric constant of the plasticizers determines the dielectric constant of the membrane. So, the dielectric constant of plasticizers employed in PVC membranes has a crucial impact on ISE.²¹³⁻²¹⁵ Two plasticizers with different dielectric constants were investigated (**Figure 3.5**). Evaluation of the peak-width at half-height and peak-to-peak separation at low scan rate (10 mV/s) indicated that there is a dramatic impact on these parameters for membranes prepared with either NPOE or DOS, but with the same composition otherwise (**Figure 3.5 a and b**). The membrane with NPOE shows a more promising response than the one with DOS. In thin films, peak-width in half-height can be attributed of electrostatic effects produced by neighbouring charged species in thin films.²¹⁶

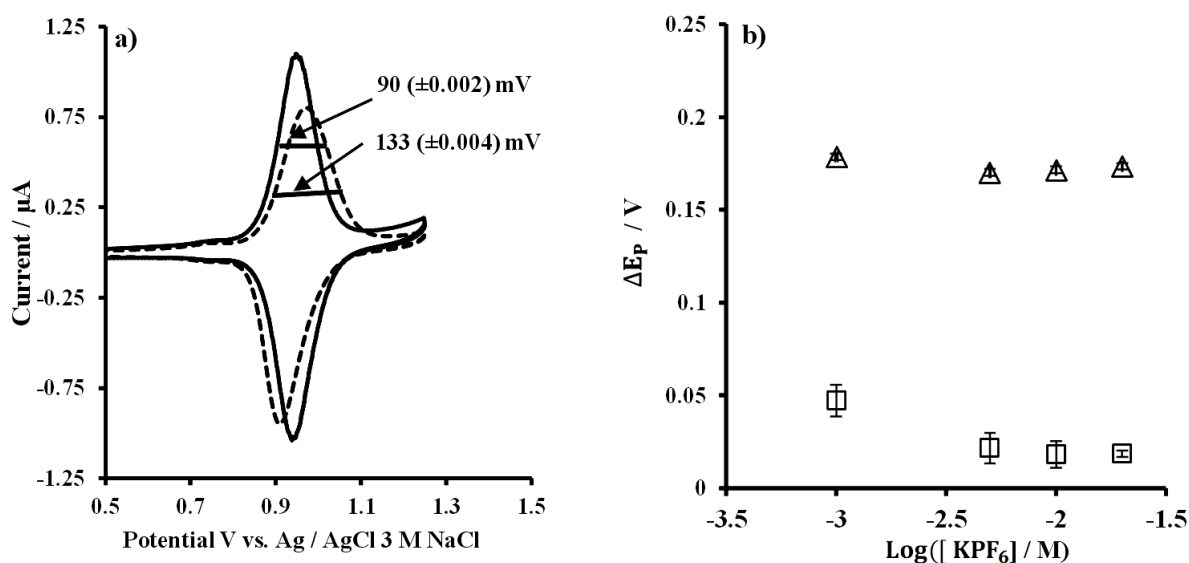


Figure 3.5 a) Comparison of half width potential by using different plasticizer of NPOE (solid line) (M5, 65 mmol/Kg Ru-bipod, 33% PVC, 66% NPOE) and DOS (dotted line) M4 (65 mmol/Kg Ru-bipod, 33% PVC, 66% DOS) in presence of 10 mM KPF_6 b) comparison of peak to peak separation by using NPOE (square shapes) and DOS (triangle shapes) as a plasticiser in presence of different concentrations of KPF_6 ($n=6$).

It is well-known in the literature that voltammetry of thin films is dependent on interactions between oxidised and reduced forms of the redox couple. This is encapsulated in the Frumkin isotherm which includes parameters for interactions of the different forms of the redox couple which also depend on the scan rate and the surface coverage. The magnitudes of these parameters determine whether peak-widths at half-height are less than, equal to or greater than $90.6/n$ mV.²¹² The greater peak-width at half-height in the presence of DOS (133 mV) can be related to the difference in dielectric constants of the two plasticizers (ca. 24 and 4 for NPOE and DOS, respectively ca. 4)²¹⁷ because, in the membrane with less dielectric constant, the Ru-bipod complexes can experience greater neighbouring electrostatic forces by charged species in the thin film. Additionally, CVs of the membranes containing NPOE or DOS at different scan rates (**Figure 3.6** a and b, respectively) revealed a substantial shift in peak potentials with scan rate in the DOS-based membrane. Also, in the presence of DOS, there is no linear relation of the peak current with scan rate while the relation is linear in the presence of NPOE, exhibiting typical thin film behaviour (**Figure 3.6** c and d). This non-linearity in the presence of DOS might be attributed to diffusion-based behaviour since there is linear relation between square root of scan rates and peak current. Since all procedures to prepare the membranes with either plasticizer was identical, it is important to investigate the reasons behind this deviation from an ideal thin film behaviour in the presence of DOS. This deviation might be attributed to ohmic drop,¹⁶⁹ but the uncompensated resistance for the DOS-based thin films was low (2 k Ω) and similar

to that for the NPOE-based films (1.7 k Ω) which were measured by CH instrument. These results have agreement with theoretical studies showed ohmic drop of thin films can be neglected.²¹⁸ Another reason for the difference might be the kinetics of electron transfer of the Ru-bipod complex at the film-electrode interface or kinetics of anion transfer at the membrane–water interface. Since voltammetric and potentiometric studies of PF₆⁻ showed Nernstian behaviour of this ion, the kinetic transfer rate of this ion at water/ membrane interface is very high and it is not limiting factor.^{161, 219} Thus, it is needed to evaluate the electron transfer rate at film-electrode interface.

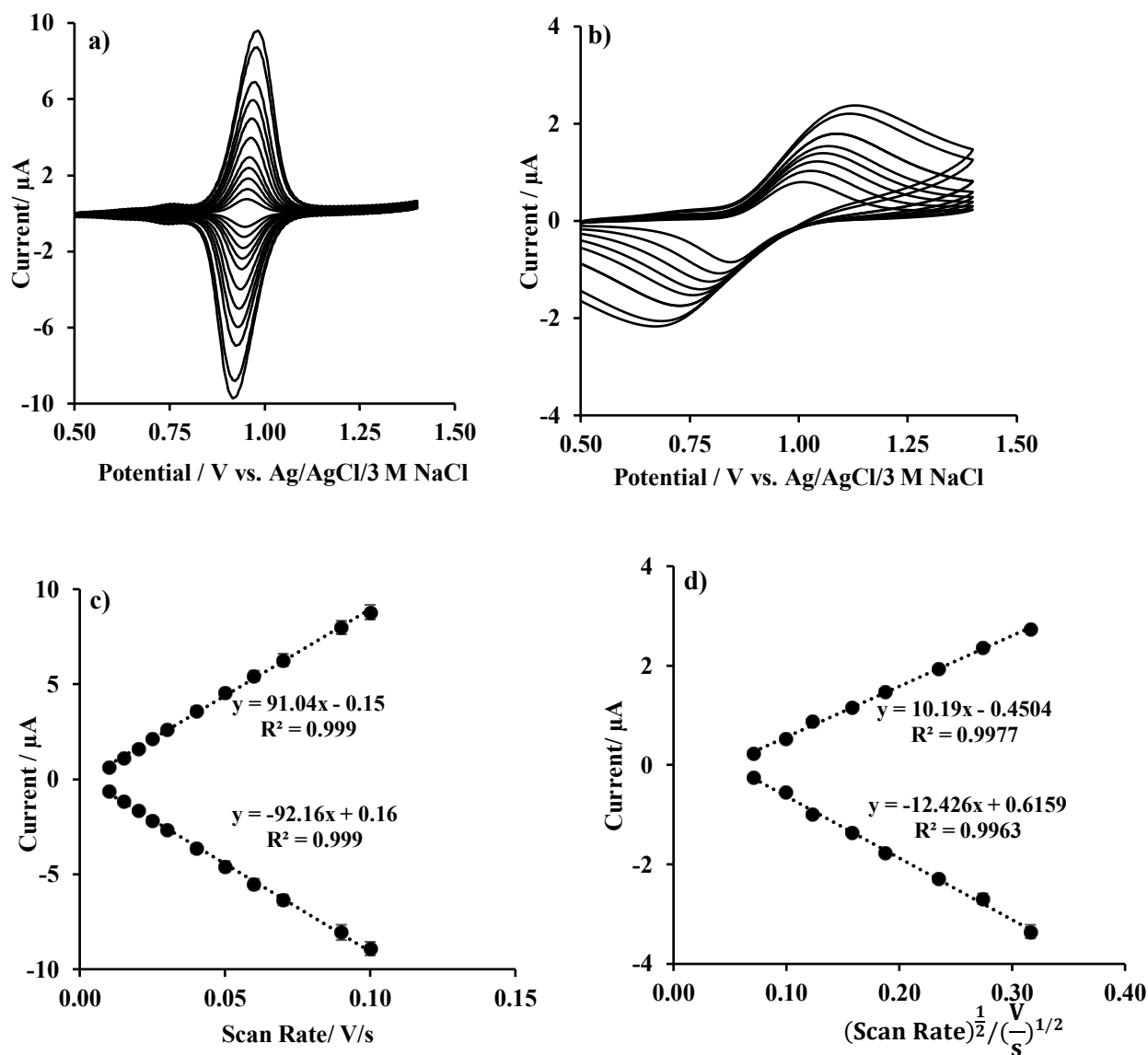


Figure 3.6 a) Cyclic voltammograms in 10 mM KPF_6 using membrane with two different plasticisers NPOE (M5, 65 mmol/kg Ru-bipod, 33% PVC, 66% NPOE) and b) DOS (M4, 65 mmol/Kg Ru-bipod, 33% PVC, 66% DOS) at different scan rates (10, 15, 20, 25, 30, 40, 50, 60, 70, 90 and 100 mV/ s), and scan rate dependence for cathodic and anodic peaks c) with NPOE and d) DOS (n=3).

3.3.2. Electron transfer kinetic study

Based on thin film behaviour, the rate of electron transfer of the Ru-bipod complex dissolved in the membrane was estimated by the Butler-Volmer approach.²²⁰ The separation of anodic and cathodic peaks with increasing of scan rates (**Figure 3.7**) was applied to calculate kinetic parameters by the Laviron model,²²⁰ according to the following equations and equations which are shown in appendix B:

$$E_{p,c} = E^{0'} - \frac{2.3RT}{\alpha nF} \log \left[\frac{\alpha nFv}{RTk_{app}} \right] \quad \text{Equation 3.1}$$

$$E_{p,a} = E^{0'} - \frac{2.3RT}{(1-\alpha)nF} \log \left[\frac{(1-\alpha)nFv}{RTk_{app}} \right] \quad \text{Equation 3.2}$$

where $E_{p,c}$ and $E_{p,a}$ are the cathodic and anodic peak potentials, respectively, $E^{0'}$ is the formal potential calculated by averaging the anodic and cathodic peak potentials at low scan rates, v is the scan rate, α is the electron transfer coefficient, k_{app} is the apparent rate constant of electron transfer, R is the ideal gas constant, T is the temperature, F is the Faraday constant, and n is the number of electrons transferred. By plotting $E_{p,c} - E^{0'}$ and $E_{p,a} - E^{0'}$ versus the logarithm of the scan rate at higher scan rates, where $E_p - E^{0'} > 100$ mV (**Figure 3.7**), α and $1 - \alpha$ can be determined from the slopes of the linear fits (**Figure 3.7**). Based on the values in Table 1, the low transfer coefficient and non-unity sum of α and $1 - \alpha$ is attributed to the structure of the polymeric membrane and is consistent with highly defective film structures on electrodes reported previously.^{221, 222} By extrapolating the linear fits to determine the corresponding intercept (**Figure 3.7**), anodic and cathodic critical scan rates (v_a and v_c , respectively) can be obtained. Then, by using equations 3, 4 and 5 (in Appendix C), anodic, cathodic and total electron transfer rate constants ($k_{app,a}$, $k_{app,c}$ and $k_{app,ET}$, respectively) can be calculated (Table 3.3). The data in Table 3.3 shows the rate of electron transfer of the Ru-bipod complex in NPOE-based membranes is four times greater than in DOS-based membranes, with this kinetic difference can be attributed to the difference in dielectric constants of these two plasticizers. The redox transducer (Ru-bipod) experiences less interactions in the membrane with higher dielectric constant compared to in the membrane with lower dielectric constant. This is seen in the CVs and associated scan rate studies of the membrane in the presence of these plasticizers (**Figure 3.6**). Maybe in the membrane with lower dielectric constant, charged species easily can influence on each other because there are not strong interactions between them and the solvent (plasticizer). In contrast, in the membrane with higher dielectric constant, both oxidized and reduced species are partially impacted by the solvent (plasticizer), and their interactions with each other is less than in the membrane with lower dielectric constant. These interactions negatively impact the electron transfer rates and with higher neighboring interactions, the electroactive species can more slowly participate

in electron transfer. This caused to more rate of electron transfer at same time in the membrane with NPOE as plasticizers with nearly 5 times more dielectric constant compared to membrane with DOS. These results agree with other reports in which electrostatic interactions or ionic interactions can result in increased ion pairing between organic molecules with same size, this effect is more pronounced in lower dielectric constant solvents. consequently, more electrostatic interactions cause electron transfer to be slower.²²³

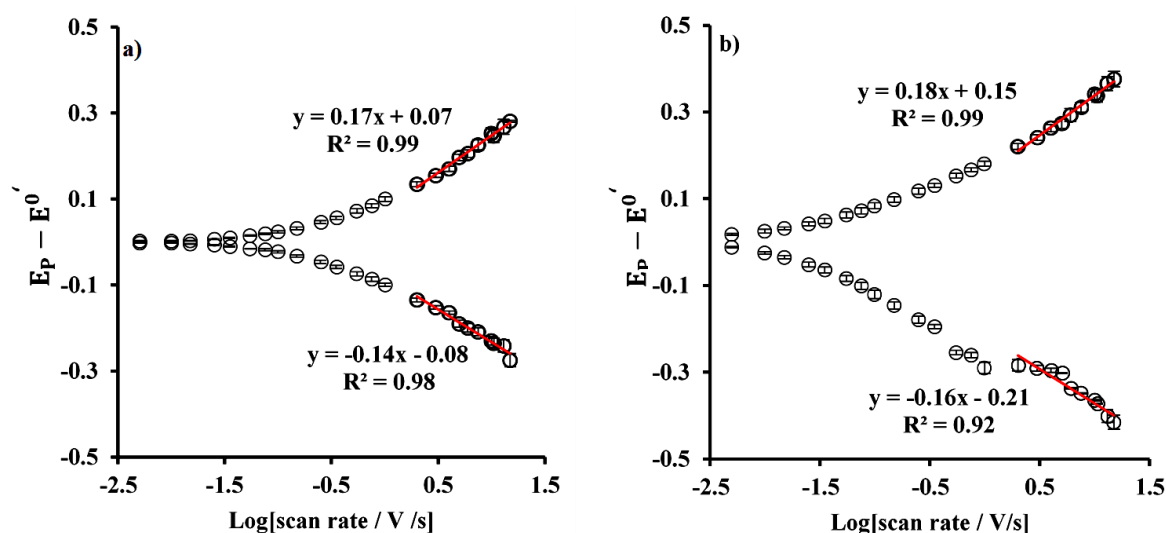


Figure 3.7 Plots of the oxidation and reduction peak potentials of the Ru-bipod complex in membranes M5 (65 mmol/kg Ru-bipod, 33% PVC , 66% NPOE) (left) and M4 (65 mmol/kg Ru-bipod, 33% PVC , 66% DOS) (right) in the presence of aqueous 10 mM KPF_6 versus logarithm of scan rate with a) NPOE (M5), b) DOS (M4). Linear regression data shown for the higher scan rates where $E_p - E^{0'} > 100$ mV). (n=3)

Table 3.3 Kinetic parameters calculated from the data in Fig5 for the kinetics of Ru-bipod in the presence of NPOE or DOS as plasticizers. α : electron transfer coefficient, v_a and v_c : anodic and cathodic critical scan rates, respectively, $k_{app,a}$ and $k_{app,c}$: anodic and cathodic electron transfer rate constants, respectively, and $k_{app,ET}$: total electron transfer rate constant

	$1-\alpha$	α	v_a (V/s)	v_c (V/s)	$k_{app,a}(s^{-1})$	$k_{app,c}(s^{-1})$	$k_{app,ET}(s^{-1})$
Ru-bipod (NPOE)	0.34 (± 0.02)	0.42 (± 0.03)	0.37 (± 0.02)	0.26 (± 0.06)	4.9 (± 0.18)	4.40 (± 0.15)	4.66 (± 0.10)
Ru-bipod (DOS)	0.32 (± 0.02)	0.37 (± 0.02)	0.14 (± 0.02)	0.04 (± 0.01)	1.8 (± 0.18)	0.64 (± 0.12)	1.2 (± 0.18)

3.3.3. Stability evaluation during potential cycling

By choosing the best membrane composition, the stability of the polymeric layer during repetitive scans was evaluated (Figure 3.8 a). In the presence of 10 mM KPF_6 , there was no significant change in the peak current for both forward and backward peaks. However, in the presence of 10 mM KNO_3

or K_2SO_4 (Figure 3.8 b and c, respectively), significant loss in signal occurred during 50 cycles and shows instability in presence of the more hydrophilic anions. It was also observed that in the presence of K_2SO_4 there is a combination of two or three peaks instead of a single sharp peak as seen with KPF_6 (Figure 3.8 b). The origin of this feature is unclear at present, but similar observations were attributed to transfer of different species or leaching of the Ru-bipod complex to the aqueous phase, as shown previously¹⁶⁹ with an osmium complex in the presence of sodium chloride. Chemical reaction between the Ru-bipod and sulfate cannot be excluded at present either.

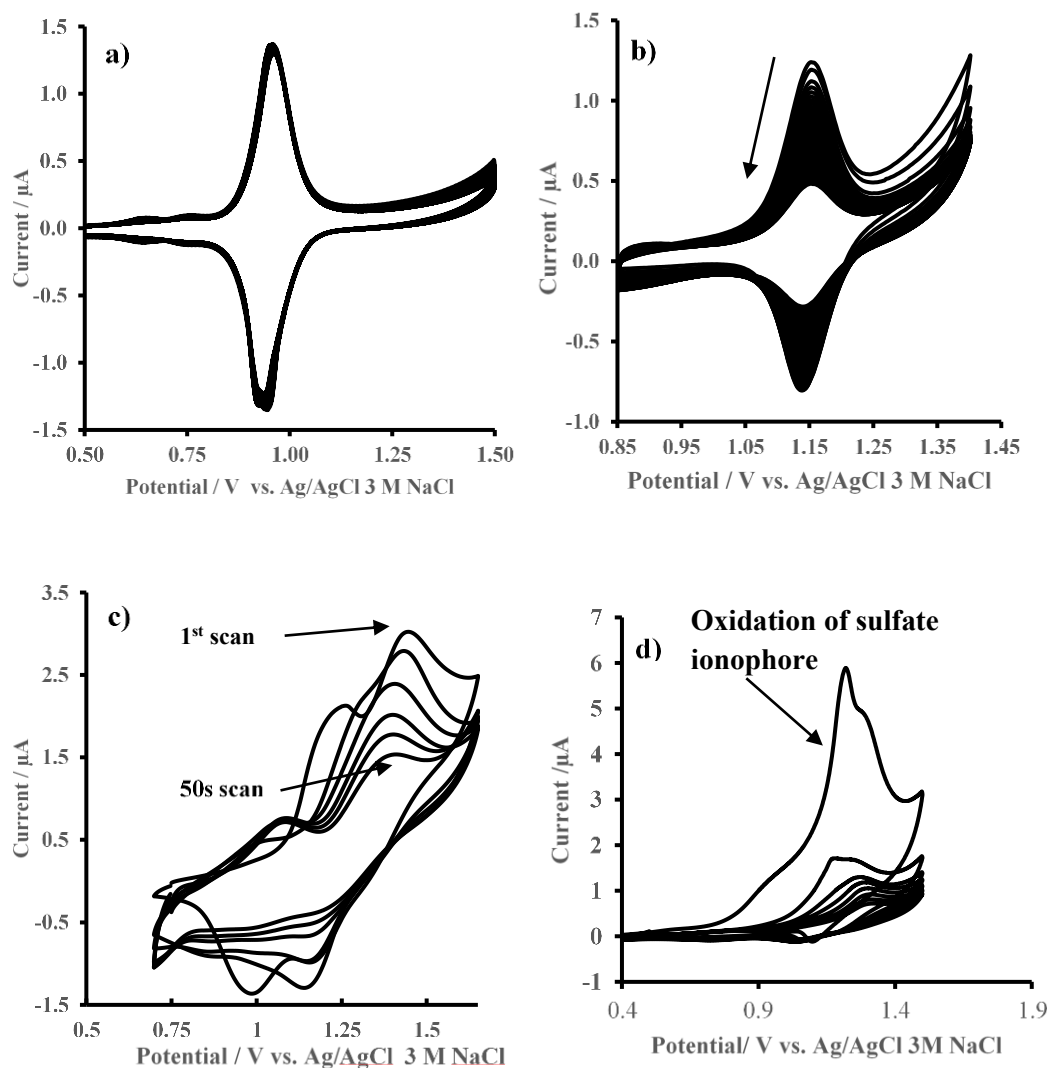


Figure 3.8 Demonstrating electrochemical stability of thin film (using membrane **M5**) in the presence of **a)** 10 mM KPF_6 , **b)** 10 mM KNO_3 , **c)** K_2SO_4 and **d)** the thin film (using membrane **M11**, with sulfate ionophore) in the presence of 10 mM K_2SO_4 , scan rate 10 mV/s (50 scans).

The instability could be attributed to the high potential of redox activity in the presence of aqueous phase sulfate, close to 1.25 V. This is shown by comparison of the first scans of membrane M5 and M11 (without and with sulfate ionophore, respectively) in the presence of 10 mM sulfate (Figure 3.8

c and d), and also the first scans of M4 and M9 (without and with ETH500) (comparison of CVs **Figure 3.9** a, c, e and g) and **Figure 3.9** b, d, f and h). These show that sulfate ionophore and ETH500 are oxidised in the membrane. In this regard, the composition of the membrane with background electrolyte and ionophore is not suitable for detection of anions, especially the more hydrophilic anions like sulfate. The comparison of the area under first peak which represents of charge of electron which are transferring by oxidation of electroactive species (Table 3.4) shows that the peak area related to first anodic peak in the presence of ETH500 is around 5 times more than the first anodic peak area in the absence of ETH500. In addition, the first anodic peak in the presence of S.I is around ten times more than the first anodic peak area in the absence of S.I (Table 3.4).

Table 3.4 The peak area under first scan which is representative of the charge which is transferred in the first peak with and without ETH500 in the presence 10 mM of KPF_6 and with and without sulfate ionophore in the presence of 10 mM of K_2SO_4 ($n = 6$).

Peak area for the first peak with ETH500 (M4)	Peak area for first peak without ETH500 (M9)	Peak area for the first peak with S.I (M11)	Peak area for first peak without S.I (M5)
$5.93(\pm 0.52) \times 10^{-7}$ C	$1.11(\pm 0.15) \times 10^{-7}$ C	$1.66(\pm 0.27) \times 10^{-6}$ C	$1.48(\pm 0.15) \times 10^{-7}$ C

3.3.4. Nernstian behaviour of the thin film:

Since more stable electrochemical responses of the Ru-bipod complex were achieved with more hydrophobic anions (PF_6^- , ClO_4^- and NO_3^-), the potentiometric response and selectivity of the membrane were carried out in the presence of these anions. Generally, based on Nernst equation (equation 3.3), by adding concentration of anions there is shift in potential from more positive to more negative potential.²²⁴ In this study, Gradual addition of PF_6^- and NO_3^- in aqueous phase provoked more shift to more negative potential (**Figure 3.10** a and **Figure 3.11** a, respectively). The Ru-bipod complex in the membrane, shows Nernstian behaviour in the presence of PF_6^- (**Figure 3.10** b) and NO_3^- (**Figure 3.11** b), with response slopes of 58 mV/dec and 60 mV/dec for PF_6^- and NO_3^- , respectively.

$$E_{mid} = E^0 - \frac{2.303RT}{nF} \log [M^-] \quad \text{Equation 3.3}$$

As mentioned earlier, the thin film shows instability to repeated scanning in the presence of NO_3^- (**Figure 3.8** b). The deterioration of the peak currents in the presence of different concentrations of nitrate (**Figure 3.11** a) can be associated to leaching of Ru-bipod complex from thin film, analogous with earlier studies^{115, 169} or to chemical reactions of Ru-pipod with nitrate within the membrane film. Despite the decrease in current magnitude, there is a Nernstian response to nitrate ions.

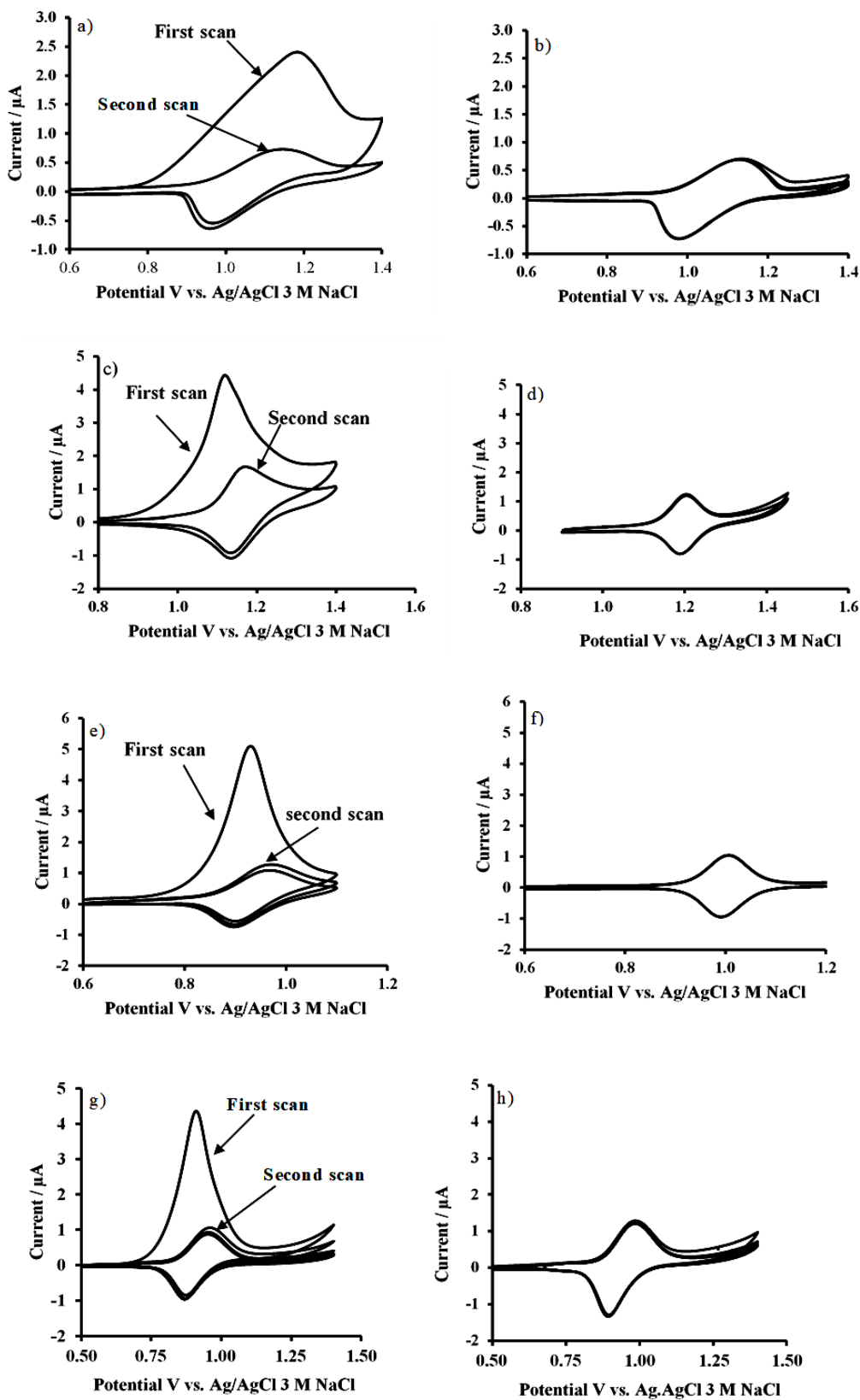


Figure 3.9 Comparison of membrane a) M5 (with ETH500) and b) M10 (without ETH500) in the presence of 0.1 mM of KPF_6 c) M5 and d) M10 in the presence of 10 mM KNO_3 , e) M5 and f) M10 in the presence of 10 mM $KClO_4$, g) M4(with ETH500) and h) M9 (without ETH500) from in the presence of 10 mM KPF_6 with scan rate 10 mV/s

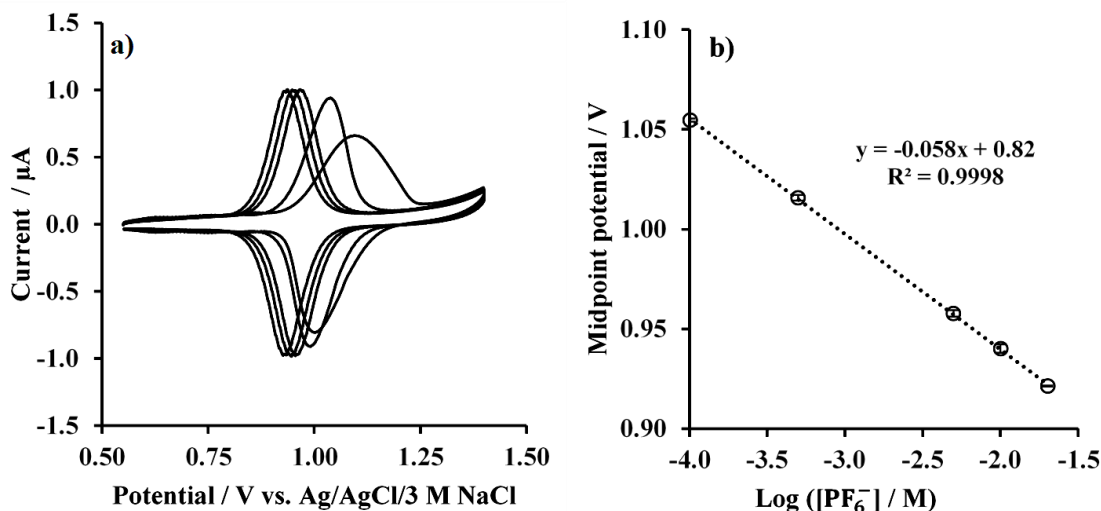


Figure 3.10 Cyclic voltammograms for increasing concentrations of a) different concentrations of KPF_6 with membrane M5 (65 mmol/kg Ru-bipod, 33% PVC, 66% NPOE). b) relationship between log of concentration and midpoint potential, with a Nernst slope for PF_6^- . Scan rate: 10 mV/s. (n=3).

3.3.5. Selectivity study:

The fixed interference method (FIM) and separate solution method (SSM) was used to investigate the selectivity of the membrane for nitrate anions over perchlorate and hexafluorophosphate anions. In this mixed solutions method,^{115, 225} CVs were recorded in different concentrations of nitrate without interference (**Figure 3.11**) and with 0.1 mM ClO_4^- (**Figure 3.12 a**) or 0.1 mM PF_6^- (**Figure 3.12 b**). Plotting the midpoint potential from these CVs versus the logarithm of nitrate concentration (**Figure 3.12 c**) for these three solutions indicates better selectivity for nitrate over perchlorate compared to hexafluorophosphate, and selectivity coefficients $K_{NO_3^-, ClO_4^-}$ and $K_{NO_3^-, PF_6^-}$ were calculated to be 25(±1) and 50(±4), respectively. Selectivity coefficient values for NO_3^- over PF_6^- and ClO_4^- by potentiometric methods reported in other studies are more promising than the values achieved in this study.^{219, 226} In addition, SSM was used to evaluate the selectivity coefficient of NO_3^- ions over ClO_4^- and PF_6^- and it is reported in table 3.5. Based on selectivity coefficients by SSM, as it is expected from Hofmeister series (**Figure 3.3 d**) selectivity of NO_3^- over PF_6^- is better than NO_3^- over ClO_4^- ions.

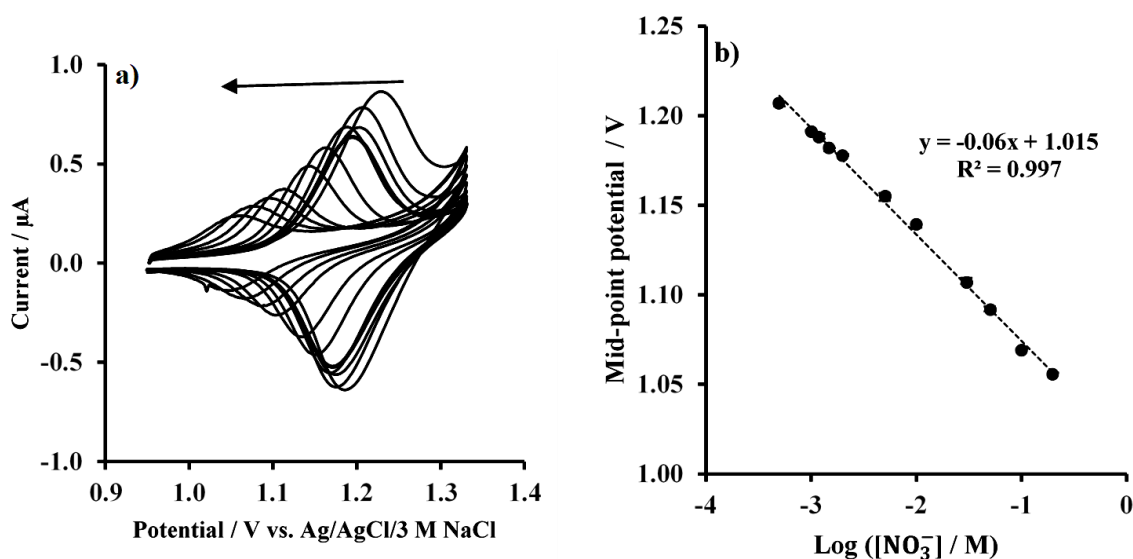


Figure 3.11 Cyclic voltammograms for increasing concentrations of a) different concentrations of KNO_3 with membrane M5 (65 mmol/kg Ru-bipod , 33% PVC , 66% NPOE). b) relationship between log of concentration and midpoint potential, with a Nernst slope for NO_3^- Scan rate: 10 mV/s. (n=3).

Table 3.5 selectivity coefficients of NO_3^- ions over PF_6^- and ClO_4^- by FIM and SSM methods

	$K_{NO_3^-,PF_6^-}$	$K_{NO_3^-,ClO_4^-}$
FIM	50(±4)	25(±1)
SSM	6.7×10^{-4}	4.2×10^{-3}

Since FIM method is more practical than SSM to evaluate the selectivity, and the numbers of selectivity coefficients by FIM are very high, it seems that selectivity of thin films without ionophore by fixed interference method is not satisfactory for application in SC-ISEs, and fouling of thin film occurs in mixed solution methods, and the membrane without selective ionophore can be responsive with other anions in mixed solutions.

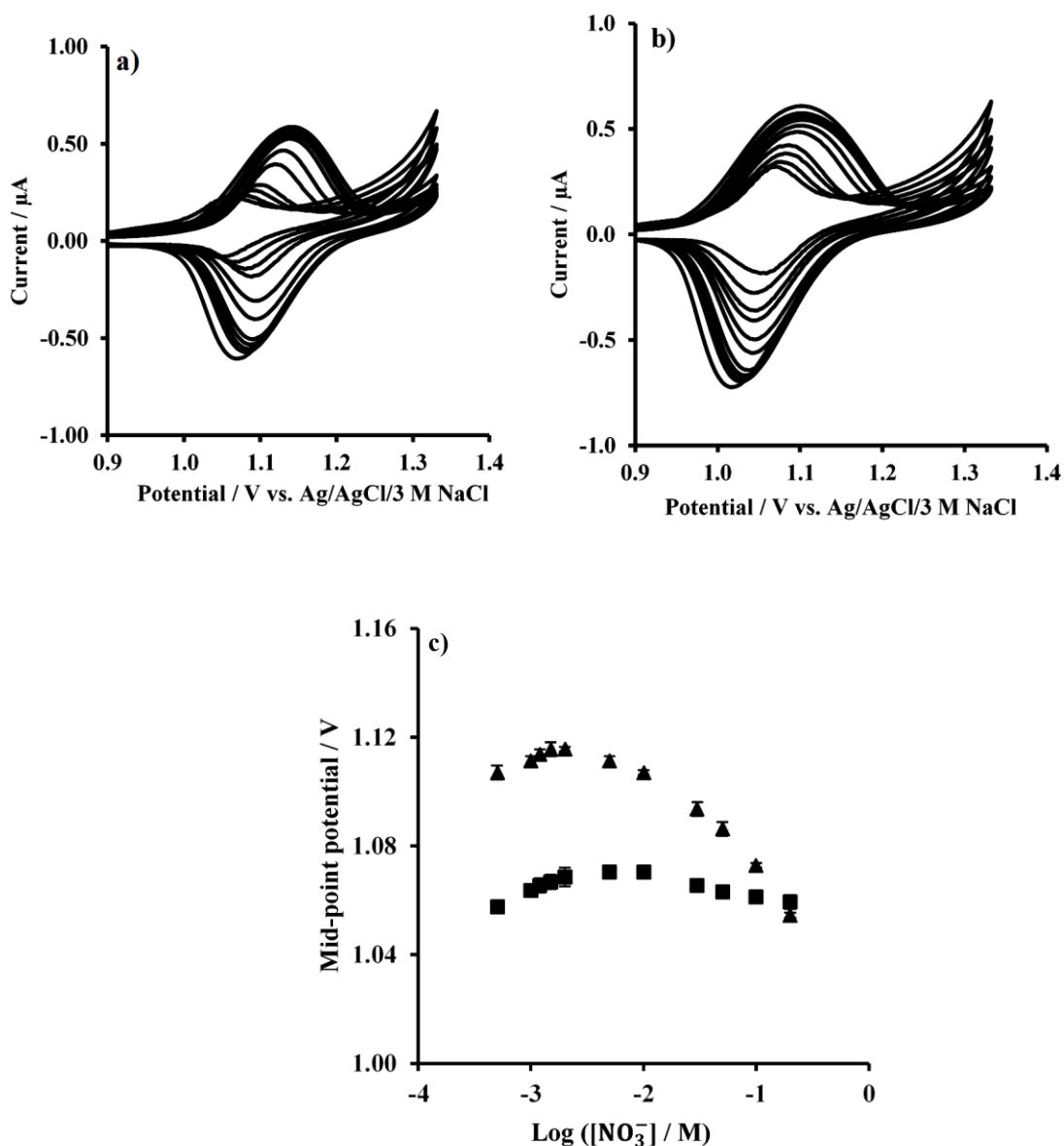


Figure 3.12 Selectivity study of solid contact with membrane M5 (65 mmol/kg Ru-bipod , 33% PVC and 66% NPOE) in the presence of different concentrations of a) NO_3^- (0.5, 1, 1.2, 1.5, 2, 5, 10, 30, 50, 100 and 200 mM); a) in presence of 0.1 mM ClO_4^- b) in presence of 0.1 mM PF_6^- and c) relation of mid-point potential to logarithm of NO_3^- concentration (n=3): NO_3^- ions in presence of 0.1 mM ClO_4^- (triangles) and NO_3^- ions in presence of 0.1 mM PF_6^- (squares) (n=3).

3.4. Conclusion

In this study, a Ru-bipod complex was investigated as a redox transducer within a thin polymeric film for detection of anions. The complex showed reversible and stable voltammetric responses in the presence of more lipophilic anions, while in the presence of sulfate and chloride the response was unstable and the resulting high redox potential of the Ru-bipod complex in the presence of these anions resulted in destruction of the complex in the film. It was also shown background electrolyte (ETH500) or sulfate ionophore in the film were susceptible to oxidation at the high potentials required in the presence of hydrophilic anions. Nevertheless, thin film behaviour was demonstrated by scan

rate dependence in the presence of lipophilic anions for thin films containing NPOE plasticizer. The rate of electron transfer of the Ru-bipod complex in thin films was substantially different when membrane plasticizers with different dielectric constants were employed. The rate of electron transfer with membranes containing NPOE (higher dielectric constant) was greater than that with membranes containing DOS (lower dielectric constant). Moreover, the Ru-bipod complex showed Nernstian responses to anions (except sulfate and chloride). Placing the thin film in solutions of mixtures of anions showed that fouling effect can reduce the selectivity of the membrane, significantly. Maybe by using selective ionophores the fouling effect can be overcome, although preliminary results using a sulfate ionophore indicate that this is oxidised within the membrane. Based on the results presented, the Ru-bipod complex is very responsive to anion detection. However, for future work, the design of new complexes with less positive redox potentials are needed to enable a stable response in the presence of ionophores.

4. New Ru complexes to develop solid contact ion selective electrodes to sense Sulfate

4.1. Introduction

Ion selective electrodes (ISEs) are representative of electrochemical sensors in clinical and environmental applications. Since the conventional configurations of ISEs with inner filling solutions do not have mechanical stability and robustness compared to more promising alternative of the solid contact ion selective electrodes (SC-ISEs). In SC-ISEs, usually a double polymeric layer was used. One layer, which is directly in contact with the metallic electrode, acts as transduction layer which contains an electroactive substance like a conducting polymer. The second layer, which is in contact with the first layer, is the sensing polymeric layer.¹⁶³⁻¹⁶⁶ However, in some new configurations, electroactive species like molecular redox probes can be dissolved directly in a sensing layer. For the first time, this configuration was used by Anson and Shi to measure the electron transfer rate of ferrocene derivatives as redox probes dissolved in an organic thin layer.^{159, 160} In this study cobalt porphyrins are used as an electroactive species on surface of electrodes and served as catalysts to reduce and oxidize O_2 , H_2O_2 , NO , CO_2 , etc. Then, ion sensing by this approach was initially introduced by Bond and his co-workers. The redox behaviour of 7,7,8,8-tetracyanoquinodimethane caused a charge imbalance in the organic film and this charge is neutralised by sourcing ions from the aqueous in contact with the organic layer.^{161, 162} Ion sensing is obtained by this mechanism. In different reports, several redox probes were used in organic films. Ferrocene derivatives like dimethyl ferrocene were used to sense heparin and in another study ferrocene that was covalently attached to polyvinylchloride (PVC) was applied to sense carbonate.¹⁰⁸⁻¹¹⁰ However, the ferrocene complex in these studies showed irreversible and unstable responses which showed that ferrocene is not a reliable choice for ion sensing. In other reports, different redox complexes were used, such as cobalt and osmium complexes.^{113, 169} Solid contact membranes containing cobalt complexes were not stable in the presence of ionophores and the redox potential for osmium complexes versus Ag/AgCl reference electrode was high, close to 1 V, and in the presence of hydrophilic anions, there were different peaks in the CVs which were suggested to be different species of the membrane components transferring to the aqueous phase. In other reports, cationic helicenes complexes were used as redox probes in SC-ISE systems.^{115, 170} However, in the presence of ionophore this complex gradually was leached to aqueous phase. In the membrane with sodium ionophore, after transferring of the ion to the membrane positively charged diaza complexes were gradually expelled from the membrane. This can be more a serious issue for the sensing of more hydrophilic anions, like sulfate, which is the purpose of this study. As shown in chapter 3, the lipophilic $Ru(bipod)_2$ complex, which had a very high redox potential in the presence of sulfate and chloride ions, was found to cause an unstable and irreversible

electrochemical response due to the oxidation of membrane components like the background electrolyte ions or ionophore. On the other hand, generally Ru complexes can be promising alternative redox probes because the redox potential of this complex can be easily changed by changing functional groups coordinated to the Ru core.²⁰⁰

In this study, in order to have capability to evaluate sulfate sensing in solid contact electrodes, by changing in chemical structure of Ru-bipod (as a homoleptic complex), two new hetroleptic Ru complexes were studied: these complexes are Ru(bipod)(bipob) and Ru(bipod)(dmbb), which contain the same core part as the homoleptic structure of Ru-bipod (discussed in chapter 3). The key difference in these structures is that one carbon instead of a nitrogen is connected to the Ru metal. By this replacement, the redox potential of the new complexes is significantly less positive than that of the Ru-bipod complex. The difference between Ru(bipod)(bipob) and Ru(bipod)(dmbb) is the number of alkyl chains in their chemical structure, which influences the complex lipophilicity.

4.2. Experimental section

4.2.1. Reagents.

Potassium chloride, potassium hexafluorophosphate, potassium nitrate, potassium perchlorate, potassium sulfate, tetrakis(4-chlorophenyl) borate tetradodecylammonium salt (ETH500), 2-nitrophenyloctylether (NPOE), anhydrous tetrahydrofuran (THF), high molecular weight PVC, polyurethane (PU) and the sulfate ionophore (S.I.) were purchased from Sigma Aldrich in analytical grade. Aqueous solutions were prepared in deionized water (resistivity 18.2 MΩcm; USF Purelab with UV). 2-Octyl-1-dodecanol (Aldrich), 2-fluoronitrobenzene (TCI) and ruthenium (III) trichloride hydrate (Heraeus GmbH) were used without further purification. 1-Bromo-2-octyl-1-dodecane and 2,6-bis(1-(2-octyldodecan) benzimidazol-2-yl) pyridine (bipop), was prepared from 2-octyl-1-dodecanol.²²⁷

4.2.2. Instrumentation and measurements.

A three-electrode electrochemical cell was used for all measurements, comprising a thin film-coated glassy carbon (GC) disc working electrode (3 mm diameter) (CH Instruments), a Ag/AgCl/3 M NaCl reference electrode (model MF-2056, BASi), and a platinum disc as counter electrode, and placed in a Faraday cage. Electrochemical experiments were conducted with an Autolab PGSTAT302N electrochemical workstation (Metrohm, The Netherlands) with NOVA software. A CH1900b potentiostat (CH Instruments Inc., USA) was used to measure uncompensated resistance. Preparation of the organic thin films is the same as in chapter 3, by spin-coating onto GC electrodes using an inverted overhead stirrer (model IKA RW20).

4.2.3. Film preparation.

According to CVs related to the different compositions of thin layer which were investigated in chapter 3 (Table 3.2 in chapter 3), M10 (65 mmol/Kg ETH500, 65 mmol/ kg the Ru complex, NPOE with two times proportion with PVC) and the composition includes 65 mmol/Kg ETH500 and 65 mmol/ kg Ru complex and same proportion PU and NPOE were used.²²⁸

4.2.4. Synthesis of Ru(bipod)(dmdb) and Ru(bipod)(bipob).

Ru(bipod)(dmdb) and Ru(bipod)(bipob) (Figure 4.1) were synthesized as described in Appendix B and then characterized by ESI-MS, ¹H NMR and cyclic voltammetry (Figure B-6, B-7 and B-8, respectively).

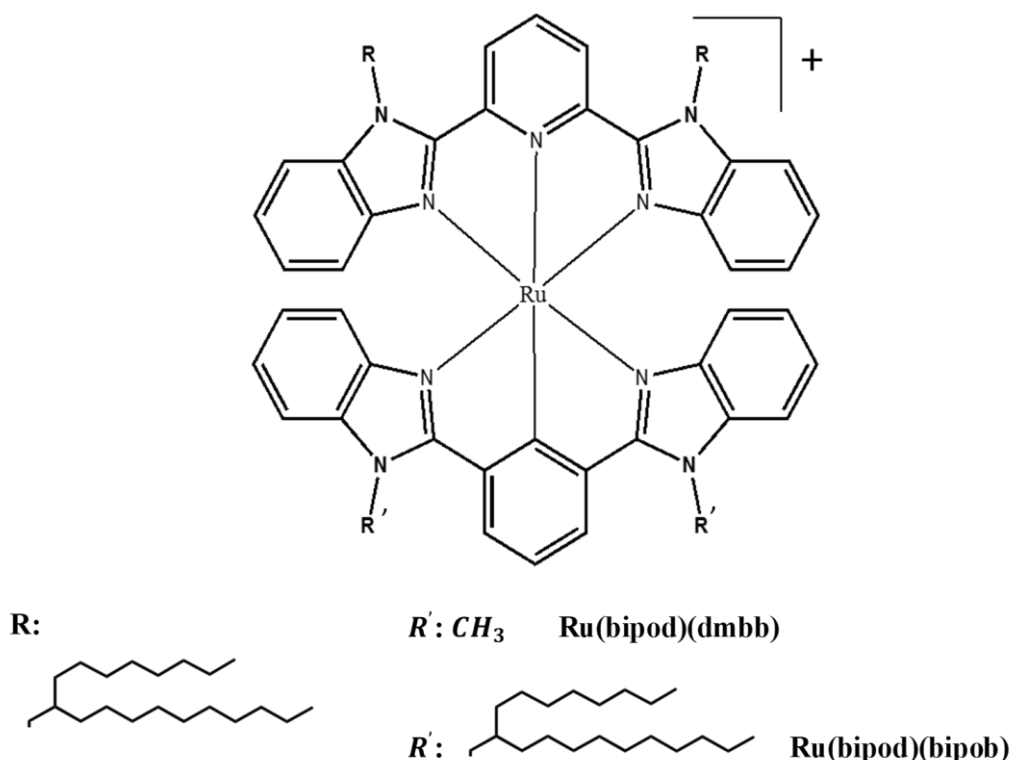


Figure 4.1 : Structure of Ru complexes: Ru(bipod)(dmdb) and Ru(bipod)(bipob).

4.3. Result and discussion

4.3.1. Electrochemical properties of the complexes

The introduction of Ru-C cyclometalated bond results in a potential shift to a more negative value by 0.6 V, which has been expected from our previous study. As is shown in Figure 4.2 (which is provided by Prof. Haga's research group, Chuo University, Japan), there is a significant difference of oxidation and reduction potentials of Ru complexes with cyclometalated bond (i.e. Ru(bipod)(bipob)) and Ru-bipod with nitrogen bond.

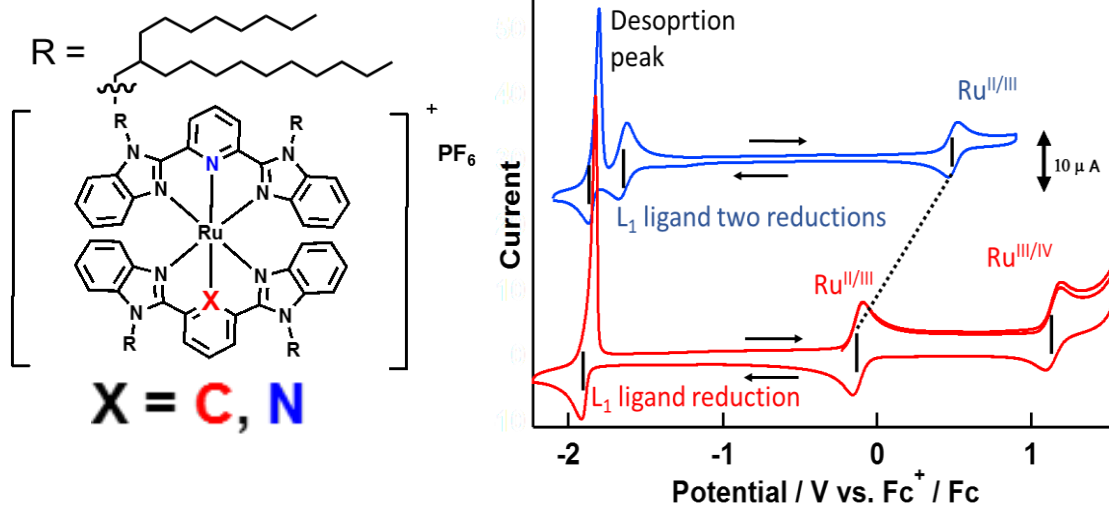


Figure 4.2 : Cyclic voltammograms of 0.5 M Ru(bipod)(bipob) together with 0.3 M Ru-bipod in CH₃CN with 0.1 M TBAPF₆ as a supporting electrolyte. Working electrode, glassy carbon electrode at 25°C (Data provided by research group of Prof. Haga, Chuo University, Japan).

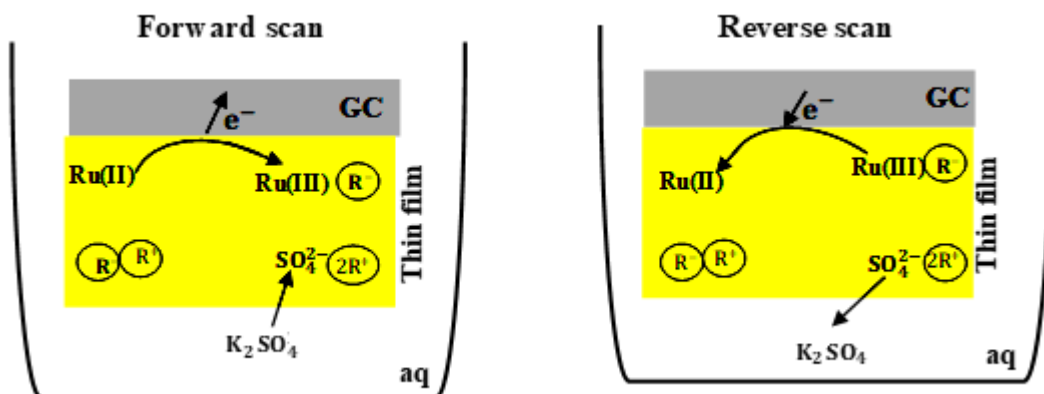


Figure 4.3 : Schematic of sulfate ions transfer in forward (left) and reverse scan (right) which is triggered by oxidation and reduction of the Ru complex, respectively.

The mechanism of sulfate transfer is illustrated in **Figure 4.3**. In forward scan by imposing potential and oxidation of the Ru complexes in thin film, the additional positive charge introduced can be stabilized by the negative charge of organic salt in thin film (tetrakis(4-chlorophenyl borate)). To compensate this charge imbalance, there is transfer of sulfate from aqueous phase to organic phase (thin film). During the reverse scan, all process are reverse. Based on this mechanism, oxidation, and reduction of Ru(bipod)(bipob) was obtained as a CV (**Figure 4.4**). As it is shown in **Figure 4.4** there is not oxidation and reduction peak in absence of PF₆⁻ ions. By imposing potential, Ru(bipod)(dmbb) is oxidised, and the positive charge of the Ru can be stabilised by organic anion in the thin film (tetrakis(4-chlorophenyl) borate) and the charge imbalance is generated in the thin film. The charge

imbalance can be compensated by PF_6^- ions transfer from aqueous phase to organic phase. This process generates the oxidation peak (**Figure 4.4**). In reverse scan, by reduction of the Ru complex, all the process is the reverse and can generate reduction peak (**Figure 4.4**). In this study, to increase the stability of the membrane, polyurethane (PU) ²²⁸ was used instead of PVC. However, to compare kinetic results of the Ru complexes with the Ru-bipod results, PVC as a polymer was used. As will be discussed below, with the new (lower) redox potential, selectivity of the membrane containing this complex was improved in the presence of new synthesised ionophore by using the separation solution method.

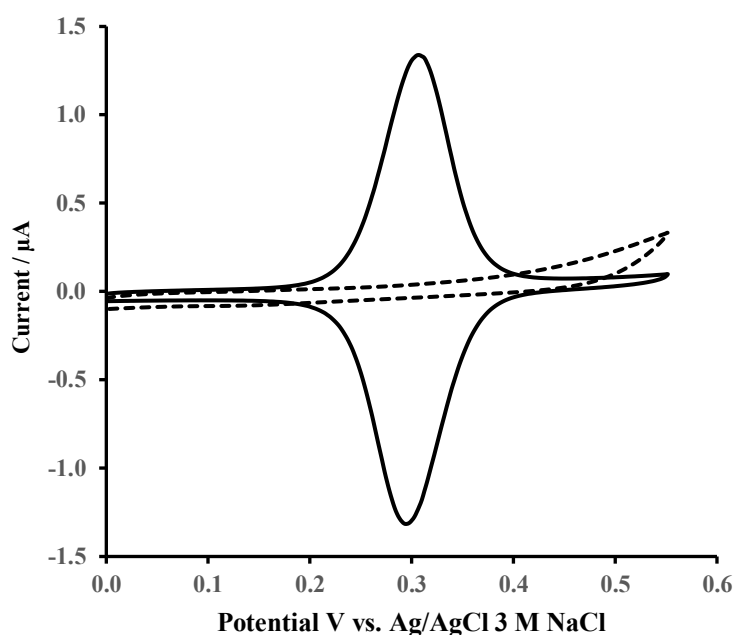


Figure 4.4 : Cyclic voltammograms of 65 mmol/kg Ru(bipod)(dmbb) complex, 65 mmol/kg ETH500, NPOE and PU, in the presence (solid line) and absence of PF_6^- (dashed line). scan rate: 10 mV/s.

In addition, CV of thin film is obtained for Ru-bipod, Ru(bipod)(bipob) and Ru(bipod)(dmbb) in the presence of 10 mM of KPF_6 and comparison of redox potential of these complexes is shown in **Figure 4.5**. The oxidation and reduction peak potential shows that the redox potential of Ru(bipod)(bipob) is 670 mV more negative than Ru-bipod. This reduction is attributed to strong electron donating property of cyclometalated bond.¹⁹⁹ In addition, based on the CVs related to Ru(bipod)(bipob) and Ru(bipod)(dmbb), there is no significant difference in redox potential with these two complexes with four and two alkyl chains, respectively.

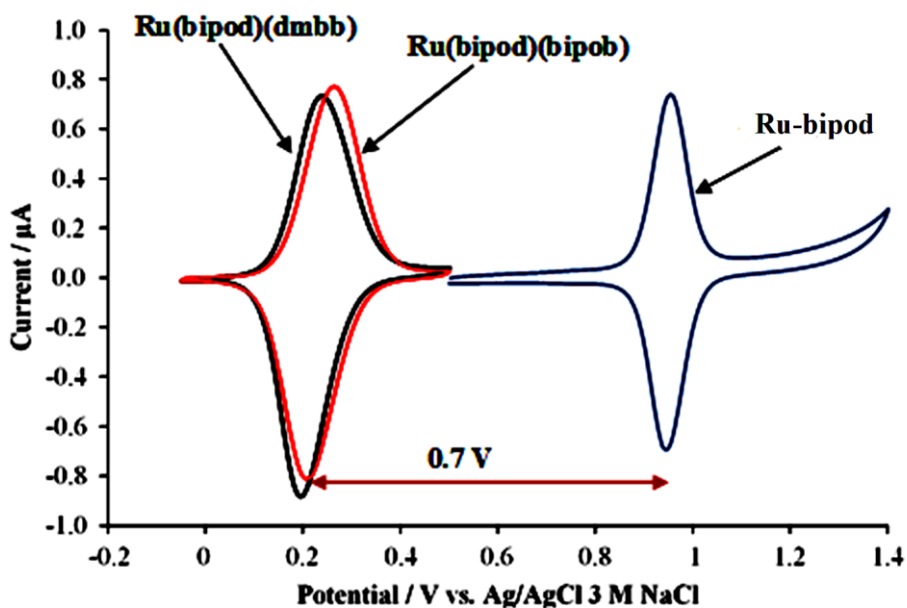


Figure 4.5 : Cyclic voltammetry obtained using membrane containing 65 mmol/kg Ru-bipod complex (blue) and 65 mmol/ kg Ru (bipod)(bipob) (red) and 65 mmol/ kg Ru(bipod)(dmbb), 33% PVC and 66% NPOE in the presence of 10 mM KPF_6 . Scan rate: 10 mV/s.

4.3.2. Stability during scans in the presence of sulfate ions:

Stability of the thin film was investigated for films containing Ru-bipod, Ru(bipod)(dmbb) and Ru(bipod)(bipob) during 50 scans. As it is shown in **Figure 4.5** a and b respectively, electrochemical response of thin films containing Ru(bipod)(bipob) and Ru(bipod)(dmbb) is stable in the presence of sulfate ion without significant drop in CV response, while thin film containing Ru(bipod)₂ in the presence of sulfate ion (**Figure 9** c, chapter 3) does not show this stability during 50 scans. The reason behind that is the lower redox potential of Ru(bipod)(bipob) and Ru(bipod)(dmbb) compared to Ru(bipod)₂ complex which has a high positive redox potential (>1 V) specifically in the presence of sulfate ions. In addition, by comparison of the CVs (**Figure 4.5**) related to Ru(bipod)(bipob) complex, with four long alkyl chains, and Ru(bipod)(dmbb), which has two alkyl chains, there is no difference in stability during scans. These results suggest that, for stability of the electrochemical response, the redox potentials of redox probe complexes are more important factor than the number of hydrophobic alkyl chain attached to the Ru complexes.

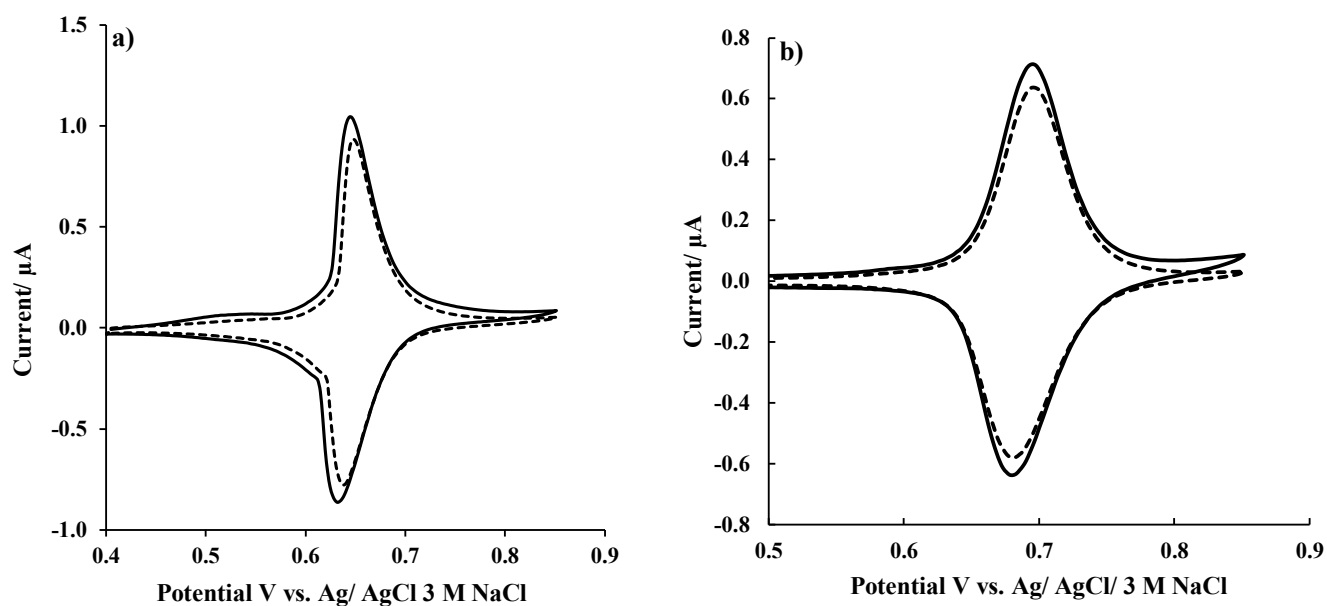


Figure 4.6. Stability of the membrane containing a) 65 mmol/kg Ru(bipod)(dmdbb) complex and b) Ru(bipod)(bipob), 65 mmol/kg ETH500, 50% NPOE and 50% PU during 50 runs in presence of 10 mM sulfate (first scan (solid line), last line (dotted line)).

As was shown in chapter 3, at high potential there is oxidation of thin film components and consequently loss of the electrochemical response. In addition, the thin films both contains ETH500 as background electrolyte and voltammograms for both complexes show multiple scans starting from the first scan. As it is shown here there is no significant difference between the first scan and the subsequent scans. In comparison to the CVs related to first scan of the thin film containing Ru(bipod)₂ and ETH500 in the presence of different anions (**Figure 3.4**), there is no response representing oxidation of ETH500. This can be attributed to the low redox potential of these new Ru complexes (**Figure 4.6**).

In another study, mechanical and physical stability of thin films was investigated by rinsing the thin film-coated electrode containing PVC or PU directly with water. In this study Ru(bipod)(dmdbb) was used as a redox probe in the membrane. As represented in **Figure 4.7**, there is no drop in electrochemical responses with thin films containing PU while there is considerable loss in the electrochemical response with thin films containing PVC. These results are in agreement with the results of the PVC and PU based thin film in other studies,^{170, 228} and suggest that PU makes thin films more stable specifically for development of sensors and is an alternative to PVC.

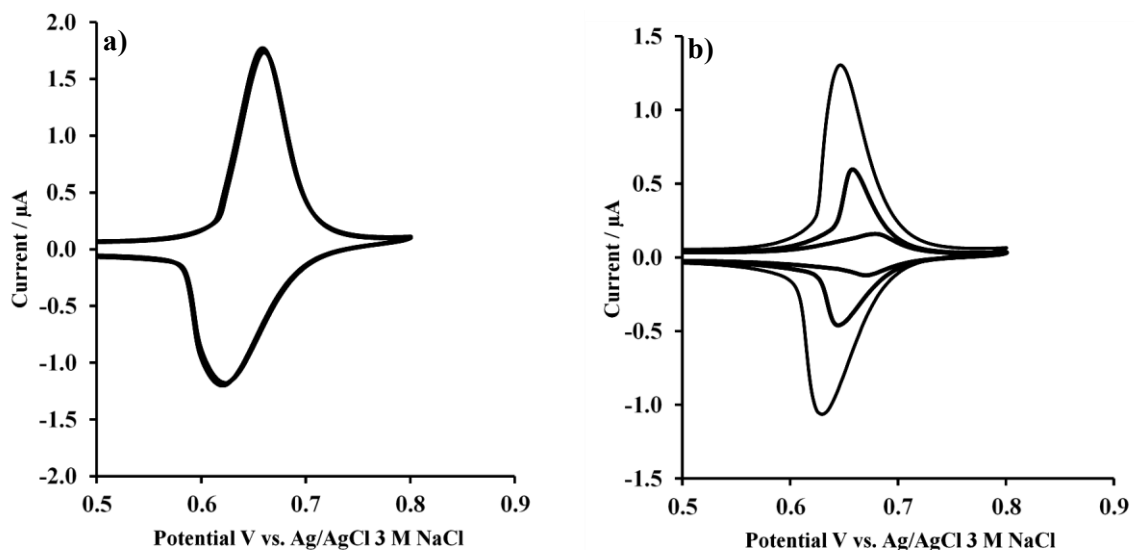


Figure 4.7 : CVs after twice rinsing of thin film containing 65mmol/kg Ru(bipod)(dmbb), 130 mmol / kg ETH500, 50% NPOE and 50% PU a) and 50% PVC b).

4.3.3. Thin film behaviour in the presence of sulfate ions:

Thin film behaviour was evaluated with both complexes by cyclic voltammetry in the presence of sulfate ions at different scan rates (**Figure 4.8 a and b**). Faradic peak current (I_p) has direct proportion with scan rate by the equation 4.1.²¹²

$$I_p = \left(\frac{n^2 F^2}{4RT}\right) \Gamma A \nu \quad \text{Equation 4.1}$$

In which, I_p is peak current, A is electrode surface area, Γ is surface coverage and ν is scan rate. The peak currents at different scan rate were plotted against scan rate (**Figure 4.8 c and d**) and as shown in the **Figure 4.8 c and d**, there is linear dependence on scan rates up to 100 mV/s for both cathodic and anodic peak currents, which confirms thin film behaviour. In theory, at low scan rate anodic and cathodic peak potentials difference is close to zero.²¹² Here, the peak-to-peak separation of the CVs for both complexes was found to be around 0 mV at 10 mV/s, which is ideal and agrees with theoretical value of surface confined or thin film one electron transfer process.

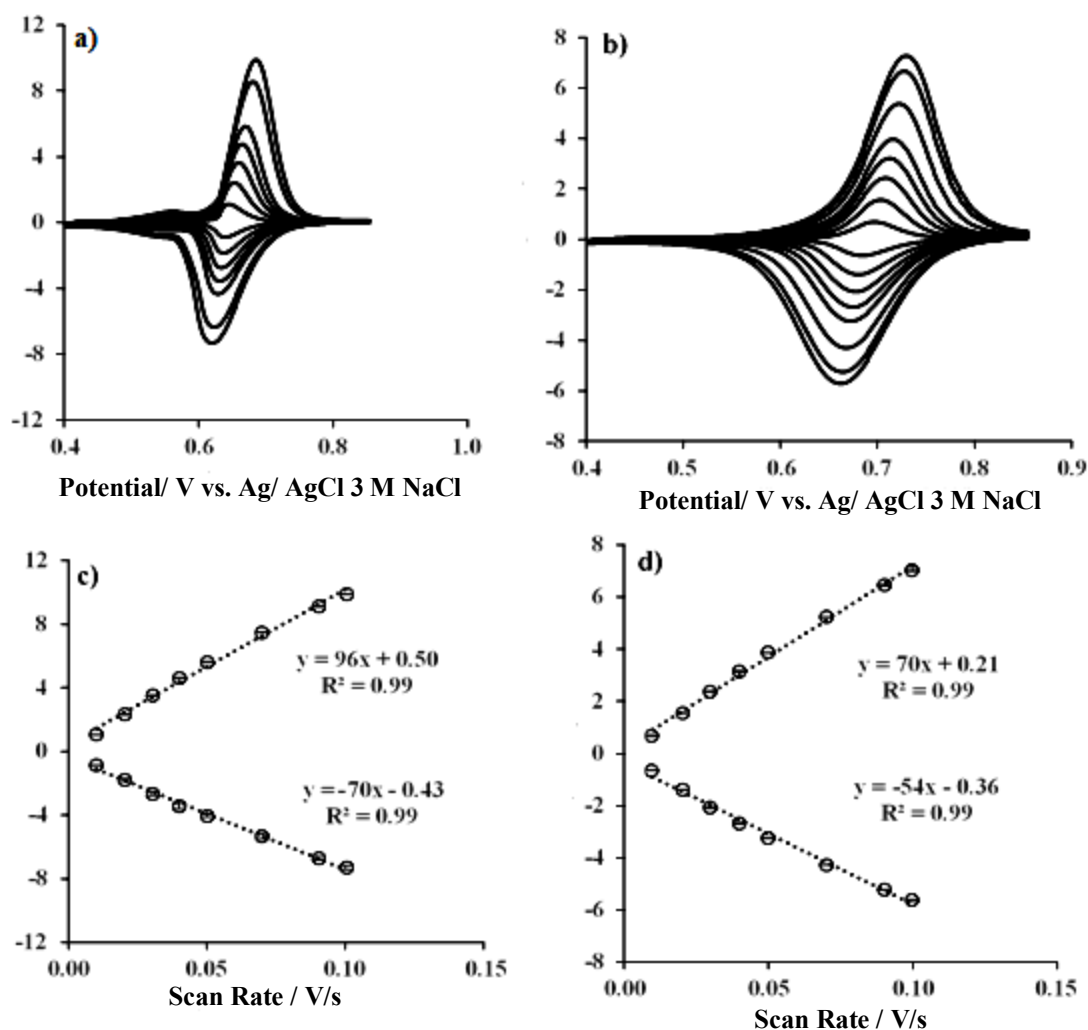


Figure 4.8 : Cyclic voltammograms in 10 mM K_2SO_4 using thin film containing a) 65 mmol/ kg Ru(bipod)(dmdbb) and b) Ru(bipod)(bipob), 130mmol/kg ETH500, PU=NPOE in different scan rate (10, 20, 30, 40, 50, 70, 90, 100 mV/s).

4.3.4. Hofmeister series and selectivity of thin film to sense sulfate over other anions:

The responses toward different anions (Hofmeister series) with thin film containing these two Ru complexes were evaluated. The CVs were obtained by thin film contains ETH500, PU, NPOE and Ru(bipod)(dmdbb) (**Figure 4.9 a**) and Ru(bipod)(bipob) (**Figure 4.9 b**) in the presence of 10 mM different anions. The difference in redox peak potentials for both complexes (**Figure 4.9 a** and **b**) showed better selectivity compared to the thin film containing Ru(bipod)₂ (**Figure 3.3**) complex, i.e. the responses in the presence of different anions are better separated along the potential axis. However, the behaviour of different anions with thin films containing Ru(bipod)(dmdbb) and Ru(bipod)(bipob) are almost the same.

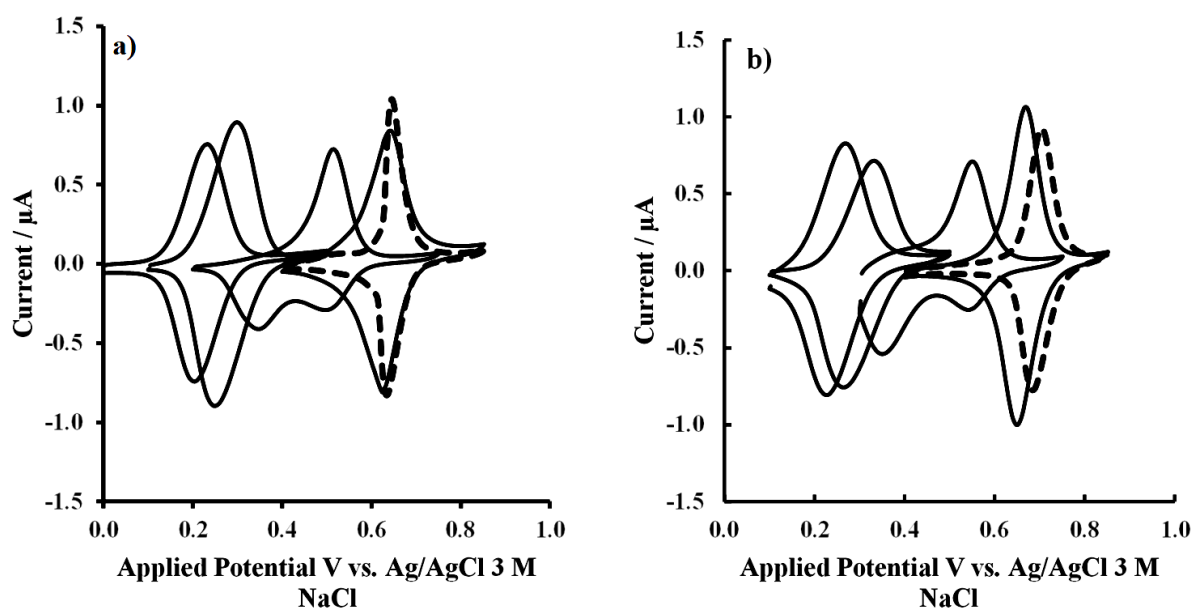


Figure 4.9 : Hofmeister series with thin film containing 65 mmol/ kg Ru(bipod)(dmdb)(a) Ru(bipod)(bipob), 130 mmol/ kg ETH500, PU=NPOE, in the presence of 10 mM (from right to left) sulfate (dotted line), chloride, nitrate, perchlorate and hexafluorophosphate. Scan rate 10 mV/s. (n=3).

4.3.5. Potentiometric behaviour of the thin films and calibration curves:

According to the Nernstian equation (equation 3.3), gradual addition of anions to aqueous solution causes a shift to more negative potentials of the CV oxidation and reduction potentials. The gradual addition of PF_6^- to the aqueous phase with the membrane containing Ru(bipod)(dmdb) causes a shifting of CVs to more negative potential (Figure 4.10 a). Then, a Nernstian slope was achieved by plotting of the mid-point potential versus the logarithm of concentration of PF_6^- (Figure 4.10 b). The same study was carried out by adding different concentrations of SO_4^{2-} with membranes containing Ru(bipod)(bipob) and Ru(bipod)(dmdb) (Figure 4.11 a and b, respectively). As expected, the addition of sulfate to the aqueous solution caused a shift of the CVs to more negative potentials. Plotting of the mid-point potential of each CV against the logarithm of concentration of sulfate shows that the slope of the best-fit straight lines are around 0.02 V/dec. According to the Nernstian behaviour of sulfate ions, which have two negative charges, the expected theoretical slope ($0.059/z$) should be around 0.03 V/dec. This deviation from the Nernstian slope might be due to kinetic effect of sulfate transfer at the interface between the aqueous medium and the thin film, or electron transfer at thin film-electrode interface. Since a Nernstian slope was obtained with the membrane containing Ru(bipod)(dmdb) in the presence of different concentrations of hexafluorophosphate (Figure 4.9), and the kinetics of facilitated sulfate transfer is fast enough at the interface between aqueous phase and organic phase,²²⁹ it seems that the kinetics of electron transfer at the membrane-electrode interface can be affected by the type of ions which are responsible for neutralisation of charge imbalance in the membrane. Based on scan rate studies with both Ru complexes (Figure 4.6), there is thin film behaviour of the membrane. In addition, the equations related to adsorbed redox species are similar with thin films containing redox probes.²¹² Electron transfer rates by the Laviron model²³⁰ were investigated with the membranes containing Ru(bipod)(dmdb) and Ru(bipod)(bipob) in the presence of both PF_6^- and SO_4^{2-} ions (Figure 4.12 and Figure 4.13, respectively). As is shown in Figure 4.12 a and b, in the presence of PF_6^- , the membranes show symmetric cathodic and anodic portions with both Ru complexes, while in the presence of SO_4^{2-} , the cathodic and anodic portions are not similar.

This asymmetry can be attributed to transfer coefficient values that exceed 0.5.²²⁰ It can be seen that in cathodic part of the kinetic study (Figure 4.13 a and b) the transfer coefficient is ca. 1, and the Laviron model does not cover this value for estimation of electron transfer kinetics. This phenomenon in the presence of SO_4^{2-} results from an imbalance of sulfate ion transfer during anodic and cathodic processes. In other words, the rate of ingress and egress of sulfate ions are not the same and based on the transfer coefficient rate value of cathodic process, which exceeds 0.5, the rate of egress of sulfate ions is higher than the rate of ingress of these ions. This difference in rate might be related to the high hydrophilicity of sulfate ions. These results agree with other studies with monolayers of redox molecules.^{231, 232} The kinetics of electron transfer data are calculated based on the Laviron model as done also in Chapter 3 and are reported in

Table 4.1 and Table 4.2. The anodic and cathodic kinetics of electron transfer nearly are the same values in the presence of PF_6^- with the membranes containing Ru(bipod)(bipob) and Ru(bipod)(dmdb).

PF_6^-	$1-\alpha$	α	v_a (V/s)	v_c (V/s)	$k_{app,a}(s^{-1})$	$k_{app,c}(s^{-1})$	$K_{app}(s^{-1})$
Ru(pod)(pob)	0.41(±0.03)	0.53(±0.05)	0.30(±0.03)	0.17(±0.04)	4.76 (±0.2)	3.56 (±0.63)	4.16 (±0.27)
Ru(pod)(dmdb)	0.30(±0.02)	0.38(±0.05)	0.40(±0.02)	0.24(±0.05)	4.56(±0.18)	3.53 (±0.26)	4.05 (±0.04)

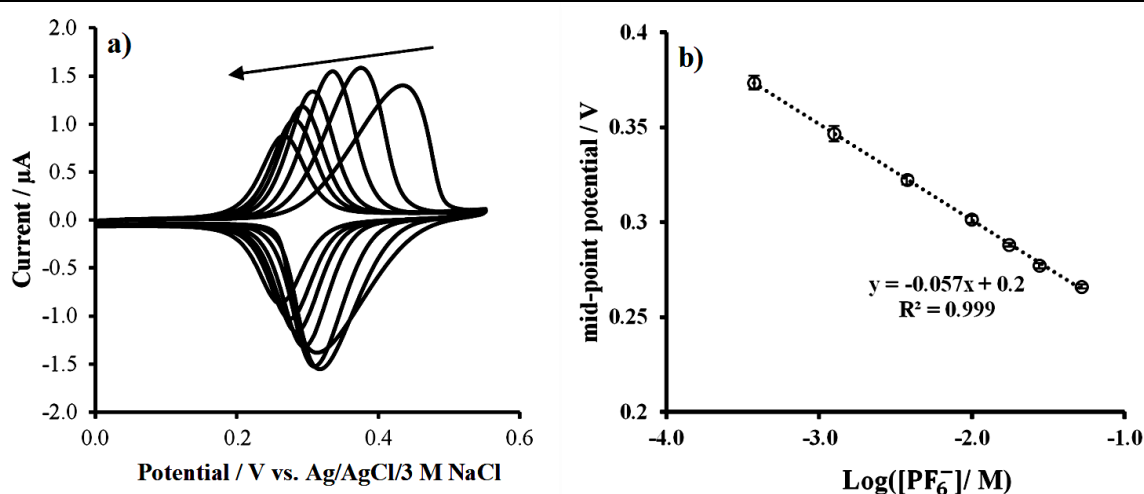


Figure 4.10 : Response of thin film membrane containing 65mmol/kg Ru (bipod) (dmdb), 130mmol/ kg ETH500, 50% NPOE and 50% PU in presence of different concentration of KPF_6 . (375 μM , 1.25 mM , 3.75 mM ,10 mM, 17.5 mM , 27.5, 52.5 mM). (n=3).

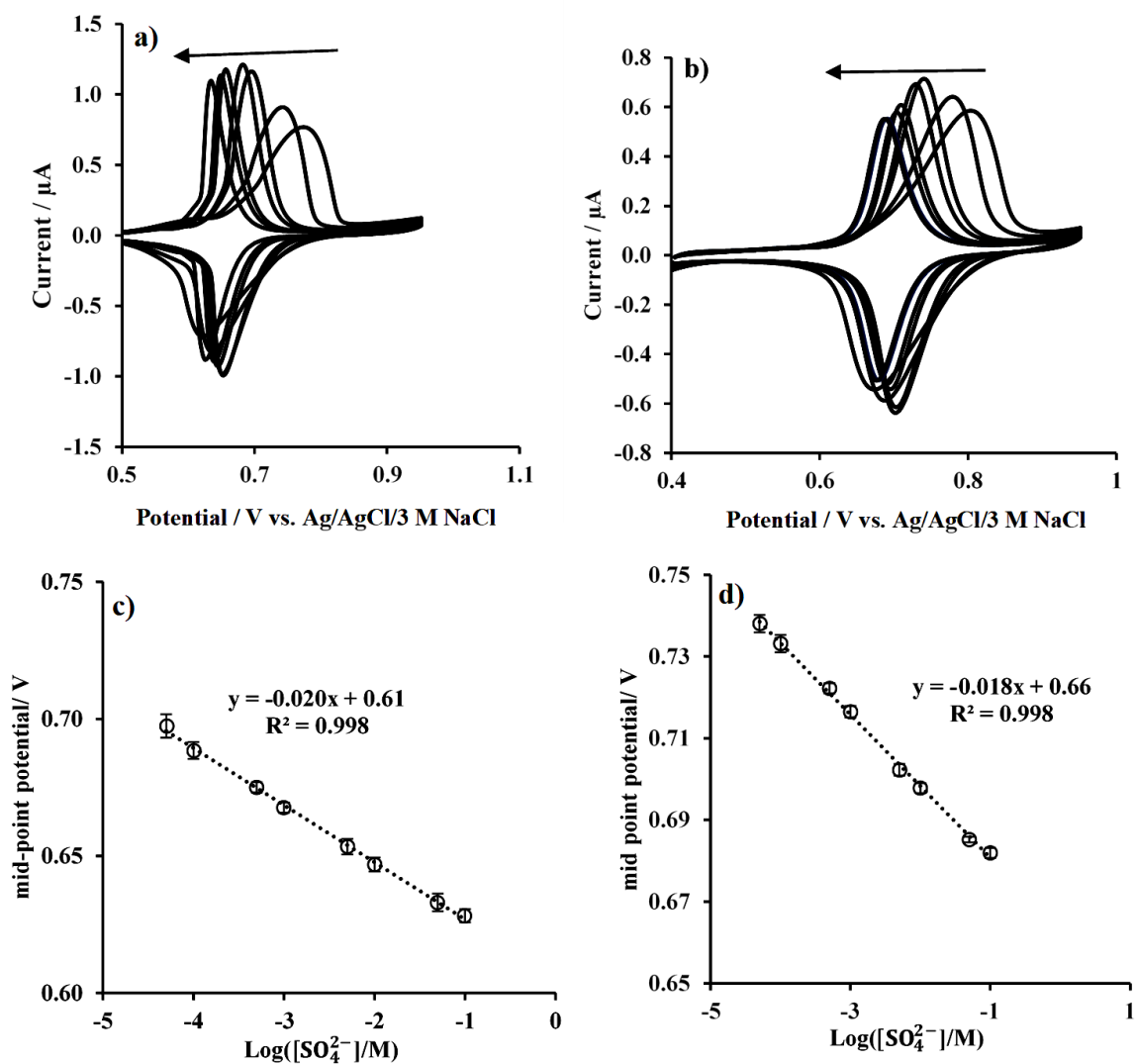


Figure 4.11 : Response of thin film membrane containing 65mmol/ kg of a) Ru (bipod) (dmdb) and b) Ru(bipod)(bipob), 130mmol/kg ETH500, NPOE=PU in presence of different concentration of SO_4^{2-} (5×10^{-5} , 10^{-4} , 5×10^{-4} , 10^{-3} , 5×10^{-3} , 10^{-2} , 5×10^{-2} , 10^{-1} M) and c) and d) relationship between log of the concentrations of SO_4^{2-} and midpoint potential related to the membrane containing Ru(bipod)(dmdb) and Ru(bipod)(bipob), respectively. (n=6).

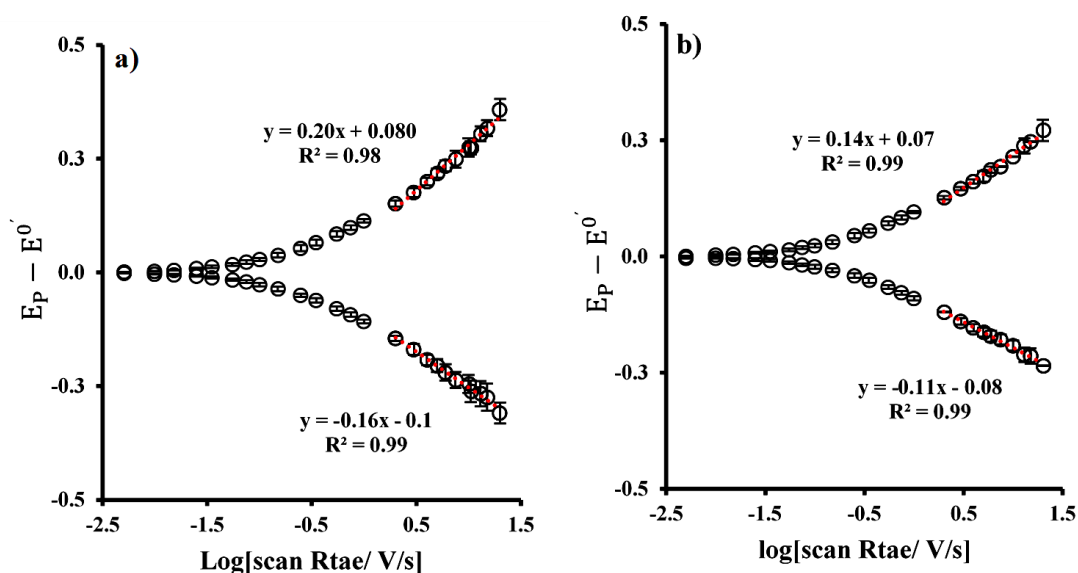


Figure 4.12 : Plots of the oxidation and reduction peak potentials of the Ru-bipod complex in membranes a) 65 mmol/kg Ru(bipod)(dmdbb), NPOE=2PVC and b) 65 mmol/ kg Ru(bipod)(bipob), 66% NPOE and 33% PVC (right) in the presence of aqueous 10 mM KPF_6 versus logarithm of scan rate with(n=3).

Table 4.1 Kinetic parameters calculated from the data in **Figure 4.13** : Plots of the oxidation and reduction peak potentials of the Ru-bipod complex in membranes a) 65 mmol/kg Ru(bipod)(dmdbb) and b) 65 mmol/ kg Ru(bipod)(bipob), 66% NPOE and 33% PVC in the presence of aqueous 10 mM K_2SO_4 versus logarithm of scan rate with(n=3). for the kinetics of Ru(pod)(pob) and Ru(pod)(dmdbb) in the presence of 10 mM KPF_6 . α : electron transfer coefficient, v_a and v_c : anodic and cathodic critical scan rates, respectively, $k_{app,a}$ and $k_{app,c}$: anodic and cathodic apparent electron transfer rate constants, respectively, and k_{app} : total apparent electron transfer rate constant.

PF_6	$1-\alpha$	α	v_a (V/s)	v_c (V/s)	$k_{app,a}(s^{-1})$	$k_{app,c}(s^{-1})$	$K_{app} (s^{-1})$
Ru(pod)(pob)	0.41(\pm 0.03)	0.53(\pm 0.05)	0.30(\pm 0.03)	0.17(\pm 0.04)	4.76 (\pm 0.2)	3.56 (\pm 0.63)	4.16 (\pm 0.27)
Ru(pod)(dmdbb)	0.30(\pm 0.02)	0.38(\pm 0.05)	0.40(\pm 0.02)	0.24(\pm 0.05)	4.56(\pm 0.18)	3.53 (\pm 0.26)	4.05 (\pm 0.04)

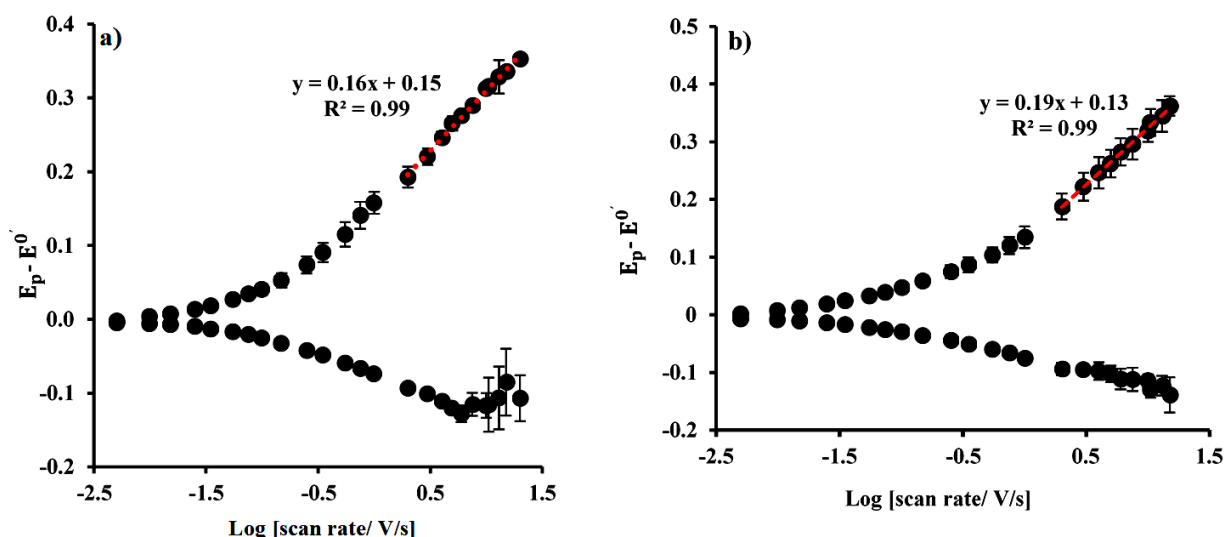


Figure 4.13 : Plots of the oxidation and reduction peak potentials of the Ru-bipod complex in membranes a) 65 mmol/kg Ru(bipod)(dmdbb) and b) 65 mmol/ kg Ru(bipod)(bipob), 66% NPOE and 33% PVC) in the presence of aqueous 10 mM K_2SO_4 versus logarithm of scan rate with(n=3).

Table 4.2 : Kinetic parameters calculated from the data in **Figure 4.13** for the kinetics of Ru(pod)(pob) and Ru(pod)(dmdbb) in the presence of 10 mM K_2SO_4 . α : electron transfer coefficient, v_a and v_c : anodic and cathodic critical scan rates, respectively, $k_{app,a}$ and $k_{app,c}$: anodic and cathodic apparent electron transfer rate constants, respectively, and k_{app} : total electron transfer rate constant.¹

SO_4	$1-\alpha$	α	v_a (V/s)	v_c (V/s)	$k_{app,a}(s^{-1})$	$k_{app,c}(s^{-1})$	$K_{app}(s^{-1})$
Ru(pod)(pob)	0.28 (± 0.02)		0.29 (± 0.09)		3.08 (± 0.8)		
Ru(pod)(dmdbb)	0.36 (± 0.01)		0.13 (± 0.03)		1.78 (± 0.41)		

4.3.6. Sensitivity and selectivity of the membrane with Ru(bipod)(dmdbb) and Ru(bipod)(bipob):

The response of the membranes to sulfate concentration and to mixtures of anions was evaluated as the basis for possible detection of sulfate. Gradual addition of sulfate ions to the aqueous phase from a low concentration of sulfate, 10 nM, to a high concentration of sulfate, 0.1 M, (**Figure 4.14** a and b) showed that the linear response range of the SC-ISE with the membranes containing Ru(bipod)(dmdbb) and Ru(bipod)(bipod) is between ca. 10^{-4} M and 0.1 M. The low detection limit was estimated from the calibration curve by linear extrapolation of mid-point potentials versus

¹ The cathodic transfer coefficient (α) is 1 and Laviron model does not cover this value for estimation of electron transfer kinetics $k_{app,c}(s^{-1})$.

logarithm of SO_4^{2-} concentrations (**Figure 4.14** c and d). For Ru(bipod)(dmdbb) and Ru(bipod)(bipod), the detection limit is around 31 and 38 μM , respectively. In addition, selectivity coefficients were measured by the separate solution method⁹²⁻⁹⁴ with sulfate over chloride and nitrate for membranes containing either Ru complex. In the membrane containing Ru(bipod)(dmdbb), the logarithm of the selectivity coefficients for sulfate ions over chloride ions $\text{Log}K_{\text{SO}_4^{2-},\text{Cl}^-}$ and for sulfate ions over nitrate ions $\text{Log}K_{\text{SO}_4^{2-},\text{NO}_3^-}$ were -0.18 and -6.39, respectively. In the membrane containing Ru(bipod)(bipob), the values of $\text{Log}K_{\text{SO}_4^{2-},\text{Cl}^-}$ and $\text{Log}K_{\text{SO}_4^{2-},\text{NO}_3^-}$ were -1.58 and -7.13, respectively. These results were achieved by Hofmeister series (**Figure 4.9** a and b) and the separate solution method. Based on these results, the membranes show better selectivity for sulfate ions over nitrate ions compared to sulfate ions over chloride ions in the presence of both Ru complexes. Also, selectivity sulfate ions over chloride and nitrate ions is better with the membrane contains Ru(bipod)(bipob) compared to the membrane with Ru(bipod)(dmdbb).

4.3.7. Electrochemical behaviour of thin film in the presence of sulfate ionophores:

To have better sensitivity and selectivity, both a commercially-available sulfate ionophore (S.I) and Tren thiourea bis CF₃ (T.Thio. bisCF₃), which is a synthesised sulfate ionophore from Prof. K. Jolliffe, University of Sydney, (see **Figure 4.15** a and b, respectively) were used in the membrane with both Ru complexes. Based on the previous studies, in order to have a stable response of the membrane containing an ionophore, it is required to add excess amount of sulfate ionophore in the membrane.^{115, 170} In addition, the first 10 scans of the membrane which contains 130 mmol/kg of S.I and with Ru(bipod)(dmdbb) shows a gradual decrease of the peak current and a shift in the peak potential (**Figure 4.16**). Thus, to have a stable response and better selectivity and sensitivity, excess amount of sulfate ionophores (260 mmol/kg) were added to the membrane until, all components are dissolved in the membrane.

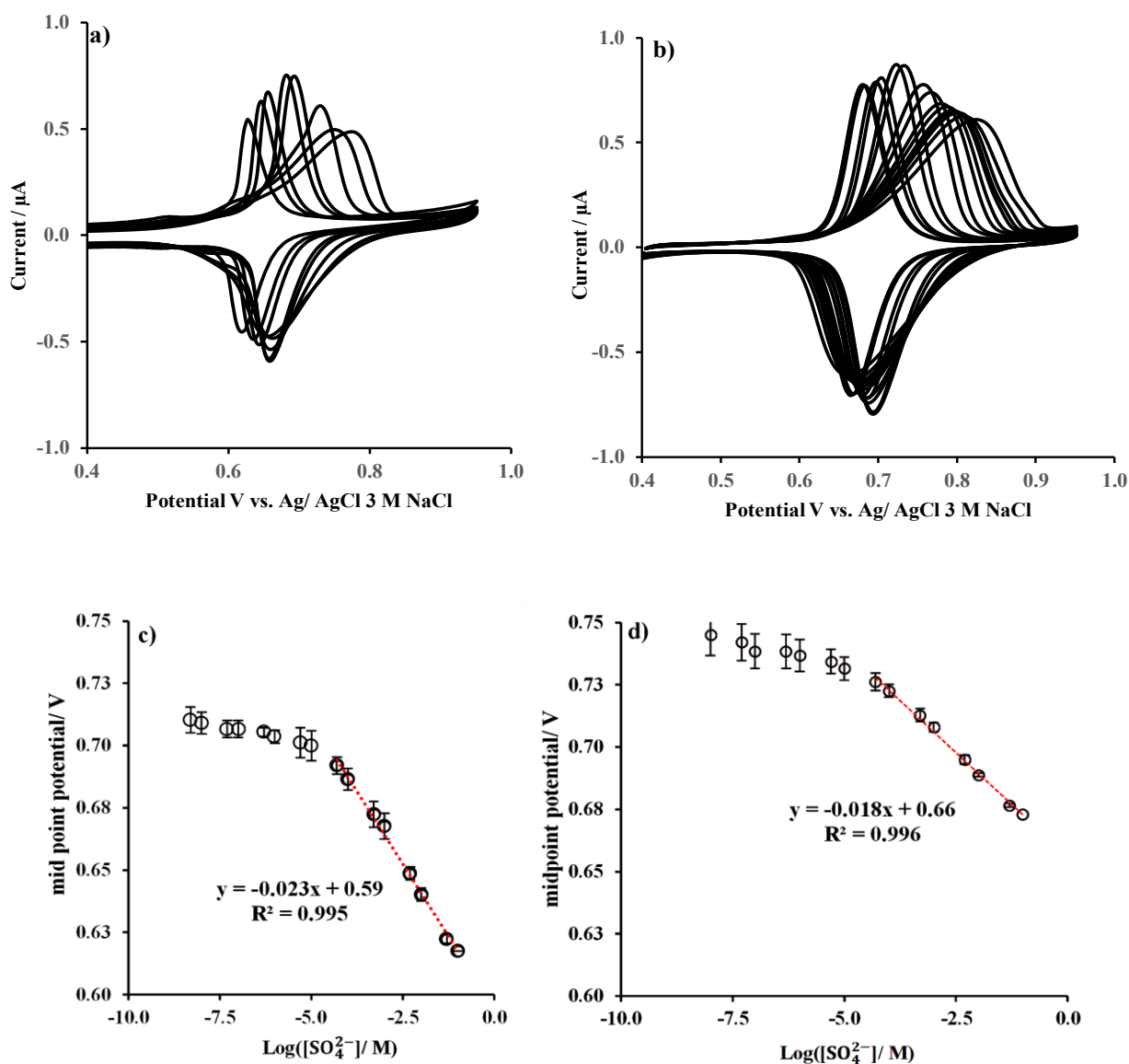


Figure 4.14 : Response of thin film membrane containing a) 65mmol/kg Ru (bipod)(dmbb), and b) 65mmol/kg Ru(bipod)(bipob), 130mmol/kg ETH500, 50% NPOE and 50% PU in presence of different concentration of KSO_4 and the midpoint potential versus logarithm of the different concentrations of sulfate ions with thin film containing c) Ru(bipod)(dmbb) and d) Ru(bipod)(bipob) ($n=3$).

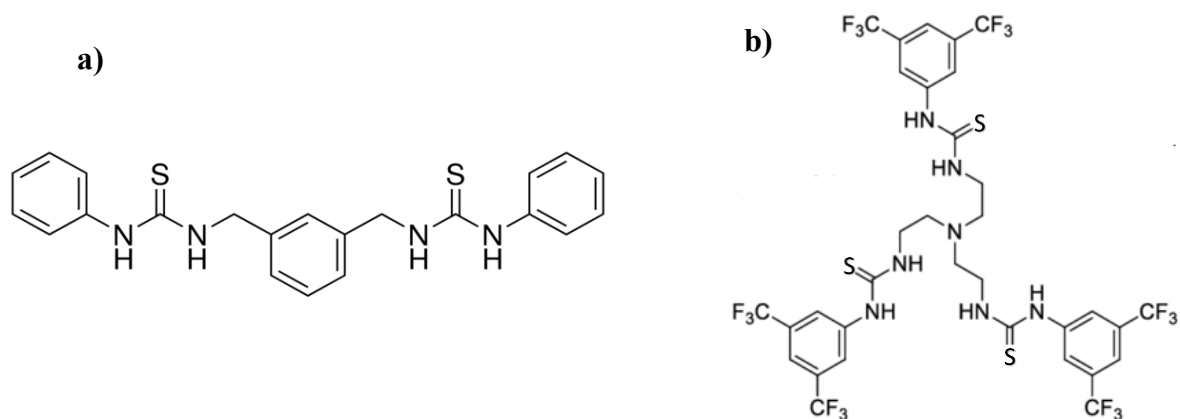


Figure 4.15 : a) structure of commercial sulfate ionophore (S.I) b) structure of Tren thiourea bis CF₃ (T.Thio. bisCF₃).

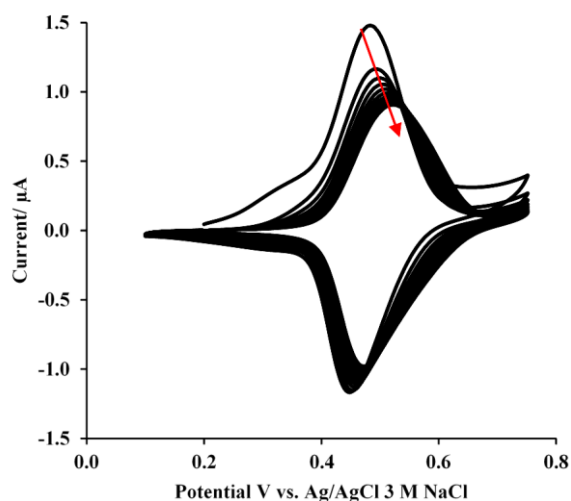


Figure 4.16 : 10 first scans of thin film containing 65 mmol/kg Ru(bipod)(dmbb), 130 mmol/ kg ETH500, 130 mmol/kg Sulfate ionophore, 50% NPOE and 50% PU.

Gradual addition of different concentrations of sulfate to the membrane with S.I together with Ru(bipod)(dmbb) or Ru(bipod)(bipob) complexes were carried out (**Figure 4.17** a and b, respectively) and also plotting of mid-point potential versus logarithm of concentration of sulfate were achieved (**Figure 4.17** c and d). These results showed that in the presence of both complexes there is not a linear response related to Nernstian behaviour with the membrane containing S.I. However, same studies in the presence of excess amount of T.Thio. bisCF₃ showed a linear response between 5 μM and 0.1 M. The limits of detection with the membrane containing either Ru(bipod)(dmbb) or Ru(bipod)(bipob) are 2.86 and 2.60 μM with the membrane with T.Thio. bisCF₃, respectively.

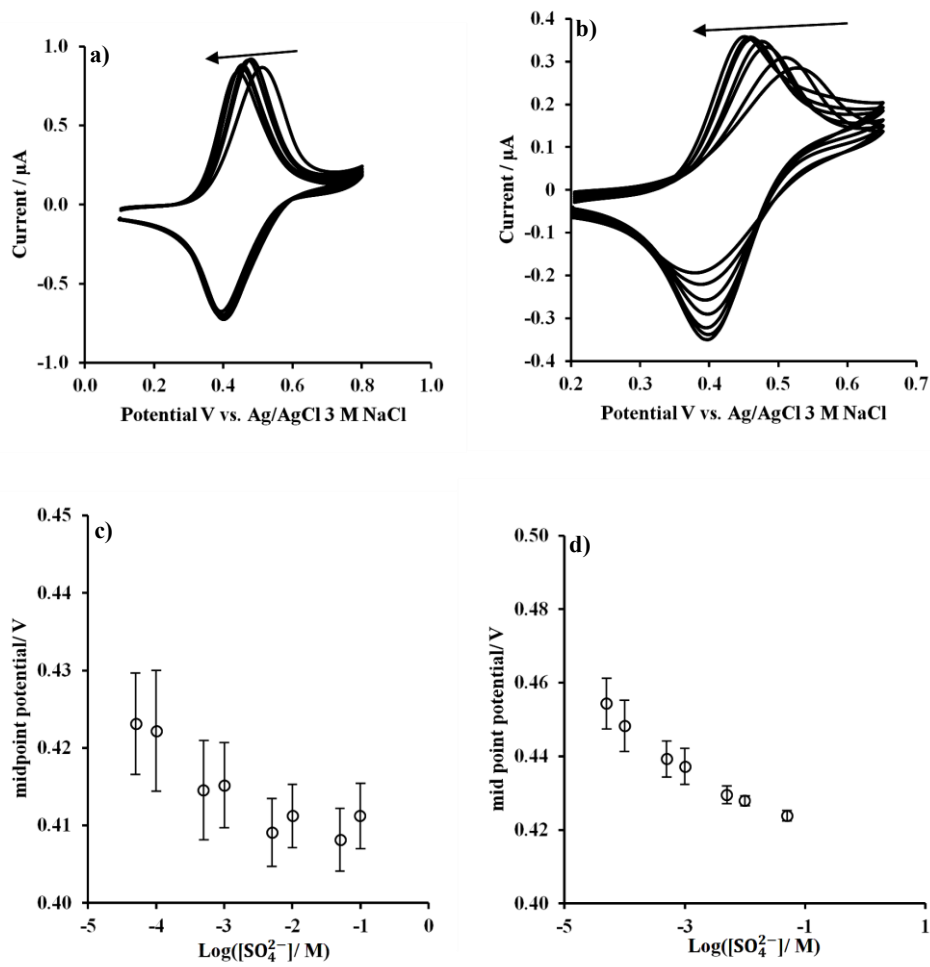


Figure 4.17 : CVs of the thin film: a) 65 mmol/ kg Ru(bipod)(dmbb) b) 65 mmol/ kg Ru(bipod)(bipob) , 130mmol/kg ETH500, 50% NPO, 50% PU and excess of S.I in the presence of different concentrations of sulfate and the midpoint potential versus logarithm of the different concentrations of sulfate ions with thin film containing c) Ru(bipod)(dmbb) and d) Ru(bipod)(bipob).

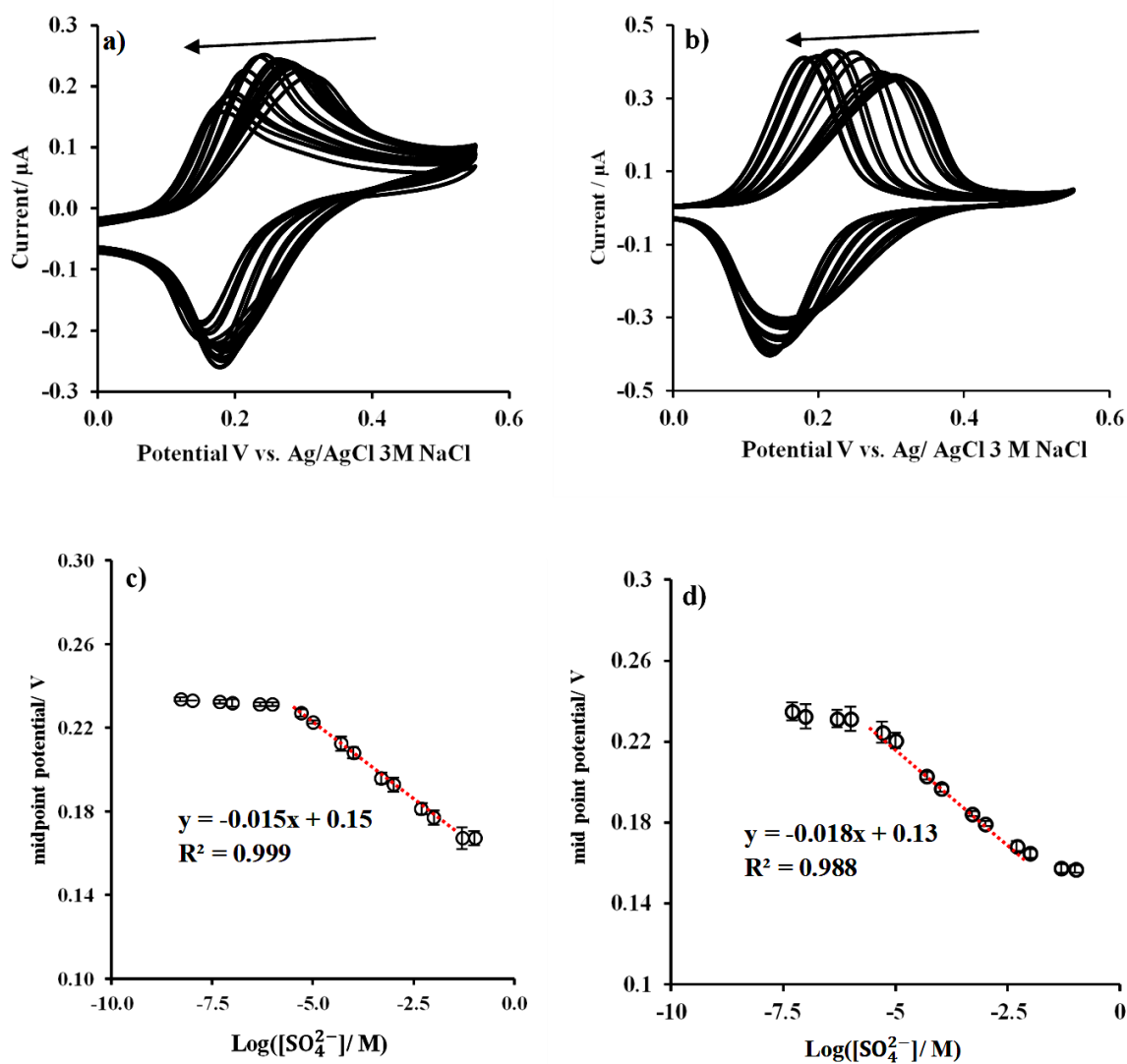


Figure 4.18 : Response of thin film membrane containing a) 65mmol/kg Ru (bipod) (dmdbb) , and b) 65mmol/kg Ru(bipod)(bipob) 130mmol/kg ETH500, excess amount of T.Thio. bisCF₃ ionophore, 50% NPOE and 50% PU in presence of different concentration of KSO₄ ((10⁻⁸, 5 × 10⁻⁸, 10⁻⁷ , 5 × 10⁻⁷, 10⁻⁶, 5 × 10⁻⁶, 10⁻⁵, 5 × 10⁻⁵, 10⁻⁴, 5 × 10⁻⁴, 10⁻³, 5 × 10⁻³, 10⁻², 5 × 10⁻², 10⁻¹ M) and the midpoint potential versus logarithm of the different concentrations of sulfate ions with thin film containing c) Ru(bipod)(dmdbb) and d) Ru(bipod)(bipob) (n=3).

In the membrane containing Ru(bipod)(dmdbb), the logarithm of selectivity coefficient of sulfate ions over chloride ions $\text{Log}K_{\text{SO}_4^{2-}, \text{Cl}^-}$ and sulfate ions over nitrate ions $\text{Log}K_{\text{SO}_4^{2-}, \text{NO}_3^-}$ was -3.91 and -6.26, respectively (**Figure 4.19 a**). Also, in the membrane contains Ru(bipod)(bipob), the logarithm selectivity of coefficient of sulfate ions over chloride ions $\text{Log}K_{\text{SO}_4^{2-}, \text{Cl}^-}$ and sulfate ions over nitrate ions $\text{Log}K_{\text{SO}_4^{2-}, \text{NO}_3^-}$ was achieved -3.25 and -5.83, respectively (**Figure 4.19 b**). Based on these results (which is collected in **Table 4.3**), the membrane shows better selectivity for sulfate ions over nitrate ions for sulfate ions over chloride with both Ru complexes in the presence of T.Thio. bisCF₃. In addition, based on the selectivity coefficients achieved without and with T.Thio. bisCF₃, selectivity of sulfate over chloride was improved by using of T.Thio. bisCF₃ ionophore. In addition, there is

significant improvement in the mid-point potential, and it is shown that by using the sulfate ionophores the ion-to-electron transduction happens easier and at significantly lower potential compared to the membrane without sulfate ionophore (Figure 4.19 a, b). Since there is not linear potentiometric response in the presence of S.I with different concentrations of sulfate, there is not possibility to investigate selectivity of sulfate over chloride and nitrate by separation solution method by the thin film contains S.I.

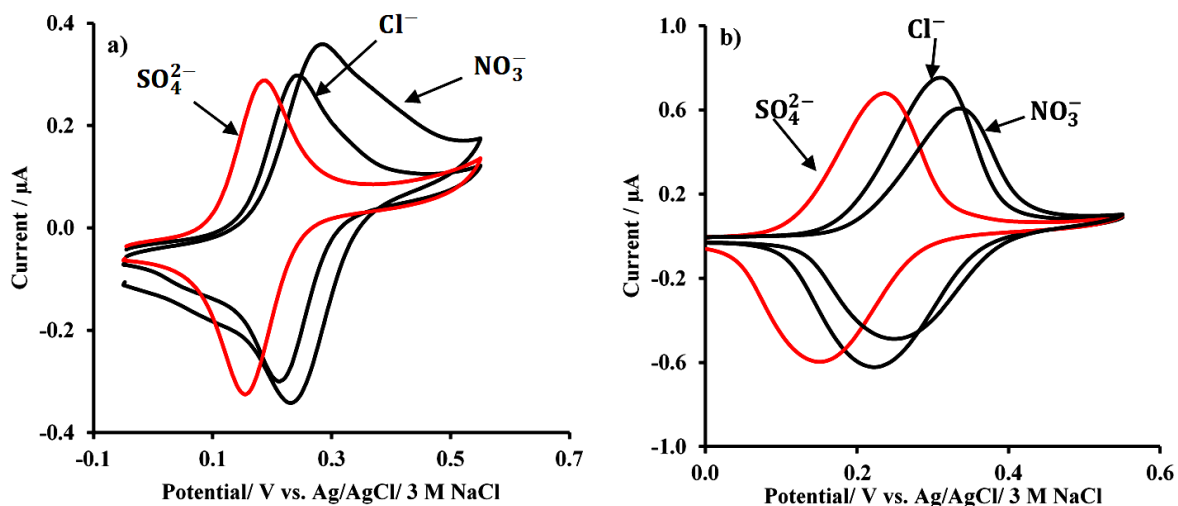


Figure 4.19 : CVs related to responses of the membrane contains a) 65 mmol/ kg Ru(bipod)(dmbb) and b) Ru(bipod)(bipob), 130 mmol/ kg ETH500, excess amount of T.Thio. bisCF₃ ionophore and 50% NPOE and 50% PU in the presence of 10 mM SO₄²⁻, Cl⁻ and NO₃⁻ ions.

Table 4.3 : selectivity coefficients of the thin film with Ru complexes in the presence and absence of T.Thio. bisCF₃ with sulfate over chloride and nitrate ions by separate solution method.

	Ru(pod)(dmbb)		Ru(pod)(pob)	
	Without T.Thio. bisCF ₃	With T.Thio. bisCF ₃	Without T.Thio. bisCF ₃	With T.Thio. bisCF ₃
$LogK_{SO_4^{2-}, Cl^-}$	-0.18	-3.91	-1.58	-3.25
$LogK_{SO_4^{2-}, NO_3^-}$	-6.39	-6.26	-7.13	-5.83

The redox potentials in the presence of sulfate ionophores (S.I and T.Thio. bisCF₃) significantly changed and reduced with thin film contains R(bipod)(dmbb) (Figure 4.20 a) and Ru(bipod)(bipob) (Figure 4.20 b). As it is shown in Figure 4.20 a and b the redox potential was less positive in the presence of T.Thio. bisCF₃.

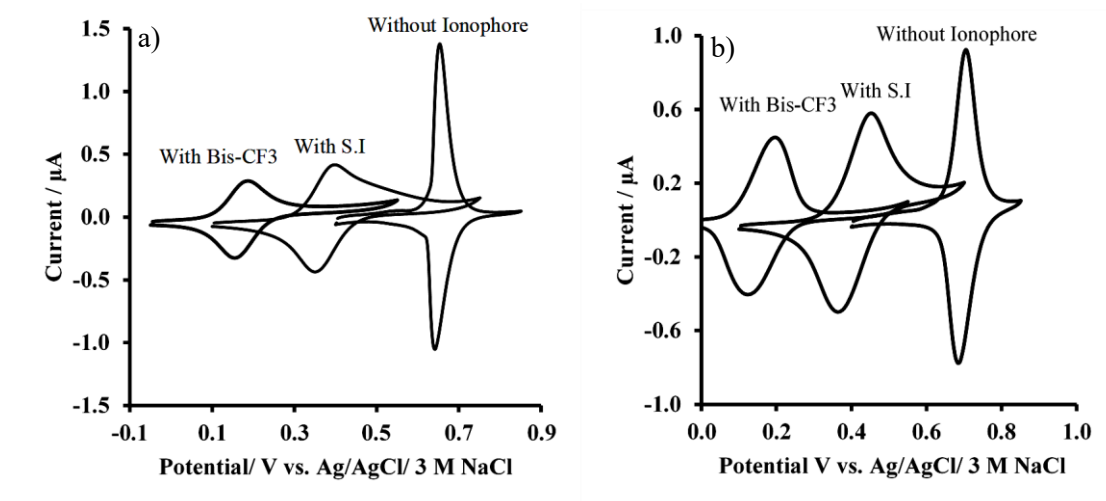


Figure 4.20 : Response of thin film in the presence of 10 mM of Sulfate ions. (scan rate: 10 mV/s) in the presence of a) Ru(bipod)(dmbb) and b) Ru(bipod)(bipob). (from right to left: without any ionophore, with S.I and with T.Thio. bisCF₃ ionophore.

4.4. Conclusion

In this study, two Ru complexes, Ru(bipod)(dmbb) and Ru(bipod)(bipob), were used as a redox transducer within a thin polymeric film for detection of sulfate ions. The complexes showed reversible and stable voltammetric responses in the presence of sulfate ions as a very hydrophilic ion. This is because the redox potential of the new Ru complexes are significantly lower than the redox potential of Ru-bipod (in chapter 3). In addition, they are very stable response in the presence of different ions. Furthermore, thin film behaviour was obtained by these two complexes. Sensitivity and selectivity studies were carried out on the thin films containing these two Ru complexes and there was not a difference in results between these two complexes. The Nernstian slope was not achieved because the balancing ion transfer process upon oxidation/reduction of the Ru complexes was reversible in the presence of PF₆⁻ while sulfate transfer indicated the imbalance ion transfer during ion-to-electron transduction process.

To improve selectivity and sensitivity, S.I and T.Thio. bisCF₃ ionophore were used in the thin films. There was not a linear response upon additions of different concentrations of sulfate ions with S.I while there was linear response with T.Thio. bisCF₃ ionophore. Separation solution method was used to investigate selectivity. Selectivity of the thin films with T.Thio. bisCF₃ ionophore was investigated. Selectivity of the membrane with sulfate over nitrate and chloride was improved compared to the membrane without the ionophore.

5. Immobilization of Janus type Ru complex on ITO electrodes and investigation of its electrochemical behaviour

5.1. Introduction

The ion transfer process between polymeric phases and aqueous phases across the interface has been developed during this decade²³³ As discussed in previous chapters, there are several approaches to sense ions by this method. One of the most recent methods is using redox molecules in thin polymeric films. One big issue related to this method is the use of high concentration of redox probe molecules in thin films by the spin coating method. Because to have effective ion transfer process by this method, a high concentration of metallic active centre is needed on the surface of the electrodes. This can be more problematic when an ionophore is used in the thin film, and there is leaching of redox probes molecules from polymeric layer to the aqueous phase.¹⁷⁰

Because of this problem, it will be required to use excess concentrations of the ionophore in the thin film, and by use of excess amount of the ionophore, the diffusion can be dominant compared to thin-film behaviour. This problem can be addressed by immobilization of the redox probes on electrode surfaces and can overcome the instability of SC-ISEs with both redox probes and ionophores. The first time this method was introduced by Pretsch and co-workers to immobilise fullerene or tetrathiafulvalene on gold electrodes.²³⁴ After immobilization of redox active compounds on gold electrode surfaces, the regular ion selective membrane with valinomycin as the ionophore was used to sense potassium. In another study, gold chips were modified by five synthesised organothiol ferrocene complexes as redox active materials; the best one was benzenethiol based self-assembled monolayer and it was used for potentiometric study of sodium ions.²³⁵ In addition, silicon-based electrodes with gold contacts were modified by immobilisation of redox-active organothiols and were coated by polymeric membranes and used for potentiometric analysis.²³⁶ In a very recent study, ferrocene was self-assembled on GC electrode, and after coating of the modified electrodes by PVC based membrane by spin coating to provide very thin layer of polymeric based membrane (with nanometer thickness), these electrodes were used to sense anions and cations.²³³ One of the most important advantages of this method is that in all modified electrodes, there is very close proximity between the molecular redox probes and the electrodes, and it helps to have very effective ion transfer. Thus, in this method it is not required to used high number of redox probes, and consequently in the presence of ionophore to have more selectivity of the sensors, and there is not leaching of the redox molecules into the aqueous phase.

In this study, in order to provide more stable and robust anion sensors with selective sensing capability of sulfate ions, the J-Ru complex (**Figure 5.1**), which was reported by Haga and co-worker,²³⁷ was immobilised on ITO electrodes and evaluated for anion sensing. The Ru complex has hydrophilic

phosphonate groups that chemisorbed onto the surface of the ITO. The polymeric based membrane was then spin coated on the modified ITO electrode and thin layer behaviour of these ITO electrodes was evaluated. Reproducibility of prepared ITO electrodes was investigated with calculation of surface coverage of the Ru complex. Then, the sensing ability of the modified ITO electrode with spin coated polymeric thin film in the presence of different concentrations of ClO_4^- and SO_4^{2-} ions was examined. Finally, the electron transfer rates were measured in the presence PF_6^- ions. This chapter presents a preliminary study of modified ITO electrodes as possible substrates for ion sensors.

5.2. Experimental

5.2.1. Reagent:

Potassium chloride, potassium hexafluorophosphate, potassium nitrate, potassium perchlorate, potassium sulfate, tetrakis(4-chlorophenyl) borate tetradodecylammonium salt (ETH500), 2-nitrophenyloctylether (NPOE), anhydrous tetrahydrofuran (THF), high molecular weight poly (vinyl chloride) (PVC), the sulfate ionophore (S.I.) were purchased from Sigma Aldrich in analytical grade, and pure Dimethylformamide (DMF) from Sigma Aldrich. Aqueous solutions were prepared in deionized water (resistivity 18.2 M Ω cm; USF Purelab with UV). Janus- Ru complex (**Figure 5.1**) was received from Prof. M.-a. Haga and was synthesized and characterized as stated in ref.²³⁷

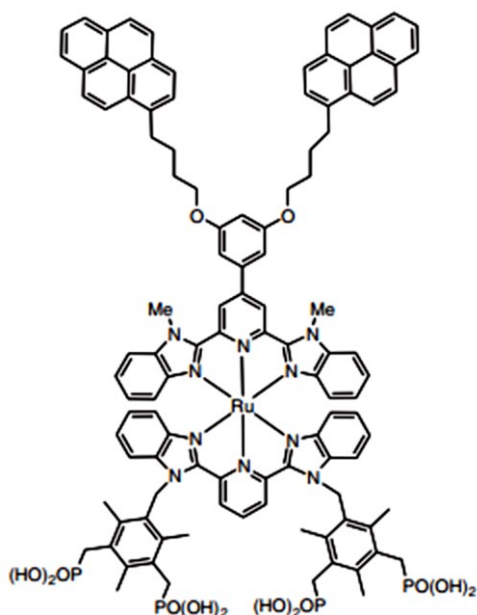


Figure 5.1 : The structure of the Janus Ru complex²³⁷ employed in this work.

5.2.2. Modification of ITO electrodes:

ITO electrodes were immersed in pH 5 aqueous DMF solution, which contained 50 μM of the Janus- Ru complex, for 24 hours. The modified electrodes, after rinsing by DMF and D.I. water and drying by nitrogen gas, are ready to use.²³⁷ The dimension of active surface area of the electrodes was measured by ruler and the average of the surface area is around 1.83 cm^2 for each electrode.

5.2.3. Instrumentation and measurement:

A three-electrode electrochemical cell was used for all measurements, comprising a Janus- Ru complex modified-ITO working electrode of rectangular shape (25 mm ×12.5 mm) on glass substrate (Sigma Aldrich)(with 8-12 Ω/sq) , a Ag/AgCl/3 M NaCl reference electrode (model MF-2056, BASi), and a platinum disc as counter electrode. The cell was placed in a Faraday cage. Electrochemical experiments were conducted with an Autolab PGSTAT302N electrochemical workstation (Metrohm, The Netherlands) with NOVA software. Preparation of the organic thin films is the same as reported in chapters 3 and 4, by using of a spin coater (Model WS-400B-6NPP/LITE) at 1500 rpm for one minute.

5.3. Results and discussion

5.3.1. Characterization of Janus-Ru complex modified ITO electrode:

Electrochemical responses of the modified ITO electrodes were evaluated by cyclic voltammetry at different scan rates (**Figure 5.2 a**). A linear response of peak current versus scan rate was achieved in this study (**Figure 5.2 b**), which shows immobilisation the Janus Ru complex on ITO electrodes which agrees with other reports.^{233,237} In addition, by the results of the scan rate study, the surface coverage of the Janus Ru complex on ITO can be calculated from equation 5.1²³⁸:

$$I_p = \left(\frac{n^2 F^2}{4RT}\right) \Gamma A \nu \quad \text{Equation 5.1}$$

In this equation, I_p is the peak current, A is the electrode surface area, Γ is the surface coverage and ν is the scan rate. Based on the slope of the straight line in **Figure 5.2 b**, and the surface area of the ITO electrodes, which is around 1.83 cm^2 , the surface coverage is estimated to be around $4.6 \times 10^{-11} \text{ mol/cm}^2$, which is comparable with the value reported in other studies which is $2.5 \times 10^{-11} \text{ mol/cm}^2$.^{237,238}

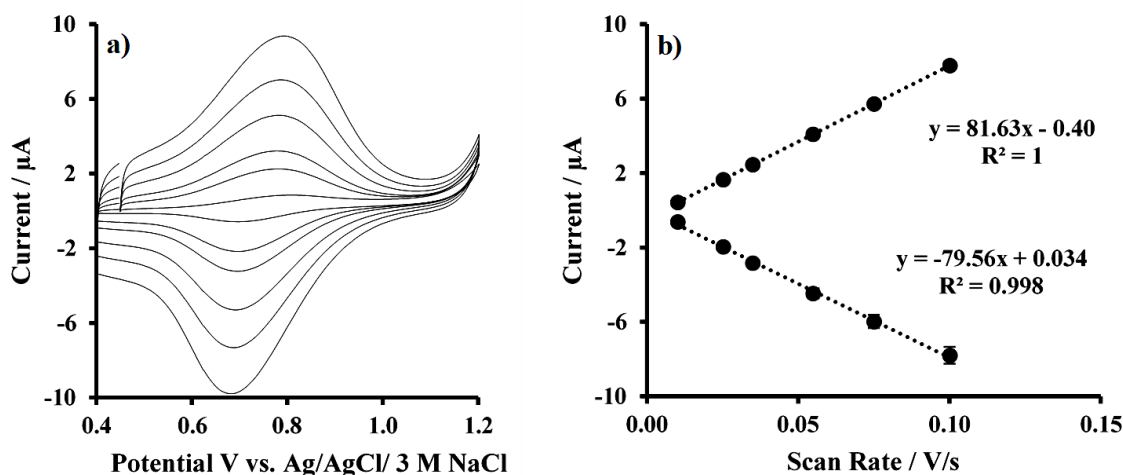


Figure 5.2 : Voltammograms of the ITO electrode which is modified with Janus Ru complex at different scan rates in aqueous solution containing 10 mM KPF_6 b) the linear relationship between peak currents and scan rates (10, 25, 35, 55, 75, 100 mV/ s) in forward and backward scans ($n=3$; error bars show standard deviation, and are not visible if smaller than the symbol size).

Half-width potentials were measured with the modified ITO electrodes. As shown in **Figure 5.3**, the half width potential is much higher (190 ± 15 mV) than the theoretical value $(90/n)^{212}$. Also, the peak-to-peak separation of the CVs of the Janus Ru complex on the ITO electrodes is 100 ± 12 mV, while the ideal value for surface-immobilised complexes is around 0 mV.²¹² These deviations can be attributed to interaction between the adsorbed Ru complexes can impose on each other.^{232, 233, 238}

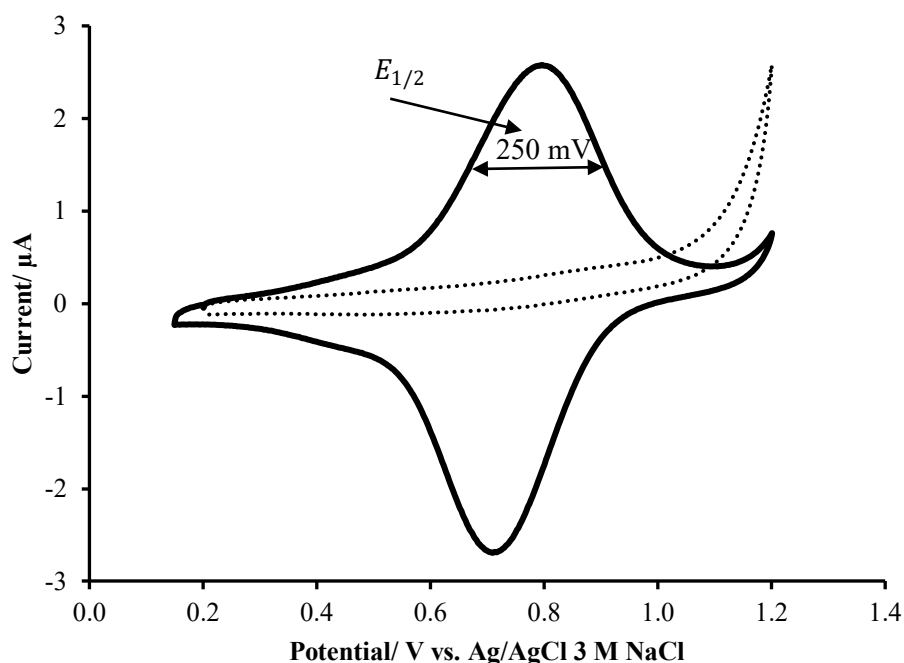


Figure 5.3 : Cyclic voltammogram of modified ITO electrode (solid line) by J-Ru complex and bare ITO electrode (dotted line) in the presence of 10 mM KPF_6 in aqueous solution (Scan rate :55 mV/s).

In next step, the thin film PVC-based membrane was spin coated on the modified ITO electrodes. The thin film is the same as the membrane used in SC-ISEs and contains plasticizer and ETH500 as background electrolyte. The mechanism of anion transfer is the same as in the membrane in SC-ISEs. Oxidation of the Janus Ru complex causes the tetrakis(4-chlorophenyl) borate (i.e. the anion of ETH500) to stabilise the oxidised Ru complex and then this imbalance in charge in the thin film can be compensated by anion transferring from aqueous phase to organic membrane phase (**Figure 5.4**).

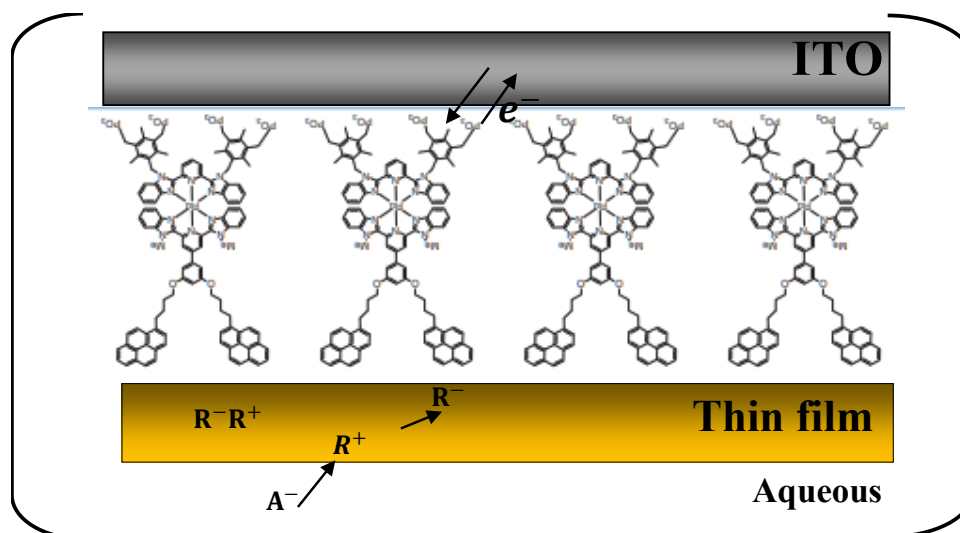


Figure 5.4 : Scheme of anion transfer by thin film which is spin coated on immobilised ITO electrode, R^+ and R^- are tetradodecylammonium and tetrakis(4-chlorophenyl)borate ions , respectively.

Electrochemical responses of the modified ITO electrodes with thin film were evaluated by cyclic voltammetry at different scan rates (**Figure 5.5 a**). A linear response of peak current versus scan rate was achieved (**Figure 5.5 b**), which indicates that the ion-to-electron transduction is controlled by thin film behaviour and not diffusion, and hence the polymeric layer on the ITO electrodes is very thin layer. peak to peak separation is 140 ± 10 mV at 10 mV/s scan rate, and halfwidth potential at 55 mV/s of scan rate is 340 mV. Comparison of these parameters with the parameters obtained by the modified ITO electrodes, shows increase peak-to-peak separation and half width potential of the modified electrodes with polymeric film compared to the modified ITO electrodes without polymeric film. These results showed that polymeric film caused the modified ITO electrodes have more deviation from theoretical values. The surface coverage of the modified ITO electrodes with the polymeric film was obtained as 1.46×10^{-11} mol/cm².

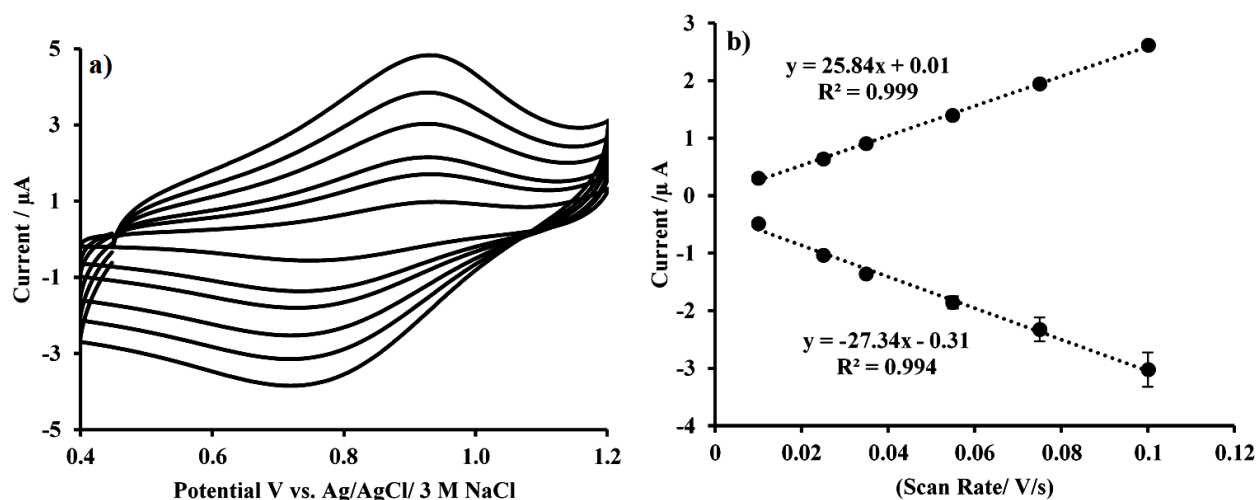


Figure 5.5 : Voltammograms of the immobilised ITO electrode with the polymeric thin film containing 65 mmol/ kg ETH00, PVC and NPOE, at different scan rates (10, 25, 35, 55, 75, 100 mV/s) in solution containing 10 mM KPF_6 ; b) the linear relationship between peak current and scan rate in forward and backward scans ($n=3$; error bars show the standard deviation; where error bars are not visible, the error bars are smaller than the symbol size).

5.3.2. Electrochemical responses of the modified ITO electrode in the presence of different anions:

Cyclic voltammetry responses of the modified ITO electrodes with spin coated by polymeric membrane were evaluated in the presence of different anions. As is shown in **Figure 4.6**, in comparison to the SC-ISE system with Ru(bipod), Ru(bipod)(dmdbb) or Ru(bipod)(bipob) (reported in chapters X and XX) in which there are significant differences between redox mid-point potential of the Ru complexes in the presence of different anions, the redox mid-point potential of the Janus Ru complex on ITO with the thin film was not sensitive to the presence of different anions. It seems that the rigid arrangement of the Janus Ru complex on the ITO and the high electrostatic forces between neighbouring complexes combined with the thin film, which is coated on the surface of the electrodes, causes the CVs to be broadened so that they are not sensitive to the different anions in the aqueous solutions.

In addition, since the redox potential of the Janus Ru complex is around 1 V vs. Ag/AgCl, the first scan of the electrode which contains of ETH500 has very large oxidation current (first scan in **Figure 5.7**) which is related to oxidation of ETH500. This oxidation can impact the response of the modified ITO electrode in the presence of each anion in the same way as the membrane containing ETH500 in SC-ISEs with Ru(bipod) in the presence of different anions was impacted (**Figure 4 a and c**, chapter 3). As it is shown in **Figure 5.6** in the presence of different anions, there is no significant difference in redox potential of the Ru complex.

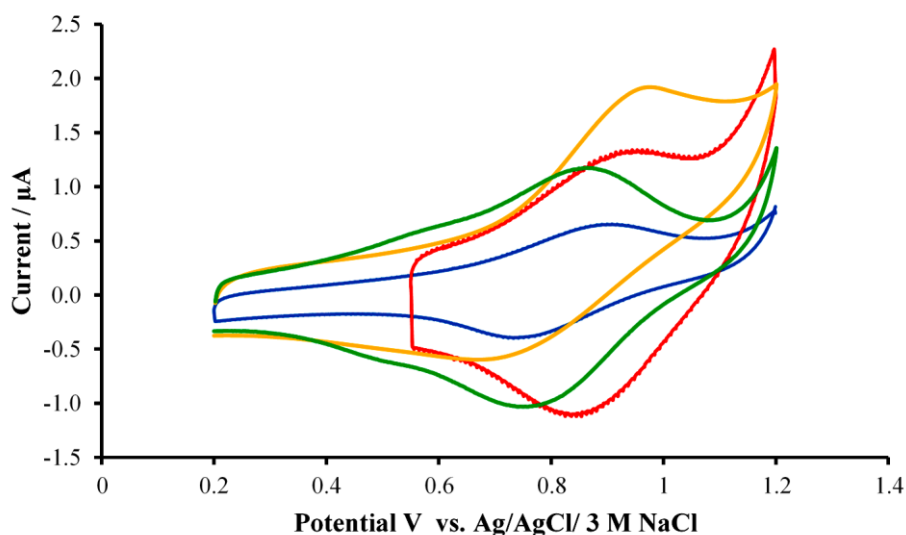


Figure 5.6 : CVs (third scan) related to immobilised ITO electrode which is spin coated by thin film (containing 65 mmol/ kg ETH500, PVC, NPOE) in the presence of different 10 mM aqueous solutions of anions, PF_6^- (orange), ClO_4^- (blue), NO_3^- (green) and SO_4^{2-} (red).

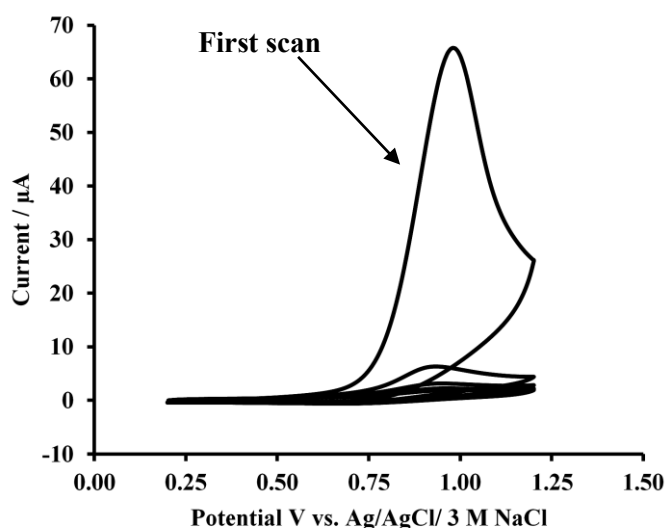


Figure 5.7 : 10 first scans of the modified ITO electrode with polymeric thin film containing 65 mmol/kg ETH500, PVC and NPOE, in the solution containing 10 mM KPF_6 (Scan rate:10 mV/s).

However, in contrast to the behaviour of the membrane in SC-ISEs with Ru(bipod) in which there was an ideal electrochemical response in the absence of ETH500, there was not a redox response of the Ru Janus with the membrane without ETH500 (**Figure 5.8**). This might be because there is not any charge in the thin film to compensate the charge imbalance due to oxidation and reduction of the Janus Ru complex and hence the thin film without ETH500 acts like non-conductive layer.

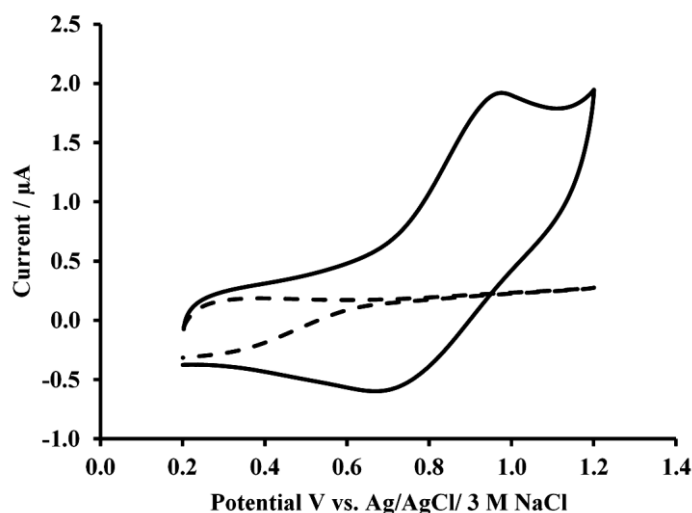


Figure 5.8 : Comparison of CV of the modified ITO with polymeric thin film membrane with (solid line) and without (dotted line) added ETH500 in the solution containing 10 mM KPF_6 (Scan rate:10 mV/s).

5.3.3. Sensitivity of the immobilised ITO electrode with the thin film:

The sensitivity of the ITO electrodes with and without the thin film in the presence of different concentrations of KPF_6 in aqueous solutions was evaluated (**Figure 5.9** and **Figure 5.10**). As shown in **Figure 5.9 a**, the CVs related to the modified ITO without polymeric thin film, the Nernstian slope was not obtained upon plotting of the mid-point potential of the CVs against the logarithm of different concentrations of PF_6^- ions (**Figure 5.9 b**). However, the potentiometric behaviour was improved by the use of modified ITO electrodes with polymeric thin film (**Figure 5.10 a, b**), but still has deviation from the ideal value ($0.059/n$).

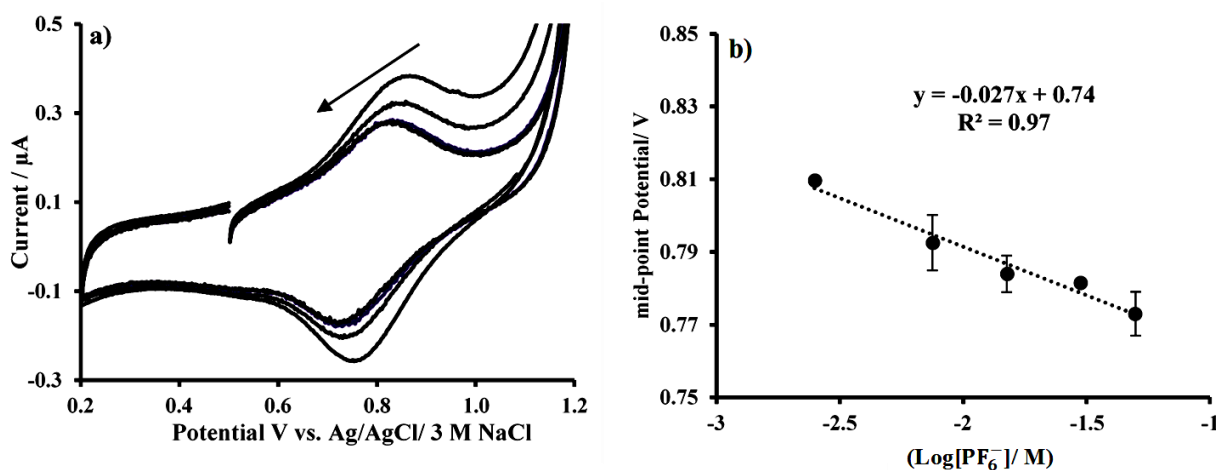


Figure 5.9 : a) Response of the immobilised ITO electrode in the presence of different concentrations of PF_6^- (2.5, 7.5, 15, 30 and 50 mM). b) relationship between log of concentration and midpoint potential, with a Nernst slope for PF_6^- Scan rate: 10 mV/s. ($n=3$).

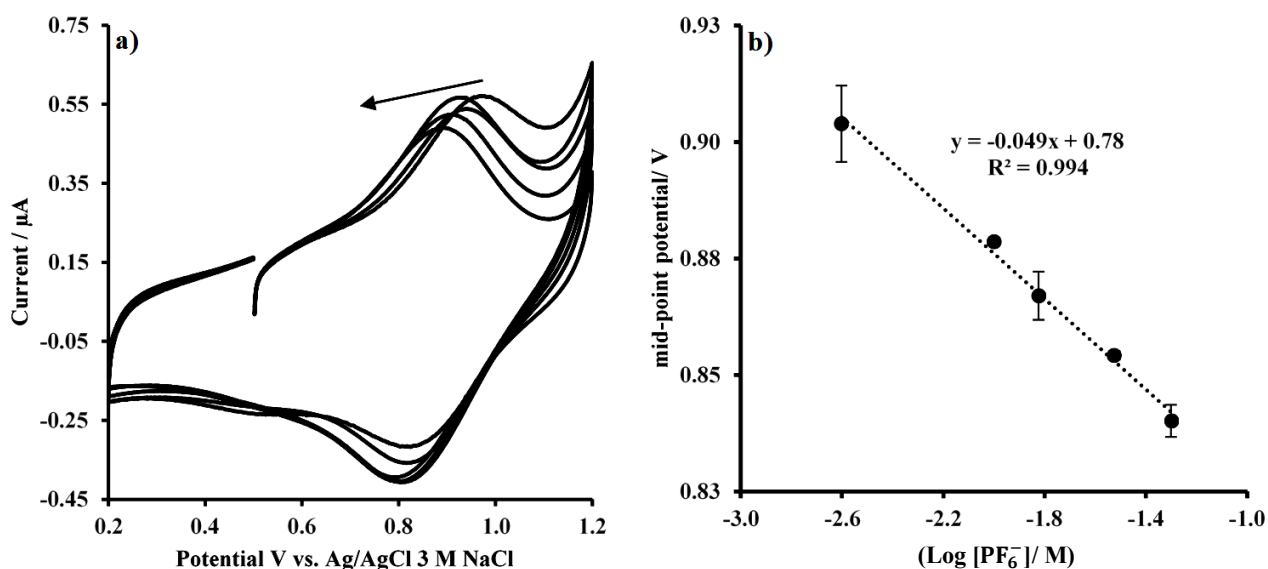


Figure 5.10 : a) Response of the immobilised ITO electrodes with thin film membrane containing 65 mmol/kg ETH500, PVC and NPOE in the presence of different concentrations of PF_6^- (2.5, 7.5, 15, 30 and 50 mM). b) relationship between log of concentration and midpoint potential, with a Nernst slope for PF_6^- Scan rate: 10 mV/s. ($n=3$).

In a similar study, the response of the modified ITO electrode with polymeric thin film with and without commercial sulfate ionophore S.I in the presence of 10 mM sulfate was evaluated (**Figure 5.11**). As shown in **Figure 5.11**, the membrane that contains S.I is not responsive to sulfate, and there is not any peak current showing the transfer of sulfate from the aqueous phase to the thin film on the modified electrode.

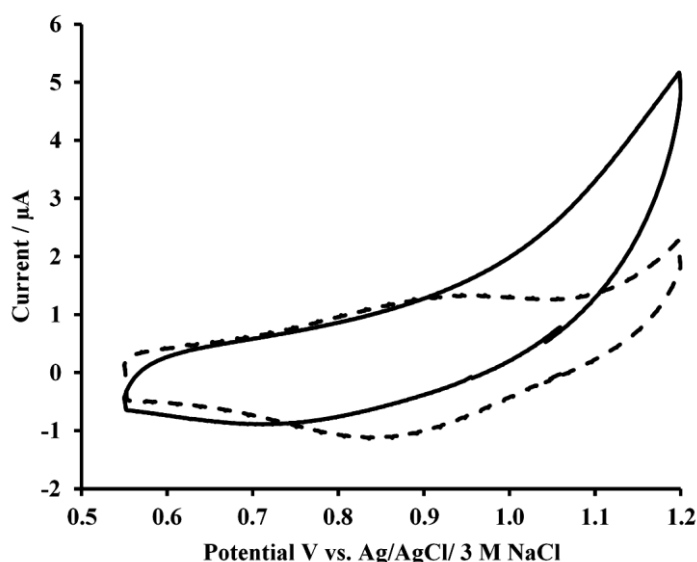


Figure 5.11 : Electrochemical response of the modified ITO with thin film contains 65mmol/kg ETH500, PVC, NPOE and with 130 mmol/ kg S.I (solid line) and without S.I (dotted line). In the solution contains 10 mM K_2SO_4 (Scan rate: 10 mV/s).

5.4. Conclusion:

Electrochemical responses of a Janus Ru complex on ITO electrodes to sense anions was investigated. A monolayer of the Janus Ru complex immobilised on ITO was investigated by scan rate study and surface coverage analysis of the Ru complex. A thin PVC-based membrane was spin coated on the modified ITO electrodes, and it was shown ion-to-electron transduction is controlled by thin film behaviour, not diffusion. The responses of the electrode were evaluated and compared in the presence of different anions, but there is no significant difference in the midpoint potential related to the ion-to-electron transduction in the presence of different anions. This can be attributed to the very high deviation of half width potential and peak to peak separation from theoretical values, which can be due to high electrostatic forces of the Janus Ru complexes on each other and also to the very high peak current of the first scan in the presence of ETH500 in the membrane, which is related to oxidation of ETH500. In addition, it was shown without ETH500 in the thin film, reversible electrochemical responses were not achieved, and the thin film without ETH500 acts as a nonconductive layer on the ITO electrodes. The sensitivity of the modified ITO electrodes with and without polymeric thin films in the presence of PF_6^- ions were evaluated. The difference in behaviour of the modified ITO electrodes with thin film without ETH500 and thin film contains Ru(bipod) complex without ETH500 can be in the last one, the mobility of Ru complexes can assist ion to electron transduction process while in the modified electrodes without ETH500, because of the rigid attachment (with four covalent bonds) of the J-Ru complexes on surface of ITO, there is not any mobility to perform ion to electron transduction process. Although the sensitivity was improved by using thin film on ITO electrodes, the potentiometric slope deviated from the theoretical (Nernstian) value and the linear range was very limited. Finally, the responses of the electrodes in the presence of sulfate ions in cases of with and without sulfate ionophore were evaluated. No response was achieved from the modified ITO electrodes with thin films containing the sulfate ionophore S.I. Modified electrodes can be more promising alternatives and they provide very stable response. This chapter represents the preliminary evaluation of the modified electrodes with redox probes for sensing purposes. The results are not promising for sensing purpose as much as the results obtained in chapter 3 and 4. However, it needs more investigations to provide different functional groups on different types of working electrodes like GC or gold electrodes and design new molecules and attachment bonds.

6. Conclusions

6.1. General Conclusions

The work presented in this thesis describes the study into using electrochemistry at the interface between two immiscible electrolyte solutions (ITIES) as a way for sensing of ions. Facilitated ion transfer was applied to sense sulfate as a challenging ion (Chapter 2). In addition, to provide more mechanical stability to a sensor, solid contact electrodes were applied to sense anions (Chapter 3). Changing in the chemical structure of the redox probe employed in solid contact sensors was investigated to provide sensing of sulfate (Chapter 4) and the modified electrodes were applied to provide more robust and sensitive sensors to detect anions (Chapter 5).

Facilitated potassium transfer by DB18-C6 was examined at micro-ITIES arrays located at glass membranes with two types of pores for interfaces, located at either the laser entry side or the laser exit side of these laser-ablated membranes. The highest mass transfer was achieved across the interfaces located at the pores on the laser entry side (which were wider in diameter). In addition, facilitated ion transfer was studied for sulfate ions by using different synthesised sulfate ionophores at water/NPOE interfaces formed at laser entry side of glass membranes. Interfacial complexation of SO_4^{2-} was investigated with two synthesised ionophores (Tren-phenyl and Tren-bis CF_3). Tren-bis CF_3 was chosen as the best ionophore and Nernstian behaviour was examined with different concentrations of SO_4^{2-} ions in the presence of Tren-bis CF_3 ionophore. Both cyclic voltammetry and differential pulse voltammetry, as a more sensitive technique, were used to sense sulfate. The results in this chapter suggest that there is no difference in thermodynamic and kinetic parameters between these two types of pore configurations. However, significant improvement in sensitivity was obtained with micro pores made at laser entry side. Although facilitated ion transfer at the ITIES can be used to develop ion sensors, it does not have mechanical stability. To address this, the solid contact sensor format can provide a more robust sensor for sulfate.

Polymer based thin films containing a Ru-bipod complex as a redox transducer were investigated for detection of anions. Although these thin films showed reversible and stable voltammetric responses in the presence of more lipophilic anions, in the presence of more hydrophilic anions like sulfate and chloride, the response was unstable. This was attributed to the high redox potential of the Ru-bipod complex in the presence of these anions; at the high positive potential different species of the thin film were oxidised. From the first CV of the thin film with background electrolyte (ETH500) or sulfate ionophore, it can be concluded that there is possibility of oxidation of ETH500 and sulfate ionophore. Two types of plasticizers (NPOE and DOS) with significant difference in dielectric constant were evaluated to study of thin film behaviour, by variation of the voltammetric scan rate.

Thin film behaviour was obtained in the presence of NPOE as the plasticizer. This difference can be related to rate of electron transfer of the Ru-bipod complex in thin films was substantially different with these two plasticizers. Moreover, the Ru-bipod complex showed Nernstian responses to lipophilic anions. These results suggest that the redox potential of the redox probe has key impact on the stability of the thin film. The more positive redox potentials can cause oxidation of components in the thin film. This phenomenon can be worse in the presence of more hydrophilic anions. To sense more hydrophilic anions like sulfate, design of new Ru complexes with less positive redox potential is needed, in order to provide more stable response in the presence of sulfate ions.

Two new Ru complexes, Ru(bipod)(dmbb) and Ru(bipod)(bipob), were utilised as redox transducers within thin polymeric films for detection of sulfate ions. Reversible and stable voltammetric responses were obtained in the presence of sulfate. In these Ru complexes, one Ru-N bond was replaced by one cyclometalated bond (Ru-C) in Ru-bipod (the complex studied in chapter 3). The cyclometalated bond has more electron donation property compared to Ru-N bond. This new design of Ru complex can facilitate electron transfer, consequently less positive redox potentials for these two new complexes were achieved. A scan rate study showed thin film behaviour for both of these complexes. Although, the Nernstian slope was achieved in the presence of PF_6^- , there was a deviation from Nernstian slope in the presence of sulfate ions. This deviation can be related to an imbalance in the ion transfer process during the ion-to-electron transduction process. A commercial sulfate ionophore (S.I) and synthesised T.Thio. bisCF₃ ionophore were used in the thin films. There was not a linear response upon additions of different concentrations of sulfate ions with S.I while there was linear response with T.Thio. bisCF₃ ionophore. Sensitivity was improved by using T.Thio. bisCF₃ compared to a thin film without ionophore. Selectivity of the thin films containing T.Thio. bisCF₃ for sulfate over chloride and nitrate ions was investigated. There was significant improvement with selectivity results for sulfate over chloride, but the measured selectivity coefficient was worse with sulfate over nitrate ions. The results in this chapter suggest that the chemical structure of redox probes and their redox potential can cause significant improvements in stability of the thin film contains redox probes in the presence of one the most hydrophilic anion such as sulfate. In addition the redox potentials of the redox probes are more important than the number of alkyl chains in the chemical structure of the redox probes to provide more lipophilic molecules dissolving in the polymeric film. One of the main issue for using redox probes when dissolved in polymeric thin films is consumption of a high amount of the redox probe to provide efficient ion transfer; this issue is worse when ionophores are used in thin film. One alternative approach is modifying the electrodes immobilisation of redox molecules onto them.

Finally, ITO electrodes modified by a Janus Ru complex were evaluated to sense different anions. Scan rate study suggest that the Janus Ru complexes are immobilised as a monolayer on ITO electrodes. Surface coverage was measured by scan rate study. Polymeric thin film was spin coated on the modified ITO electrodes and scan rate study suggested thin film behaviour. The half width potential of CVs achieved by the modified ITO electrodes is deviated from theoretical values and the peaks are broad. This broadening in peaks causes the modified electrodes were not sensitive in the presence of different anions. In addition, sensitivity of the modified ITO electrodes were evaluated in the presence of different concentrations of PF_6^- ions. There is significant deviation from the Nernstian slope.

In this report, anion sensing is achieved at liquid-liquid interface. Sensing of sulfate as one the most challenging anion is obtained by using solid contact ion selective electrodes and this achievement can be attractive in practical applications such as development of sulfate sensors which can be applied for different applications such as sulfate sensing in wastewater recycling plants to monitor performance integrity of reverse osmosis membrane.

6.2. Suggestions for future work

This thesis explores how electrochemistry at the interface between two immiscible electrolyte solutions can shed light on the transfer of ions at polarized soft interfaces. This topic has been a significant driving force behind the research reported. According to this study, detecting sulfate, which is one of the most hydrophilic anions, is very difficult, and additional research is necessary to develop this method to a point where it can be utilized commercially or for routine sulfate detection. As a result, several crucial aspects or research domains in this area could benefit from more research investigations.

Detecting sulfate in the presence of other anions, such as chloride and nitrate, presents a significant obstacle in sulfate sensing. While the research presented here demonstrated that modifying the chemical structure of the Ru complexes used as ion-to-electron transducers can enhance the selective detection of sulfate over the interferences, detecting sulfate in water samples with elevated levels of chloride and nitrate remains a difficult task. New designs of Ru complexes that act as redox transducers and have functional groups to attach to different working electrodes (such as glassy carbon and gold electrodes) might provide better selectivity in the presence of different anions. These new designs ideally will have less electrostatic neighbouring effects and less positive redox potentials. In addition, in this approach, leaching of ionophores from the thin film to the aqueous phase can be reduced because of less consumption of the Ru complexes.

In this study, cyclic voltammetry was used to investigate sulfate sensing. To increase electrochemical responses and consequently achieve more competitive detection limits for sulfate sensing, more sensitive methods such as differential pulse voltammetry and stripping voltammetry²³⁹ can be applied. To assess the practicality of these techniques, one could investigate the new Ru complexes with functional groups that enable their attachment to the electrode surface, followed by coating with a thin polymeric layer. By using of stripping voltammetry, preconcentration of sulfate in the polymeric layer can provide better sensitivity to sulfate and achieve lower detection limits. To facilitate the commercialization of this approach to sulfate detection, the various enhancements that have been made to create a more sensitive and selective sensor can be integrated with ion chromatography approach. This would result in a more reliable and standardized system that is suitable for industrial applications.^{240, 241}

References:

1. Bard, A. J.; Faulkner, L. R., *Electrochemical Methods: Fundamentals and Applications*. 2001; p 339.
2. Wang, J., *Analytical electrochemistry / Joseph Wang*. 2nd ed.. ed.; New York : John Wiley & Sons: New York, 2000.
3. Bard, A. J., Faulkner, L., *Electrochemical Methods, Fundamentals and applications*. **2001**, 2 (482), 580-632.
4. Bond, A. M., *Broadening electrochemical horizons: principles and illustration of voltammetric and related techniques*. Portland: Ringgold Inc: Portland, 2003; Vol. 27.
5. Zoski, C. G., *Handbook of electrochemistry / Cynthia G. Zoski*. 1st ed.. ed.; Amsterdam, Boston : Elsevier: 2007.
6. Samec, Z., *Electrochemistry at the interface between two immiscible electrolyte solutions (IUPAC Technical Report)*. **2004**, 76 (12), 2147.
7. Arrigan, D. W. M., *Bioanalytical Detection Based on Electrochemistry at Interfaces between Immiscible Liquids*. *Analytical Letters* **2008**, 41 (18), 3233-3252.
8. Vanýsek, P.; Basáez Ramírez, L., *Interface between two immiscible liquid electrolytes: a review*. *Journal of the Chilean Chemical Society* **2008**, 53 (2), 1455-1463.
9. Lillie, G. C.; Holmes, S. M.; Dryfe, R. A. W., *Electrochemistry of Cytochrome c at the Liquid–Liquid Interface*. *The Journal of Physical Chemistry B* **2002**, 106 (47), 12101-12103.
10. Blank, M.; Feig, S., *Electric Fields across Water-Nitrobenzene Interfaces*. *Science (New York, N.Y.)* **1963**, 141 (3586), 1173-1174.
11. Santos, H. A.; García-Morales, V.; Pereira, C. M., *Electrochemical properties of phospholipid monolayers at liquid-liquid interfaces*. *Chemphyschem* **2010**, 11 (1), 28-41.
12. Arrigan, D. W. M., *Voltammetry of proteins at liquid–liquid interfaces*. *Annual Reports Section "C" (Physical Chemistry)* **2013**, 109 (0), 167-188.
13. Uyanik, I., *Transfer of the protonable surfactant dipalmitoyl-phosphatidylcholine across a large liquid/liquid interface: a voltammetric study*. *Turkish Journal of Chemistry* **2018**, 42 (2), 264-273.
14. Koryta, J., *Electrochemical polarization phenomena at the interface of two immiscible electrolyte solutions*. *Electrochimica Acta* **1979**, 24 (3), 293-300.
15. Taylor, G.; Girault, H. H. J., *Ion transfer reactions across a liquid—liquid interface supported on a micropipette tip*. *Journal of Electroanalytical Chemistry and Interfacial Electrochemistry* **1986**, 208 (1), 179-183.
16. Campbell, J. A.; Girault, H. H., *Steady state current for ion transfer reactions at a micro liquid/liquid interface*. *Journal of Electroanalytical Chemistry* **1989**, 266 (2), 465-469.
17. Campbell, J. A.; Stewart, A. A.; Girault, H. H., *Determination of the kinetics of facilitated ion transfer reactions across the micro interface between two immiscible electrolyte solutions*. *Journal of the Chemical Society, Faraday Transactions 1: Physical Chemistry in Condensed Phases* **1989**, 85 (4), 843-853.
18. Shao, Y.; Mirkin, M. V., *Fast Kinetic Measurements with Nanometer-Sized Pipets. Transfer of Potassium Ion from Water into Dichloroethane Facilitated by Dibenzo-18-crown-6*. *Journal of the American Chemical Society* **1997**, 119 (34), 8103-8104.
19. Scanlon, M. D.; Arrigan, D. W. M., *Enhanced Electroanalytical Sensitivity via Interface Miniaturisation: Ion Transfer Voltammetry at an Array of Nanometre Liquid–Liquid Interfaces*. *Electroanalysis* **2011**, 23 (4), 1023-1028.
20. Rimboud, M., Hart, R., Becker, T., Arrigan, D., *Electrochemical behaviour and voltammetric sensitivity at arrays of nanoscale interfaces between immiscible liquids*. *Analyst* **2011**.
21. Nernst, W.; Riesenfeld, E. H., *Ueber elektrolytische Erscheinungen an der Grenzfläche zweier Lösungsmittel*. *Annalen der Physik* **1902**, 313 (7), 600-608.
22. Gavach, C.; Seta, P.; D'Epenoux, B., *The double layer and ion adsorption at the interface between two non miscible solutions. Part I. Interfacial tension measurements for the water-nitrobenzene tetraalkylammonium bromide systems*. *Journal of Electroanalytical Chemistry* **1977**, 83 (2), 225-235.
23. Samec, Z.; Mareček, V.; Koryta, J.; Khalil, M. W., *Investigation of ion transfer across the interface between two immiscible electrolyte solutions by cyclic voltammetry*. *Journal of Electroanalytical Chemistry and Interfacial Electrochemistry* **1977**, 83 (2), 393-397.

24. Arrigan, D. W. M.; Ghita, M.; Beni, V., Selective voltammetric detection of dopamine in the presence of ascorbate. *Chemical Communications* **2004**, (6), 732-733.
25. Wilke, S.; Franzke, H.; Müller, H., Simultaneous determination of nitrate and chloride by means of flow-injection amperometry at the membrane-stabilized water/nitrobenzene interface. *Analytica Chimica Acta* **1992**, 268 (2), 285-292.
26. Lee, H. J., Pereira, C. M., Silva, A. F., Girault, H. H., Pulse amperometric detection of salt concentrations by flow injection analysis using ionodes. *Analytical chemistry* **2000**, 72 (22), 5562-5566.
27. Lee, H. J.; Beriet, C.; Girault, H. H., Amperometric detection of alkali metal ions on micro-fabricated composite polymer membranes. *Journal of Electroanalytical Chemistry* **1998**, 453 (1-2), 211-219.
28. Hossain, M., Lee, S., Girault, H.H., Devaud, V., Lee, H., Voltammetric studies of hexachromic anion transfer reactions across micro-water/polyvinylchloride-2-nitrophenyloctylether gel interfaces for sensing applications. *Electrochimica Acta* **2012**, 82 (C), 12-18.
29. Samec, Z.; Mareček, V.; Colombini, M. P., Standard Gibbs energies of transfer of alkali metal cations from water to 1,2-dichloroethane: A critique. *Journal of Electroanalytical Chemistry* **1988**, 257 (1-2), 147-154.
30. Lagger, G.; Tomaszewski, L.; Osborne, M. D.; Seddon, B. J.; Girault, H. H., Electrochemical extraction of heavy metal ions assisted by cyclic thioether ligands. *Journal of Electroanalytical Chemistry* **1998**, 451 (1-2), 29-37.
31. Herzog, G., Moujahid, W., Strutwolf, J., Arrigan, D., Interactions of proteins with small ionised molecules: electrochemical adsorption and facilitated ion transfer voltammetry of haemoglobin at the liquid|liquid interface. *Analyst (London)* **2009**, Vol.134 (8), p.1608-1613.
32. Alvarez de Eulate, E.; Arrigan, D., Adsorptive stripping voltammetry of hen-egg-white-lysozyme via adsorption-desorption at an array of liquid-liquid microinterfaces. *Analytical chemistry (Washington)* p.2505-2511 **2012**, Vol.84 (5), p.2505-2511.
33. Atkins, P. W., *The elements of physical chemistry / P.W. Atkins*. Oxford : Oxford University Press: Oxford, 1992.
34. Gavach, C.; Seta, P.; D'Epenoux, B., The double layer and ion adsorption at the interface between two non miscible solutions: Part I. Interfacial tension measurements for the water-nitrobenzene tetraalkylammonium bromide systems. *Journal of Electroanalytical Chemistry and Interfacial Electrochemistry* **1977**, 83 (2), 225-235.
35. Gros, M.; Gromb, S.; Gavach, C., The double layer and ion adsorption at the interface between two non-miscible solutions: Part II. Electrocapillary behaviour of some water-nitrobenzene systems. *Journal of Electroanalytical Chemistry and Interfacial Electrochemistry* **1978**, 89 (1), 29-36.
36. Seta, P.; d'Epenoux, B.; Gavach, C., The double layer and ion adsorption at the interface between two immiscible solutions: Part III. Long chain alkyl-trimethylammonium halides at partition equilibrium between water and nitrobenzene. *Journal of Electroanalytical Chemistry and Interfacial Electrochemistry* **1979**, 95 (2), 191-199.
37. Takashi, K.; Mitsugi, S., Structure of the Electrical Double Layer at the Interface between Nitrobenzene Solution of Tetrabutylammonium Tetraphenylborate and Aqueous Solution of Lithium Chloride. *Bulletin of the Chemical Society of Japan* **1983**, 56 (6), 1753-1760.
38. Gschwend, G. C., Olaya, A., Peljo, P., Girault, H.H., , Structure and reactivity of the polarised liquid-liquid interface: what we know and what we do not. *Current Opinion in Electrochemistry* **2020**, 19, 137-143.
39. Girault, H. H. J.; Schiffrin, D. J., Theory of the kinetics of ion transfer across liquid/liquid interfaces. *Journal of Electroanalytical Chemistry and Interfacial Electrochemistry* **1985**, 195 (2), 213-227.
40. Pereira, C. M. S., W., Silva, F., Sousa, M. J., Ion association at liquid|liquid interfaces. *Journal of Electroanalytical Chemistry* **1997**, 436 (1), 9-15.
41. Mitrinović, D. M. T., A. M.Li, M.Huang, Z., Schlossman, M. L., Noncapillary-wave structure at the water-alkane interface. *Physical review letters* **2000**, 85 (3), 582-5.
42. Mitrinovic, D. M. Z., Z.Williams, S.M., Huang, Z., Schlossman, M.L., X-ray Reflectivity Study of the Water-Hexane Interface. *The Journal of Physical Chemistry B* **1999**, 103 (11), 1779-1782.
43. Schlossman, M. L., Liquid-liquid interfaces: studied by X-ray and neutron scattering. *Current Opinion in Colloid & Interface Science* **2002**, 7 (3), 235-243.

44. Strutwolf, J., Barker, A.L., Gonsalves, M., Caruana, D.J., Unwin, P.R., Williams, D.E., Webster, J.R. P., Probing liquid|liquid interfaces using neutron reflection measurements and scanning electrochemical microscopy. *Journal of Electroanalytical Chemistry* **2000**, 483 (1), 163-173.
45. Bard, A. J.; Zoski, C. G., *Electroanalytical chemistry : a series of advances / edited by Allen J. Bard and Cynthia G. Zoski*. Boca Raton, FL : CRC Press: 2014.
46. Molina, Á.; Serna, C.; Ortuño, J. A.; Torralba, E., Studies of ion transfer across liquid membranes by electrochemical techniques. *Annual Reports Section "C" (Physical Chemistry)* **2012**, 108 (1), 126-176.
47. Girault, H. H., Charge Transfer across Liquid—Liquid Interfaces. In *Modern Aspects of Electrochemistry: Volume 25*, Bockris, J. O. M.; Conway, B. E.; White, R. E., Eds. Springer US: Boston, MA, 1993; pp 1-62.
48. Liu, B.; Mirkin, M. V., Electrochemistry at Microscopic Liquid–Liquid Interfaces. *Electroanalysis* **2000**, 12 (18), 1433-1446.
49. Liu, S.; Li, Q.; Shao, Y., Electrochemistry at micro- and nanoscopic liquid/liquid interfaces. *Chemical Society Reviews* **2011**, 40 (5), 2236-2253.
50. Beattie, P. D.; Delay, A.; Girault, H. H., Investigation of the kinetics of assisted potassium ion transfer by dibenzo-18-crown-6 at the micro-ITIES by means of steady-state voltammetry. *Journal of Electroanalytical Chemistry* **1995**, 380 (1-2), 167-175.
51. Shao, Y.; Mirkin, M. V., Voltammetry at micropipet electrodes. *Anal Chem* **1998**, 70 (15), 3155-61.
52. Cai, C.; Tong, Y.; Mirkin, M. V., Probing rapid ion transfer across a nanoscopic liquid-liquid interface. *Journal of Physical Chemistry B* **2004**, 108 (46), 17872-17878.
53. Zazpe, R., Hibert, C., O'Brien, J., Lanyon, Y.H., Arrigan, D.W. M., Ion-transfer voltammetry at silicon membrane-based arrays of micro-liquid–liquid interfaces. *Lab on a Chip* **2007**, 7 (12), 1732-1737.
54. Scanlon, M.; Herzog, G.; Arrigan, D., Electrochemical Detection of Oligopeptides at Silicon-Fabricated Micro-Liquid|Liquid Interfaces. *American Chemical Society* **2008**, 80 (15), 5743-5749.
55. Liu, S.; Li, Q.; Shao, Y., Electrochemistry at micro- and nanoscopic liquid/liquid interfaces. *Chem. Soc. Rev.* **2011**, 40 (5), 2236-2253.
56. Liu, S. G., Dong, Y., Zhao, W., Xie, X., Ji, T., Yin, X., Liu, Y., Liang, Z., Momotenko, D., Liang, D., Girault, H.H., Shao, Y., , Studies of ionic current rectification using polyethyleneimines coated glass nanopipettes. *Analytical chemistry* **2012**, 84 (13), 5565-5573.
57. Wilke, S.; Osborne, M. D.; Girault, H. H., Electrochemical characterisation of liquid|liquid microinterface arrays. *Journal of Electroanalytical Chemistry* **1997**, 436 (1), 53-64.
58. Peulon, S.; Guillou, V.; L'Her, M., Liquid |liquid microinterface. Localization of the phase boundary by voltammetry and chronoamperometry; influence of the microchannel dimensions on diffusion. *Journal of Electroanalytical Chemistry* **2001**, 514 (1), 94-102.
59. Faisal, S. N., Pereira, C.M., Rho, S., Lee, H., , Amperometric proton selective sensors utilizing ion transfer reactions across a microhole liquid/gel interface. *Physical Chemistry Chemical Physics* **2010**, 12 (46), 15184-15189.
60. Lee, H., Beattie, P.D., Seddon, B.J., Osborne, M.D., Girault, H.H., Amperometric ion sensors based on laser-patterned composite polymer membranes. *Journal of Electroanalytical Chemistry* **1997**, 440 (1), 73-82.
61. Alvarez de Eulate, E., Strutwolf, J., Liu, Y., O'Donnell, K., Arrigan, D.W. M., An Electrochemical Sensing Platform Based on Liquid–Liquid Microinterface Arrays Formed in Laser-Ablated Glass Membranes. *Analytical Chemistry* **2016**, 88 (5), 2596-2604.
62. Scanlon, M. D., Strutwolf, J., Blake, A., Iacopino, D., Quinn, A.J., Arrigan, D.W. M., , Ion-Transfer Electrochemistry at Arrays of Nanointerfaces between Immiscible Electrolyte Solutions Confined within Silicon Nitride Nanopore Membranes. *Analytical Chemistry* **2010**, 82 (14), 6115-6123.
63. Rimboud, M., Hart, R., Becker, T., Arrigan, D., Electrochemical behaviour and voltammetric sensitivity at arrays of nanoscale interfaces between immiscible liquids. *Analyst* **2011**, 136 (22), 4674-4681.
64. Zoski, C. G.; Mirkin, M. V., Steady-State Limiting Currents at Finite Conical Microelectrodes. *Analytical Chemistry* **2002**, 74 (9), 1986-1992.
65. Bond, A. M., Luscombe, D., Oldham, K.B., Zoski, C.G., A comparison of the chronoamperometric response at inlaid and recessed disc microelectrodes. *Journal of Electroanalytical Chemistry and Interfacial Electrochemistry* **1988**, 249 (1), 1-14.

66. Davies, T. J.; Ward-Jones, S.; Banks, C. E.; Del Campo, J.; Mas, R.; Muñoz, F. X.; Compton, R. G., The cyclic and linear sweep voltammetry of regular arrays of microdisc electrodes: Fitting of experimental data. *Journal of Electroanalytical Chemistry* **2005**, *585* (1), 51-62.
67. Davies, T. J., Compton, R.G., The cyclic and linear sweep voltammetry of regular and random arrays of microdisc electrodes: Theory. *Journal of Electroanalytical Chemistry* **2005**, *585* (1), 63-82.
68. Strutwolf, J.; Scanlon, M. D.; Arrigan, D. W. M., Electrochemical ion transfer across liquid/liquid interfaces confined within solid-state micropore arrays – simulations and experiments. *Analyst* **2009**, *134* (1), 148-158.
69. Saito, Y., A Theoretical Study on the Diffusion Current at the Stationary Electrodes of Circular and Narrow Band Types. *Review of Polarography* **1968**, *15* (6), 177-187.
70. Fletcher, S.; Horne, M. D., Random assemblies of microelectrodes (RAM™ electrodes) for electrochemical studies. *Electrochemistry Communications* **1999**, *1* (10), 502-512.
71. Davies, T. J.; Compton, R. G., The cyclic and linear sweep voltammetry of regular and random arrays of microdisc electrodes: Theory. *Journal of Electroanalytical Chemistry* **2005**, *585* (1), 63-82.
72. Bates, R. G.; Macaskill, J. B., Standard Potential of the Silver-Silver Chloride Electrode. *Pure and Applied Chemistry* **1978**, *50* (11-12), 1701-1706.
73. Mikhelson, K. N., Ionophore-Based ISEs. In *Ion-Selective Electrodes*, Mikhelson, K. N., Ed. Springer Berlin Heidelberg: Berlin, Heidelberg, 2013; pp 51-95.
74. Lee, H., Arrigan, D., Karim, M., Kim, H., Electrochemical Strategies in Detection Science: Chapter 9: Amperometric ion sensing approaches at liquid/liquid interfaces for inorganic, organic and biological ions. 2016; pp (pp.296-340).
75. Reymond, F., Carrupt, P., Girault, H.H., Facilitated ion transfer reactions across oil|water interfaces. Part I. Algebraic development and calculation of cyclic voltammetry experiments for successive complex formation. *Journal of Electroanalytical Chemistry* **1998**, *449* (1), 49-65.
76. Matsuda H., Y. Y., Kanamori K., Kudo Y., Takeda Y. , On the Facilitation Effect of Neutral Macrocyclic Ligands on the Ion Transfer across the Interface between Aqueous and Organic Solutions. I. Theoretical Equation of Ion-Transfer-Polarographic Current-Potential Curves and Its Experimental Verification. *Journal of Electroanalytical Chemistry* **1991**, *64* (5), 1497-1508.
77. Girma, G., Yu, L., Huang, L., Jin, S., Wu, D., Zhan, D. , Alkali metal ions transfer across the water/1,2-dichloroethane interface facilitated by a series of crown ethers. *Analytical Methods* **2013**, *5* (18), 4666-4670.
78. Qiao, Y., Zhang, B., Zhu, X., Ji, T., Li, B., Li, Q., Chen, E., ; Shao, Y., Facilitated Ion Transfers at the Micro-Water/1,2-Dichloroethane Interface by Crown Ether Derivatives. *Electroanalysis* **2013**, *25* (4), 1080-1084.
79. Durmaz, M., Zor, E., Kocabas, E., Bingol, H., Akgemci, E.G., Voltammetric characterization of selective potassium ion transfer across micro-water/1,2-dichloroethane interface facilitated by a novel calix[4]arene derivative. *Electrochimica Acta* **2011**, *56* (15), 5316-5321.
80. Wickens, J., Dryfe, R.A. W., Mair, F.S., Pritchard, R.G., Hayes, R., Arrigan, D.W. M., Calixarene-facilitated transfer of alkali metal ions across the polarised liquid-liquid interface. *New Journal of Chemistry* **2000**, *24* (3), 149-154.
81. Ribeiro, J. A., Miranda, I.M., Silva, F., Pereira, C.M., Electrochemical study of dopamine and noradrenaline at the water/1,6-dichlorohexane interface. *Physical Chemistry Chemical Physics* **2010**, *12* (46), 15190-15194.
82. Chen, Y., Yuan, Y., Zhang, M., Li, F., Sun, P., Gao, Z., Shao, Y., , Systematic study of the transfer of amino acids across the water/l,2-dichloroethane interface facilitated by dibenzo-18-crown-6. *Science in China Series B: Chemistry* **2004**, *47* (1), 24-33.
83. Scanlon, M. D.; Herzog, G.; Arrigan, D. W. M., Electrochemical Detection of Oligopeptides at Silicon-Fabricated Micro-Liquid|Liquid Interfaces. *Analytical Chemistry* **2008**, *80* (15), 5743-5749.
84. Beer, P. D.; Gale, P. A., Anion Recognition and Sensing: The State of the Art and Future Perspectives. *Angewandte Chemie International Edition* **2001**, *40* (3), 486-516.
85. Zhang, J., Harris, A.R., Cattral, R.W., Bond, A.M., Voltammetric Ion-Selective Electrodes for the Selective Determination of Cations and Anions. *Analytical Chemistry* **2010**, *82* (5), 1624-1633.

86. Harris, A. R., Zhang, J., Cattral, R.W., Bond, A.M., Applications of voltammetric ion selective electrodes to complex matrices. *Analytical Methods* **2013**, *5* (16), 3840-3852.
87. Compton, R. G. a., *Understanding voltammetry / Richard G Compton, Craig E Banks*. 2nd edition.. ed.; London : Imperial College Press: 2011.
88. Fisher, A. C., *Electrode dynamics / A.C. Fisher*. Oxford, New York : Oxford University Press: 1996.
89. Matsuura, T., Progress in membrane science and technology for seawater desalination — a review. *Desalination* **2001**, *134* (1), 47-54.
90. Scholz, F., *Electroanalytical Methods: Guide to Experiments and Applications*. 2. Aufl. ed.; Berlin, Heidelberg: Springer-Verlag: Berlin, Heidelberg, 2010.
91. Bobacka, J., Conducting Polymer-Based Solid-State Ion-Selective Electrodes. *Electroanalysis (New York, N.Y.)* **2006**, *18* (1), 7-18.
92. Lai, C., Fierke, M.A., da Costa, R.C., Gladysz, J.A., Stein, A., Bühlmann, P., , Highly Selective Detection of Silver in the Low ppt Range with Ion-Selective Electrodes Based on Ionophore-Doped Fluorous Membranes. *Analytical Chemistry* **2010**, *82* (18), 7634-7640.
93. Anastasova-Ivanova, S., Mattinen, U., Radu, A., Bobacka, J., Lewenstam, A., Migdalski, J., Danielewski, M., Diamond, D.,, Development of miniature all-solid-state potentiometric sensing system. *Sensors and Actuators B: Chemical* **2010**, *146* (1), 199-205.
94. Peshkova, M. A. S., T., Mikhelson, K.N., Lewenstam, A., Obtaining Nernstian Response of a Ca²⁺-Selective Electrode in a Broad Concentration Range by Tuned Galvanostatic Polarization. *Analytical Chemistry* **2008**, *80* (23), 9181-9187.
95. Bieg, C.; Fuchsberger, K.; Stelzle, M., Introduction to polymer-based solid-contact ion-selective electrodes—basic concepts, practical considerations, and current research topics. *Analytical and Bioanalytical Chemistry* **2017**, *409* (1), 45-61.
96. Boswell, P. G.; Anfang, A. C.; Bühlmann, P., Preparation of a highly fluorophilic phosphonium salt and its use in a fluoruous anion-exchanger membrane with high selectivity for perfluorinated acids. *J Fluor Chem* **2008**, *129* (10), 961-967.
97. Veder, J. P., De Marco, R., Clarke, G., Chester, R., Nelson, A., Prince, K., Pretsch, E., Bakker, E. , Elimination of Undesirable Water Layers in Solid-Contact Polymeric Ion-Selective Electrodes. *Analytical Chemistry* **2008**, *80* (17), 6731-6740.
98. Shao, Y.; Ying, Y.; Ping, J., Recent advances in solid-contact ion-selective electrodes: functional materials, transduction mechanisms, and development trends. *Chem Soc Rev* **2020**, *49* (13), 445-4465.
99. Lindner, E.; Gyurcsányi, R. E., Quality control criteria for solid-contact, solvent polymeric membrane ion-selective electrodes. *Journal of Solid State Electrochemistry* **2009**, *13* (1), 51-68.
100. Ammann, D.; Worsfold, P. J., Ion-selective microelectrodes, principles, design and application: Springer, Berlin, 1986 (ISBN 3-540-16222-4). xv + 346 pp. Price DM 158. *Analytica Chimica Acta* **1987**, *199*, 271.
101. Freiser, H., Coated Wire Ion-Selective Electrodes. In *Ion-Selective Electrodes in Analytical Chemistry*, Freiser, H., Ed. Springer US: Boston, MA, 1980; pp 85-105.
102. Michalska, A., All-Solid-State Ion Selective and All-Solid-State Reference Electrodes. *Electroanalysis* **2012**, *24* (6), 1253-1265.
103. Enger, O., Nuesch, F., Fibbioli, M., Echegoyen, L., Pretsch, E., Diederich, F., Photocurrent generation at a fullerene self-assembled monolayer-modified gold electrode cast with a polyurethane membrane. *Journal of materials chemistry* **2000**, *10* (10), 2231-2233.
104. Hu, J., Zou, X. Stein, A., Bühlmann, P., Ion-Selective Electrodes with Colloid-Imprinted Mesoporous Carbon as Solid Contact. *Analytical Chemistry* **2014**, *86* (14), 7111-7118.
105. Paczosa-Bator, B.; Pięk, M.; Piech, R., Application of Nanostructured TCNQ to Potentiometric Ion-Selective K⁺ and Na⁺ Electrodes. *Analytical Chemistry* **2015**, *87* (3), 1718-1725.
106. Crespo, G. A.; Cuartero, M.; Bakker, E., Thin Layer Ionophore-Based Membrane for Multianalyte Ion Activity Detection. *Analytical Chemistry* **2015**, *87* (15), 7729-7737.
107. Cuartero, M., Acres, R.G., De Marco, R., Bakker, E., Crespo, G.A., Electrochemical Ion Transfer with Thin Films of Poly(3-octylthiophene). *Analytical Chemistry* **2016**, *88* (13), 6939-6946.

108. Jarolímová, Z., Crespo, G.A., Afshar, M.G., Pawlak, M., Bakker, E., All solid state chronopotentiometric ion-selective electrodes based on ferrocene functionalized PVC. *Journal of Electroanalytical Chemistry* **2013**, *709*, 118-125.
109. Pawlak, M.; Grygoliowicz-Pawlak, E.; Bakker, E., Ferrocene Bound Poly(vinyl chloride) as Ion to Electron Transducer in Electrochemical Ion Sensors. *Analytical Chemistry* **2010**, *82* (16), 6887-6894.
110. Langmaier, J., Olšák, J., Samcová, E., Samec, Z., Trojánek, A., Amperometry of Heparin Polyion Using a Rotating Disk Electrode Coated with a Plasticized PVC Membrane. *Electroanalysis* **2006**, *18* (2), 115-120.
111. Langmaier, J., Olšák, J., Samcová, E., Samec, Z., Trojánek, A., Amperometric Sensor for Heparin: Sensing Mechanism and Application in Human Blood Plasma Analysis. *Electroanalysis* **2006**, *18* (13-14), 1329-1338.
112. Zou, X. U., Cheong, J.H., Taitt, B.J., Bühlmann, P., Solid Contact Ion-Selective Electrodes with a Well-Controlled Co(II)/Co(III) Redox Buffer Layer. *Analytical Chemistry* **2013**, *85* (19), 9350-9355.
113. Zou, X. U., Zhen, X.V., Cheong, J.H., Bühlmann, P., Calibration-Free Ionophore-Based Ion-Selective Electrodes With a Co(II)/Co(III) Redox Couple-Based Solid Contact. *Analytical Chemistry* **2014**, *86* (17), 8687-8692.
114. Jansod, S., Wang, L., Cuartero, M., Bakker, E., Electrochemical ion transfer mediated by a lipophilic Os(II)/Os(III) dinonyl bipyridyl probe incorporated in thin film membranes. *Chemical Communications* **2017**, *53* (78), 10757-10760.
115. Jarolímová, Z., Bosson, J., Labrador, G.M., Lacour, J., Bakker, E., Ion Transfer Voltammetry at Thin Films Based on Functionalized Cationic [6]Helicenes. *Electroanalysis* **2018**, *30* (4), 650-657.
116. Jarolímová, Z., Bosson, J., Labrador, G.M., Lacour, J., Bakker, E., Ion Transfer Voltammetry in Polyurethane Thin Films Based on Functionalised Cationic [6]Helicenes for Carbonate Detection. *Electroanalysis* **2018**, *30* (7), 1378-1385.
117. Velázquez-Manzanares, M., Fundamentals and Applications in Electrochemistry of Liquid-liquid Interfaces. *Procedia Chemistry* **2014**, *12*, 100-107.
118. Shao, Y., 17.3 - ELECTROCHEMISTRY AT LIQUID/LIQUID INTERFACES. In *Handbook of Electrochemistry*, Zoski, C. G., Ed. Elsevier: Amsterdam, 2007; pp 785-809.
119. Arrigan, D. W. M.; Alvarez de Eulate, E.; Liu, Y., Electroanalytical Opportunities Derived from Ion Transfer at Interfaces between Immiscible Electrolyte Solutions. *Australian Journal of Chemistry* **2016**, *69* (9), 1016-1032.
120. Kudo, Y.; Takeda, Y.; Matsuda, H., On the facilitating effect of neutral macrocyclic ligands on ion transfer across the interface between aqueous and organic solutions II: Alkali metal ion complexes with hydrophilic crown ethers. *Journal of Electroanalytical Chemistry* **1995**, *396* (1), 333-338.
121. Beni, V.; Ghita, M.; Arrigan, D. W. M., Cyclic and pulse voltammetric study of dopamine at the interface between two immiscible electrolyte solutions. *Biosensors and Bioelectronics* **2005**, *20* (10), 2097-2103.
122. Nishi, N., Murakami, H., Imakura, S., Kakiuchi, T., Facilitated Transfer of Alkali-Metal Cations by Dibenzo-18-crown-6 across the Electrochemically Polarized Interface between an Aqueous Solution and a Hydrophobic Room-Temperature Ionic Liquid. *Analytical Chemistry* **2006**, *78* (16), 5805-5812.
123. Kaykal, F., Kocabas, E., Bingol, H., Akgemci, E.G., Coskun, A., Selective sodium ion transfer across a water/1,2-dichloroethane micro-interface by a calix[4]arene derivative. *Journal of Electroanalytical Chemistry* **2011**, *654* (1), 96-101.
124. Li Q., X. S., Liang Z., Meng X., Liu S., Girault H.H., Shao Y., Fast Ion-Transfer Processes at Nanoscopic Liquid/Liquid Interfaces. *Angewandte Chemie International Edition* **2009**, *48* (43), 8010-8013.
125. Ribeiro, J. A.; Silva, F.; Pereira, C. M., Electrochemical sensing of ammonium ion at the water/1,6-dichlorohexane interface. *Talanta* **2012**, *88*, 54-60.
126. Shao, Y.; Liu, B.; Mirkin, M. V., Studying Ionic Reactions by a New Generation/Collection Technique. *Journal of the American Chemical Society* **1998**, *120* (48), 12700-12701.
127. Arrigan, D. W. M., Banks, C., Reddy, S.M., Thompson, M., Economou, A., Del Campo, J., Lunte, S., Kranz, C., Compton, R., O'Riordan, A., *Electrochemical Strategies in Detection Science*. Royal Society of Chemistry: Cambridge, UNITED KINGDOM, 2015.
128. Campbell, J. A.; Girault, H. H., Steady state current for ion transfer reactions at a micro liquid/liquid interface. *Journal of Electroanalytical Chemistry and Interfacial Electrochemistry* **1989**, *266* (2), 465-469.

129. Zazpe, R., Hibert, C., O'Brien, J., Lanyon, Y.H., Arrigan, D.W. M., Ion-transfer voltammetry at silicon membrane-based arrays of micro-liquid-liquid interfaces. *Lab on a Chip* **2007**, *7* (12), 1732-1737.
130. Su, B., Zhang, S., Yuan, Y., Guo, J., Gan, L., Shao, Y., Investigation of Ion Transfer Across the Micro-Water/Nitrobenzene Interface Facilitated by a Fullerene Derivative. *Analytical Chemistry* **2002**, *74* (2), 373-378.
131. Senō, M.; Iwamoto, K.; Chen, Q.-z., Kinetic study of ion transport facilitated by crown ethers across water—nitrobenzene interface. *Electrochimica Acta* **1990**, *35* (1), 127-134.
132. Heitzsch, O., Gloe, K., Sabela, A., Koryta, J., Weber, E., Complex forming and extraction properties of oligo benzo-fused crown ethers. *Journal of inclusion phenomena and molecular recognition in chemistry* **1992**, *13* (4), 311-319.
133. Hofmanová, A., Koryta, J., Březina, M., Mittal, M. L., Electrochemical reduction of monovalent cation complexes of macrocyclic ionospheres. I. crown polyether complexes. *Inorganica Chimica Acta* **1978**, *28*, 73-76.
134. Matsuura N., U. K., Takeda Y., Sasaki A., Formation Constants of Dibenzo-18-crown-6 Complexes with Alkali Metal Ions in DMSO, DMF, and PC at 25°C. *Bulletin of the Chemical Society of Japan* **1976**, *49* (5), 1246-1249.
135. Shchori, E.; Nae, N.; Jagur-Grodzinski, J., Stability constants of complexes of a series of metal cations with 6,7,9,10,17,18,20,21-octahydrodibenzo[b,k][1,4,7,10,13,16]hexa-oxa-cyclo-octadecin (dibenzo-18-crown-6) in aqueous solutions. *Journal of the Chemical Society, Dalton Transactions* **1975**, (22), 2381-2386.
136. Nishi, N., Murakami, H., Imakura, S., Kakiuchi, T., Facilitated transfer of alkali-metal cations by dibenzo-18-crown-6 across the electrochemically polarized interface between an aqueous solution and a hydrophobic room-temperature ionic liquid. *Analytical Chemistry* **2006**, *78* (16), 5805-5812.
137. Katano, H.; Tatsumi, H.; Senda, M., Ion-transfer voltammetry at 1,6-dichlorohexane|water and 1,4-dichlorobutane|water interfaces. *Talanta* **2004**, *63* (1), 185-193.
138. Samec, Z.; Papoff, P., Electrolyte dropping electrode polarographic studies. Solvent effect on stability of crown ether complexes of alkali-metal cations. *Analytical Chemistry* **1990**, *62* (10), 1010-1015.
139. Cuartero, M., Ortuño, J. A., García, M. S., Sánchez, G., Más-Montoya, M., Curiel, D., Benzodipyrrole derivatives as new ionophores for anion-selective electrodes: Improving potentiometric selectivity towards divalent anions. *Talanta* **2011**, *85* (4), 1876-1881.
140. Langton, M. J.; Serpell, C. J.; Beer, P. D., Anion Recognition in Water: Recent Advances from a Supramolecular and Macromolecular Perspective. *Angewandte Chemie International Edition* **2016**, *55* (6), 1974-1987.
141. Sabek, J., Adriaenssens, L., Guinovart, T., Parra, E.J., Rius, F. X., Ballester, P., Blondeau, P., Chloride-Selective Electrodes Based on "Two-Wall" Aryl-Extended Calix[4]Pyrroles: Combining Hydrogen Bonds and Anion- π Interactions to Achieve Optimum Performance. *Chemistry – A European Journal* **2015**, *21* (1), 448-454.
142. Liu, Y.; Qin, Y.; Jiang, D., Squaramide-based tripodal ionophores for potentiometric sulfate-selective sensors with high selectivity. *Analyst* **2015**, *140* (15), 5317-5323.
143. Burgess, J., Ion-solvent interactions. In *Ions in Solution*, Burgess, J., Ed. Woodhead Publishing: 1999; pp 45-61.
144. Delgado-Pinar, E., Rotger, C., Costa, A., Piña, M.N., Jiménez, H.R., Alarcón, J., García-España, E., Grafted squaramide monoamine nanoparticles as simple systems for sulfate recognition in pure water. *Chemical Communications* **2012**, *48* (20), 2609-2611.
145. Pype, M. L., Lawrence, M.G., Keller, J., Gernjak, W., Reverse osmosis integrity monitoring in water reuse: The challenge to verify virus removal – A review. *Water Res* **2016**, *98*, 384-395.
146. Gomez, G. G.; Sandler, R. S.; Seal, E., Jr., High levels of inorganic sulfate cause diarrhea in neonatal piglets. *J Nutr* **1995**, *125* (9), 2325-32.
147. Markovich, D., Physiological Roles and Regulation of Mammalian Sulfate Transporters. *Physiological Reviews* **2001**, *81* (4), 1499-1533.
148. Cole, D. E.; Evrovski, J., Quantitation of sulfate and thiosulfate in clinical samples by ion chromatography. *J Chromatogr A* **1997**, *789* (1-2), 221-32.

149. Zhao, D., Chen, C., Lu, L., Yang, F., Yang, X., A label-free colorimetric sensor for sulfate based on the inhibition of peroxidase-like activity of cysteamine-modified gold nanoparticles. *Sensors and Actuators B: Chemical* **2015**, *215*, 437-444.
150. Zhang, M.; Liu, Y. Q.; Ye, B. C., Colorimetric assay for sulfate using positively-charged gold nanoparticles and its application for real-time monitoring of redox process. *Analyst* **2011**, *136* (21), 4558-62.
151. Valent, O.; Koryta, J.; Panoch, M., Voltammetric study of ion transfer across the water/o-nitrophenyloctyl ether interface: Part I. Reversible process. *Journal of electroanalytical chemistry and interfacial electrochemistry* **1987**, *226* (1-2), 21-25.
152. Samec, Z.; Langmaier, J.; Trojánek, A., Polarization phenomena at the water | o-nitrophenyl octyl ether interface. Part 1. Evaluation of the standard Gibbs energies of ion transfer from the solubility and voltammetric measurements. *Journal of Electroanalytical Chemistry* **1996**, *409* (1), 1-7.
153. Bakker, E.; Pretsch, E., Potentiometry at trace levels. *TrAC, Trends Anal. Chem.* **2001**, *20* (1), 11-19.
154. Konopka, A., Sokalski, T., Michalska, A., Lewenstam, A., Maj-Zurawska, M., Factors Affecting the Potentiometric Response of All-Solid-State Solvent Polymeric Membrane Calcium-Selective Electrode for Low-Level Measurements. *Anal.Chem.* **2004**, *76* (21), 6410-6418.
155. Cuartero, M., Chai, L., Zahang, B., De Marco, R., Crespo, G.A., Ferrocene self assembled monolayer as a redox mediator for triggering ion transfer across nanometer-sized membranes. *Electrochim.Acta* **2019**, *315*, 84-93.
156. Cuartero, M., Crespo, G.A., Bakker, E., Thin Layer Samples Controlled by Dynamic Electrochemistry. *Chimia* **2015**, *69* (4), 203-6.
157. Crespo, G. A., Bakker, E., Dynamic electrochemistry with ionophore based ion-selective membranes. *RSC Adv.* **2013**, *3* (48), 25461-25474.
158. Nikolskii, B. P., Materova, E.A., Solid Contact in Membrane Ion-Selective Electrodes. In *Ion-Select. Electrode Rev.*, Elsevier: 1985; Vol. 7, pp 3-39.
159. Shi, C., Anson, F.C., A Simple Method for Examining the Electrochemistry of Metalloporphyrins and Other Hydrophobic Reactants in Thin Layers of Organic Solvents Interposed between Graphite Electrodes and Aqueous Solutions. *Anal. Chem.* **1998**, *70* (15), 3114-3118.
160. Shi, C., Anson, F.C., Selecting Experimental Conditions for Measurement of Rates of Electron-Transfer at Liquid/Liquid Interfaces by Thin-Layer Electrochemistry. *J. Phys. Chem. B.* **2001**, *105* (5), 1047-1049.
161. Zhang, J., Harris, A.R., Cattral, R.W., Bond, A.M., Voltammetric Ion-Selective Electrodes for the Selective Determination of Cations and Anions. *Anal.Chem.* **2010**, *82* (5), 1624-1633.
162. Harris, A. R., Zhang, J., Cattral, R.W., Bond, A.M., Applications of voltammetric ion selective electrodes to complex matrices. *Anal. Methods* **2013**, *5* (16), 3840-3852.
163. Garada, M. B., Kabagambe, B., Kim, Y., Amemiya, S., Ion-Transfer Voltammetry of Perfluoroalkanesulfonates and Perfluoroalkancarboxylates: Picomolar Detection Limit and High Lipophilicity. *Anal.Chem.* **2014**, *86* (22), 11230-11237.
164. Guo, J., Amemiya, S., Voltammetric heparin selective electrode based on thin liquid membrane with conducting polymer-modified solid support. *Anal. Chem.* **2006**, *78* (19), 6893-6902.
165. Si, P., Bakker, E., Thin layer electrochemical extraction of non-redoxactive cations with an anion-exchanging conducting polymer overlaid with a selective membrane. *Chemical communications (Cambridge, England)* **2009**, (35), 5260-2.
166. Michalska, A., All-Solid-State Ion Selective and All-Solid-State Reference Electrodes. *Electroanalysis*, **2012**, *24* (6), 1253-1265.
167. Cuartero, M., Acres, R.G., De Marco, R., Bakker, E., Crespo, G.A., Electrochemical Ion Transfer with Thin Films of Poly(3-octylthiophene). *Anal.Chem.* **2016**, *88* (13), 6939-6946.
168. Cuartero, M., Acres, R., Bradley, J., Jarolímová, Z., Wang, L., Bakker, E., Crespo, G.A., DeMarco, R., Electrochemical Mechanism of Ferrocene-Based Redox Molecules in Thin Film Membrane Electrodes. *Electrochim.Acta* **2017**, *238*, 357-367.
169. Jansod, S., Wang, L., Cuartero, M., Bakker, E., Electrochemical ion transfer mediated by a lipophilic Os(ii)/Os(iii) dinonyl bipyridyl probe incorporated in thin film membranes. *Chem. Commun.* **2017**, *53* (78), 10757-10760.

170. Jarolímová, Z., Bosson, J., Labrador, G.M., Lacour, J., Bakker, E., Ion Transfer Voltammetry in Polyurethane Thin Films Based on Functionalised Cationic [6]Helicenes for Carbonate Detection, *Electroanalysis* **2018**, *30* (7), 1378-1385.
171. Jarolímová, Z., Crespo A.G., Ghahraman Afshar, M., Pawlak, M., Bakker, E., All solid state chronopotentiometric ion-selective electrodes based on ferrocene functionalized PVC. *J. Electroanal. Chem.* **2013**, *709*, 118-125.
172. Pawlak, M., Grygolowicz-Pawlak, E., Bakker, E., Ferrocene Bound Poly(vinyl chloride) as Ion to Electron Transducer in Electrochemical Ion Sensors. *Anal.Chem.* **2010**, *82* (16), 6887-6894.
173. Lei, H., Liu, C., Wang, Z., Zhang, Z., Zhang, M., Chang, X., Zhang, W., Cao, R., Noncovalent Immobilization of a Pyrene-Modified Cobalt Corrole on Carbon Supports for Enhanced Electrocatalytic Oxygen Reduction and Oxygen Evolution in Aqueous Solutions. *ACS Catal.* **2016**, *6* (10), 6429-6437.
174. Wadsworth, B. L., Beiler, A.M., Khusnutdinova, D., Jacob, S.I., Moore, J.F., Electrocatalytic and Optical Properties of Cobaloxime Catalysts Immobilized at a Surface-Grafted Polymer Interface. *ACS Catal.* **2016**, *6* (12), 8048-8057.
175. Cattrall, R. W.; Freiser, H., Coated wire ion-selective electrodes. *Analytical Chemistry* **1971**, *43* (13), 1905-1906.
176. Cadogan, A., Gao, Z., Lewenstam, A., Ivaska, A., Diamond, D., All-solid-state sodium-selective electrode based on a calixarene ionophore in a poly(vinyl chloride) membrane with a polypyrrole solid contact. *Analytical Chemistry* **1992**, *64* (21), 2496-2501.
177. Bobacka, J., McCarrick, M., Lewenstam, A., Ivaska, A., All solid-state poly(vinyl chloride) membrane ion-selective electrodes with poly(3-octylthiophene) solid internal contact. *Analyst* **1994**, *119* (9), 1985-1991.
178. Bobacka, J., Lindfors, T., McCarrick, M., Ivaska, A., Lewenstam, A., Single-piece all-solid-state ion-selective electrode. *Analytical Chemistry* **1995**, *67* (20), 3819-3823.
179. Bobacka, J., Potential Stability of All-Solid-State Ion-Selective Electrodes Using Conducting Polymers as Ion-to-Electron Transducers. *Analytical Chemistry* **1999**, *71* (21), 4932-4937.
180. Fibbioli, M., Bandyopadhyay, K., Liu, S. G., Echevoyen, L., Enger, O., Diederich, F., Bühlmann, P., Pretsch, E., Redox-active self-assembled monolayers as novel solid contacts for ion-selective electrodes. *Chemical Communications* **2000**, (5), 339-340.
181. Fouskaki, M.; Chaniotakis, N., Fullerene-based electrochemical buffer layer for ion-selective electrodes. *Analyst* **2008**, *133* (8), 1072-1075.
182. Crespo, G. A.; Macho, S.; Rius, F. X., Ion-Selective Electrodes Using Carbon Nanotubes as Ion-to-Electron Transducers. *Analytical Chemistry* **2008**, *80* (4), 1316-1322.
183. Lai, C. Z., Fierke, M.A., Stein, A., Bühlmann, P., Ion-Selective Electrodes with Three-Dimensionally Ordered Macroporous Carbon as the Solid Contact. *Analytical Chemistry* **2007**, *79* (12), 4621-4626.
184. Jaworska, E., Wójcik, M., Kisiel, A., Mieczkowski, J., Michalska, A., Gold nanoparticles solid contact for ion-selective electrodes of highly stable potential readings. *Talanta* **2011**, *85* (4), 1986-1989.
185. Ping, J., Wang, Y., Wu, J., Ying, Y., Development of an all-solid-state potassium ion-selective electrode using graphene as the solid-contact transducer. *Electrochemistry Communications* **2011**, *13* (12), 1529-1532.
186. Paczosa-Bator, B., Cabaj, L., Piech, R., Skupień, K., Platinum nanoparticles intermediate layer in solid-state selective electrodes. *Analyst* **2012**, *137* (22), 5272-5277.
187. Zhou, M., Gan, S., Cai, B., Li, F., Ma, W., Han, D., Niu, L., Effective Solid Contact for Ion-Selective Electrodes: Tetrakis(4-chlorophenyl)borate (TB⁻) Anions Doped Nanocluster Films. *Analytical Chemistry* **2012**, *84* (7), 3480-3483.
188. Paczosa-Bator, B., All-solid-state selective electrodes using carbon black. *Talanta* **2012**, *93*, 424-427.
189. Ping, J., Wang, Y., Ying, Y., Wu, J., Design and synthesis of a task-specific ionic liquid as a transducer in potentiometric sensors. *RSC Advances* **2013**, *3* (43), 19782-19784.
190. Komaba, S., Suzuki, C., Yabuuchi, N., Akatsuka, T., Kanazawa, S., Hasegawa, T., Redox-Active Alkali Insertion Materials as Inner Contact Layer in All-Solid-State Ion-Selective Electrodes. *ECS Transactions* **2013**, *50* (12), 279-287.

191. Yin, T.; Pan, D.; Qin, W., All-Solid-State Polymeric Membrane Ion-Selective Miniaturized Electrodes Based on a Nanoporous Gold Film as Solid Contact. *Analytical Chemistry* **2014**, *86* (22), 11038-11044.
192. Pięk, M.; Piech, R.; Paczosa-Bator, B., Improved Nitrate Sensing Using Solid Contact Ion Selective Electrodes Based on TTF and Its Radical Salt. *Journal of The Electrochemical Society* **2015**, *162* (10), B257-B263.
193. Zeng, X., Yu, S., Yuan, Q., Qin, W., Solid-contact K⁺-selective electrode based on three-dimensional molybdenum sulfide nanoflowers as ion-to-electron transducer. *Sensors and Actuators B: Chemical* **2016**, *234*, 80-83.
194. Weber, A. W.; O'Neil, G. D.; Kounaves, S. P., Solid Contact Ion-Selective Electrodes for in Situ Measurements at High Pressure. *Analytical Chemistry* **2017**, *89* (9), 4803-4807.
195. Garland, N. T., McLamore, E.S., Cavallaro, N.D., Mendivelso-Perez, D., Smith, E.A., Jing, D., Claussen, J.C., Flexible Laser-Induced Graphene for Nitrogen Sensing in Soil. *ACS Applied Materials & Interfaces* **2018**, *10* (45), 39124-39133.
196. Mendecki, L.; Mirica, K. A., Conductive Metal–Organic Frameworks as Ion-to-Electron Transducers in Potentiometric Sensors. *ACS Applied Materials & Interfaces* **2018**, *10* (22), 19248-19257.
197. Lenar, N.; Paczosa-Bator, B.; Piech, R., Ruthenium Dioxide as High-Capacitance Solid-Contact Layer in K⁺-Selective Electrodes Based on Polymer Membrane. *Journal of The Electrochemical Society* **2019**, *166* (15), B1470-B1476.
198. Shao, Y., Yao, Y., Jiang, C., Zhao, F., Liu, X., Ying, Y., Ping, J., Two-dimensional MXene nanosheets (types Ti₃C₂T_x and Ti₂C₂T_x) as new ion-to-electron transducers in solid-contact calcium ion-selective electrodes. *Microchimica Acta* **2019**, *186* (12), 750.
199. Yang, W. W., Zhong, Y.W., Yoshikawa, S., Shao, J.Y., Masaoka, S., Sakai, K., Yao, J., Haga, M.A., Tuning of Redox Potentials by Introducing a Cyclometalated Bond to Bis-tridentate Ruthenium(II) Complexes Bearing Bis(N-methylbenzimidazolyl)benzene or -pyridine Ligands. *Inorganic Chemistry* **2012**, *51* (2), 890-899.
200. R.S, V., Haga, M.A., Watanabe, T., Witkowska Nery, E., Jönsson-Niedziółka, M., Three-phase electrochemistry of a highly lipophilic neutral ru-complex having tridentate bis(benzimidazolate)pyridine ligands. *Electrochimica Acta* **2020**, *362*, 137090.
201. Han, W. S., Kim, J.K., Chung, K.C., Hong, J.Y., Hong, J.K., Kim, J.H., Hong, T.K., Poly(aniline) solid contact ion selective electrode for udenafil. *Journal of analytical chemistry (New York, N.Y.)* **2010**, *65* (10), 1035-1040.
202. Zhu, J., Li, X., Qin, Y., Zhang, Y., Single-piece solid-contact ion-selective electrodes with polymer–carbon nanotube composites. *Sensors and actuators. B, Chemical* **2010**, *148* (1), 166-172.
203. Bobacka, J., Alaviuhkola, T., Hietapelto, V., Koskinen, H., Lewenstam, A., Lämsä, M., Pursiainen, J., Ivaska, A., Solid-contact ion-selective electrodes for aromatic cations based on π -coordinating soft carriers. *Talanta* **2002**, *58* (2), 341-349.
204. Eugster, R., Rosatzin, T., Rusterholz, B., Aebersold, B., Pedrazza, U., Rüegg, D., Schmid, A., Spichiger, U.E., Simon, W., Plasticizers for liquid polymeric membranes of ion-selective chemical sensors. *Analytica chimica acta* **1994**, *289* (1), 1-13.
205. Prajapati, G. K.; Roshan, R.; Gupta, P. N., Effect of plasticizer on ionic transport and dielectric properties of PVA–H₃PO₄ proton conducting polymeric electrolytes. *Journal of Physics and Chemistry of Solids* **2010**, *71* (12), 1717-1723.
206. Chintapalli, S.; Frech, R., Effect of Plasticizers on Ionic Association and Conductivity in the (PEO)₉LiCF₃SO₃ System. *Macromolecules* **1996**, *29* (10), 3499-3506.
207. Sharma, J. P.; Singh, V., Influence of high and low dielectric constant plasticizers on the ion transport properties of PEO: NH₄HF₂ polymer electrolytes. *High Performance Polymers* **2020**, *32* (2), 142-150.
208. de los A. Arada Pérez, M., Marín, L.P., Quintana, J.C., Yazdani-Pedram, M., Influence of different plasticizers on the response of chemical sensors based on polymeric membranes for nitrate ion determination. *Sensors and Actuators B: Chemical* **2003**, *89* (3), 262-268.
209. Mohammad, L., *Recent Advances in Plasticizers*. IntechOpen: 2012.
210. Hooz, J.; Gilani, S. S. H., A rapid, mild procedure for the preparation of alkyl chlorides and bromides. *Canadian Journal of Chemistry* **1968**, *46* (1), 86-87.

211. Bodor, S., Zook, J.A., Lindner, E., Toth, K., Gyurcsanyi, R.E., Electrochemical methods for the determination of the diffusion coefficient of ionophores and ionophore–ion complexes in plasticized PVC membranes. *Analyst* **2008**, *133* (5), 635–642.
212. Bard, A. J.; Faulkner, L. R., *Electrochemical Methods, Fundamentals and applications*. 2001; Vol. 2, p 580-632.
213. Zahran, E. M., Hua, Y., Li, Y., Flood, A.H., Bachas, L.G. , Triazolophanes: A New Class of Halide-Selective Ionophores for Potentiometric Sensors. *Anal.Chem.* **2010**, *82* (1), 368-375.
214. Bereczki, R., Gyurcsanyi, R.E., Agai, B., Toth, K., Synthesis and characterization of covalently immobilized bis-crown ether based potassium ionophore. *Analyst* **2005**, *130* (1), 63-70.
215. Ascione, L., Ambrogi, V., Pannico, M., Carfagna, C., Persico, P., Highly branched poly(butylene adipate) for PVC plasticization: synthesis and blend characterisation. *Funct. Mater. Lett.* **2011**, *04* (04), 361-364.
216. Eckermann, A. L., Feld, D.J., Shaw, J.A., Meade, T.J., Electrochemistry of redox-active self-assembled monolayers. *Coordination Chemistry Reviews* **2010**, *254* (15), 1769-1802.
217. Paczosa-Bator, B., Piech, R., Lewenstam, A., Determination of the leaching of polymeric ion-selective membrane components by stripping voltammetry. *Talanta* **2010**, *81* (3), 1003-1009.
218. Garay, F.; Vettorelo, S. N., How to obtain kinetic information in thin-film voltammetry from the comparison of SCV and SWV responses. *Journal of Electroanalytical Chemistry* **2020**, *878*, 114647.
219. Reinsfelder, R. E.; Schultz, F. A., Anion selectivity studies on liquid membrane electrodes. *Analytica Chimica Acta* **1973**, *65* (2), 425-435.
220. Laviron, E., The use of linear potential sweep voltammetry and of a.c. voltammetry for the study of the surface electrochemical reaction of strongly adsorbed systems and of redox modified electrodes. *J. Electroanal. Chem. Interfacial Electrochem.* **1979**, *100* (1), 263-270.
221. Hong, H. G., Mallouk, T.E, Electrochemical measurements of electron transfer rates through zirconium 1,2-ethanediylbis(phosphonate) multilayer films on gold electrodes. *Langmuir* **1991**, *7* (10), 2362-2369.
222. Finklea, H. O., Avery, S., Lynch, M., Furtch, T., Blocking oriented monolayers of alkyl mercaptans on gold electrodes. *Langmuir* **1987**, *3* (3), 409-413.
223. Hsu, S. H., Reinhoudt, D., Huskens, J., Velders, A., Lateral interactions at functional monolayers. *Journal of materials chemistry* **2011**, *21* (8), 2428-2444.
224. Mikhelson, K. N., *Ion-Selective Electrodes / by Konstantin N. Mikhelson*. Berlin, Heidelberg : Springer Berlin Heidelberg : Imprint: Springer: Berlin, Heidelberg, 2013.
225. Bieg, C., Fuchsberger, K., Stelzle, M., Introduction to polymer-based solid-contact ion-selective electrodes-basic concepts, practical considerations, and current research topics. *Anal. Bioanal. Electrochem.* **2017**, *409* (1), 45-61.
226. Hutchins, R. S., Bachas, L.G., Nitrate-Selective Electrode Developed by Electrochemically Mediated Imprinting/Doping of Polypyrrole. *Anal.Chem.* **1995**, *67* (10), 1654-1660.
227. Haga, M. A., Kato, N., Monjushiro, H., Wang, K., Hossain, M.D., Metal coordination to amphiphilic Ru complexes at the air–water interface. *Supramolecular Science* **1998**, *5* (3), 337-342.
228. Cuartero, M.; Crespo, G. A.; Bakker, E., Polyurethane Ionophore-Based Thin Layer Membranes for Voltammetric Ion Activity Sensing. *Analytical Chemistry* **2016**, *88* (11), 5649-5654.
229. Nishizawa, S., Bühlmann, P., Xiao, K.P., Umezawa, Y., Application of a bis-thiourea ionophore for an anion selective electrode with a remarkable sulfate selectivity. *Analytica Chimica Acta* **1998**, *358* (1), 35-44.
230. Laviron, E., The use of linear potential sweep voltammetry and of a.c. voltammetry for the study of the surface electrochemical reaction of strongly adsorbed systems and of redox modified electrodes. *Journal of Electroanalytical Chemistry and Interfacial Electrochemistry* **1979**, *100* (1), 263-270.
231. Horie, M.; Sakano, T.; Osakada, K., Preparation and electrochemical properties of SAM of alkanethiols functionalized with 2-aza[3]ferrocenophane on gold electrode. *Journal of Organometallic Chemistry* **2006**, *691* (26), 5935-5945.
232. Hanna, C. M., Sanborn, C.D., Ardo, S., Yang, J.Y., Interfacial Electron Transfer of Ferrocene Immobilized onto Indium Tin Oxide through Covalent and Noncovalent Interactions. *ACS Applied Materials & Interfaces* **2018**, *10* (15), 13211-13217.

233. Cuartero, M., Chai, L., Zahang, B., De Marco, R., Crespo, G.A., Ferrocene self assembled monolayer as a redox mediator for triggering ion transfer across nanometer-sized membranes. *Electrochimica Acta* **2019**, *315*, 84-93.
234. Fibbioli, M., Bandyopadhyay, K., Liu, S. G., Echegoyen, L., Enger, O., Diederich, F., Bühlmann, P., Pretsch, E., Redox-active self-assembled monolayers as novel solid contacts for ion-selective electrodes. *Chemical Communications* **2000**, (5), 339-340.
235. Sęk, S., Bilewicz, R., Grygołowicz-Pawlak, E., Grudzień, I., ; Brzózka, Z., Malinowska, E., Design of ferrocene organothiol monolayer as intermediate phase for miniaturized electrochemical sensors with gold contact. *Polish Journal of Chemistry* **2004**, *78* (9), 1655-1665.
236. Grygołowicz-Pawlak, E., Wyglądacz, K., Sęk, S., Bilewicz, R., Brzózka, Z., Malinowska, E., Studies on ferrocene organothiol monolayer as an intermediate phase of potentiometric sensors with gold inner contact. *Sensors and Actuators B: Chemical* **2005**, *111-112*, 310-316.
237. Yang, L., Ozawa, H., Koumoto, M., Oshikawa, K.Y., Matsunaga, M., Haga, M.A., "Janus-type" Ruthenium Complex Bearing Both Phosphonic Acids and Pyrene Groups for Functionalization of ITO and HOPG Surfaces. *Chemistry Letters* **2015**, *44* (2), 160-162.
238. Prodromidis, M. I., Florou, A.B., Tzouwara-Karayanni, S.M., Karayannis, M.I., The Importance of Surface Coverage in the Electrochemical Study of Chemically Modified Electrodes. *Electroanalysis (New York, N.Y.)* **2000**, *12* (18), 1498-1501.
239. Izadyar, A., Stripping Voltammetry at the Interface between two Immiscible Electrolyte Solutions: A Review Paper. *Electroanalysis* **2018**, *30* (10), 2210-2221.
240. Isildak, I.; Covington, A. K., Ion-selective electrode potentiometric detection in ion-chromatography. *Electroanalysis* **1993**, *5* (9-10), 815-824.
241. Lee, D. K., Lee, H.J., Cha, G.S., Nam, H., Paeng, K., Ion chromatography detector based on solid-state ion-selective electrode array. *Journal of Chromatography A* **2000**, *902* (2), 337-343.
242. Hooz, J., Gilani, S.S.H., A rapid, mild procedure for the preparation of alkyl chlorides and bromides. *Can. J. Chem.* **1968**, *46* (1), 86-87.
243. Smith, D. W., Ionic hydration enthalpies. *Journal of Chemical Education* **1977**, *54* (9), 540.

Appendix A: Synthesizing the Ru-bipod complex and its characterisation (all the information in this section is the group of Pro. Haga, Chuo University, Japan) (related to chapter 3)

A-1: Synthesis of Ru-bipod and its characterisation:

To synthesis the Ru-bipod complex, firstly $\text{RuCl}_3 \cdot 3\text{H}_2\text{O}$ (0.050 g or 0.19 mmol) was heated in glycerol (10 mL) at 100°C , during which time the solution turned greenish in colour. Then from 2-octyl-1-dodecanol, 1-Bromo-2-octyl-1-dodecane and 2, 6-bis (1-(2-octyl-dodecan) benzimidazol-2-yl) pyridine) (as a ligand LR₂₀)²⁴². The ligand LR₂₀ (0.36 g, 0.42 mmol) in *tert*-butanol (8 mL) was added into the solution, and the mixture was heated at 150°C for 24 h. After cooled to room temperature, water (50 ml) was added to obtain a red-brown precipitate, which was collected by filtration and dried in vacuo (Figure A-1). The crude complex was purified by the silica gel column chromatography with toluene-methanol (10: 1v/v) as an eluent. The separated brown band was collected, and the solvent was removed. The resulting residue was dissolved in small amounts of CH_3CN , and the addition of KPF_6 saturated aqueous solution (5 ml) and methanol (82 ml) affected the brown precipitation, which was collected by filtration and dried. Yield of the Ru complex is 0.20 g (56 % yield) with melting point $158 - 160^\circ\text{C}$. The ^1H NMR(500 MHz, $\text{DMSO-}d_6$) δ (ppm) data including 9.02(d, $J=8.3$, 4H), 8.77(t, $J=8.2$, 2H), 7.76(d, $J=8.3$, Hz, 4H), 7.27(t, $J=7.6$ Hz, 4H), 6.99(t, $J=7.7$, 4H), 5.96(d, $J= 8.3$ Hz, 4H), 4.89(s, 8H), 1.93(s, 4H), 1.28-0.73(m, 152H) is shown in figure S.9. The spectrum related to ESI-TOF-MS is $m/z = 1283.75$ $[\text{M-H}]^+$ (Calcd. for $[\text{C}_{78}\text{H}_{105}\text{N}_{10}\text{Ru}]$, 1283.76) and FT-IR is equal to 829 cm^{-1} (P-F) (Figure S2).

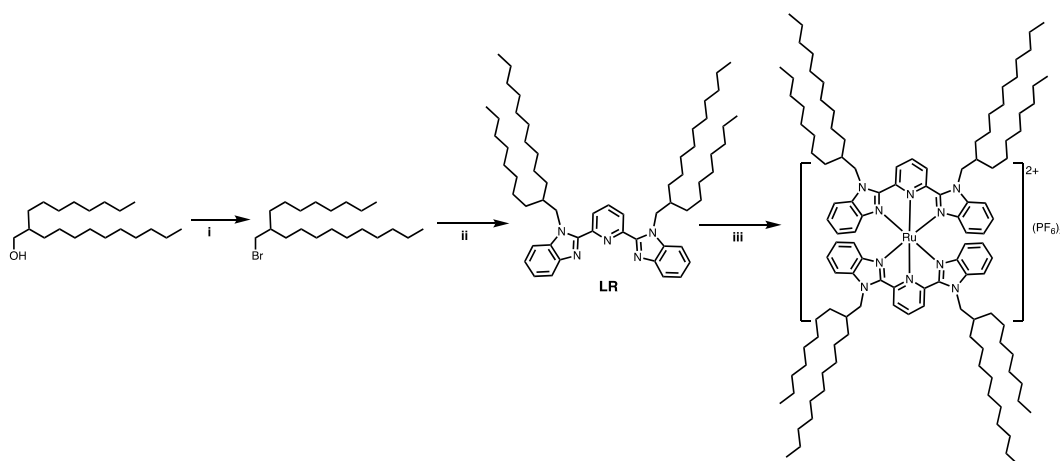


Figure A-1: Synthetic route to amphiphilic Ru-bipod : (i) PPh_3 , CBr_4 in CH_2Cl_2 , (ii) Na_2CO_3 in DMF, (iii) glycerol and *tert*-butyl alcohol at 150°C under N_2 , and then KPF_6 in water

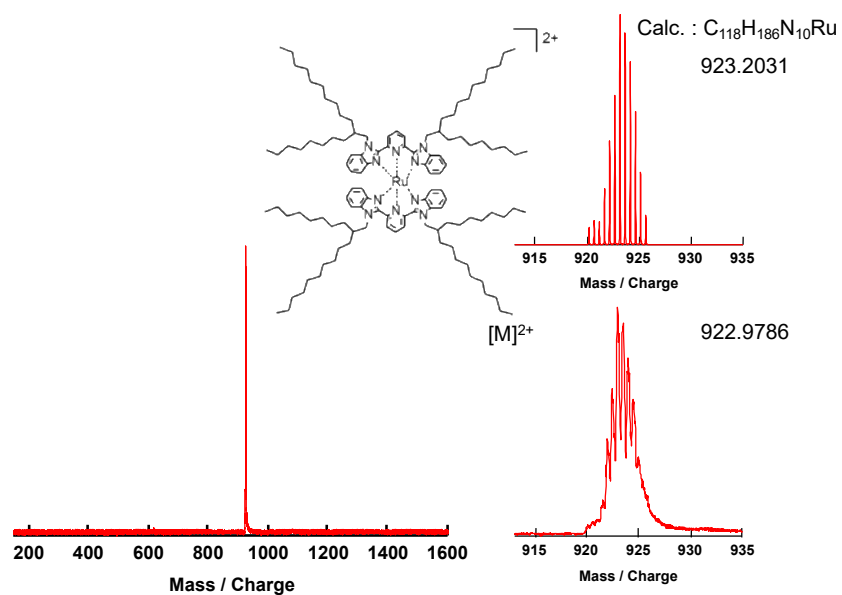


Figure A-2: ESI-MS spectra of Ru-bipod: (a) full spectrum, and (b) the observed and calculated isotope patterns of the molecular peak.

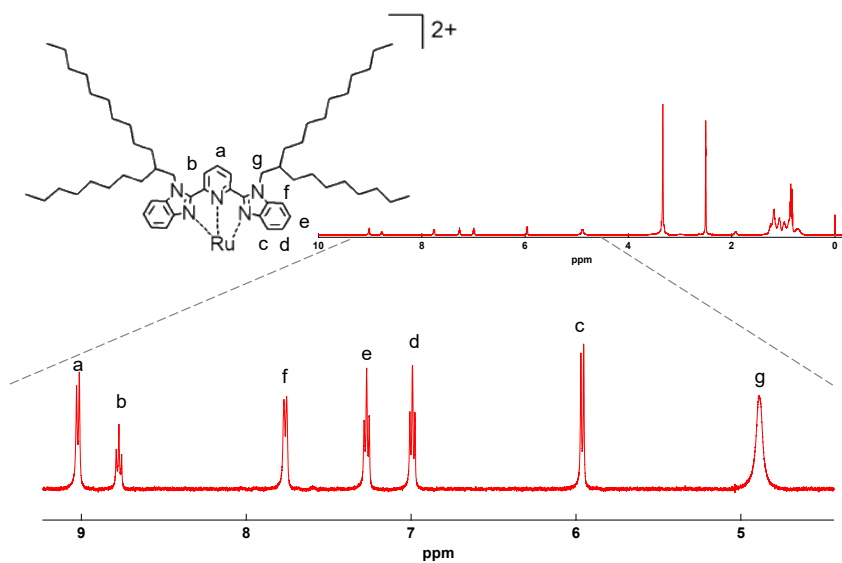


Figure A-3: ^1H NMR (500 MHz) spectra of Ru-bipod in DMSO-d_6

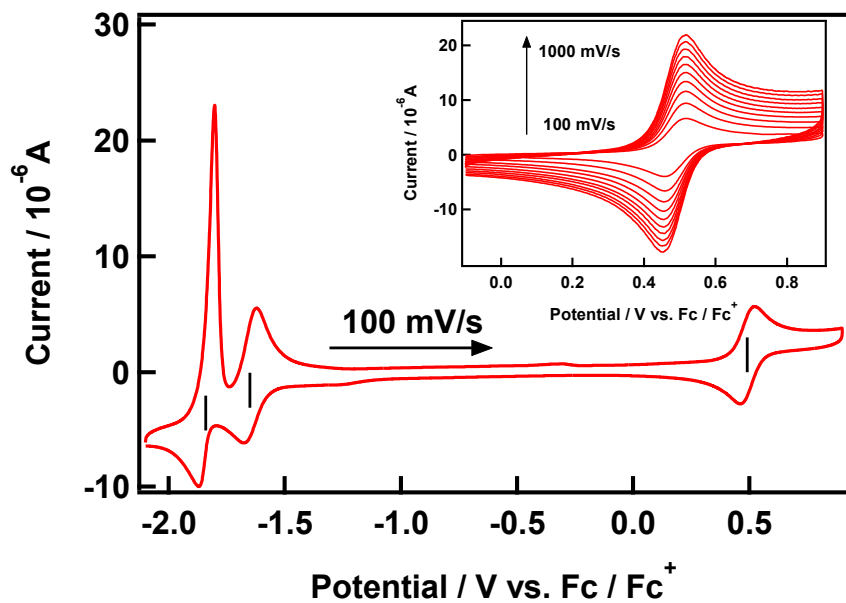


Figure A-4: Cyclic voltammogram of Ru-bipod in CH₃CN (0.1 M TBAPF₆). WE: electrode: Glassy carbon electrode, RE: Ag/AgNO₃ in CH₃CN, CE: platinum wire.

Appendix B: Synthesis of Ru(bipod)(bipob) and Ru(bipod)(dmbb) and their characterisation (all the information in this section is the group of Pro. Haga, Chuo University, Japan) (related to Chapter 4)

B-1: Materials:

2-Octyl-1-dodecanol (Aldrich), 2-fluoronitrobenzene (TCI) and ruthenium(III) trichloride hydrate (Heraeus GmbH) were used without further purification. 1-Bromo-2-octyl-1-dodecane and 2,6-bis(1-(2-octyldodecan)benzimidazol-2-yl)pyridine (bipop), was prepared from 2-octyl-1-dodecanol.^[1] All other supplied chemicals were of standard reagent grade quality.

B-2: Physical Measurements:

¹H NMR, ESI-MS, MALDI-TOF-MS, and UV-VIS spectra were recorded with a JNM-ECA 500 (JEOL) spectrometer, a JEOL JMS-T100 LC AccuTOF, Shimadzu MALDI-TOF AXIMA-CFR mass spectrometer, and Hitachi U-3210 UV-vis spectrophotometer, respectively. The electrochemical measurements were carried out in a standard one-compartment cell under N₂ gas flow equipped with a BAS glass-carbon ($\phi = 3$ mm) working electrode, Pt-wire counter electrode, and Ag/Ag⁺ reference electrode along with an ALS/CH model 660A electrochemical analyzer. The reference electrode was Ag/AgNO₃ (0.01 M in 0.1 M TBAPF₆ CH₃CN), which was abbreviated as Ag/Ag⁺. For a X-ray single crystal analysis, the diffraction data for [Ru(bipod)(bipob)](PF₆) were collected using a Bruker SMART APEXII ULTRA CCD-detector diffractometer on a rotating anode (Mo-K α radiation; graphite monochromator; $\lambda = 0.71073$ Å). The structure was solved using direct methods and refined using SHELXL-2014 (full-matrix least-squares on F^2) in APEX2. Unfortunately, the trial of refinement for the diffraction data in [Ru(bipod)(bipob)](PF₆) was unsuccessful to achieve the publishable accuracy because of the heavily disordered alkyl chain in the molecules.

Differential scanning calorimeter (DSC) Shimadzu Type DSC-60 was used for the DSC measurements.

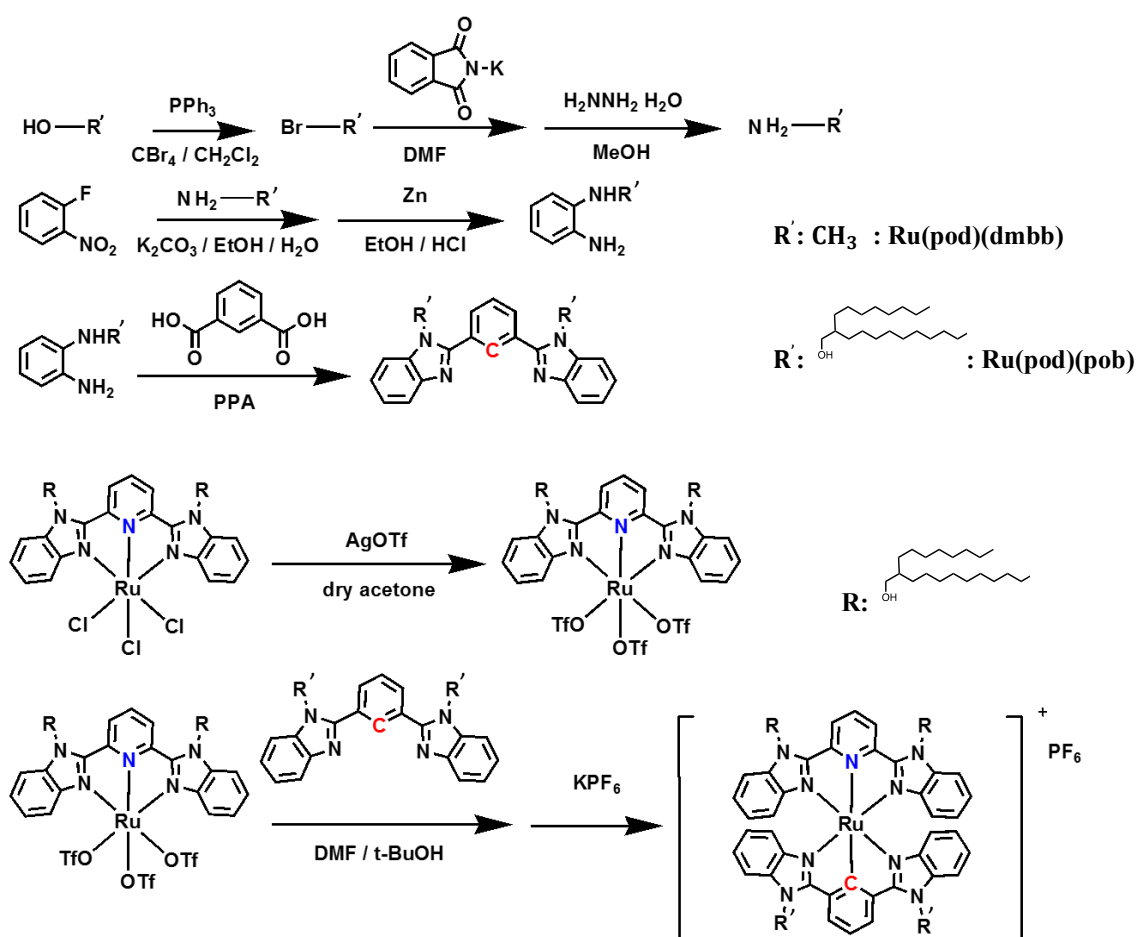


Figure B-1: Synthetic route to amphiphilic Ru complex, [Ru(bipod)(bipob)](PF₆)

(i) 2-octyl-dodecylamine Na₂CO₃ under microwave irradiation, in EtOH-H₂O, (ii) Zn/HCl in EtOH, (iii) isophthalic acid in polyphosphoric acid at 200 °C, (iv) AgOTf in acetone, (v) DMF and *tert*-butanol at 120 °C.

B-3: Synthesis of (2-nitrophenyl)-(2-octyldodecyl)amine.

2-Octyldodecylamine was mixed with potassium carbonate (4.56 g, 33.3 mmol), ethanol (15 mL), and pure water (5 ml) by stirring and then 2-fluoronitrobenzene (2.84 g, 1.34 mL, 20.2 mmol) was added dropwise. The resulting mixture was heated by the aid of intermittent microwave irradiation at 625 W for 25 min with 2 min interval, and dissolved in dichloromethane (30 ml). After washing with brine, the dichloromethane layer was collected and evaporated in vacuo. The residue was purified by silica column chromatography with ethyl acetate and hexane mixture (2:3 v/v) as an eluent, and obtained as a yellow oil (3.56 g).

¹H NMR (500 MHz, CDCl₃): δ = 8.16 (2H, m), 7.43 (1H, t, J = 4.3 Hz), 6.84 (1H, d, J = 8.6 Hz), 6.62 (1H, t, J = 10.0 Hz), 3.20 (2H, t, J = 5.4 Hz), 1.76 (1H, m), 1.27 (32H, m),

0.876 (m, 6H).

B-4: Synthesis of N-(2-octyl dodecyl)-benzene-1,2-diamine.

To the solution of (2-nitrophenyl)-(2-octyldodecyl)amine (3.56 g, 8.50 mmol) in ethanol (70 ml) zinc powder (2.60 g, 39.8 mmol) was added. The mixture was heated with stirring at 100 °C for 7 h, during time 2 mL of a 10 % diluted hydrochloric acid solution was added 5 times intermittently. After being cooled to room temperature, the solution was filtered through Celite(Sigma-Aldrich) and neutralized by the dropwise addition of 1 M sodium hydroxide solution. The resulting solution was extracted with dichloromethane, and the organic layers were combined and washed by brine several times, dried over anhydrous magnesium sulfate. A yellow oily product was obtained after evaporation of dichloromethane. Yield: 3.45 g.

¹H-NMR (500 MHz, acetone-d₆): δ = 6.66 (1H, d, J = 7.4 Hz), 6.62 (1H, t, J = 7.7 Hz), 6.55 (1H, t, J = 4.0 Hz), 6.49 (1H, t, J = 7.4 Hz), 3.02 (2H, d, J = 5.7 Hz), 1.69 (1H, m), 1.49-1.09 (32H, m), 0.88 (6H, m).

B-5: 1,3-Bis(N-(2-octyl dodecyl)benzimidazol-2-yl)benzene (bipob).

N-(2-octyl dodecyl)-benzene-1,2-diamine (3.45 g, 8.88 mmol) was heated at 150 °C with stirring for 1 h in polyphosphoric acid (25 ml), and then isophthalic acid (0.736 g, 4.48 mmol) and polyphosphoric acid (25 ml) were added into the solution and the heating at 200°C was continued for 23 h. After being cooled, the mixture was poured into water (400 ml), and the resulting solution including black precipitate was neutralized with 5 M sodium hydroxide. The brown residue was collected by filtration, and then dissolved in acetone, followed by celite filtration. The filtrate was dried in vacuo. The resulting residue was purified by column chromatography on a silica gel with a solvent mixtures of chloroform and ethyl acetate by changing the mixing ratio of 100/0 to 0/100 v/v. The product was obtained as a third band, which was collected to obtain the reddish-yellow oil. Yield: 1.31 g (42 %).

¹H-NMR (500 MHz, acetone-d₆): δ = 8.24 (1H, s), 8.02 (2H, m), 7.80 (1H, t, J = 7.7 Hz), 7.72 (2H, d, J = 7.4 Hz), 7.61 (2H, d, J = 8.0 Hz), 7.29 (4H, m), 4.44 (4H, d, J = 7.4 Hz), 1.95 (2H, m), 1.35 - 0.96 (64H, m), 0.86 (12H, m). ESI-TOF MS. *m/z* = 871.88 (Calcd. for [C₆₀H₉₄N₄]⁺, 871.76)

B-6: Synthesis of [Ru(bipod)Cl₃].

This Ru complex was synthesized in a similar manner to [RuL18]Cl₃, except that the bipod ligand was used instead of L18 ligand.[1]

B-7: Synthesis of [Ru(bipod)(bipob)](PF₆).

Under shading condition a mixture of Ru(bipod)Cl₃ (0.20 g, 0.18 mmol) and silver trifluoroacetate (AgOTf) (0.149 g, 0.581 mmol) were refluxed with stirring for 2 h. After being cooled, the solution was filtered through celite in order to remove grey-colored AgCl solid, and the solvent was removed

in vacuo. To the resulting violet solid residue DMF (10 ml), *tert*-butanol (10 ml), and the bipob ligand (0.161 g, 0.185 mmol) were added, and the mixture was heated at 120 °C for 25 h, during which time the solution turned reddish violet in color. The solvent was concentrated by evaporating the solvent up to one third of its total volume. After being cooled to room temperature, the addition of KPF₆ saturated aqueous solution (5 ml) led to the precipitation, which was collected. After the crude product was dissolved in dichloromethane, the purification was performed by the silica gel column chromatography with a mixture of dichloromethane-ethyl acetate by changing the volume ratio from 100:0 to 0:100 v./v as an eluent. The separated third violet band was collected to obtain the violet solid. Yield: 0.15 g (42 % yield). ¹H NMR (500 MHz, DMSO-*d*₆) δ: 8.88 (2H, d, J = 8.2 Hz), 8.45 (3H, m), 7.68 (1H, t, J = 7.2 Hz), 7.55 (2H, d, J = 8.3 Hz), 7.40 (2H, d, J = 7.9 Hz), 7.10 (2H, t, J = 7.5 Hz), 6.93 (2H, t, J = 7.7 Hz), 6.73 (2H, t, J = 7.9 Hz), 6.65 (2H, t, J = 7.9 Hz), 6.05 (2H, d, J = 8.2 Hz), 5.72 (2H, d, J = 8.0 Hz), 4.82 (4H, s), 4.67 (4H, s), 2.07 (2H, s), 1.95 (2H, s), 1.28~ 0.733 (m, 168H).

ESI TOF MS: $m/z = 1843.07$ (Calcd. for [C₁₁₉H₁₈₅N₉Ru]⁺, 1843.39. (ESI TOF spectra shown in Figure 1) Anal. Calcd for C₁₁₉H₁₈₆N₉RuPF₆: C, 71.86; H, 9.43; N, 6.34. Found: C, 71.63; H, 9.62; N, 6.56

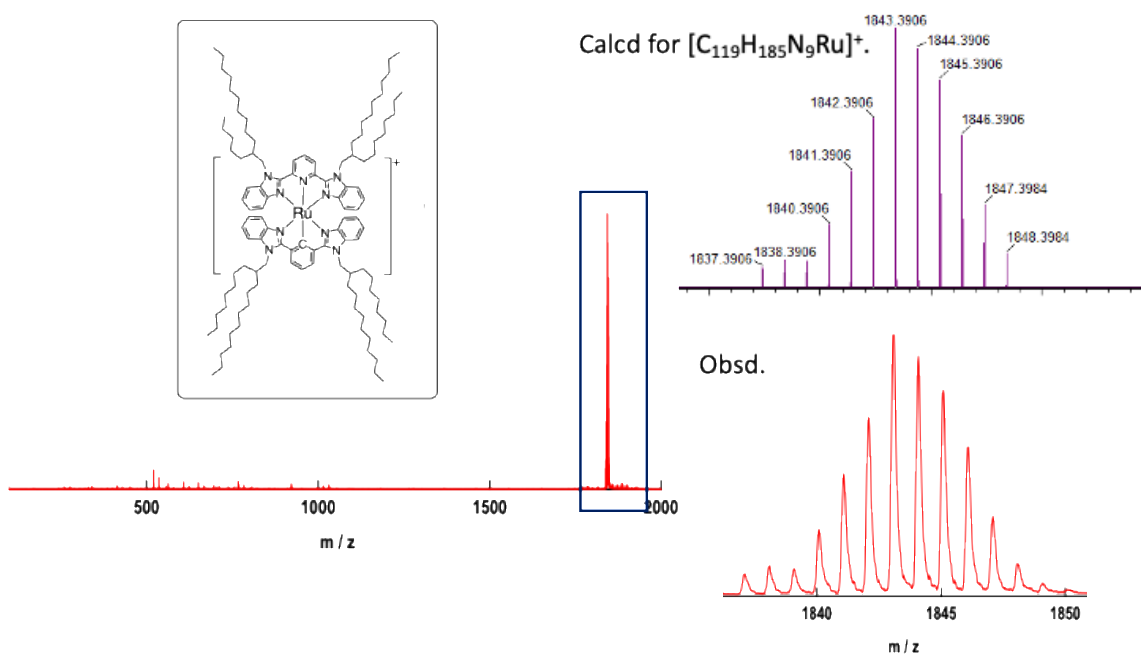


Figure B-2: ESI-MS spectra of [Ru(bipod)(bipob)](PF₆): (a) full spectrum, and (b) the observed and calculated isotope patterns of the molecular peak

B-8: Result and discussion:

B-8-1: Synthesis.

Synthetic route to target amphiphilic Ru complex $[\text{Ru}(\text{bipod})(\text{bipob})](\text{PF}_6)$ is summarized in Scheme 1. The ligand, 1,3-bis(*N*-(2-octyl dodecyl)benzimidazol-2-yl)benzene (bipob) was synthesized by the condensation reaction of *N*-(2-octyl dodecyl)-benzene-1,2-diamine with isophthalic acid in polyphosphoric acid. At first, we tried to synthesize the bipod ligand by the alkylation of 2,6-bis(benzimidazol-2-yl)benzene with alkyl bromide, but the double N-H alkylation reaction did not proceed to completion, which is in sharp contrast to the reaction with 2,6-bis(benzimidazol-2-yl)pyridine. Therefore, the condensation reaction was selected as a synthetic route. Heteroleptic bis-tridentate $[\text{Ru}(\text{bipod})(\text{bipob})](\text{PF}_6)$ complex was obtained by the reaction of $[\text{Ru}(\text{bipod})(\text{OTf})_3]$ with bipob in DMF- *tert*-butanol mixture at 120°C, during which time the Ru-C cyclometallation and the reduction from Ru(III) to Ru(II) state took place. The complex, $[\text{Ru}(\text{bipod})(\text{bipob})](\text{PF}_6)$, was soluble in CH_2Cl_2 , DMF, DMSO, toluene, but insoluble in water.

Surprisingly, ^1H nmr spectra of $[\text{Ru}(\text{bipod})(\text{bipob})](\text{PF}_6)$ showed strong dependence on the kind of solvent; the two spectra in CDCl_3 and DMSO-d_6 were shown in Figure 2. In nonpolar solvent such as CDCl_3 , all ^1H nmr signals showed broadened and up-field shifted compared to those in polar solvents such as DMSO-d_6 . This result suggested the strong intermolecular interaction between aromatic rings.

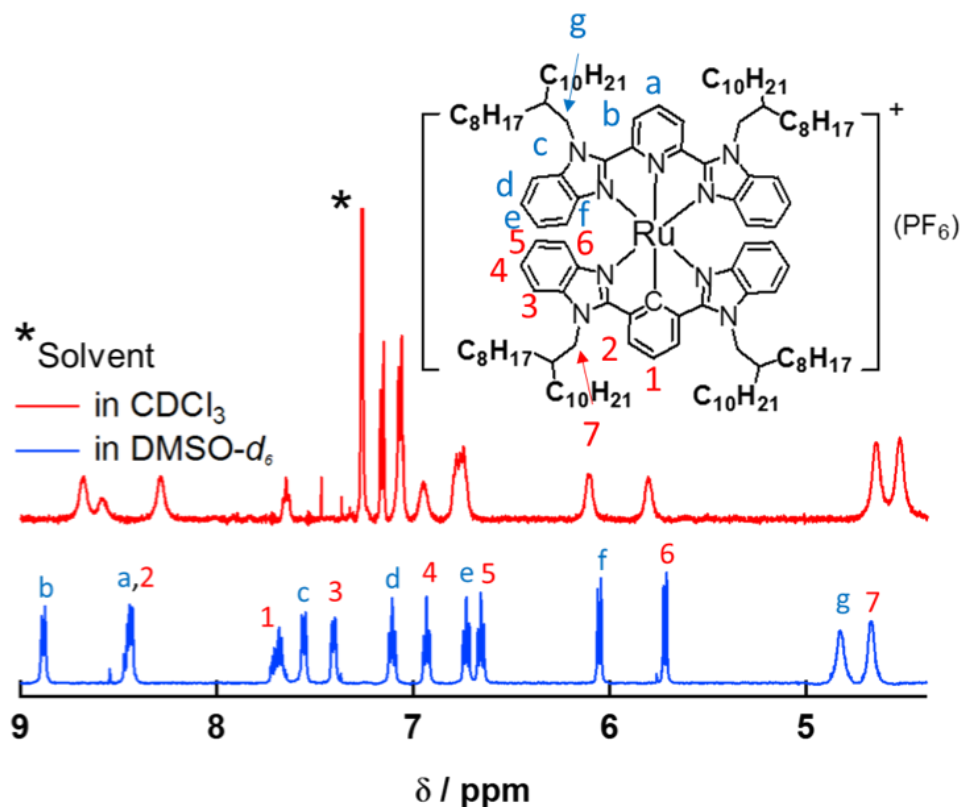


Figure B-3: ^1H NMR spectra of $[\text{Ru}(\text{bipod})(\text{bipob})](\text{PF}_6)$ in CDCl_3 (red) and $\text{DMSO-}d_6$ (blue line). (The atom numbering and the signal assignment in $\text{DMSO-}d_6$ are shown).

B-8-2: Electrochemical properties:

$[\text{Ru}(\text{bipod})(\text{bipob})](\text{PF}_6)$ showed two reversible one-electron oxidations at -0.11 V ($\Delta E_p = 59\text{ mV}$) and $+1.16\text{ V}$ ($\Delta E_p = 61\text{ mV}$) vs Fc^+/Fc , which were assigned for the $\text{Ru}(\text{II})/\text{Ru}(\text{III})$ and $\text{Ru}(\text{III})/\text{Ru}(\text{IV})$ processes, respectively. Only one-electron reduction wave at $E_{pc} = -1.81\text{ V}$ vs Fc^+/Fc was observed, accompanied by a large anodic desorption peak at -1.78 V vs Fc^+/Fc . This reduction occurred on the coordinated bipod ligand by comparing the redox behavior of homoleptic $[\text{Ru}(\text{bipod})_2](\text{PF}_6)$ complex. Since $[\text{Ru}(\text{bipod})(\text{bipob})](\text{PF}_6)$ lost the total charge by the reduction, which led to the deposition of the reduced species on the electrode surface. The comparison of cyclic voltammograms of two homo- and heteroleptic Ru complexes is shown in Figure B-2. The introduction of Ru-C cyclometalated bond results in a potential shift to a large negative shift by 0.6 V , which has been expected from our previous study[2].

B-8-3: UV-vis spectral change by chemical oxidation of $[\text{Ru}(\text{bipod})(\text{bipob})]^+$ by $\text{Ce}(\text{IV})$ ion

Figure B-4 exhibits the UV-vis spectral change of $[\text{Ru}(\text{bipod})(\text{bipob})](\text{PF}_6)$ in CH_3CN upon the dropwise addition of ammonium cerium(IV) nitrate in CH_3CN . The MLCT band at 517 nm derived

from the Ru(II) oxidation state gradually decreased with increasing the amount of Ce(IV) ion and at the same time a new strong band at 417 nm and a weak band at 730 nm appeared, keeping the isosbestic points at 451, 648, 800 nm. The solution color was changed from violet to yellow.

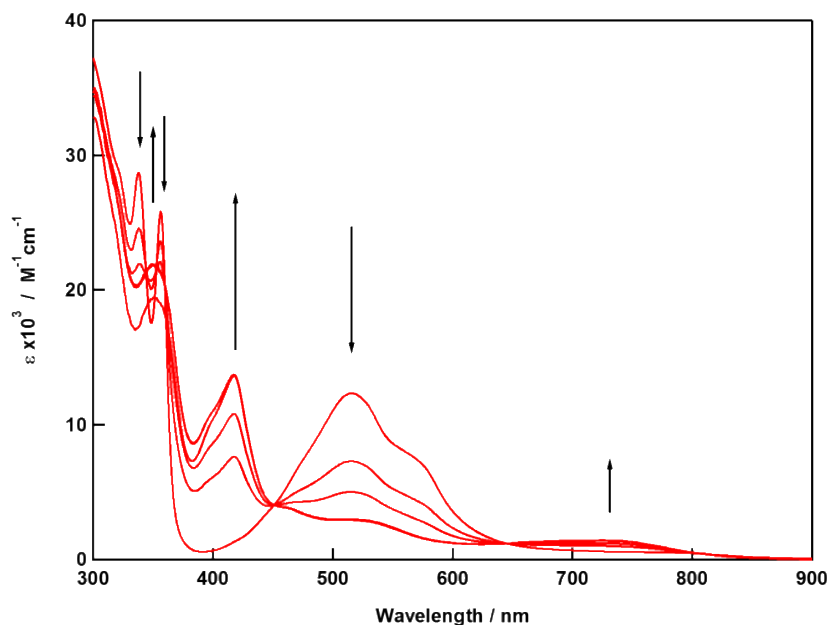


Figure B-4: UV-vis spectral change of [Ru(bipod)(bipob)](PF₆) in CH₃CN upon the dropwise addition of ammonium cerium(IV) nitrate in CH₃CN.

B-8-4: Preliminary result of X-ray single crystal analysis.

Needle-shaped single crystals were obtained from DMSO-methanol-water (1:5:3 v/v/v) mixed solvent system by the slow evaporation of the solvent at room temperature. Unfortunately, the structure refinement on experimental data, in particularly for the longer alkyl chain parts, was unsuccessful because of the heavily disordered alkyl chains and the presence of optical isomers in the alkyl chains, but at least the molecular packing around the rigid Ru center in the crystals was clearly observed, which is shown in Figure B-5. In the crystals, two bis(benzimidazol-2-yl)pyridine moieties in bipod ligands was closely located through $\pi\pi\pi\pi$ interactions, on the other hand bis(benzimidazol-2-yl)benzene moieties were located away from each other. The flexible soft alkyl chains were sandwiched by the rigid Ru bis(tridentate ligand) core to form the layered structure. (Please see the checkcif file.)

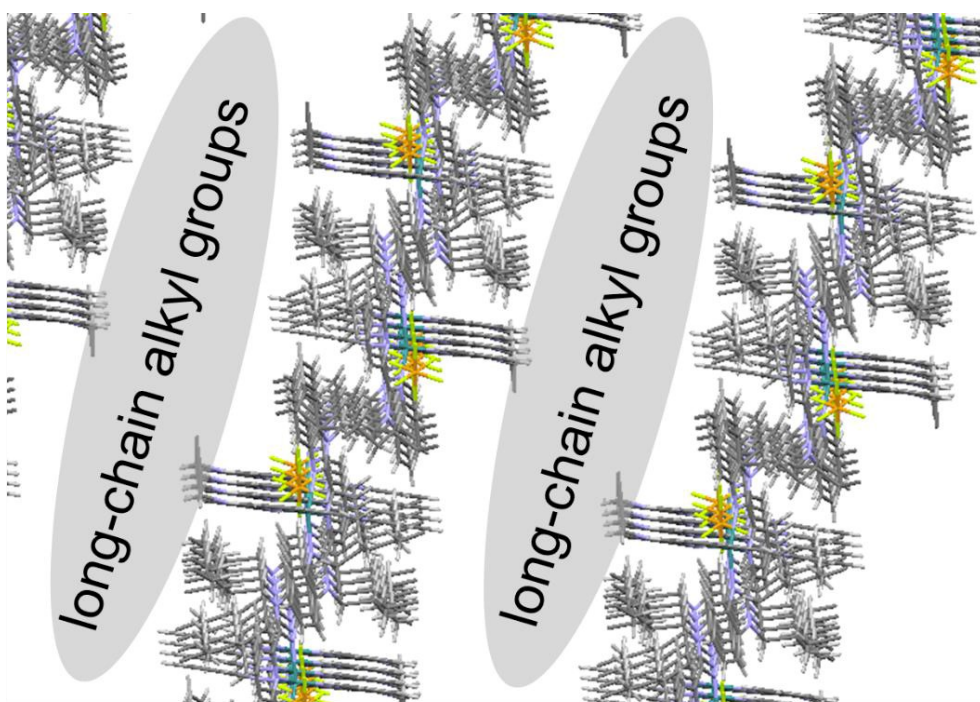


Figure B-5: Molecular packing image in [Ru(bipod)(bipob)](PF₆) crystals from a single crystal X-ray analysis. (The refinement was not completed because of heavy disordered in flexible long alkyl chains and the presence of optical isomers.

B-8-5: Phase transitions from DSC measurement

DSC curves of [Ru(bipod)(bipob)](PF₆) for heating and cooling processes is shown in Figure B-6, suggesting a phase transition at 60 °C. Further, a structural phase transition occurred at 110 °C and crystals appeared at 120 °C and became an isotropic liquid at 140 °C, which was also supported by the polarized microscopic images (Figure B-7). Upon cooling process, a clear DSC peak did not appear but on the polarized microscopic image showed the clear change of the phase, depending on the cooling processes. (Figure B-8)

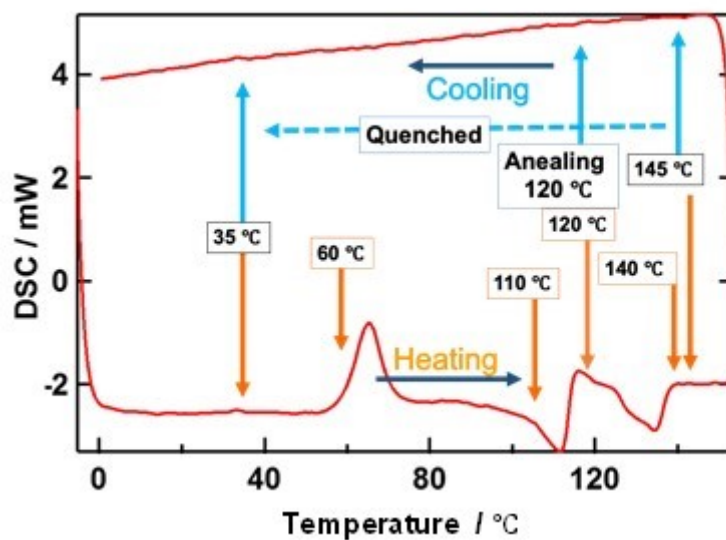


Figure B-6: DSC curves of [Ru(bipod)(bipob)](PF₆) on heating and cooling processes.

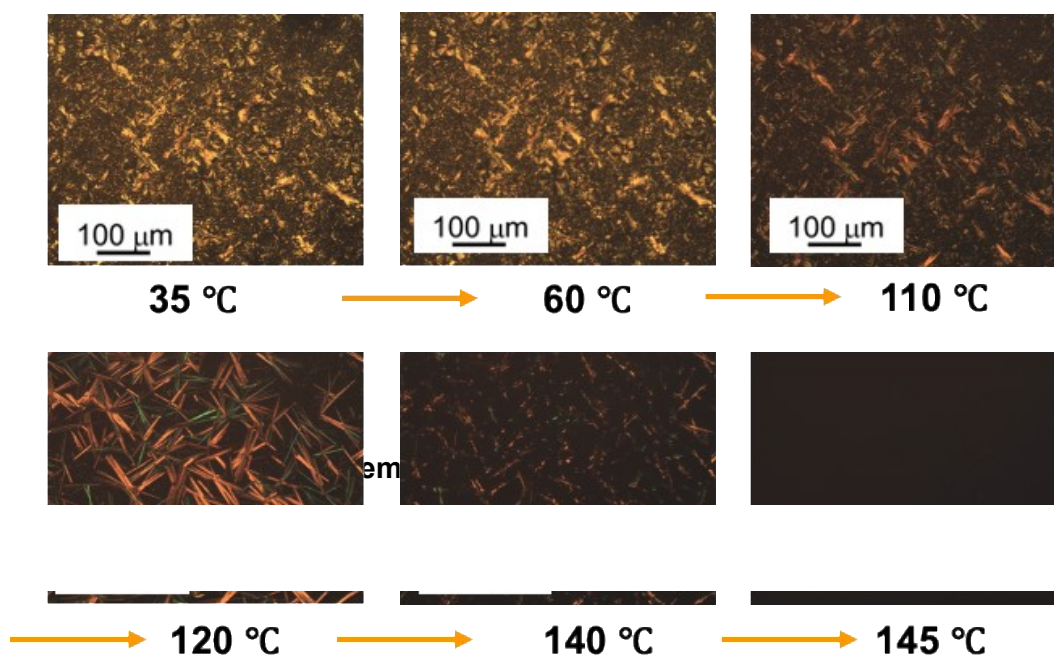


Figure B-7: Polarized microscopic images of [Ru(bipod)(bipob)](PF₆) N upon heating process.

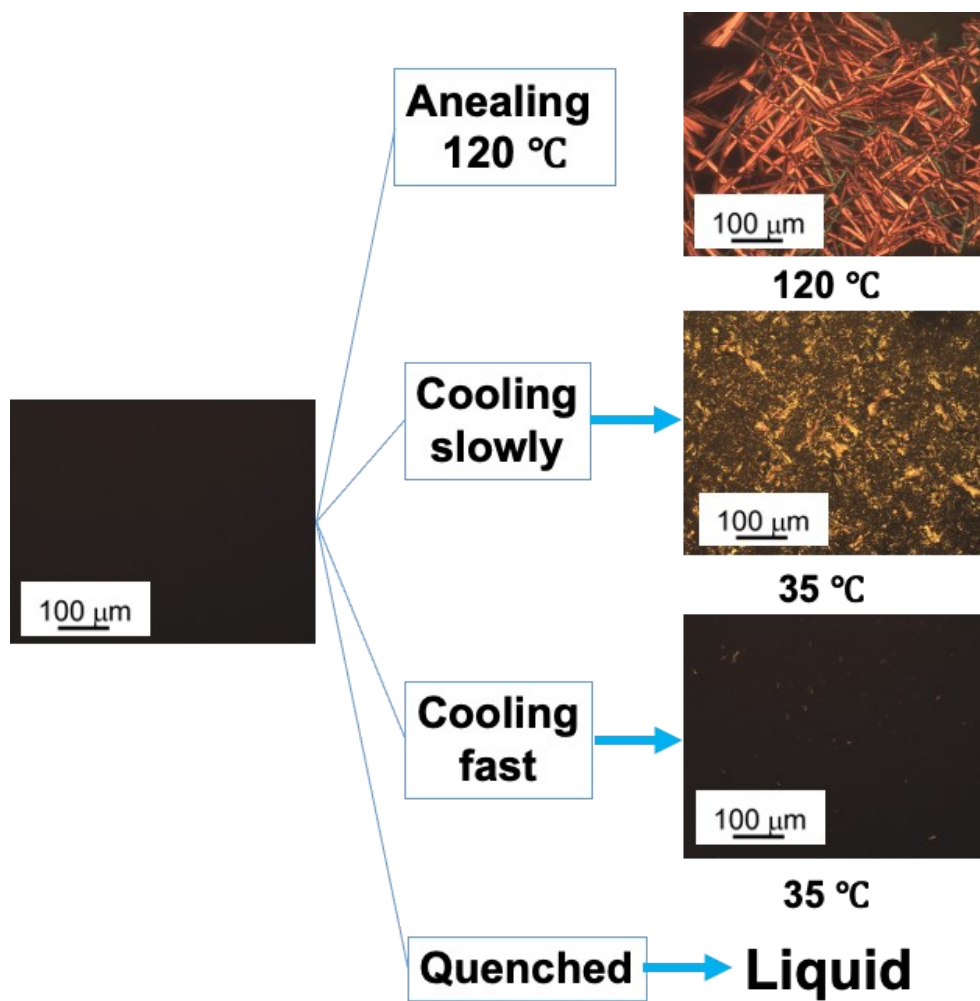


Figure B-8: Polarized microscopic images of [Ru(bipod)(bipob)](PF₆) upon cooling process.

Appendix C: Results (related to chapter 3)

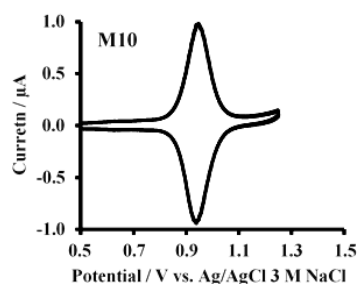
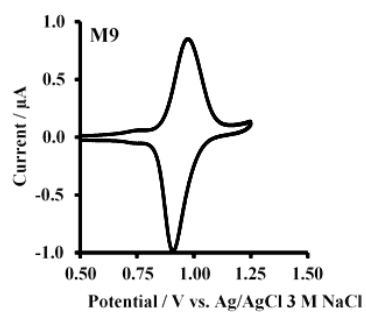
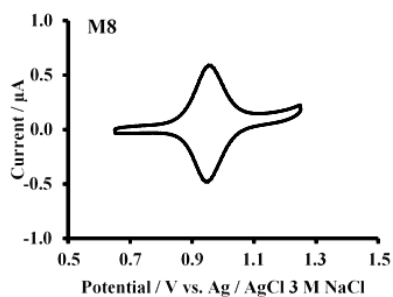
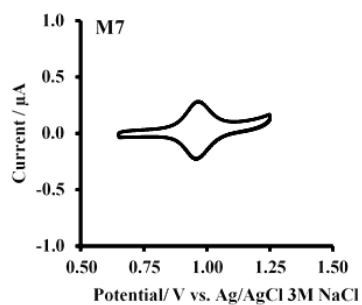
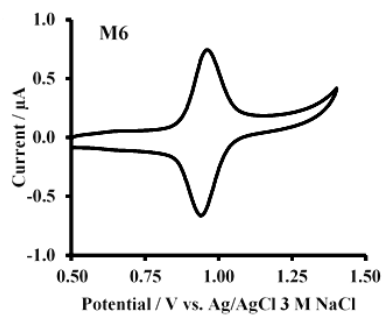
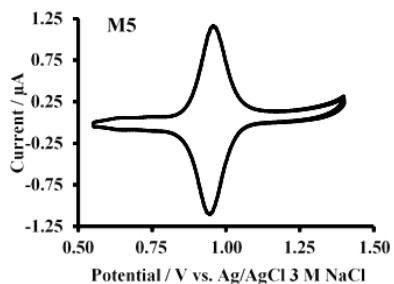
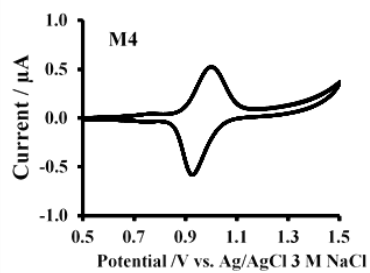
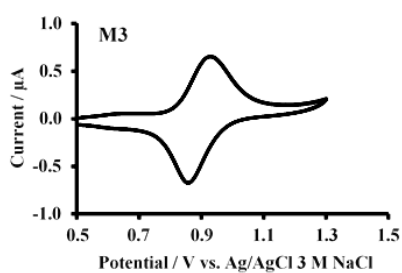
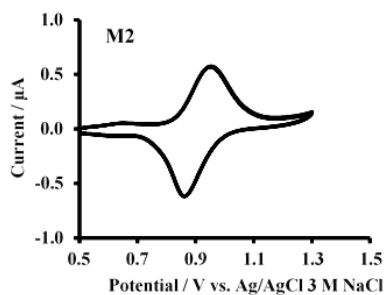
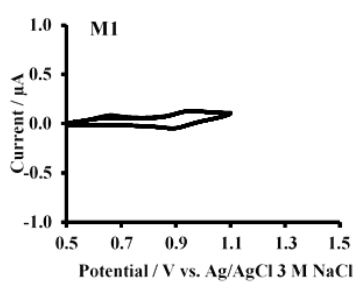


Figure C-1: Cyclic voltammetry obtained using membrane with different combinations of membrane (M1-M10) demonstrating in table 1. With 10 mM KPF_6 with scan rate 10 mV/s ($n=3$).

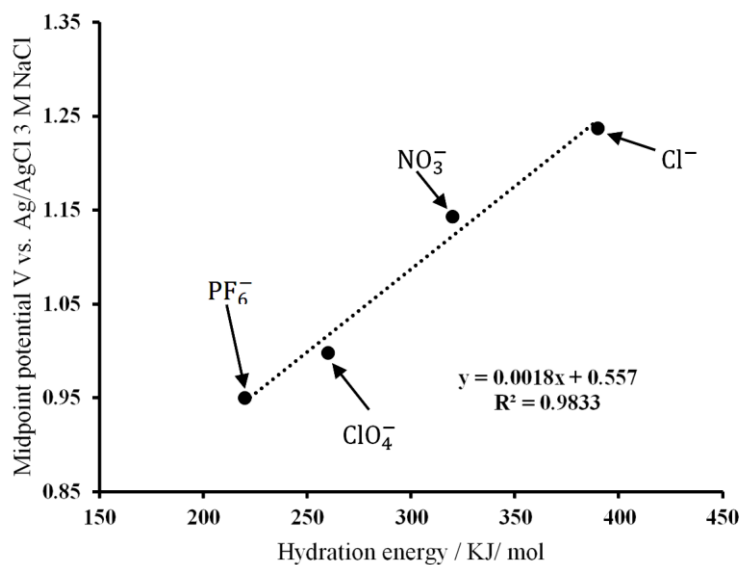


Figure C-2. Linear relation between mid- point potentials of the membrane M5 in the presence of 10 mM of different anions and hydration energies of different anions²⁴³

Equations to calculate electron transfer coefficients (α and $1 - \alpha$), anodic and cathodic critical scan rates (v_a and v_c , respectively) and anodic and cathodic and total electron transfer rate constant ($k_{\text{app},a}$, $k_{\text{app},c}$ and $k_{\text{app},\text{ET}}$, respectively):

$$k_{\text{app},a} = \frac{(1-\alpha)nFv_a}{RT} \quad \text{eq.3} \quad , \quad k_{\text{app},c} = \frac{\alpha nFv_c}{RT} \quad \text{eq.4} \quad , \quad k_{\text{app},\text{ET}} = \frac{k_{\text{app},a} + k_{\text{app},c}}{2} \quad \text{eq.5}$$

Appendix D: Attribution Statement

To Whom It May Concern

In relation to a planned draft manuscript to be submitted for journal publication:

I, Nasib Khalei, contributed to the design of experiments, the gathering of data by performing these experiments, undertaking of data analysis and interpretation, and preparation of the draft manuscript prepared under the draft title of “facilitated ion transfer of potassium ions at micro-interfaces between immiscible electrolyte solutions supported on laser-ablated glass membranes”.



Nasib Khalei

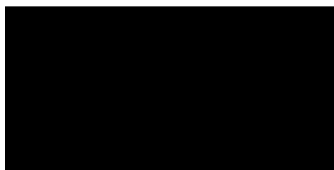
I, as a Co-Author, endorse that this level of contribution by the candidate indicated above is appropriate.



Prof. Damien W.M. Arrigan



Dr. Terence G. Henares



Dr Gazi Jahirul Islam

To Whom It May Concern

In relation to a planned draft manuscript to be submitted for journal publication:

I, Nasib Khalei, contributed to the design of thin film electrochemical experiemnts, the gathering of data by performing these experiments, undertaking of data analysis and interpretation, and preparation of the draft manuscript prepared under the draft title of "Evaluation of a Ru-bipod complex as a redox transducer for membrane-based voltammetry of anions".



Nasib Khalei

I, as a Co-Author, endorse that this level of contribution by the candidate indicated above is appropriate.



Prof. Damien W.M. Arrigan

Besides the above co-authors, the contributions of additional co-authors will be solely in the synthesis and characterisation of the synthesised ruthenium complex studied.

To Whom It May Concern

In relation to a planned draft manuscript to be submitted for journal publication:

I, Nasib Khalei, contributed to the design of thin film electrochemical experiemnts, the gathering of data by performing these experiments, undertaking of data analysis and interpretation, and preparation of the draft manuscript prepared under the draft title of “membrane-based voltammetry of anions using a heteroleptic ruthenium complex as a redox transducer”.



Nasib Khalei

I, as a Co-Author, endorse that this level of contribution by the candidate indicated above is appropriate.



Prof. Damien W.M. Arrigan

Beside the above co-authors, the contributions of additional co-authors will be solely in the synthesis and characterisation of the new compounds employed in the study, either new ruthenium complex or new sulfate ionophores.